

https://dspace.org/

Formulating a procedure for conducting studies for evaluating the transient recovery voltage for line circuit breakers connected to evolving, series and shunt compensated transmission lines

Naidoo, Krishna

2022

https://hdl.handle.net/10539/34143

Downloaded from a DSpace repository. https://dspace.org/

MASTER'S DISSERTATION

Formulating a procedure for conducting studies for evaluating the transient recovery voltage for line circuit breakers connected to evolving, series and shunt compensated transmission lines



Author:
K. Naidoo

Supervisor:
Prof. J.M van Coller

Co-Supervisor:
Prof. C. Gomes

A dissertation submitted to the Faculty of Engineering and the Built Environment, University of the Witwatersrand, Johannesburg, in fulfilment of the requirements for the degree of Master of Science in Engineering

in the

High Voltage Research Group

School of Electrical and Information Engineering

Johannesburg, November 2021 South Africa

DECLARATION

I hereby declare that this dissertation is my own unaided work. It is being submitted to the Degree of Master of Science to the University of the Witwatersrand, Johannesburg. It has not been submitted before for any degree or examination to any other University.

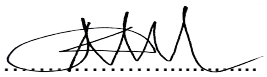

Krishna Naidoo

20th day of November year 2021

ABSTRACT

The objective of this dissertation is to develop a procedure to evaluate TRVs for Line Circuit Breakers (LCBs) connected to evolving series and shunt compensated transmission lines.

The LCBs of a compensated circuit may be exposed to the effects of the change in compensation factor due to the integration of new voltage sources in this circuit which could result in higher stresses during switching. The insulation stresses related to switching the LCBs are to be evaluated in this changing environment to ensure the specified withstand requirements are adequate for the new configuration. The objective of this research is to develop an approach taking into consideration various factors that would influence the decision to uprate existing LCBs in an evolving, series and shunt compensated typical transmission network.

Three scenarios were investigated in evaluating TRVs of LCBs connected to evolving series and shunt compensated transmission lines.

A procedure was developed describing the approach to conducting TRV studies of LCBs connected to evolving series and shunt compensated transmission lines. Figure 1-1 presents this high-level procedure to follow. The existing network configuration must be established. This will include the fault level of the network, the fault type to apply to the simulation model (i.e. three-phase, three-phase-to-ground, etc.) and the phase angles of voltage sources. Next, the simulation model is to be developed by applying the appropriate component models. Input data such as transmission line tower geometry, conductors, conductor geometry, surge arrester V-I curves, series capacitor size damping circuit sizing, shunt reactor size, etc., will be required to develop an accurate model of the network being studied. Future network plans associated with the circuit being studied must be identified as this will provide input to the various scenarios to be modelled and simulated. The model should then be validated against existing fault recording data. Once the model is validated, the simulations for the various scenarios may be conducted. The results of the simulations will determine fault current limits that would result in the peak recovery voltage and RRRV ratings of the LCB being exceeded. These fault current levels will then form a trigger when these magnitudes are being reached to reassess the TRV ratings of LCBs in the circuit. This may either result in the LCB being uprated or mitigation strategies applied.

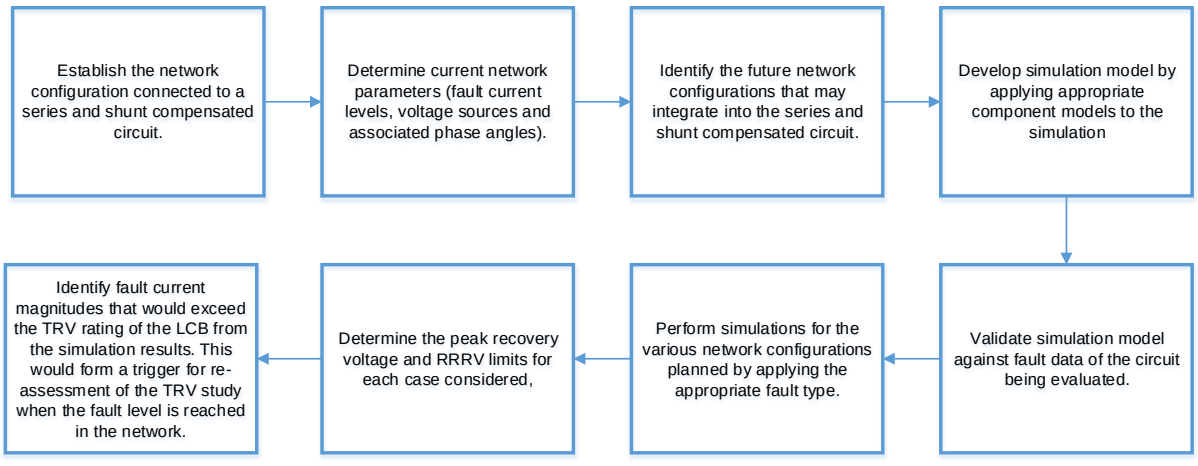

Figure 1-1: High level procedure in evaluating the TRV for LCBs connected to evolving, series and shunt compensated transmission lines

It was found that a change in fault level of the network had a direct influence on the required TRV rating of the LCB. Additionally, a change in the line length of a series and shunt compensated circuit was shown to influence the required peak recovery voltage rating of an LCB. An increase in line length increases the peak recovery voltage, making it susceptible to exceeding its LCB ratings. The compensation factor was shown to have a minimal impact on the required TRV rating of the LCB.

However, failure of the series capacitor protection to operate correctly upon fault detection could result in the series capacitor bypass circuit breaker not to close. This would result in severe peak recovery voltages being imposed on the LCB.

ACKNOWLEDGEMENTS

The completion of this research would not have been possible without the patience, guidance and expertise of my academic supervisor, Prof. J. M Van Coller. I am thankful for the numerous hours of guidance that he afforded me over the past two years.

A special thanks to Prof. Chandima Gomes for his weekly support and motivation to progress with my research.

I wish to acknowledge Peet Schutte who guided me over the first six months in introducing the topic of research as well as the simulation software tool utilised in this work.

I would like to express my appreciation to my managers, Mr Bheki Ntshangase and Mr Benny Tladi, who afforded me the opportunity to participate in the Eskom Power Plant Engineering Institute (EPPEI) programme to pursue my post graduate studies.

Lastly, and importantly, my sincere gratitude to my wife, Vasanta Naidoo, my children, Bhavani and Devanya, my parents and a close colleague, Mr Mohammad Nabbie for all the encouragement, support and sacrifices that were made to complete this research.

TABLE OF CONTENTS

1 INTRODUCTION 1

1.1 Background 1

1.2 Scope 1

1.3 Research question 2

1.4 Research objective 2

1.5 Research approach 2

1.6 Chapter Summary 3

2 THE THEORY ON THE ORIGIN OF THE NATURE OF TRANSIENT RECOVERY VOLTAGES (TRV) 4

2.1 Insulation Coordination to mitigate effects of overvoltages 4

2.2 Transients in Power Systems 6

2.2.1 Temporary Overvoltages 7
2.2.2 Slow-Front Overvoltages 7
2.2.3 Fast-Front Overvoltages 8
2.2.4 Very-Fast-Front Overvoltages 8

2.3 The origin and nature of Transient Recovery Voltages 8

2.3.1 TRV Characteristics 8
2.3.2 Transient Response Analysis 10
2.3.3 Travelling Wave Effects 14
2.3.4 Terminal Faults of TRV travelling waves 16
2.3.4.1 First-Pole-To-Clear Factor 16
2.3.4.2 Underdamped TRV 21
2.3.5 Short-Line Faults 22
2.3.5.1 Overdamped TRV 22
2.3.6 Out-of-Phase Condition 23
2.3.7 TRV Calculations 23

2.4 Circuit Breakers 24

2.4.1 SF_6 Circuit Breakers 25

2.5 Black Box Arc Modelling 25

2.5.1 The Cassie Black Box Model 26
2.5.2 The Mayr Black Box Model 27

2.6 Arc Interruption Process 28

2.6.1 Interruption of Capacitive Currents 28
2.6.1.1 Shunt Capacitance in transmission lines 28
2.6.1.2 Series Capacitors used with transmission lines 29
2.6.2 Interruption of Inductive Currents 35
2.6.2.1 Shunt Reactors 35
2.6.2.2 Series Reactors 35

2.7 Metal Oxide Varistors (MOVs)(Zinc Oxide (ZnO) Arresters) (Surge Arresters (SAs)) 36
2.8 Probabilistic Approach to TRV Evaluation 37
2.9 Existing Statistical Analysis Methods 37
2.9.1 Monte Carlo Approach 37
2.9.2 Kernel Density Estimation via Diffusion Process 37
2.10 Transient Modelling Theory 38
2.10.1 Simulation Time Step 39
2.10.2 Overhead Transmission Lines 39
2.11 A literature review of TRV case studies 41
3 CASE STUDY: TRV EVALUATION OF LCBS CONNECTED TO AN EVOLVING SERIES AND SHUNT COMPENSATED TRANSMISSION LINE 44
3.1 Procedure to conduct TRV studies for LCBs connected to evolving series and shunt compensated transmission lines 44
3.2 Network Configuration 44
3.3 Component Modelling 46
3.3.1 Overhead Transmission Line Modelling 46
3.3.2 Source Modelling 48
3.3.3 Surge Arrester Modelling 49
3.3.4 Line Arrester Modelling 50
3.3.5 Series Capacitor Bank 51
3.3.6 Compensation Factor 51
3.3.7 Current Limiting Damping Circuit 52
3.3.8 Line Circuit Breaker TRV specifications 52
3.3.9 Equivalent Capacitance of HV equipment 53
3.3.10 Fault Arc Resistance 54
3.4 Simulation model assumptions 55
3.5 Simulation methodology and accuracy 55
3.5.1 Simulation model accuracy 55
3.5.2 Sequence of the simulation procedure on ATPDraw 57
3.6 Circuit analysis of the three circuit configurations 61
3.6.1 Case 1: No Sub C 63
3.6.1.1 Steady State/Pre-fault condition (No Sub C) 63
3.6.1.2 Three-phase-to-ground fault application (No Sub C) 64
3.6.1.3 Series Capacitor Bank bypassed (No Sub C) 67
3.6.1.4 Sub B LCB Opens (No Sub C) 67
3.6.1.5 Sub A LCB Opens (No Sub C) 68
3.6.2 Sub C – Fault current contribution of 5 kA (Line A-C 1) 69
3.6.2.1 Steady State/Pre-fault condition (Line A-C 1) 69
3.6.2.2 Three-phase-to-ground fault application (Line A-C 1) 70
3.6.2.3 Series Capacitor Bank bypassed (Line A-C 1) 72
3.6.2.4 Sub A LCB Opens (Line A-C 1) 73
3.6.2.5 Sub C LCB Opens (Line A-C 1) 74

3.6.3 Sub C – Fault current contribution of 5 kA (Line C-B 1) 74
3.6.3.1 Steady State/Pre-fault condition (Line C-B 1) 75
3.6.3.2 Three-phase-to-ground fault application (Line C-B 1) 75
3.6.3.3 Series Capacitor Bank bypassed (Line C-B 1) 78
3.6.3.4 Sub B LCB Opens (Line C-B 1) 78
3.6.3.5 Sub C LCB Opens (Line C-B 1) 80
3.7 Simulation Results 80
3.7.1 Simulation Results: Case 1 82
3.7.2 Simulation Results: Case 2a (Sub C – 5 kA) 90
3.7.3 Simulation Results: Case 2b (Sub C – 10 kA) 99
3.7.4 Simulation Results: Case 3a (Sub C – 5 kA) 109
3.7.5 Simulation Results: Case 3b (Sub C – 10 kA) 119
3.7.6 Series Compensated Transmission Line Protection Malfunction 127
4 DISCUSSION OF RESULTS 130
4.1 Peak Recovery Voltages and RRRVs for Sub A 130
4.2 Peak Recovery Voltages and RRRVs for Sub B 132
4.3 Peak Recovery Voltages and RRRVs for Sub C 134
5 CONCLUSION 137
5.1 Future work and recommendations 137
6 REFERENCES 138
7 APPENDICES 140
7.1 V-I data for Surge Arrester 140

LIST OF FIGURES

Figure 1-1: High level procedure in evaluating the TRV for LCBs connected to evolving, series and shunt compensated transmission lines ii
Figure 2-1: Standard wave shape for a lightning voltage impulse 5
Figure 2-2: Standard wave shape for a switching impulse 5
Figure 2-3: Cumulative Distribution for the probability of flashover for insulation strength 6
Figure 2-4: Two-Parameter Envelope [11] 9
Figure 2-5: Four-Parameter Envelope [11] 9
Figure 2-6: Simplified RLC circuit with voltage injection 10
Figure 2-7: Pre-charged capacitor circuit 13
Figure 2-8: Generic damping curves for a series RLC circuit with step voltage injection 14
Figure 2-9: Equivalent segment for a two conductor transmission line model [9] 14
Figure 2-10: Unbalanced set of phasors represented by balanced set of symmetrical components 16
Figure 2-11: Equivalent circuit for a two-phase-to-earth fault 18
Figure 2-12: Sequence network circuit diagram for a two phase-to-earth fault 18
Figure 2-13: Equivalent circuit for a two phase fault 19
Figure 2-14: Sequence network circuit diagram for a two phase fault 20
Figure 2-15: TRV Capability for a 132 kV circuit breaker in an underdamped condition [3] 22
Figure 2-16: TRV for a Short-Line Fault [9] 23
Figure 2-17: Circuit diagram of a shunt capacitance circuit 28
Figure 2-18: Capacitive current interruption and re-ignition in a circuit breaker [9] 29
Figure 2-19: Circuit diagram of Fixed Series Capacitor [25] 29
Figure 2-20: Circuit Diagram of Thyristor Controlled Series Capacitor 30
Figure 2-21: V-I curve of a MOV across a series capacitor 30
Figure 2-22: Linear approximation of and MOV protected series capacitor 31
Figure 2-23: Relationship between Normalised MOV resistance and capacitive impedance with respect to current 31
Figure 2-24: X-R diagram of the series combination of Xc' and Rc' 31
Figure 2-25: X-R diagrams comparing an uncompensated line and a compensated line and the influence of the MOV 32
Figure 2-26: Example of voltage reversal of a 60% series compensated line. 33
Figure 2-27: Example of current reversal with a series capacitor connected to the line terminal 33
Figure 2-28: Simplified series resonant circuit 34
Figure 2-29: Typical V-I curve of MOV with the characteristic regions [5] 36
Figure 2-30: Increased bandwidth (a) vs reduced bandwidth (b) [39] 38
Figure 2-31: Internal AC resistance of a copper conductor 40
Figure 2-32: Internal inductance of copper conductor 40
Figure 3-1: High level procedure in evaluating the TRV for LCBs connected to evolving, series and shunt compensated transmission lines 44
Figure 3-2: Case 1 - Base case network configuration to be analysed for the case study 45
Figure 3-3: Case 2 - network configuration to be analysed for the case study 45
Figure 3-4: Case 3 - network configuration to be analysed for the case study 46
Figure 3-5: Transmission line tower configuration models 47
Figure 3-6: Thévenin equivalent modelling 48
Figure 3-7: X-R diagrams of source impedances 49
Figure 3-8: V-I curve of the surge arrester 50
Figure 3-9: V-I curve of rated line arrester 50
Figure 3-10: Current Limiting Damping Circuit 52
Figure 3-11: TRV ratings for various test duties of a 420 kV circuit breaker 53
Figure 3-12: Fault recording measured peak load current [A] 56
Figure 3-13: Simulated peak load current [A] 56

Figure 3-14: Fault recording measurement: peak fault current [A] 57
Figure 3-15: Simulated peak fault current [A] 57
Figure 3-16: Flow diagram of the simulation algorithm 58
Figure 3-17: Three-phase voltage waveform across line circuit breaker contacts 58
Figure 3-18: Three phase current waveform through the LCB 59
Figure 3-19: RRRV across LCB contacts 59
Figure 3-20: Series capacitor bank discharging into series capacitor damping reactor 60
Figure 3-21: Arc resistance for LCBs at Sub C 60
Figure 3-22: Closer view of the arc resistance response for Phase A 61
Figure 3-23: Characteristic response of fault arc resistance of three-phase-to-ground fault 61
Figure 3-24: Network configuration of Case 1 62
Figure 3-25: Network configuration of Case 2a and 2b 62
Figure 3-26: Network configuration of Case 3a and 3b 63
Figure 3-27: Single phase representation of the Network Configuration for Case 1 (No Sub C) 63
Figure 3-28: Circuit diagram of steady state pre-fault network configuration 64
Figure 3-29: Three-phase-to-ground fault applied to the series compensated circuit (No Sub C) 64
Figure 3-30: Thévenin equivalent circuit to determine fault current 64
Figure 3-31: Thévenin equivalent impedance Z_{th} at the point of the fault applied (Line A-C 1) 65
Figure 3-32: Delta- Star impedance transformation 65
Figure 3-33: Thévenin equivalent impedance reduced circuit 66
Figure 3-34: Fault applied through the arc impedance when the series capacitor bank was bypassed 67
Figure 3-35: LCB at Sub B was opened after the series capacitor bank was bypassed 67
Figure 3-36: Thévenin equivalent impedance when the LCB at Sub B was opened 68
Figure 3-37: Single phase representation of the Network Configuration for Case 2: Line A-C 1 (Sub C – 5 kA contribution) 69
Figure 3-38: Circuit diagram of steady state pre-fault network configuration for the series compensated line A-C 1 70
Figure 3-39: Three-phase-to-ground fault applied to the series compensated circuit Line A-C 1 70
Figure 3-40: Thévenin equivalent impedance Z_{th} at the point of the fault applied (Line A-C 1) 70
Figure 3-41: First Delta-Star impedance transformation applied to determine the Thévenin equivalent impedance (Line A-C 1) 71
Figure 3-42: Second Delta-Star impedance transformation applied to determine the Thévenin equivalent impedance (Line A-C 1) 71
Figure 3-43: Final Thévenin equivalent impedance for a fault applied with the integration of Sub C (Line A-C 1) 72
Figure 3-44: Series bypass capacitor bank circuit breaker closed Line A-C 1 (Sub C – 5 kA) 73
Figure 3-45: LCB at Sub A was opened after the series capacitor bank was bypassed 73
Figure 3-46: Thévenin equivalent impedance after LCB at Sub A was opened 74
Figure 3-47: Single phase representation of the Network Configuration for Case 2: Line C-B 1 (Sub C – 5 kA contribution) 75
Figure 3-48: Circuit diagram of the steady state pre-fault network configuration for the series compensated line C-B 1 75
Figure 3-49: Three-phase-to-ground fault applied to the series compensated circuit Line A-C 1 76
Figure 3-50: Thévenin equivalent impedance Z_{th} at the location of the fault (Line C-B 1) 76
Figure 3-51: Delta-Star impedance transformation applied to determine the Thévenin equivalent impedance (Line C-B 1) 76
Figure 3-52: Second Delta-Star impedance transformation applied to determine the Thévenin equivalent impedance (Line C-B 1) 77
Figure 3-53: Series bypass capacitor bank circuit breaker closed Line C-B 1 (Sub C – 5 kA) 78
Figure 3-54: LCB at Sub B was opened after the series capacitor bank was bypassed 79
Figure 3-55: Thévenin equivalent impedance after LCB at Sub B was opened 79

Figure 3-56: Network configuration of Case 1 80
Figure 3-57: Network configuration of Case 2a and 2b 81
Figure 3-58: Network configuration of Case 3a and 3b 81
Figure 3-59: Single Line Diagram of Case 1 82
Figure 3-60: Circuit configuration of case 1 82
Figure 3-61: Peak fault current (50 Hz) for LCBs at Sub A – Case 1 83
Figure 3-62: Peak fault current (50 Hz) for LCBs at Sub B – Case 1 83
Figure 3-63: Test duties for LCBs at Sub A – Case 1 84
Figure 3-64: Test duties for LCBs at Sub B – Case 1 84
Figure 3-65: Peak recovery voltage profile for LCBs at Sub A – Case 1 85
Figure 3-66: Peak recovery voltages and limits for LCBs at Sub A – Case 1 85
Figure 3-67: Underdamped response of Sub A LCB for a fault at 140 km away from Sub A 86
Figure 3-68: Peak recovery voltage profile for LCBs at Sub B – Case 1 86
Figure 3-69: Peak recovery voltages and limits for LCBs at Sub B – Case 1 87
Figure 3-70: RRRV profile for LCBs at Sub A – Case 1 87
Figure 3-71: RRRV and limits for LCBs at Sub A – Case 1 88
Figure 3-72: RRRV profile for LCBs at Sub B – Case 1 89
Figure 3-73: RRRV and limits for LCBs at Sub B – Case 1 89
Figure 3-74: Single Line Diagram of Case 2a 90
Figure 3-75: Peak fault current (50 Hz) for LCBs at Sub A – Case 2a 91
Figure 3-76: Peak fault current (50 Hz) for LCBs at Sub C– Case 2a 92
Figure 3-77: Circuit configuration of case 2a 92
Figure 3-78: Test duties for LCBs at Sub A – Case 2a 93
Figure 3-79: Test duties for LCBs at Sub C – Case 2a 94
Figure 3-80: Peak Recovery Voltage profiles for LCBs at Sub A for line lengths of 200 km and 240 km for Line A-C 1: Case 2a 94
Figure 3-81: Peak Recovery Voltage profiles for LCBs at Sub C for line lengths of 200 km and 240 km for Line A-C 1: Case 2a 95
Figure 3-82: Underdamped Response at the line side terminal of the LCB at Sub C for a fault approximately 140 km from Sub A – Case 2a 95
Figure 3-83: Peak Recovery Voltage profiles for the LCB at Sub A for Sub C at 200 km – Case 2a .. 96
Figure 3-84: Peak Recovery Voltage profiles for the LCB at Sub A for Sub C at 240 km – Case 2a .. 96
Figure 3-85: Peak Recovery Voltage profiles for the LCB at Sub C for Sub C at 200 km– Case 2a ... 97
Figure 3-86: Peak Recovery Voltage profiles for the LCB at Sub C for Sub C at 240 km – Case 2a .. 97
Figure 3-87: RRRV for the LCB at Sub A for Sub C at 200 km – Case 2a 98
Figure 3-88: RRRV for the LCB at Sub A for Sub C at 240 km – Case 2a 98
Figure 3-89: RRRV for the LCB at Sub C for Sub C at 200 km – Case 2a 99
Figure 3-90: RRRV for the LCB at Sub C for Sub C at 240 km – Case 2a 99
Figure 3-91: Single Line Diagram of Case 2b (Sub C at 10 kA) 100
Figure 3-92: Peak fault current (50 Hz) for LCBs at Sub A – Case 2b 101
Figure 3-93: Peak fault current (50 Hz) for LCBs at Sub C– Case 2b 101
Figure 3-94: Test duties for LCBs at Sub A – Case 2b 102
Figure 3-95: Test duties for LCBs at Sub C – Case 2b 103
Figure 3-96: Peak Recovery Voltage profiles for LCBs at Sub A for line lengths of 200 km and 240 km for Line A-C 1 - Case 2b 104
Figure 3-97: Peak Recovery Voltage profiles for LCBs at Sub C for line lengths of 200 km and 240 km for Line A-C 1 - Case 2b 104
Figure 3-98: Peak Recovery Voltage profiles for the LCB at Sub A for Sub C at 200 km – Case 2b 105
Figure 3-99: Peak Recovery Voltage profiles for the LCB at Sub A for Sub C at 240 km – Case 2b 106
Figure 3-100: Peak Recovery Voltage profiles for the LCB at Sub C for Sub C at 200 km – Case 2b 106

Figure 3-101: Peak Recovery Voltage profiles for the LCB at Sub C for Sub C at 240 km – Case 2b 107
Figure 3-102: RRRV for the LCB at Sub A for Sub C at 200 km – Case 2b 107
Figure 3-103: RRRV for the LCB at Sub A for Sub C at 240 km – Case 2b 108
Figure 3-104: RRRV for the LCB at Sub C for Sub C at 200 km – Case 2b 108
Figure 3-105: RRRV for the LCB at Sub C for Sub C at 240 km – Case 2b 109
Figure 3-106: Single Line Diagram of Case 3a 109
Figure 3-107: Peak fault current (50 Hz) for LCBs at Sub C – Case 3a 110
Figure 3-108: Peak fault current (50 Hz) for LCBs at Sub B– Case 3a 111
Figure 3-109: Circuit configuration of case 3a 111
Figure 3-110: Fault current split from the fault to Sub C and Sub B 112
Figure 3-111: Test duties for LCBs at Sub C – Case 3a 112
Figure 3-112: Test duties for LCBs at Sub B – Case 3a 113
Figure 3-113: Peak Recovery Voltage profiles for LCBs at Sub C for line lengths of 20 km and 40 km for Line C-B 1 – Case 3a 114
Figure 3-114: Peak Recovery Voltage profiles for LCBs at Sub B for line lengths of 20 km and 40 km for Line C-B 1 – Case 3a 114
Figure 3-115: Peak Recovery Voltage profiles for the LCB at Sub B for Sub C at 20 km – Case 3a 115
Figure 3-116: Peak Recovery Voltage profiles for the LCB at Sub B for Sub C at 40 km – Case 3a 115
Figure 3-117: Peak Recovery Voltage profiles for the LCB at Sub C for Sub C at 20 km – Case 3a 116
Figure 3-118: Peak Recovery Voltage profiles for the LCB at Sub C for Sub C at 40 km – Case 3a 116
Figure 3-119: RRRV for the LCB at Sub B for Sub C at 20 km– Case 3a 117
Figure 3-120: RRRV for the LCB at Sub B for Sub C at 40 km – Case 3a 117
Figure 3-121: RRRV for the LCB at Sub C for Sub C at 20 km from Sub A – Case 3a 118
Figure 3-122: RRRV for the LCB at Sub C for Sub C at 40 km from Sub A – Case 3a 118
Figure 3-123: Single Line Diagram of Case 3b 119
Figure 3-124: Peak fault current (50 Hz) for LCBs at Sub B – Case 3b 119
Figure 3-125: Peak fault current (50 Hz) for LCBs at Sub C– Case 3b 120
Figure 3-126: Test duties for LCBs at Sub C – Case 3b 121
Figure 3-127: Test duties for LCBs at Sub B – Case 3b 121
Figure 3-128: Peak Recovery Voltage profiles for LCBs at Sub C for line lengths of 212.5 km and 232.5 km for Line C-B 1 – Case 3b 122
Figure 3-129: Peak Recovery Voltage profiles for LCBs at Sub B for line lengths of 212.5 km and 232.5 km for Line C-B 1 – Case 3b 122
Figure 3-130: Peak Recovery Voltage profiles for the LCB at Sub B for Sub C at 20 km – Case 3b 123
Figure 3-131: Peak Recovery Voltage profiles for the LCB at Sub B for Sub C at 40 km – Case 3b 123
Figure 3-132: Peak Recovery Voltage profiles for the LCB at Sub C for Sub C at 20 km – Case 3b 124
Figure 3-133: Peak Recovery Voltage profiles for the LCB at Sub C for Sub C at 40 km – Case 3b 124
Figure 3-134: RRRV for the LCB at Sub B for Sub C at 20 km – Case 3b 125
Figure 3-135: RRRV for the LCB at Sub B for Sub C at 40 km – Case 3b 125
Figure 3-136: RRRV for the LCB at Sub B for Sub C at 20 km – Case 3b 126
Figure 3-137: RRRV for the LCB at Sub B for Sub C at 40 km – Case 3b 126
Figure 3-138: Fault current through LCB at Sub A 127
Figure 3-139: Voltage profile of TRV across the LCB terminals at Sub A 127
Figure 3-140: Fault current through LCB at Sub C 128
Figure 3-141: Voltage profile of TRV across the LCB terminals at Sub C 128
Figure 3-142: Trapped charge due to the series capacitor bank seen after 80 ms 128
Figure 4-1: Peak recovery voltage profiles for Sub A LCB 131
Figure 4-2: RRRV profiles for Sub A LCB 132
Figure 4-3: Peak recovery voltage profiles for Sub B LCB 133
Figure 4-4: RRRV profiles for Sub B LCB 134
Figure 4-5: Peak recovery voltage profiles for Sub C LCB for Cases 2a and 2b 135

Figure 4-6: RRRV profiles for Sub C LCB for Case 2a and 2b 135
Figure 4-7: Peak recovery voltage profiles for Sub C LCB for Cases 3a and 3b 136
Figure 4-8: RRRV profiles for Sub C LCB for Case 3a and 3b 136

LIST OF TABLES

Table 2-1: Classification of Frequency Ranges [7] 6
Table 2-2: Origins of electrical transients and typical frequency ranges [7][8] 7
Table 2-3: RRRV for circuit breakers at rated voltages 100 kV to 800 kV 23
Table 2-4: Amplitude Factors for Circuit Breakers [4] 24
Table 2-5: Time t_2 for a four parameter circuit breaker rating 24
Table 2-6: Factors to consider when modelling overhead lines [33][40] 39
Table 3-1: Transmission line model parameters 47
Table 3-2: Input data for source impedances for the 48
Table 3-3: Calculated source impedance parameters 49
Table 3-4: Surge Arrester Parameters 49
Table 3-5: Line Arrester Parameters 50
Table 3-6: V-I data of the line arrester 51
Table 3-7: Series capacitor bank parameters 51
Table 3-8: Compensation factor of existing series compensated transmission line 52
Table 3-9: Current Limiting Damping circuit parameters 52
Table 3-10: TRV ratings of a 420 kV circuit breaker [4] 53
Table 3-11: Equivalent capacitance of HV equipment 54
Table 3-12: Comparison of calculated and measured parameters for series capacitor bypass circuit 73
Table 3-13: Comparison of calculated and measured parameters when the LCB at Sub A was opened 74
Table 3-14: Comparison of calculated and measured parameters for series capacitor bypass circuit 78
Table 3-15: Comparison of calculated and measured parameters when the LCB at Sub B was opened 80
Table 3-16: Sub C source impedance parameters 90
Table 3-17: Compensation factor for studies conducted for Line A- C 1 90
Table 3-18: Sub C source impedance parameters (10 kA) – Case 2b 100
Table 3-19: Comparison of fault currents for LCBs at Sub A and Sub C 102
Table 3-20: Sub C source impedance parameters (5 kA) 110
Table 3-21: Compensation factor for studies conducted for Line B - C 1 110
Table 3-22: Comparison of fault currents for LCBs at Sub A and Sub C 120

ABBREVIATIONS

AC	Alternating Current
DC	Direct Current
LIWL	Lightning Impulse Withstand Level
SIWL	Switching Impulse Withstand Level
CFO	Critical Flashover Voltage
EHV	Extra High Voltage
FFO	Fast-Front Overvoltage
FSC	Fixed Series Capacitor
GIS	Gas Insulated Switchgear
HV	High Voltage
IEC	International Electrotechnical Commission
IEEE	Institute of Electrical and Electronics Engineers
IPP	Independent Power Producer
KDE	Kernel Density Estimate
KVL	Kirchoff's Voltage Law
LCB	Line Circuit Breaker
LOV	Lightning Overvoltage
MISE	Mean Integrated Square Error
MOV	Metal Oxide Varistor
OP	Out-of-Phase
P.U.	Per Unit
RLC	Resistor, Inductor and Capacitor
RRRV	Rate of Rise of Recovery Voltage
SF_6	Sulphur Hexaflouride
SFO	Slow-Front Overvoltage
SLF	Short Line Faults
SOV	Switching Overvoltage
TCR	Thyristor Controlled Reactor
TCSC	Thyristor Controlled Series Capacitor
TOV	Temporary Overvoltage
TRV	Transient Recovery Voltage
UHV	Ultra-High Voltage
VFFO	Very-Fast-Front Overvoltage

1 INTRODUCTION

1.1 Background

The Southern African Power System is constantly evolving as a result of new loads and sources being introduced into the network. These changes include the introduction of new connections tying into existing, long series and shunt compensated transmission lines. These new connections would facilitate the integration of remotely located renewable energy sources such as large wind and solar photovoltaic Independent Power Producers (IPPs).

There is a paradigm shift in the approach to the current energy landscape with focus towards the integration of renewable energy. The Southern African Power Pool Annual Report indicated that renewable energy sources accounted for approximately 60% of the new generation sources commissioned in 2018 [1]. These sources are usually not located close to large load centers and are required to be integrated into the remote parts of the transmission system where the network is weak.

As part of the Integrated Resource Plan 2019 (IRP2019) issued by the Department of Energy in South Africa, indicated that approximately 20 GW of renewable generation will be commissioned by 2030. The majority of renewable generation will be evacuated out of the Northern Cape province due to favorable wind and solar conditions. Significant network strengthening is required to evacuate the power to the distant load centers. The use of series capacitor banks assists in the increase in the power transfer capacity of the transmission lines through the existing main power corridors. As part of the network strengthening initiatives, this may require interconnecting onto existing series and shunt compensated transmission lines. As a result, the TRV capability of the LCBs (existing and new) for the evolved compensated circuit needs to be studied to ensure that they still operate within their withstand capability.

The original purpose of long Alternating Current (AC) interconnections at Extra High Voltage (EHV) level was for long distance power transmission. These interconnections were optimized to operate at their Surge Impedance Loading (SIL) and therefore usually include of Fixed Series Compensation (FSC) [2]. Additionally, shunt reactors are utilized for long EHV transmission lines to compensate for the Ferranti effect.

The Line Circuit Breakers (LCBs) of a compensated circuit may be exposed to the effects of the change in compensation factor due to the integration of new voltage sources in this circuit which could result in higher stresses during switching. The insulation stresses associated with the switching of the LCBs need to be re-evaluated in this changing environment to ensure the specified withstand requirements are adequate for the new configuration. Although the fault current in a power system varies throughout the day based on the network configuration, the evaluation of the TRVs for LCBs are based on the worst-case fault level.

If the series capacitor is not bypassed when opening the LCB, the LCB is exposed to additional Transient Recovery Voltage (TRV) stresses. Additionally, if the TRV capability of the LCB is exceeded, there is a possibility of a restrike or re-ignition. This could be detrimental to the circuit breaker and result in catastrophic failure.

1.2 Scope

This research covers LCBs connected to evolving (network changes due to addition of new loads, voltage sources, transmission lines, transmission nodes (e.g. substations) and reactive compensation), series and shunt compensated transmission lines. The objective of this research aims to address the approach for conducting studies for evaluating the TRVs for LCBs connected to evolving, series and shunt compensated transmission lines.

The focus of this study is to develop a procedure to evaluate TRV stresses imposed on the LCBs in an evolving series and shunt compensated transmission line. This will be achieved by evaluating the key factors that determine the peak recovery voltage and rate of rise of recovery voltage.

Although there are guidelines available for the evaluation of TRVs of circuit breakers, the aim of this research is to clarify the approach when the circuit configuration of compensated transmission line evolves or there is an increase in the fault level of the system.

This research creates an awareness amongst switchgear specialists, transmission network planning engineers as well as substation design engineers regarding the required TRV ratings for LCBs connected to evolving series and shunt compensated transmission lines. This is done to prevent damage to equipment, while maintaining a level of reliability and availability of the power system.

1.3 Research question

1. What are the key properties of a transmission network that need to be studied as part of the procedure in evaluating LCB TRVs in an evolving network?
2. How can a procedure be formulated to evaluate the TRVs on a LCB in an evolving, transmission network?

1.4 Research objective

The objective of the proposed research is to answer the research question by developing a procedure taking into consideration:

1. Factors common to all applications.
2. Factors that require special consideration for evolving networks where new generation sources are added along existing series and shunt compensated transmission lines.

1.5 Research approach

The IEEE guide for the application of Transient Recovery Voltage for AC High Voltage Circuit Breakers [3] defines the approach to determining the required TRV rating of circuit breakers. The TRV ratings for HV circuit breakers are defined in SANS 62271-100:2017 [4]. The TRV stresses imposed on the circuit breaker are determined through studies conducted and an appropriate circuit breaker is selected based in its insulation strength to match the determined stresses.

A review and assessment of fundamental concepts of insulation coordination and transient recovery voltage formed the basis on which a procedure was developed to evaluate TRVs of LCBs connected to evolving series and shunt compensated transmission lines. The literature review also included mitigation strategies in limiting the TRV stresses imposed on the LCB.

An existing series and shunt compensated transmission line network configuration was studied. This assisted in identifying the network configurations that resulted in excessive LCB stresses. A simulation model was developed on transient simulation modelling software. This model was then validated against actual fault waveform data for the circuit.

The TRV rating of the LCBs was analyzed by splitting the existing compensated transmission line by looping in and looping out a new voltage source. The ratings of the series capacitor bank and shunt reactor remained fixed for all the simulations conducted. As a result, the compensation factor was not adjusted. The position of the new voltage source was varied such that the compensation factor of the circuit did not exceed 90% (for practical purposes). The fault current contribution of the new voltage source was varied to determine the TRV stresses imposed on the LCB as a result. The fault position was also varied along the transmission line for each scenario.

The magnitude of the fault current that flowed through the LCBs due to a fault applied determined the test duty of the circuit breaker. The test duty determined the required TRV withstand parameters of the LCB. The TRV stresses on the LCB were evaluated for various network configurations. The peak recovery voltage and the rate of rise of recovery voltage were the two main parameters to evaluate the required TRV ratings of the LCBs.

1.6 Chapter Summary

Chapter 1 - Introduction

Chapter 1 provides background to the problem identified and highlights the need to investigate and address it. The scope of the work is defined, and the research questions and objectives are outlined.

Chapter 2 – The theory on the origin of the nature of Transient Recovery Voltages (TRVs)

Chapter 2 provides an overview of the fundamentals of insulation coordination and transient recovery voltages. The circuit breaker technology as well as the arc interruption process are discussed. Furthermore, an appraisal of existing, relevant literature by identifying, evaluating, and interpreting the research evidence is presented. The literature review will guide the development of the research questions and objectives by identifying the research gaps.

Chapter 3 – Case Study: TRV Evaluation of LCBs connected to an evolving series and shunt compensated transmission line

Chapter 3 presents the procedure developed to evaluate TRVs of LCBs connected to evolving series and shunt compensated transmission lines. The network topology that was utilized in the study is also presented. The input data required to accurately model the various components in the simulation software is detailed. The assumptions that were made to conduct this study are discussed. This includes the series capacitor sizing for each of the cases studied, the shunt reactor requirements as well as the protection settings. The verification of the simulation model against fault waveform recording data is then presented. The methodology and sequence of conducting the simulations is then discussed. The circuit analysis conducted for the various cases is then presented. The results of the analysis were compared against the simulation conducted for those specific cases. The simulation results and the analysis of the results are then discussed. The simulation results include the fault current profiles, test duty profiles of the LCBs and a comparison of the peak recovery voltage and rate of rise of recovery voltage (RRRV) against the LCB ratings.

Chapter 4 – Discussion of Results

Chapter 4 presents the discussion of the results for the case study. The results are presented in a consolidated view for the LCBs for Sub A, Sub B and Sub C. The LCB at Sub A was evaluated for Case 1 and Case 2, while the LCB at Sub B was evaluated for Case 1 and 3 and finally the LCB at Sub C was evaluated for Cases 2 and 3. Furthermore, the discussion aims to highlight the influence of integrating a voltage source along varied points of a compensated circuit as well as emphasizing the impact of varying the fault current contribution of the new voltage source.

Chapter 5 – Conclusion

Finally, this chapter presents the conclusions derived from this research as well as addressing the research question and objectives. Additionally, recommendations and future work was presented.

2 THE THEORY ON THE ORIGIN OF THE NATURE OF TRANSIENT RECOVERY VOLTAGES (TRV)

2.1 Insulation Coordination to mitigate effects of overvoltages

The objective of insulation coordination is to select the insulation strength of equipment in relation to the voltages that they may be exposed to due to the service environment as well as the characteristics of the available protective devices for an acceptable risk [5][6]. This is achieved by selecting the minimum insulation/clearance to reduce cost. The process to conduct an insulation coordination study generally entails the following [5]:

- Selection of the reliability criteria
- A study to determine the electrical stresses that the insulation or clearance will be exposed to
- Comparison between the electrical stresses and insulation strength characteristic
- Selection of insulation strength

If the insulation strength requirements are considered to be excessive in matching the stress, protective devices such as surge arresters, protective gaps, shield wires or closing resistors may be considered as mitigating measures to reduce the exposure of the electrical stresses.

Insulation coordination is typically categorized into two sections: line (transmission and distribution) and station (generation, transmission, and distribution) insulation coordination. All electrical stresses that may be applied to a piece of equipment or power line tower should be considered when conducting an insulation coordination study. These stresses include [5]:

- Lightning overvoltages (LOV) produced by lightning strikes
- Switching overvoltages (SOV) as a result of switching of circuit breakers and disconnectors
- Temporary overvoltages (TOV) generated typically by power system faults, generator over-speed or ferro-resonance
- Power frequency voltage

The conventional or deterministic and statistical methods are currently the two approaches utilized in conducting insulation coordination studies [5]. The deterministic approach considers specifying the minimum strength of the insulation or clearance according to the maximum stress it would be exposed to in a specific power system configuration. The probabilistic approach entails selecting an insulation strength or clearance based on a specific reliability criterion [5]. The reliability criterion is essentially a function of the consequence of failure and life span of the equipment.

All specifications of insulation strength are specified under standard/normal conditions [5]:

- Ambient temperature: 20°C
- Air pressure: 101.3 kPa
- Absolute humidity: 11 g of water/m^{3} of air
- Wet tests: 1 mm to 1.5 mm of water/minute

The strength of insulation, measured in voltage, is corrected to standard values where atmospheric conditions vary from standard/normal conditions.

Insulation is classified into four categories [5][6]:

- External insulation - which is either the surface of an insulating medium (e.g. porcelain) which is in contact with air or a distance in open air which is subjected to a dielectric stress and the atmosphere.
- Internal insulation – which is a solid, liquid or gas medium enclosed within the electrical equipment which is not exposed to the atmosphere.

- Self-restoring insulation - completely recovers its insulating properties after being exposed to a disruptive discharge (e.g. air).
- Non-self-restoring insulation – loses its insulating properties or does not fully recover its insulating properties after being exposed to a disruptive discharge (e.g. porcelain).

The electrical strength of insulation may be expressed by either the Lightning Impulse Withstand Level (LIWL), the Switching Impulse Withstand Level (SIWL) or the Critical Flashover Voltage (CFO) [5].

The LIWL refers to the crest value of a standard lightning impulse for a given electrical strength of insulation [5]. The lightning impulse wave shape is defined as the time to crest to the time to half value of the tail ($\frac{t_C}{t_T}$) which is standardized as 1.2/50 μs (Figure 2-1).

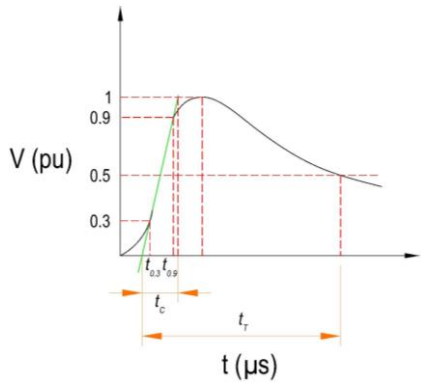

Figure 2-1: Standard wave shape for a lightning voltage impulse

The time to crest is calculated by constructing a line between the time to 30% and 90% of the crest value. This line intersects the point of zero voltage resulting in a virtual origin.

The SIWL refers to the crest value of a standard switching impulse for a given electrical strength of insulation [5]. The standard switching impulse wave shape is defined similarly to the standard lightning impulse wave shape however the time to crest and the time to half value of the tail are calculated from the origin (Figure 2-2). Additionally, the time to crest to the time to half value of the tail (t_C/t_T) is standardized as 250/2500 μs [5].

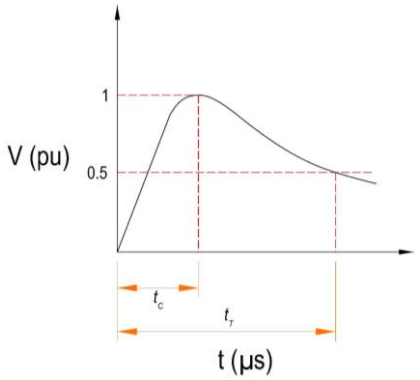

Figure 2-2: Standard wave shape for a switching impulse

The statistical LIWL and SIWL are applicable only to self-restoring insulation while conventional/deterministic LIWL and SIWL are applicable to non-self-restoring insulation. The statistical LIWL and SIWL are based on the premise that the insulation strength would have a 90% probability of withstand for a crest value of a lightning impulse or 10% probability of flashover or failure.

The conventional/deterministic LIWL and SIWL refer to the crest value of a lightning or switching impulse respectively for which the insulation does not exhibit a disruptive discharge when subjected to a specified number of impulses.

The insulation strength may be represented by a cumulative Gaussian distribution where the mean or 50% value is known as the CFO [5]. The CFO represents a 50% probability of failure/flashover and represents another measure of insulation strength. The statistical BIL/BSL is the 10% probability of failure or 1.28σ (standard deviations) from the mean (Figure 2-3) [5].

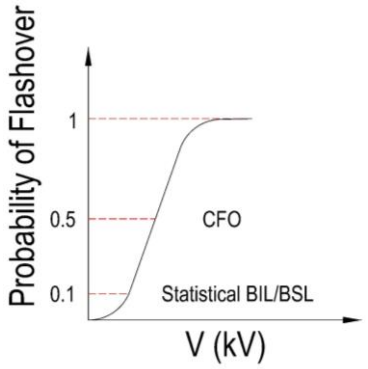

Figure 2-3: Cumulative Distribution for the probability of flashover for insulation strength

2.2 Transients in Power Systems

The analysis of the electrical transient phenomena ranges from DC up to 50 MHz and in some instances higher [7]. The transition from one steady state to another due to an electrical disturbance in a power system defines the transient phenomenon. These electrical disturbances originate from the opening or closing of power system switchgear (e.g. circuit breakers) or short circuits, earth faults or lightning strikes [7]. The consequence of these electrical disturbances result in electromagnetic phenomena such as travelling waves along electrical power lines/cables or electrical conductor and oscillations due to the interaction between the inductance and capacitance inherent in a power system [7].

The network elements need to be modelled accurately to the particular frequency range being studied in order to reliably perform the transient analysis. Therefore, the frequency ranges have been classified into four groups (Table 2-1):

Table 2-1: Classification of Frequency Ranges [7]

Group	Frequency Range	Shape Designation	Representation for
I	0.1 Hz – 3 kHz	Low Frequency Transients	Temporary Overvoltages (TOV)
II	50/60 Hz – 20 kHz	Slow Front Overvoltages	Switching Overvoltages (SFO)
III	10 kHz – 3 MHz	Fast Front Overvoltages	Lightning Overvoltages
IV	100 kHz – 50 MHz	Very Fast Front Overvoltages	Restrike Overvoltages

Based on Table 2-1, the electrical disturbances or transients have been categorized into their origins and respective typical frequency ranges (Table 2-2) [7][8].

Table 2-2: Origins of electrical transients and typical frequency ranges [7][8]

Origin of Electrical Transient	TOV	Transient Overvoltages		
		SFO	FFO	VFFO
Transformer Energization	X	X		
Ferroresonance	X	X		
Load Rejection	X			
Parallel Line Resonance	X			
Uneven Breaker Poles	X			
Back-feeding	X			
Fault Clearing	X	X		
Fault Initiation	X	X		
Line Energization	X	X		
Line Reclosing	X	X		
AIS Busbar Switching			X	*
Switching of inductive and capacitive currents	X	X	X	
Back Flashover			X	
Transient Recovery Voltage				
• Terminal Faults	X	X		
• Short Line Faults	X		X	
Multiple Restrikes of Circuit Breaker	X		X	
Lightning surges; faults in substations			X	
Disconnector Switching (single restrike) and fault in GIS				X
SF_6 circuit breaker inductive and capacitive switching	X	X	X	*
Flashover in GIS substation				X
Vacuum circuit breaker switching			X	X

** - In the case of short distance busbars and low damping, very-fast-front overvoltages can also occur* **[8]**.

Switching impulses are generally not critical for voltage levels up to 245 kV while lightning impulses have to be carefully evaluated for this range [8]. Switching impulses becomes critical for voltages especially in the UHV range where lightning impulses are not an essential consideration. Terminal faults and Short Line Faults (SLFs) were the focus of this study.

2.2.1 Temporary Overvoltages

Temporary overvoltages refer to the electrical stress imposed on equipment by power frequency withstand voltages. MOVs are particularly stressed due to the energy generated by the TOV [8]. Transformers and reactors may also be stressed by TOVs due to over-fluxing which affects the operational performance of the equipment. Over-fluxing results in heat generation and consequently affects the life span of the equipment.

2.2.2 Slow-Front Overvoltages

Slow-front overvoltages influence the energy rating requirements for MOVs in addition to the selection of the withstand voltage rating of equipment and the air gap requirement for transmission line towers.

Electrical transient events that should be considered for slow-front overvoltage analysis are generated by switching or disconnecting operations [8].

2.2.3 Fast-Front Overvoltages

Fast-Front Overvoltages are typically generated by lightning impulses. These overvoltages are analyzed to select the appropriate voltage withstand levels based on the configuration of the protective equipment installed as well as the earthing arrangement [8].

2.2.4 Very-Fast-Front Overvoltages

Very-Fast-Front Overvoltages refer to overvoltages that occur due to internal flashovers in GIS as well as the operating of vacuum circuit breakers [8]. These overvoltages may generate high touch voltages.

The phenomenon of Transient Recovery Voltage will be presented in section 2.3. An overview into the fundamentals of transient recovery voltages will be presented focusing on TRV characteristic parameters, the effects on travelling wave on TRVs and the various types of TRVs.

2.3 The origin and nature of Transient Recovery Voltages

When the terminals of a pole of a circuit breaker are opened, there will be the presence of ionized gas between the fixed terminal and the moving contact resulting in a conductive channel between the two contacts usually forming an arc [9]. If the dielectric strength of the insulating medium between the circuit breaker contacts is recovered faster than the rate of rise of the recovery voltage (RRRV) of the circuit breaker then the arc is extinguished. The Recovery Voltage is the longitudinal voltage across the terminals of a pole of a circuit breaker based on the difference between the power system voltage on the source side and the load side after interruption. IEEE defines this voltage in two successive time intervals [3]:

1. During the transient voltage.
2. During the time that the power-frequency voltage alone exists.

The breaking operation is considered successful if it withstands both these voltages. While three-phase unearthed faults generate the highest TRV peaks, the probability of occurrence is very low, therefore TRV ratings as stipulated in the IEC 62271-100 are calculated based on three-phase to earth faults [10].

TRVs have oscillatory, triangular, or exponential shapes or a combination of these. Capacitive current or out of phase current interruption will result in the highest peak TRVs whereas terminal faults (e.g. due to a current transformer that fails next to a circuit breaker) or short line fault interruptions will result in TRVs related to the highest short-circuit currents.

2.3.1 TRV Characteristics

A circuit breaker TRV capability is defined either by a two parameter (u_c, t_3) (Figure 2-4) or a four parameter (u_1, t_1, u_c, t_2) (Figure 2-5) envelope as stipulated in IEC 62271-100 [4].

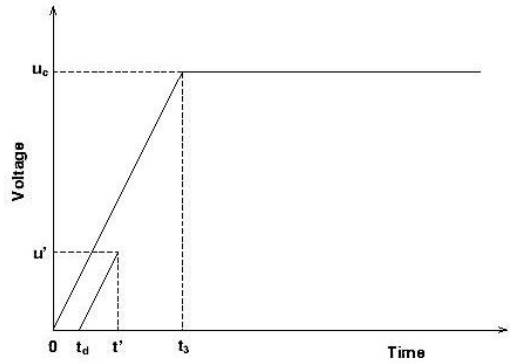

Figure 2-4: Two-Parameter Envelope [11]

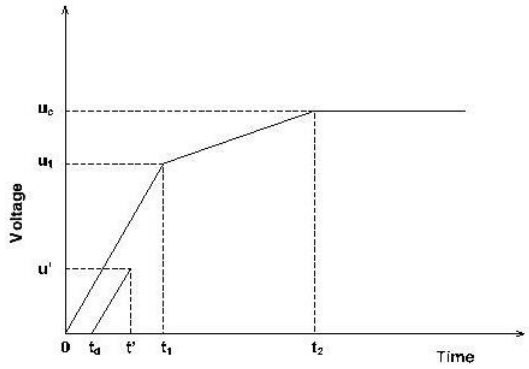

Figure 2-5: Four-Parameter Envelope [11]

The envelope defines a voltage withstand boundary of the circuit breaker. The parameter values of the voltage withstand boundaries were developed based on network studies conducted by the French and Italian power utilities in the 1960's for nominal system voltages up to 245 kV [12]. These studies were based on three-phase ungrounded faults and first-pole-to-clear. It is worth observing that the voltage withstand boundaries that were developed were from a statistical perspective. These values were then extrapolated for nominal system voltages up to 765 kV based on the preceding data.

The voltage withstand boundary parameters are grouped into four groups which are based on a percentage of the maximum short-circuit current ratings, known as test duties. The values of the test duties are classified as 10%, 30%, 60% and 100% of the maximum short-circuit current rating. The magnitude of short-circuit current that is required to be cleared as well as the rate of rise and magnitude of the TRV, governs the stress that a circuit breaker is subjected to [9].

Circuit breakers rated 100 kV and above which clear terminal fault currents higher than 30% of the circuit breaker rating would result in a four parameter envelope [3]. This is based on evaluations conducted on various system configurations. A four-parameter envelope is utilised in the cases of overdamped (exponential) TRVs. These TRVs are typical for faults on transmission lines. The exponential part of the TRV is transmitted as a travelling wave and the reflections due to the open point or discontinuity on the transmission line results in superimposing a "1-cosine" waveshape.

The two parameter envelope is utilised for terminal fault current ratings between 10% and 30% of the circuit breaker rating for circuit breakers 100 kV and above and for all terminal fault currents for circuit breakers below 100 kV [3]. These TRVs are typically underdamped/oscillatory in nature and where the fault current is limited by a transformer or series reactor. The TRV is rated based on a "1-cosine" waveshape.

2.3.2 Transient Response Analysis

In order to understand TRVs, it is imperative to establish the transition from a state prior to the switching event/transient to a state after the event. This implies that all transients have a starting point, target point and maximum point. The transient response of a switching event can be associated with either a series or parallel RLC circuit taking into consideration specific initial or boundary conditions [11]. Current interruption and circuit breaker restrikes or re-ignitions may be analysed by evaluating four basic circuit configurations which broadly cover most switching events. These include but are not limited to the switching of shunt capacitor banks resulting in inrush currents, inductive load switching and the associated TRVs as well as TRVs for terminal faults [11].

The transient response for the inrush currents associated with the switching of capacitive or inductive loads may be derived by analysing a simplified Resistor, Inductor and Capacitor (RLC) circuit (Figure 2-6).

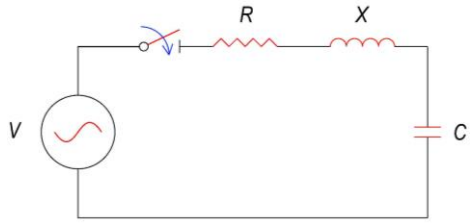

Figure 2-6: Simplified RLC circuit with voltage injection

Taking Kirchhoff's Voltage Law of this circuit results in the following equation [11]:

$$V(t) = Ri(t) + L\frac{di(t)}{dt} + \frac{1}{C}\int i(t)\,dt \tag{2-1}$$

The source impedance is considered negligible in the analysis of the RLC circuit. However, it is noted that the source impedance is made up of resistance, inductance, and capacitance. The resistance and inductance are determined from the X/R ratio of the source busbars and the fault level.

Differentiating Equation (2-1) with respect to *i(t)* results in a second order linear homogenous differential equation:

$$\frac{d^2i(t)}{dt^2} + \frac{R}{L}\frac{di(t)}{dt} + \frac{i(t)}{LC} = 0 \tag{2-2}$$

The characteristic equation derived from equation (2-2) is therefore:

$$x^2 + \frac{R}{L}x + \frac{1}{LC} = 0 \tag{2-3}$$

The roots of the characteristic equation (2-3) can then be calculated using the quadratic formula:

$$x = \frac{-b \pm \sqrt{b^2 - 4ac}}{2a} = -\frac{b}{2a} \pm \sqrt{\frac{b^2}{(2a)^2} - \frac{4ac}{(2a)^2}} \tag{2-4}$$

Therefore:

$$x_1, x_2 = -\frac{R}{2L} \pm \sqrt{\left(\frac{R}{2L}\right)^2 - \frac{1}{LC}} \tag{2-5}$$

If

$$\alpha = \frac{R}{2L} \tag{2-6}$$

(α is known as the damping co-efficient. The resistive component supresses or dampens the natural oscillating frequency.)

And

$$\omega = \frac{1}{\sqrt{LC}} \tag{2-7}$$

(The natural oscillating frequency of the circuit is given by the Inductor-capacitor (LC) combination as determined in equation (2-7).)

The roots of the characteristic equation are given as:

$$x_1 = -\propto + \sqrt{\propto^2 - \omega^2} = -\alpha + \beta \tag{2-8}$$

And

$$x_2 = -\propto - \sqrt{\propto^2 - \omega^2} = -\alpha - \beta \tag{2-9}$$

The homogenous solution for this case is given in the form [13]:

$$i_h(t) = C_1 e^{x_1 t} + C_2 e^{x_2 t} = C_1 e^{(-\alpha+\beta)t} + C_2 e^{(-\alpha-\beta)t} \tag{2-10}$$

Therefore, the combination of the RLC components of the circuit dictates the transient response. There are three resultant cases based on equations (2-8) and (2-9):

Case 1: $\alpha^2 > \omega^2$, known as the **OVERDAMPED CASE**

Initial or boundary conditions are required to determine a particular solution. The initial conditions in this case are given as follows:

$$i(0) = 0 = C_1 + C_2 \Rightarrow C_1 = -C_2 \tag{2-11}$$

And

$$\frac{\partial(0^+)}{\partial t} = \frac{V(t)}{L} = (-\alpha + \beta)C_1 + (-\alpha - \beta)C_2 \tag{2-12}$$

Using the identity:

$$\sinh(x) = \frac{e^x - e^{-x}}{2} \tag{2-13}$$

And substituting for C_1 and C_2 into equation (2-10) the particular solution becomes:

$$i_p(t) = \frac{V(t)}{\beta L} e^{-\alpha t} \sinh(\beta t) \tag{2-14}$$

Case 2: $\alpha^2 = \omega^2$, known as the **CRITICALLY DAMPED CASE**

In the critically damped case, since $\alpha^2 = \omega^2$ and $\beta = 0$, the homogenous solution becomes:

$$i_h(t) = (C_1 + C_2 t)e^{-\alpha t} \tag{2-15}$$

Using the initial condition:

$$i(0) = 0 = C_1 \tag{2-16}$$

Taking the second initial condition:

$$\frac{\partial(0^+)}{\partial t} = \frac{V(t)}{L} = C_2 \tag{2-17}$$

The particular solution becomes:

$$i_p(t) = \frac{V(t)}{L} t e^{-\alpha t} \tag{2-18}$$

Case 3: $\alpha^2 < \omega^2$, known as the **UNDERDAMPED CASE**

The roots for the underdamped case become complex conjugates of the characteristic equation. Using Euler's formula:

$$e^{ix} = cosx + isinx \tag{2-19}$$

The homogenous equation becomes [13]:

$$i(t) = e^{-\alpha t}(C_1 \cos(\beta t) + C_2 \sin(\beta t)) \tag{2-20}$$

Applying the initial conditions:

$$i(0) = 0 = C_1 \tag{2-21}$$

And

$$\frac{\partial(0^+)}{\partial t} = \frac{V(t)}{\beta L} = C_2 \tag{2-22}$$

Therefore, the particular solution becomes:

$$i(t) = \frac{V(t)}{\beta L} e^{-\alpha t} \sin(\beta t) \tag{2-23}$$

The analysis presented is the initial transient response and does not consider the travelling wave theory.

In order to determine the critical damping resistance $R_{critical}$, the damping coefficient α is equated to the natural oscillating frequency ω. This will result in:

$$R_{critical} = 2\sqrt{\frac{L}{C}} \tag{2-24}$$

Utilizing the critical damping resistance (2-24), the degree of damping may be determined calculating the ratio of the damping coefficient to the natural oscillating frequency:

$$d = \frac{\alpha}{\omega} = \frac{R}{R_{critical}} \tag{2-25}$$

The transient response of a faulted transmission line may also be determined in the event of a line circuit breaker opening. This will result in the transmission line behaving as a pre-charged capacitance discharging into the fault through the transmission line (Figure 2-7).

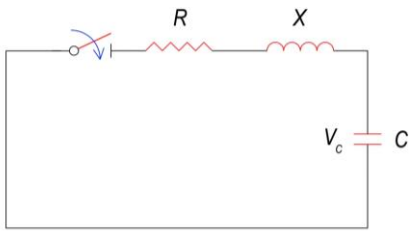

Figure 2-7: Pre-charged capacitor circuit

The same approach may be used to derive the equations for the scenario of the pre-charged capacitor circuit for the overdamped, critically damped, and underdamped cases. Utilising (2-1) and setting *V(t)* to zero and taking into consideration the boundary conditions:

- V(0) = V_c (initial voltage across the capacitance)
- $\frac{dV(0)}{dt} = 0$ (due to the inductance *X* in the circuit)

The equations for the three cases discussed above are calculated as:

Case 1: $\alpha^2 > \omega^2, d > 1, R > R_{critical}$, known as the **OVERDAMPED CASE**

$$V(t) = e^{-dt}\left(cosh\sqrt{d^2-1}t\right) + \frac{d}{\sqrt{d^2-1}}\left(sinh\sqrt{d^2-1}t\right) \quad (2\text{-}26)$$

Case 2: $\alpha^2 = \omega^2, d = 1, R = R_{critical}$, known as the **CRITICALLY DAMPED CASE**

$$V(t) = e^{-t}(1+t) \quad (2\text{-}27)$$

Case 3: $\alpha^2 < \omega^2, d < 1, R < R_{critical}$, known as the **UNDERDAMPED CASE**

$$V(t) = e^{-dt}\left(cos\sqrt{1-d^2}t\right) + \frac{d}{\sqrt{1-d^2}}\left(sin\sqrt{1-d^2}t\right) \quad (2\text{-}28)$$

Figure 2-8 is the resultant generic damping curves for the series RLC circuit with step voltage injection as described by equations (2-26) to (2-28). Damping factors less than one (underdamped), result in oscillations of varying magnitude prior to reaching a steady-state based on the degree of the damping. The critically damped case (d = 1) results in a smooth transition to the next steady-state. The overdamped case (d>1) results in no oscillations however the steady-state is attained in a longer duration than the critically damped case.

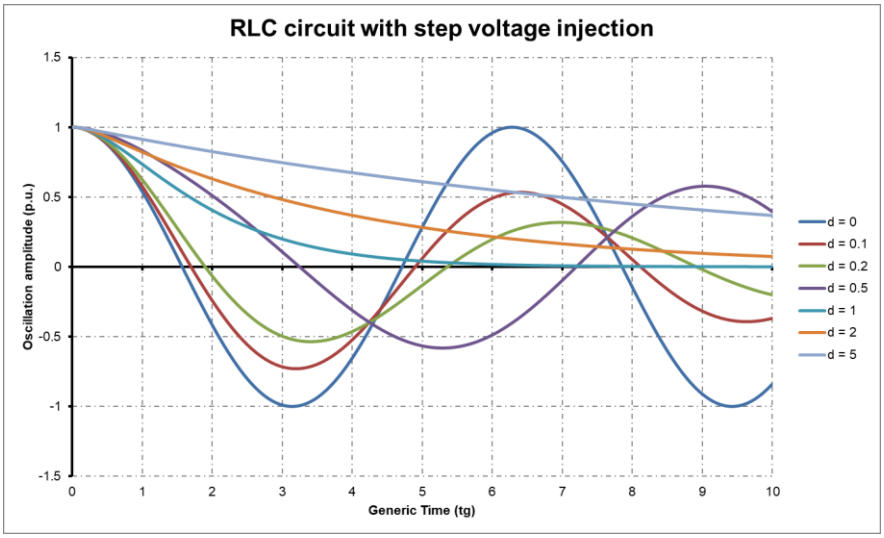

Figure 2-8: Generic damping curves for a series RLC circuit with step voltage injection

2.3.3 Travelling Wave Effects

A lumped model representation of a power system may be adequate for steady-state analysis of the system. However the travel time of electromagnetic waves in a power system needs to be taken into consideration when conducting a transient analysis study [9].

A transmission line can be considered as a combination of resistive, inductive, capacitive and conductive components distributed along the length of the transmission line (Figure 2-9). These components represent the resistivity of the transmission line conductor, the inductance due to the stored magnetic energy of the transmission line conductor, the capacitance due to the stored electrical energy between conductors and the conductance of the dielectric between conductors.

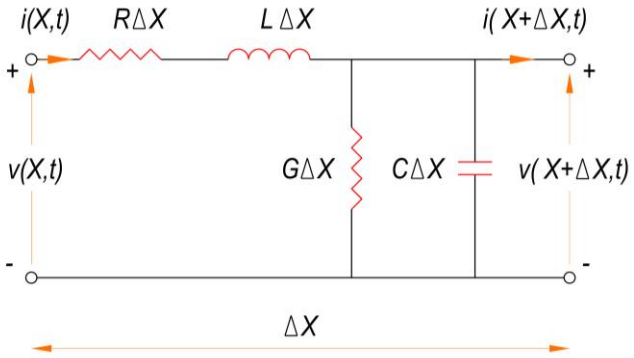

Figure 2-9: Equivalent segment for a two conductor transmission line model [9]

The two-conductor transmission line model, as shown in Figure 2-9, is defined by equations known as the Telegraph equations. Applying Kirchhoff's Voltage Law to the above circuit results in:

$$v(x,t) - v(x+\Delta x,t) = i(x,t)R\Delta x + L\Delta x\frac{\partial i(x,t)}{\partial t} \quad (2\text{-}29)$$

Taking the limit as $\Delta x \to 0$, the equation becomes:

$$-\frac{\partial v(x,t)}{dx} = i(x,t)R + L\frac{\partial i(x,t)}{\partial t} \quad (2\text{-}30)$$

Similarly applying Kirchhoff's Current law and taking the limit as $\Delta x \to 0$ results in the following equation:

$$-\frac{\partial i(x,t)}{\partial x} = v(x,t)G + C\frac{\partial v(x,t)}{\partial t} \quad (2\text{-}31)$$

Taking the Fourier Transform of equations (2-30) and (2-31) respectively:

$$-\frac{dv(x)}{dx} = (R + j\omega L)i(x) \quad (2\text{-}32)$$

$$-\frac{di(x)}{dx} = (G + j\omega C)v(x) \quad (2\text{-}33)$$

Differentiating equations (2-32) and (2-33):

$$-\frac{d^2v(x)}{dx^2} = (R + j\omega L)\frac{di(x)}{dx} \quad (2\text{-}34)$$

$$-\frac{d^2i(x)}{dx^2} = (G + j\omega C)\frac{dv(x)}{dx} \quad (2\text{-}35)$$

Substituting equations (2-32) and (2-33) into equations (2-34) and (2-35) respectively resulting in the final form of the wave equations:

$$\frac{d^2v(x)}{dx^2} = (R + j\omega L)(G + j\omega C)v(x) \quad (2\text{-}36)$$

$$\frac{d^2i(x)}{dx^2} = (G + j\omega C)(R + j\omega L)i(x) \quad (2\text{-}37)$$

The propagation constant is then defined as $\gamma = \sqrt{(G + j\omega C)(R + j\omega L)}$. Finding the solutions of equations (2-36) and (2-37) results in:

$$v(x) = {v_0}^+ e^{-\gamma x} + {v_0}^- e^{\gamma x} \quad (2\text{-}38)$$

$$i(x) = {i_0}^+ e^{-\gamma x} + {i_0}^- e^{\gamma x} \quad (2\text{-}39)$$

${v_0}^+ e^{-\gamma x}$ and ${i_0}^+ e^{-\gamma x}$ refer to the forward-traveling waves in the positive 'z' direction and ${v_0}^- e^{\gamma x}$ and ${i_0}^- e^{\gamma x}$ are the backward-traveling waves in the negative 'z' direction). From the above equations the characteristic impedance Z_0 can be derived as the following:

$$Z_0 = \frac{{V_0}^+}{{I_0}^+} = \frac{R + j\omega L}{\gamma} = \sqrt{\frac{R + j\omega L}{G + j\omega C}} \quad (2\text{-}40)$$

There is a relationship between current and voltage, as shown above, when electromagnetic waves propagate along a transmission line. When electromagnetic waves approach a point of discontinuity (e.g. open circuit or short circuit) there is a mismatch in characteristic impedance resulting in either the energy being reflected and superimposed on the incident wave or refracted by penetrating through the point of discontinuity. Consequently, the amplitudes of current and voltage are adjusted accordingly at this point complying with the law of conservation of energy [14].

Consider a junction between two power transmitting media with characteristic impedances Z_a and Z_b respectively. Assume that a voltage signal, V_i, is transmitted through medium A (known as the incident wave) towards the junction. This wave would then result in a reflected wave, V_r, and a refracted wave, V_t. The current and voltage waveforms are continuous through the junction between transmitting media *A* and *B*. This implies that:

$$V_i + V_r = V_t \quad (2\text{-}41)$$

$$\frac{V_i}{Z_a} - \frac{V_r}{Z_a} = \frac{V_t}{Z_b} \tag{2-42}$$

The reflected voltage wave can be derived in terms of the incident voltage wave:

$$V_r = V_i\left(\frac{Z_a - Z_b}{Z_a + Z_b}\right) \tag{2-43}$$

$\frac{Z_a - Z_b}{Z_a + Z_b}$ is known as the reflection coefficient, r, where $-1 \leq r \leq 1$. The reflected current wave can also be derived as a function of the incident current wave:

$$I_r = I_i\left(\frac{Z_b - Z_a}{Z_a + Z_b}\right) \tag{2-44}$$

Similarly, the refracted/transmitted voltage and current wave can also be derived as a function of the incident voltage and current waves:

$$V_t = V_i\left(\frac{2Z_b}{Z_a + Z_b}\right) \tag{2-45}$$

$$I_t = I_i\left(\frac{2Z_a}{Z_a + Z_b}\right) \tag{2-46}$$

The reflection of voltage and current waves has a significant influence on TRVs with respect to terminal faults and Short Line Faults (SLFs). Section 2.3.4 and Section 2.3.5 will present the effects of travelling waves and the impact to TRVs.

2.3.4 Terminal Faults of TRV travelling waves

Terminal faults are limited to power transformers or series reactors where transmission lines or cables are not present to provide damping due to the surge impedance. When a fault occurs, the transient produced due to the operation of the circuit breaker generates a travelling wave from the circuit breaker [11]. The travelling wave travels through a conductor with surge impedance until it encounters a discontinuity. Assuming the worst case where the discontinuity is an open circuit, the travelling wave reflects fully and returns to the circuit breaker where it superimposes on the initial transient.

2.3.4.1 First-Pole-To-Clear Factor

Although symmetrical components are utilised in fault calculations, this approach may also be utilised in evaluating the power frequency voltage that occurs across the circuit breaker when interrupting fault current. A three phase unbalanced system may be represented by a set of balanced sequence or symmetrical components (Figure 2-10) [11].

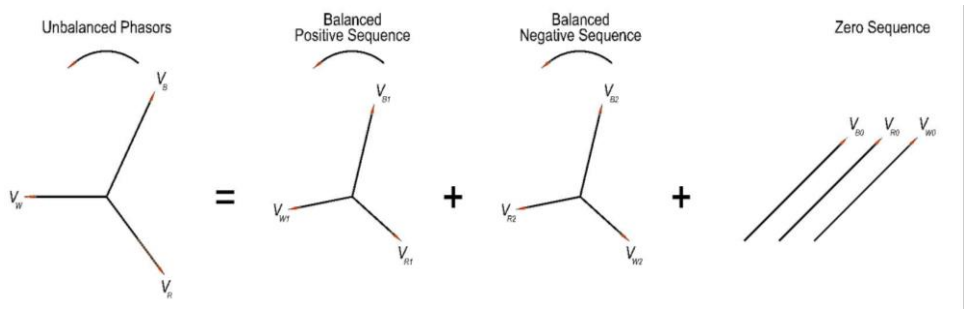

Figure 2-10: Unbalanced set of phasors represented by balanced set of symmetrical components

From Figure 2-10 the unbalanced phasors are expressed as a function of the sequence components as follows:

$$V_B = V_{B0} + V_{B1} + V_{B2} \quad (2\text{-}47)$$

$$V_R = V_{R0} + V_{R1} + V_{R2} \quad (2\text{-}48)$$

$$V_W = V_{W0} + V_{W1} + V_{W2} \quad (2\text{-}49)$$

The positive-sequence and negative-sequence components have phases of equal magnitude and are equally displaced 120° apart with a phase rotation of BRW and BWR respectively. The zero-sequence components have voltages of equal magnitude and are unidirectional with no phase angle displacement.

The phasors for the positive and negative sequence components are rotated using the *a* operator which is defined using Euler's formula:

$$e^{j\theta} = cos\theta + jsin\theta \quad (2\text{-}50)$$

Therefore:

$$a = e^{j120} = cos120 + jsin120 = -0.5 + j0.866 \quad (2\text{-}51)$$

The unbalanced phasors may be expressed as a function of the sequence components (positive, negative and zero sequence components) with reference to the reference phase voltage V_{B1}, V_{B2} and V_{B0} using the *a* operator. This would result in the following matrix:

$$\begin{bmatrix} V_B \\ V_R \\ V_W \end{bmatrix} = \begin{bmatrix} 1 & 1 & 1 \\ 1 & a^2 & a \\ 1 & a & a^2 \end{bmatrix} \begin{bmatrix} V_{B0} \\ V_{B1} \\ V_{B2} \end{bmatrix} \quad (2\text{-}52)$$

Where the transformation matrix is defined as $T = \begin{bmatrix} 1 & 1 & 1 \\ 1 & a^2 & a \\ 1 & a & a^2 \end{bmatrix}$

Similarly, the sequence components (positive, negative and zero sequence components) may be expressed as a function of the unbalanced phasors by taking the inverse:

$$\begin{bmatrix} V_{B0} \\ V_{B1} \\ V_{B2} \end{bmatrix} = \frac{1}{3} T^{-1} \begin{bmatrix} V_B \\ V_R \\ V_W \end{bmatrix} \quad (2\text{-}53)$$

Where the inverse transformation matrix is $T^{-1} = \begin{bmatrix} 1 & 1 & 1 \\ 1 & a & a^2 \\ 1 & a^2 & a \end{bmatrix}$.

Circuit breakers may be installed in either an effectively earthed or non-effectively earthed system. The rating of a circuit breaker is based on a three-phase-to-earth fault for an effectively earthed system and three-phase fault for a non-effectively earthed system. As a result of these faults, the circuit breaker poles will clear sequentially due to the current zeros of the respective phases being 120° apart.

After the first pole clears in an effectively earthed system, the other two phases remain connected to the system resulting in a two phase-to-earth fault (Figure 2-11).

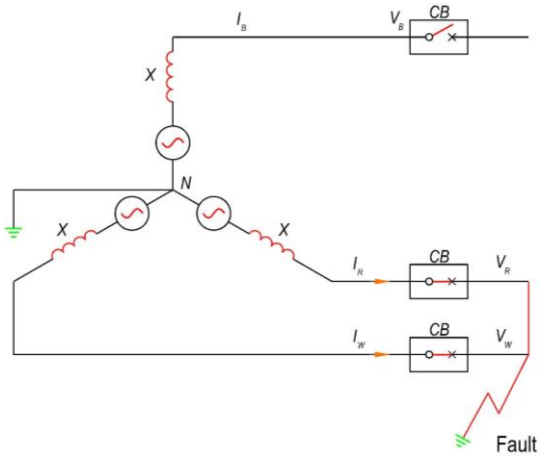

Figure 2-11: Equivalent circuit for a two-phase-to-earth fault

As a result, $I_B = 0$ and $V_R = V_W = 0$. This implies that:

$$I_B = I_{B0} + I_{B1} + I_{B2} = 0 \tag{2-54}$$

And

$$\begin{bmatrix} V_{B0} \\ V_{B1} \\ V_{B2} \end{bmatrix} = \frac{1}{3}\begin{bmatrix} 1 & 1 & 1 \\ 1 & a & a^2 \\ 1 & a^2 & a \end{bmatrix}\begin{bmatrix} V_B \\ V_R = 0 \\ V_W = 0 \end{bmatrix} \tag{2-55}$$

Therefore

$$V_{B0} = V_{B1} = V_{B2} = \frac{1}{3}V_B \tag{2-56}$$

Since the sum of the sequence component currents equals to zero (Equation (2-54)), and the terminal voltages are equal for the sequence components (Equation (2-56)), the sequence components are configured in parallel for the aforementioned to be true. As a result, the sequence network for a two phase-to-earth fault are configured as follows (Figure 2-12):

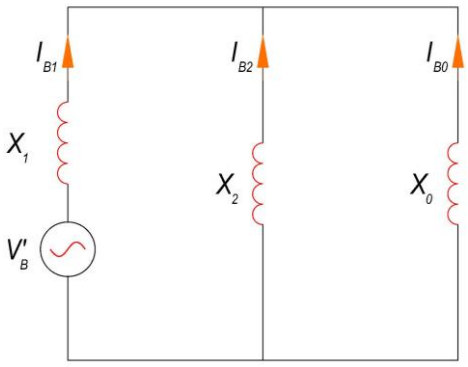

Figure 2-12: Sequence network circuit diagram for a two phase-to-earth fault

V_B': Phase-to-earth voltage before the fault

The positive sequence current I_{B1} is calculated from the positive sequence component as follows:

$$V_{B1} = V'_B - I_{B1}X_1 = \frac{1}{3}V_B \tag{2-57}$$

Taking Kirchhoff's Voltage Law for Figure 2-12 will result in I_{B1} being:

$$I_{B1} = \frac{V_B{}'}{X_1 + \frac{X_0 X_2}{X_0 + X_2}} \tag{2-58}$$

X_0: Zero sequence reactance in Ω
X_1: Positive sequence reactance in Ω

The first pole to clear factor is given as the ratio of the recovery voltage for the first pole to clear and the phase-to-earth voltage prior to the fault (Equation (2-59)).

$$k_{pp1} = \frac{V_B}{V_B{}'} \tag{2-59}$$

Therefore equating (2-57) and Equation (2-58) will result in:

$$k_{pp1} = \frac{V_B}{V_B{}'} = \frac{3X_0 X_2}{X_1 X_2 + X_0 X_1 + X_0 X_2} \tag{2-60}$$

Since $X_1 = X_2$ for transmission systems then [11]:

$$k_{pp1} = \frac{3X_0}{X_1 + 2X_0} \tag{2-61}$$

$X_0 = 3X_1$ for an effectively earthed system therefore $k_{pp1} \approx 1.3$ [3]. This factor represents the ratio of the zero-sequence reactance of the system to the combination of the positive and zero sequence reactance

For a circuit breaker installed in a non-effectively earthed system, the first pole-to-clear results in a line-to-line fault (Figure 2-13).

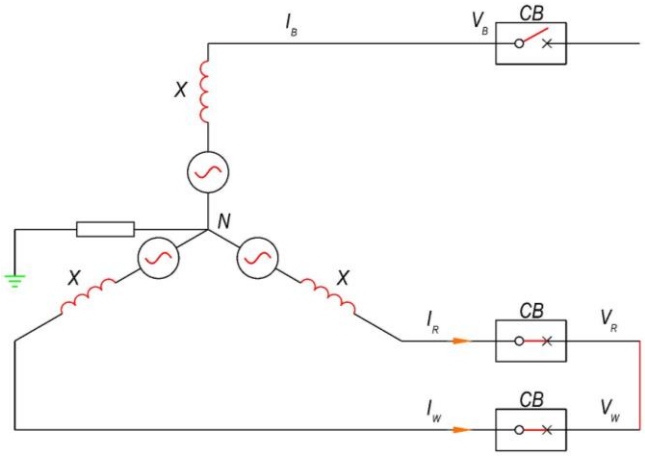

Figure 2-13: Equivalent circuit for a two phase fault

In this case, $I_R = -I_W$, $I_B = 0$ and $V_R = V_W$. The sequence components current can be written as a function of the unbalanced phases as follows:

$$\begin{bmatrix} I_{B0} \\ I_{B1} \\ I_{B2} \end{bmatrix} = \frac{1}{3} T^{-1} \begin{bmatrix} 0 \\ I_R \\ -I_R \end{bmatrix} \tag{2-62}$$

Therefore

$$I_{B0} = \frac{1}{3}(0 + I_R - I_R) = 0 \tag{2-63}$$

$$I_{B1} = \frac{1}{3}(0 + aI_R - a^2 I_R) = \frac{1}{3} I_R (a - a^2) \tag{2-64}$$

$$I_{B2} = \frac{1}{3}(0 + a^2 I_R - aI_R) = -\frac{1}{3} I_R (a - a^2) \tag{2-65}$$

From equation (2-63) $I_{B0} = 0$ and $I_{B1} = -I_{B2}$ (equations (2-64) and (2-65)). Since $I_{B0} = 0$ this suggests that the zero-sequence component does not exist. This is also confirmed from the equivalent circuit due to the absence of a path for fault current to flow through ground. The unbalanced phase voltages may be written as a function of the sequence components as follows:

$$\begin{bmatrix} V_B \\ V_R \\ V_W \end{bmatrix} = T \begin{bmatrix} V_{B0} \\ V_{B1} \\ V_{B2} \end{bmatrix} \tag{2-66}$$

Since $V_R = V_W$ and substituting from equation (2-66) then:

$$V_R = V_W \rightarrow V_{B0} + a^2 V_{B1} + a V_{B2} = V_{B0} + a V_{B1} + a^2 V_{B2} \tag{2-67}$$

Therefore

$$V_{B1} = V_{B2} \tag{2-68}$$

And

$$V_B = 0 + V_{B1} + V_{B1} = 2V_{B1} \tag{2-69}$$

Since the sum of the sequence component currents equals to zero (equation (2-62)), and the terminal voltages are equal for the sequence components (equation (2-68)), the sequence components are configured in parallel noting the absence of the zero sequence components. As a result, the sequence network for a two-phase fault are configured as follows (Figure 2-14):

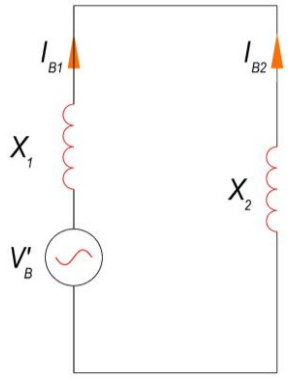

Figure 2-14: Sequence network circuit diagram for a two phase fault

The positive sequence terminal voltage may be written as:

$$V_{B1} = V'_B - I_{B1} X_1 \tag{2-70}$$

The positive sequence current may also be derived by applying Ohm's law to Figure 2-14:

$$I_{B1} = \frac{V'_B}{X_1 + X_2} \tag{2-71}$$

Substituting equation (2-71) into equation (2-70) then:

$$V_{B1} = V'_B - \frac{V'_B}{X_1 + X_2} X_1 \tag{2-72}$$

Since $X_1 = X_2$ for transmission systems then [11]:

$$V_{B1} = 0.5 V'_B \tag{2-73}$$

Substituting equation (2-69) into equation (2-73) the first pole to clear factor is given as:

$$k_{pp1}{}^{*} = \frac{V_B}{V_B{}'} = 1 \tag{2-74}$$

However, there is a recovery voltage that occurs across the phase B circuit breaker between the period of interruption of the phase B and the simultaneous interruption of phases R and W. This recovery voltage is calculated by determining either V_R or V_W using equations (2-66) and (2-68):

$$V_R = 0 + a^2 V_{B1} + a V_{B1} = -V_{B1} \tag{2-75}$$

Substituting for V_{B1} from equation (2-73):

$$V_R = -0.5 V_B' \tag{2-76}$$

Therefore, the recovery voltage across the circuit breaker on phase R is given as:

$$V_{BR} = V_B' - (-0.5 V_B') = 1.5 V_B' \tag{2-77}$$

Therefore, the first pole to clear factor for non-effectively earthed systems is given as:

$$\frac{V_{BR}}{V_B'} = 1.5 \tag{2-78}$$

The recovery voltage is higher on the first pole to clear during a three-phase fault. This factor (k_{pp}) is classified into three categories [4]:

- Terminal fault breaking by circuit-breakers with rated voltages higher than 800 kV in effectively earthed neutral systems where the k_{pp} is 1,2.
- Terminal fault breaking by circuit-breakers for rated voltages up to and including 800 kV in effectively earthed neutral systems where the k_{pp} is 1,3.
- Terminal fault breaking by circuit-breakers for rated voltages less than 245 kV in non-effectively earthed neutral systems where the k_{pp} is 1,5.
- Interrupting in an out-of-phase condition in systems with effectively earthed neutral where the k_{pp} is 2.
- Interrupting in an out-of-phase conditions in systems with non-effectively earthed neutral where the k_{pp} is 2,5.

The TRV ratings for circuit breakers installed on power systems operated at 72,5 kV and below assume that the system neutrals are non-effectively earthed and circuit breakers installed in systems at 245 kV and above assume that the system neutrals are effectively earthed [10].

2.3.4.2 Underdamped TRV

A high frequency transient may also occur where the transient may exceed the TRV capability of the circuit breaker (underdamped) [3] (Figure 2-15). An example of this is where the short circuit occurs directly outside the transformer and there is not substantial capacitance between the transformer and the circuit breaker to dampen the transient.

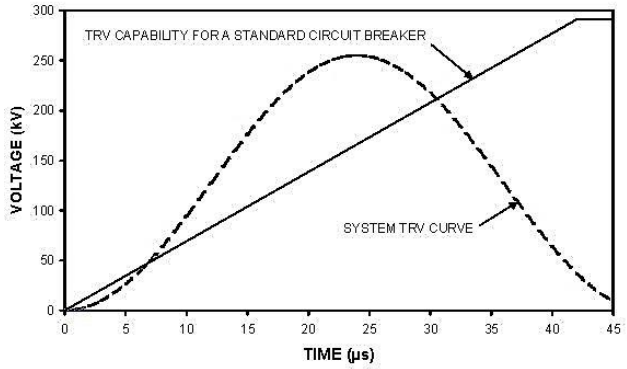

Figure 2-15: TRV Capability for a 132 kV circuit breaker in an underdamped condition [3]

A TRV is considered underdamped/oscillatory when:

$$R > \frac{1}{2}\sqrt{\frac{L}{C}} \tag{2-79}$$

In this case it is assumed that the network may be reduced to a simplified RLC parallel circuit [3][10].

The two-parameter envelope is utilized in this instance where:

- The circuit breaker is rated less than 100 kV for all current interruption values.
- The circuit breaker is rated at 100 kV and above and if the short circuit current is less than or equal to 30% of the rated current interruption [10]. The four-parameter envelope is utilised for instances above the 30% value.

2.3.5 Short-Line Faults

A TRV is considered a short line fault where the travelling waves are reflected at the point of interruption/discontinuity on a transmission line such that the circuit breaker terminal perceives the reflected wave in typically hundreds of microseconds.

The short-line fault is deemed one of the harshest short-circuit duties on a circuit breaker [9]. A very steep voltage oscillation on the line side of a circuit breaker terminal develops after current interruption due to the reflected waves [9]. This may cause thermal breakdown on the arc channel due to the high stress imposed on the still-hot plasma channel. The circuit breaker fails short-circuit current interruption since the arcing time is sustained and thermal breakdown occurs in the subsequent current zero crossing. The oscillating waveform on the line side is typically a triangular or saw-toothed waveform. Grading capacitors are installed across the circuit breaker terminals to reduce the rate of rise of the TRV [10] and improve the Short Line Fault (SLF) performance. The grading capacitor decreases the oscillation frequency on the line side of the circuit breaker resulting in a reduced contribution of the RRRV to the TRV [10]. Opening resistors are also utilized predominantly with air blast circuit breakers for short circuit interruption and to assist in the interruption of fast TRVs in selected SF_6 circuit breakers.

2.3.5.1 Overdamped TRV

This is also known as an overdamped condition (see Figure 2-16) where:

$$R \leq \frac{1}{2}\sqrt{\frac{L}{C}} \tag{2-80}$$

Similarly to the underdamped TRV, the network may be reduced to a simplified RLC parallel circuit [3][10].

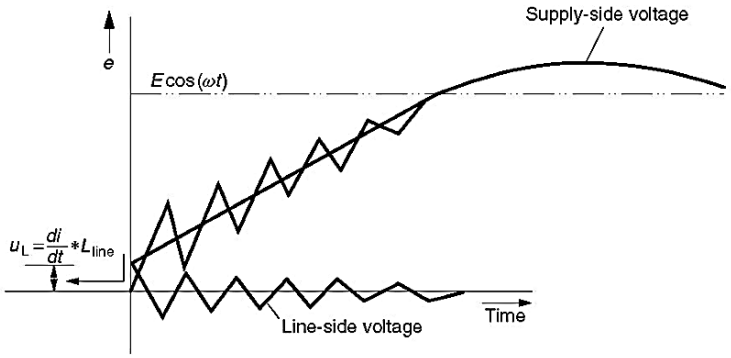

Figure 2-16: TRV for a Short-Line Fault [9]

2.3.6 Out-of-Phase Condition

One of the consequences of operating a long high voltage transmission line near their stability limits as a result of a high loading of the line is that the line circuit breakers of this transmission line may be occasionally subjected to an out-of-phase switching duty [15][16]. This out-of-phase switching duty may be attributed to faults or disturbances and may result in a system separation [16]. When a circuit breaker operates for current interruption in the above scenario, a TRV develops across the circuit breaker contacts until the travelling wave returns from the remote end substation of the transmission line. The out-of-phase current that develops between the circuit breaker contacts is determined by the phase angle between the busbar side voltage of the circuit breaker and the transmission line side. This condition could occur when closing a circuit breaker between two power systems which may not be synchronised.

2.3.7 TRV Calculations

TRV parameters are defined as a function of the amplitude factor (k_{af}), the first-pole-to-clear (k_{pp}) and the rated voltage (U_r).

The first reference voltage u_1 for circuit breakers at rated voltages 100 kV to 800 kV are derived at a time t_1 calculated by the equation [4]:

$$u_1 = (0.75 \times k_{pp} \times \frac{\sqrt{2}}{\sqrt{3}} U_r) kV \quad (2\text{-}81)$$

The first-pole-to-clear is determined as indicated in section 2.3.4.1. The RRRV for circuit breakers at rated voltages 100 kV to 800 kV are specified as follows [4]:

Table 2-3: RRRV for circuit breakers at rated voltages 100 kV to 800 kV

Test Duty	RRRV (kV/µs)
T100	2
T60	3
T30	5
T10	7
OP	1.54

The corresponding t_1 or t_3 value is derived taking voltage u_1 and dividing by the RRRV for a given circuit breaker for a specific test duty as specified in the SANS 62271-100:2017 [4]:

$$t_1 = \frac{u_1}{RRRV}\mu s \tag{2-82}$$

The TRV peak voltage value for circuit breakers rated up to 800 kV is calculated using the following equation [4]:

$$u_c = (k_{pp} \times k_{af} \times u_r \times \sqrt{\frac{2}{3}})kV \tag{2-83}$$

The amplitude factors for various test duties of circuit breakers are specified in SANS 62271-100:2017 [4] as follows:

Table 2-4: Amplitude Factors for Circuit Breakers [4]

Test Duty	Amplitude Factors			
	U_r<100 kV (Type S1)	U_r<100 kV (Type S2)	100 kV ≤U_r< 800 kV	≥ 800 kV
T10	1.7	1.8	1.7	1.76
T30	1.6	1.74	1.54	1.54
T60	1.5	1.65	1.5	1.5
T100	1.4	1.54	1.4	1.5
OP	1.25	1.25	1.25	1.25

The time t_2 may be calculated as follows for circuit breakers at rated voltages 100 kV to 800 kV:

Table 2-5: Time t_2 for a four parameter circuit breaker rating

Test Duty	Time t_2 (µs)
T100	4 x t_1 (for T100)
T60	6 x t_1 (for T60)
OP	2 x t_2 (for T100)

The circuit breaker technology will be presented in section 2.4 with specific focus on the SF_6 type circuit breaker which is the dominant technology for the transmission system studied.

2.4 Circuit Breakers

In order to have a complete understanding of TRVs it is essential to understand the physical processes that occur between the circuit breaker contacts. One of the main functions of a circuit breaker is to break fault currents in order to isolate faulted portions of a power system. In addition, a circuit breaker may interrupt capacitive, inductive or load currents [9]. Current interruption in a circuit breaker is achieved by cooling the arc plasma such that the electric arc that forms between the breaker contacts after contact separation, disappears [9]. Circuit breakers are classified in accordance with their arc extinguishing medium (i.e. oil-filled, air-blast, vacuum and SF_6).

Circuit breakers are further classified as class E1, E2, C1, C2, M1, M2, S1 and S2 [4]: Classes E1 and E2 defines the designs of the circuit breaker by its electrical endurance capability, while classes C1 and C2 are designed for capacitive current switching. Classes M1 and M2 are circuit breakers designed for mechanical endurance and classes S1 and S2 are circuit breakers designed for cable systems and line systems respectively [4].

2.4.1 SF_6 Circuit Breakers

SF_6 gas is known for its high dielectric strength as well as good thermal conductivity properties. This gas has been employed in HV circuit breakers internationally for over thirty years as an insulating as well as an arc extinguishing medium.

Two technologies were developed for the breaking of current in SF_6 circuit breakers [9][17]:

- Puffer (piston) – type circuit breaker
    - Designed for breaking higher current capacities
- Self-blast circuit breaker
    - Designed for breaking medium current capacities

The puffer type interrupter is used in the live tank circuit breaker where the current interruption chamber is enclosed with SF_6 gas at a pressure of 0.5-0.6MPa [18]. During current interruption the breaker contacts part and the puffer cylinder, which forms part of the moving arcing contact, directs the compressed gas to the arc which forms between the arcing contacts. The arc is cooled as a result of the gas flow and the arcing current is extinguished at a current zero. The Short Line Fault is also an important test duty for these types of circuit breakers.

The modelling of the arc behaviour of circuit breakers during the interruption process is presented in section 2.5. The Cassie and Mayr models will be focussed on as they were the models used in the simulation model.

2.5 Black Box Arc Modelling

The arcing phenomena in circuit breakers may be described by three modelling tools [19]:

- Black Box models
- Physical arc models
- Parameter arc models

The black box model describes the circuit breaker arc behaviour by a mathematical transfer function which defines the relationship between the arc conductance and measurable parameters such as the arc voltage and the arc current. This approach is not suitable for the design of circuit breaker interrupters but rather for simulation purposes in understanding the interaction of the switching arc and the response of the power system during current interruption. Cassie and Mayr models are classical black box models utilised extensively in power system simulations.

The physical arc models are based on the combination of the laws of fluid dynamics and Maxwell's equations and comply with the laws of thermodynamics. This model also details the exchange processes of radiation and conduction and various chemical reactions [9].

Parameter arc models are similar to black box arc models however they are described by more complex functions and tables [19].

The arc conductance is defined as a function of the power supplied to and transmitted from the arc channel during the duration of the arc interruption process. A difference in the power supplied to and transmitted from the arc channel will result in energy being stored in the arc channel [9]:

$$g = f(Q) = f\left[\int_0^t P_{in} - P_{out}\, dt\right] \tag{2-84}$$

The general arc equation can then be derived as a function of the arc conductance as follows:

$$\frac{1}{g}\frac{dg}{dt} = \frac{f'(Q)}{f(Q)}(P_{in} - P_{out}) \tag{2-85}$$

2.5.1 The Cassie Black Box Model

The *Cassie black box model* is based on a cylindrical arc channel where the temperature, current density and electric field strength are constant [19]. The arc channel is cooled down due to gas flow or convection and the arc channel diameter varies. This black box arc model is suitable for modelling the arcing characteristics representative for SF_6 and air circuit breakers for relatively high currents (in the order of hundreds of amperes) [20].

The arc conductance is calculated as the product of the arc channel diameter (*D*) and the arc conductance per unit volume (g_0) [9]:

$$g_c = f(Q) = D_{arc} g_0 \tag{2-86}$$

g_o: conductance per unit volume
D_{arc}: arc diameter as a function of time

The energy in the arc channel is a function of the arc channel diameter and the energy per unit volume:

$$Q = D_{arc} Q_0 \rightarrow D_{arc} = \frac{Q}{Q_0} \tag{2-87}$$

Q_0: energy per unit volume

Combining equations (2-86) and (2-87) and differentiating results in the following:

$$f'(Q) = \frac{g_0}{Q_0} \tag{2-88}$$

The dissipated power is also a function of the arc channel diameter:

$$P_{out} = D_{arc} P_0 = \frac{Q}{Q_0} P_0 \tag{2-89}$$

P_0: power loss per unit volume

Substituting equations (2-86), (2-88) and (2-89) into the general arc equation (2-85):

$$\frac{1}{g_c}\frac{dg}{dt} = \frac{g_0}{Q_o}\frac{Q_0}{Q g_0}\frac{Q}{Q_0} P_0 \left(\frac{P_{in}}{P_{out}} - P_{out}\right) \tag{2-90}$$

The time constant is then defined as:

$$\tau = \frac{P_0}{Q_o} \tag{2-91}$$

Therefore, the rate of change of conductance is given by:

$$\frac{dg_c}{dt} = \frac{1}{\tau}\left(\frac{g_c \cdot {v_{arc}}^2}{{v_{out}}^2} - g_c\right) \tag{2-92}$$

Letting $v_{arc} = \frac{i_{arc}}{g}$ and substituting into equation (2-92) then:

$$\frac{dg_c}{dt} = \frac{1}{\tau}\left(\frac{{i_{arc}}^2}{g_c \cdot {v_{out}}^2} - g_c\right) \tag{2-93}$$

Applying the Laplace transform to equation (2-93) [20]:

$$sG_c = \frac{1}{\tau}\left(\frac{{i_{arc}}^2}{G_c \cdot {v_{out}}^2} - G_c\right) \tag{2-94}$$

Finally the arc conductance is derived from equation (2-94) [20]:

$$G_c = \sqrt{\frac{{i_{arc}}^2}{{v_{out}}^2}\left(\frac{1}{1+\tau s}\right)} \tag{2-95}$$

The arc resistance for the Cassie black box model is then given by:

$$R_c = \frac{1}{G_c + 1 \times 10^{-6}} \tag{2-96}$$

The term 1 x 10^{-6} is to prevent a division by zero.

2.5.2 The Mayr Black Box Model

The *Mayr black box model* describes the arcing characteristics representative for SF_6 and air circuit breakers around current zero [20]. The arc channel was considered to be cylindrical with a constant diameter. The arc column loses its energy by thermal conduction at constant power loss [19]. The temperature of the arc channel varies exponentially and may be expressed as an approximation of Saha's equation [9]:

$$g_m = f(Q) = ke^{Q/Q_0} \tag{2-97}$$

Substituting into the arc equation (Equation (2-85)) results in:

$$\frac{dg_m}{dt} = \frac{g_m k e^{Q/Q_0}}{Q_0 k e^{Q/Q_0}}(P_{in} - P_{out}) \tag{2-98}$$

Since the power in the arc loss and arc diameter are constant then $P_{out} = P_0$. As per the time constant defined in equation (2-91) and substituting into equation (2-98) then:

$$\frac{dg_m}{dt} = \frac{g_m}{\tau_m}\left(\frac{P_{in}}{P_0} - 1\right) = \frac{1}{\tau_m}\left(\frac{{i_{arc}}^2}{P_0} - g_m\right) \tag{2-99}$$

Applying the Laplace transform to equation (2-99):

$$sG_m = \frac{1}{\tau_m}\left(\frac{{i_{arc}}^2}{P_0} - G_m\right) \tag{2-100}$$

The conductance for the Mayr model is then calculated as:

$$G_m = \frac{{i_{arc}}^2}{P_0}\left(\frac{1}{1+s\tau}\right) \tag{2-101}$$

The arc resistance for the Mayr black box model is then given by:

$$R_m = \frac{1}{G_m + 1 \times 10^{-6}} \tag{2-102}$$

The term 1 x 10^{-6} is to prevent a division by zero.

A model was formulated combining both the Cassie and Mayr models [21][22] from equations (2-96) and (2-102) to describe the arc characteristic in SF_6 circuit breakers:

$$R_{total} = R_c + R_m \tag{2-103}$$

The arc interruption process is presented in section 2.6. The processes and consequences of interrupting series and shunt capacitors and inductors are then discussed.

2.6 Arc Interruption Process

An electric arc in a circuit breaker is described as the plasma channel that is established after a gas discharge in the extinguishing medium [9]. During breaker contact separation, a high current density develops between the contacts due to the small surface area between them. The contact material melts and explodes, generating a gas discharge in the extinguishing medium. With an increase in kinetic energy of the gas molecules, in combination with an increase in temperature, this gas discharge is then transformed into a plasma state which forms the plasma channel. This plasma channel is highly conductive and therefore sustains current flow between the circuit breaker contacts after contact separation [9]. One of the requirements to extinguish an electric arc/plasma channel within a circuit breaker, is for current to pass through zero [23]. At this point, the energy input to the arc channel is relatively low. By design, the cooling properties of the circuit breaker extinguishing medium should be at its maximum where the current is then interrupted [9]. It is therefore imperative for the de-ionization of the arc gap close to current zero. If the dielectric strength of the arc gap is greater than the increasing voltage that is imposed across the gap, this would indicate a successful current interruption.

2.6.1 Interruption of Capacitive Currents

2.6.1.1 Shunt Capacitance in transmission lines

Capacitor devices are installed in power systems for either voltage regulation or to increase the power transfer capacity in transmission lines. Figure 2-17 is a typical configuration of a shunt capacitor installed in the power system.

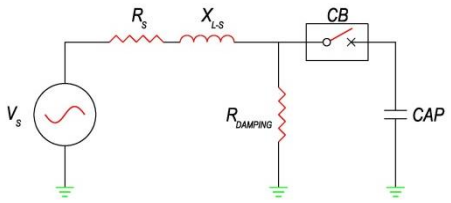

Figure 2-17: Circuit diagram of a shunt capacitance circuit

Since current leads voltage in a capacitive circuit by ninety degrees, the voltage will be at its maximum during the current interruption of a capacitive load at current zero. The capacitive load will contain the electrical charge (known as trapped charge) at a constant voltage after current interruption [9]. When the source side voltage reaches the opposite polarity to the load voltage, nearly two times the voltage peak develops across the circuit breaker contacts. This voltage build up across the circuit breaker contacts could result in the dielectric breakdown of the arc gap within a circuit breaker and initiate a re-ignition in the arc gap. The capacitor will discharge into the re-ignited channel. This transient voltage phenomenon is initiated by the sinusoidal source side voltage. The transient oscillation frequency is dependent of the source inductance and capacitance of the circuit:

$$f = \frac{1}{2\pi\sqrt{LC}} \tag{2-104}$$

When the current is extinguished at the subsequent zero crossing, the voltage across the breaker contacts is now four times the peak voltage. A second re-ignition occurs and this process repeats (see Figure 2-18) until the voltage that builds up across the breaker contacts is high enough to eventually flash over across the external insulation of the circuit breaker chamber [9]. Therefore, it is imperative that the circuit breaker that is required to switch capacitive currents should be re-strike free.

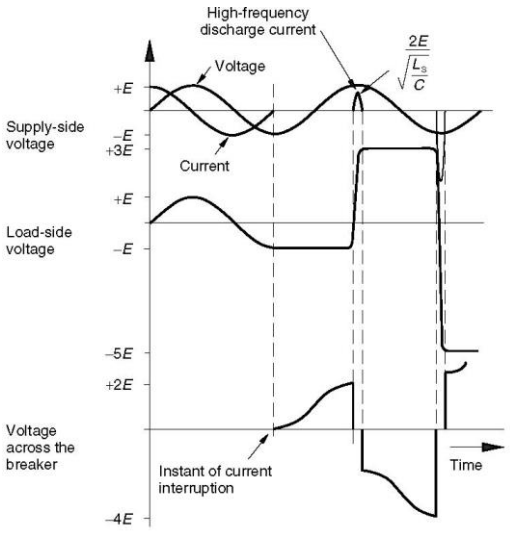

Figure 2-18: Capacitive current interruption and re-ignition in a circuit breaker [9]

2.6.1.2 Series Capacitors used with transmission lines

Series capacitors are used extensively on long transmission lines to increase the power transfer capacity of the line by decreasing the overall reactive impedance of the line. In addition, series capacitors improve the transient stability of synchronous generators connected to long transmission lines. The disadvantages of series compensation are the risk of subsynchronous resonance and the increase in the magnitudes of the TRV peaks. The increase in the TRV is attributed to the trapped charge that may remain on the series capacitor which combines with the TRV which occurs without the series cap [24]. The phenomenon of trapped charge in a series cap bank protected by the conventional spark gap occurs when the fault current is relatively small and associated increase in the TRV does not trigger the spark gap. There are currently two types of series compensators: Fixed Series Capacitors (FCS) (Figure 2-19) and Thyristor Controlled Series Capacitors (TCSC) [2] (see Figure 2-20). TCSCs are typically utilized in power systems to mitigate against resonance and subsynchronous resonance phenomena as the series capacitor is connected in parallel with a Thyristor Controlled Reactor (TCR).

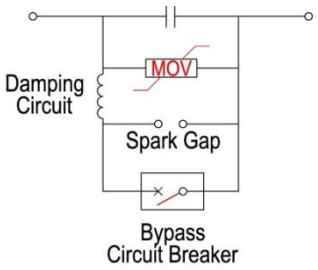

Figure 2-19: Circuit diagram of Fixed Series Capacitor [25]

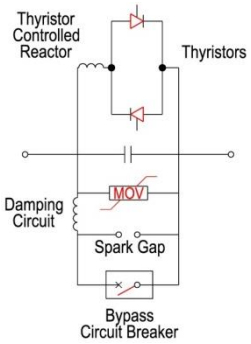

Figure 2-20: Circuit Diagram of Thyristor Controlled Series Capacitor

The apparent impedance of the transmission line decreases due to the addition of a series capacitor. As a result, the breaking current as well as the voltage peak of the TRV that the circuit breaker is exposed to increases [16]. During fault clearing of an overhead line, the combination of the trapped charge of the capacitance of the line and the series capacitor leads to a rise in peak value of the TRV which may exceed the circuit breaker TRV rating. The series capacitor bank is bypassed by closing the series capacitor bank bypass circuit breaker (Figure 2-20). The capacitor bank is discharged through the damping circuit reducing the impact of the series capacitor on the TRV imposed on the LCBs. The bypassing of the series capacitor results in an uncompensated line and the line protection operates accordingly. This is done in practice.

There are two main protection aspects that are considered when integrating a series capacitor into a power system: the protection of the series capacitor bank from overvoltages/surges or switching and the second aspect is the fault clearing on the respective transmission line.

Series capacitors have a dielectric strength described in terms of a power frequency voltage withstand level. If a fault occurs this would result in the dielectric strength of the series capacitor being exceeded. An overvoltage protection device is installed in parallel with the capacitor to limit these overvoltage stresses These are typically spark gaps and more recently Metal Oxide Varistors (MOVs). The series capacitor protection includes a high current bypass circuit breaker for faults internal to the capacitor bank and which also bypasses the MOV when external faults could cause the energy rating of the MOV to be exceeded [26]. When the voltage across capacitor is below the Maximum Continuous Operating Voltage (MCOV) of the MOV, the MOV is seen as an open circuit. If the voltage across the series capacitor exceeds the MCOV rating of the MOV, the MOV will start conducting. This will continue for as long as the voltage across the capacitor exceeds the MOV protective level as indicated in Figure 2-21.

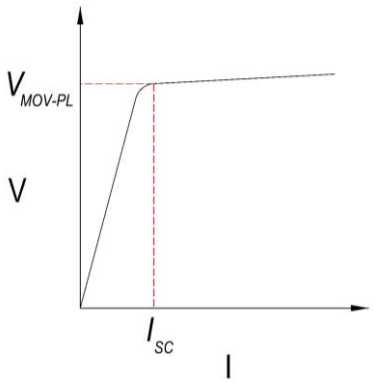

Figure 2-21: V-I curve of a MOV across a series capacitor

The combination of the non-linear MOV and capacitor may be represented as a variable resistor in series with the capacitor as opposed to the MOV in parallel to the capacitor (Figure 2-22) [27].



Figure 2-22: Linear approximation of and MOV protected series capacitor

This was a significant development as the apparent impedance of the combination of the capacitor and MOV has an impact on the way the impedance protection settings are determined. Empirical formulae were developed to determine the magnitude of the resistance of the MOV and the reactance of the capacitor as a function of fault current shown in [27]:

$$R_c' = X_c(0.0745 + 0.49e^{-0.243I_{ln}} - 35e^{-5I_{ln}} - 0.6e^{-1.4I_{ln}}) \quad (2\text{-}105)$$

$$X_c' = X_c(0.101 - 0.005749I_{ln} + 2.088e^{-0.8566I_{ln}}) \quad (2\text{-}106)$$

X_c: Capacitor reactance in Ω
R_c': MOV equivalent resistance in Ω
I_{ln}: Ratio of the capacitive current to the capacitive current protective level

As the fault current increases through the capacitor, and the voltage across the capacitor exceeds the MCOV rating of the MOV, R_c' increases and X_c' decreases (Figure 2-23).

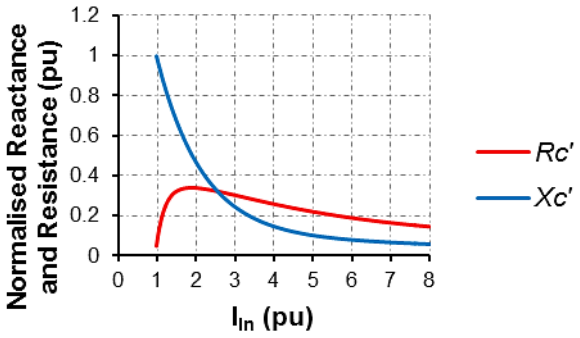

Figure 2-23: Relationship between Normalised MOV resistance and capacitive impedance with respect to current

Figure 2-24 is a locus representation of the equivalent impedance representing the combination of the MOV resistance and capacitive impedance for varying fault current. This X-R diagram is utilised in determining the protection settings for the impedance relay.

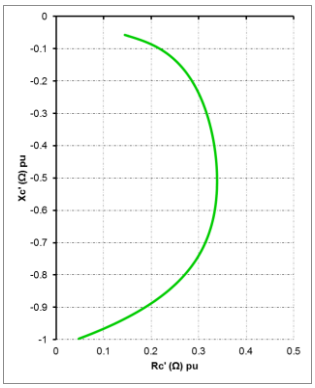

Figure 2-24: X-R diagram of the series combination of Xc' and Rc'

In order to prevent damage to the MOVs during line faults, a bypass circuit breaker is installed across the MOV such that it is triggered when the energy that is dissipated from the MOV exceeds its energy rating. One of the consequences of closing the bypass circuit breaker is that a high frequency transient oscillation is generated due to the resonance between the capacitor and the damping reactor. This could contribute significantly to the TRV that the LCBs could be exposed to. A damping resistor is installed as part of the damping circuit to reduce the impact of the high frequency transient voltage generated. In order to minimize the impact of the high frequency transient voltage or the stored charge on the series capacitor, the LCBs should open after a reasonable amount of time after the bypass circuit breaker has closed.

One of the challenges associated with series compensated transmission lines is the ability of the impedance/distance protection system to detect an internal fault and respond correctly in isolating the fault by firstly closing the series capacitor bank bypass circuit breaker and subsequently open the LCBs. Failure of the protection system in detecting a fault could result in the series capacitor bypass circuit breaker not closing prior to the LCBs opening resulting in a significant trapped charge and consequently high TRVs that the LCBs are exposed to. The following discussion presents the complexity associated with fault detection on series compensated transmission lines.

Typically, transmission lines utilise distance protection as they are simple to apply and in operation. Since the impedance of a transmission line is proportional to the length of the line, a relay is designed to measure the impedance between itself and a fixed point along the transmission line for which it would operate for faults [28]. This is achieved by measuring the voltage and current at the relay and calculating the impedance. This approach works well for the conventional uncompensated transmission line. However, series compensation of a transmission line adds further complexity to impedance protection of the line. As shown in Figure 2-25 (a), the impedance of a transmission line is typically a linear relationship between the inductive reactance and resistance of the line conductor. When a series capacitor is installed along the same transmission line, the apparent impedance of the line is altered as a result of the negative reactance introduced by the capacitor (Figure 2-25 (b)). The MOV that protects the series capacitor also has an influence of the apparent impedance of the transmission line as discussed above and shown in Figure 2-25 (c).

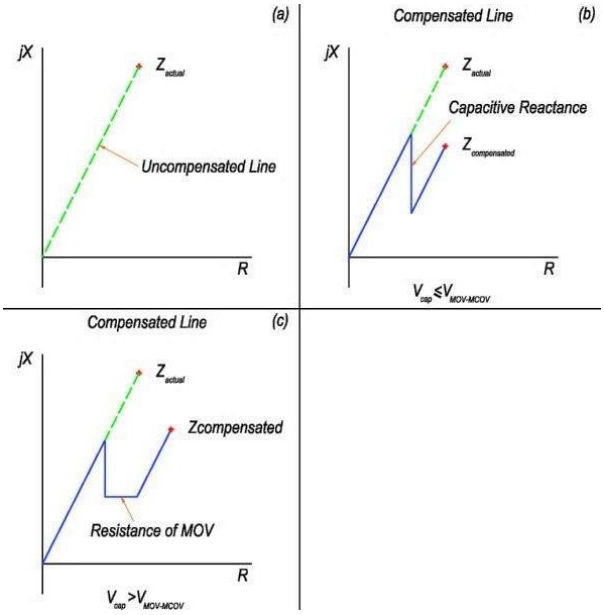

Figure 2-25: X-R diagrams comparing an uncompensated line and a compensated line and the influence of the MOV

There are three aspects to consider when evaluating the impedance protection of a series compensated circuit:

- Voltage reversal
- Current reversal
- 50 Hz resonance

Voltage reversal occurs when the impedance of the transmission line between the relay point and the fault is less than the impedance of the series capacitor (Figure 2-26). In the example below, the line impedance is split equally on either side of the series capacitor ($Z_{L\text{-}A}$=$Z_{L\text{-}B}$). The line is taken to be 60% compensated, therefore the equivalent impedance of the series capacitor is given by:

$$Z_{CAP} = 0.6(2Z_{L-A}) \tag{2-107}$$

If a fault occurs just after the capacitor then the net impedance measured from the relay to the faulted point is given by:

$$Z_{measured} = Z_{L-A} - Z_{CAP} \equiv Z_{L-A} - 0.6(2Z_{L-A}) = -0.2Z_{L-A} \tag{2-108}$$

In this case the fault current lags the source voltage. Additionally, the voltage measured by the relay is 180^0 out of phase with the source voltage and leads the fault current. The apparent measurement of the fault is perceived closer than the actual fault position due to the negative capacitive impedance (Figure 2-26). The position of the series capacitor also has an influence on whether the fault is perceived as internal or external. The closer the capacitor is positioned with respect to the relay could result in fault being measured to occur behind the relay or externally.

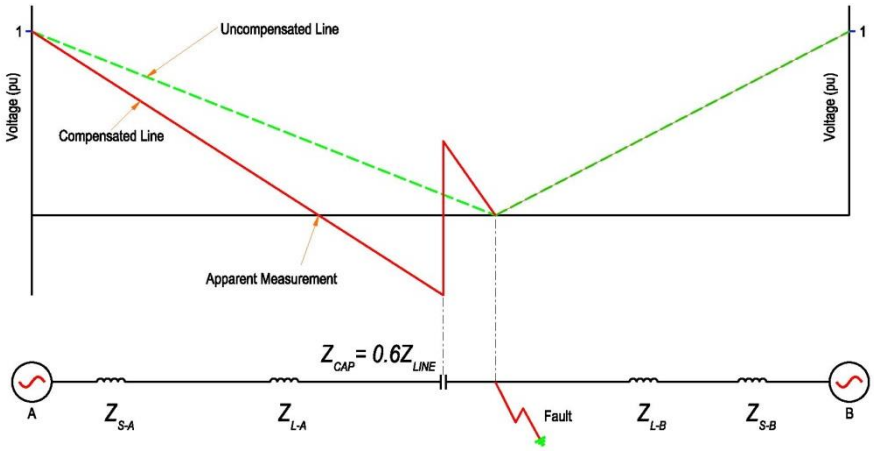

Figure 2-26: Example of voltage reversal of a 60% series compensated line.

Current reversal occurs when the impedance between source and fault along a series compensated circuit is capacitive (i.e. the series capacitive reactance exceeds the inductive reactance of a circuit) [26]. A typical example of such an application is a series capacitor connected to a line terminal (Figure 2-27).

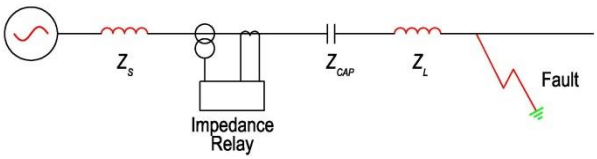

Figure 2-27: Example of current reversal with a series capacitor connected to the line terminal

In this scenario, current leads voltage due to the impedance between source and fault being capacitive. An interesting observation is that the measured voltage by the relay for the above circuit would be higher than the source voltage but in phase. This is due to the capacitive current flowing through the source inductance which results in the voltage across the source inductance being 180^0 out of phase with the source voltage.

Resonance occurs when the electrical field energy equals the magnetic field energy in an electrical circuit [29]. This phenomenon occurs when the capacitive reactance matches the inductive reactance of a circuit at a specific frequency. The resonant/natural frequency is calculated as per equation (2-104). A 50 Hz resonance could lead to significant overvoltages and stresses to the power system. A simplified diagram of a series resonant circuit is shown below in Figure 2-28:

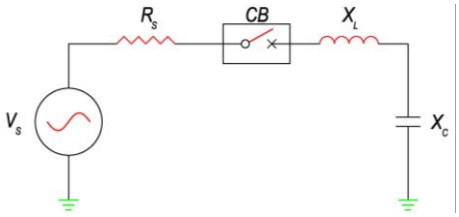

Figure 2-28: Simplified series resonant circuit

The impedance of the above circuit is given by:

$$Z = R_S + j(\omega L - \frac{1}{\omega C}) \quad (2\text{-}109)$$

At low frequencies, the capacitive reactance dominates the impedance and current leads voltage [29]. At resonant frequency the inductive reactance matches and cancels the capacitive reactance which results in the effective impedance being purely resistive. Subsequently the current and voltage are in phase. The circuit current is limited by the resistance in the circuit. The inductive reactance dominates the impedance of the circuit at high frequencies and current lags voltage in this instance.

Wilson [30] concluded that:

- Line circuit breaker terminals on series compensated circuits may be exposed to reclosing surges in excess of non-compensated lines.
- Line circuit breakers on series compensated circuits may be exposed to severe TRVs if no opening resistors are installed.
- Arresters installed on the line terminals can significantly reduce TRVs across line circuit breakers.
- MOVs installed across series capacitors may be subjected to significant thermal requirements due to power frequency overvoltages.
- Lower TRVs will be experienced by the line circuit breaker in weak source networks.
- Line circuit breakers will be exposed to severe voltages for faults occurring beyond the series capacitor.

Bladow and Weaver [31] demonstrated that the installation of line MOVs in combination with pre-insertion circuit breaker resistors in certain instances are effective in limiting TRVs on line circuit breakers of series compensated lines. The line MOVs are effective in controlling the line energisation voltage along the transmission line while the closing resistors are effective in limiting the voltage during a three-phase reclosing. Three-pole reclosing however is typically not utilised in the application of a series compensated transmission line therefore this aspect is not a critical consideration. Additionally, closing resistors increase the mechanical complexity and maintenance requirements of a circuit breaker. Closing resistors are also known to fail catastrophically resulting in severe damage to

equipment and raises the concern of personnel safety. The MOVs limit the voltage for a single-phase reclosing operations to within the switching surge withstand level.

Iliceto et. al [24] however highlighted that SF_6 circuit breakers may be installed with closing resistors and very few exceptions with opening resistors or the combination of opening and closing resistors.

The idea of the MOV installed across the line circuit breaker terminals was also evaluated in limiting the TRV across the circuit breaker [24]. During normal operation, the MOV has no applied voltage across it therefore is not exposed to the risk of the phenomenon of thermal runaway. The MOV will be exposed to:

- Power frequency voltage when the circuit breaker is open and one or both terminals of the circuit breaker are energised.
- TRVs due to switching surges, especially when clearing faults through series capacitors.

2.6.2 Interruption of Inductive Currents

2.6.2.1 Shunt Reactors

Shunt compensation of reactive power may be either capacitive or inductive [2]. Shunt reactors are utilized to absorb reactive power from the power system. Typically, these shunt reactors are installed at the remote ends of transmission lines to compensate for either the Ferranti effect or energized during lightly loaded conditions. Due to an increase in the integration of renewable energy into power systems, this has resulted in an increase in the switching duty of shunt reactors. There are two types of reactors i.e. oil-immersed/filled iron core reactors and air-core reactors.

Oil-filled reactors are utilized at the higher voltage levels (up to 1200 kV) for large reactive power ratings. These reactors are utilized to minimize losses and reduce audible noise and vibrations. They are not environmentally friendly considering oil spillages or catastrophic failure of the reactor which may result in fires. The cost of these reactors is very high and requires a large area.

The air-core reactor on the other hand is utilized at the lower voltage levels for lower reactive power ratings.

Shunt reactors are utilised on typically long transmission lines (approximately 200km or more) to compensate the effects of the line capacitance to limit the voltage rise at the remote ends of the line (known as the Ferranti rise/effect) [2]. Voltage leads current by ninety degrees for inductive loads. The stray capacitance in the load side discharges into the inductive load which triggers a high frequency oscillation during current interruption. The risk associated with this high frequency oscillation is that the dielectric strength of the extinguishing medium may not recover as fast as the high rate of rise of the recovery voltage between the breaker contacts. As a result, this could lead to the dielectric breakdown of the arc channel and subsequently re-ignition [9]. One of the challenges associated with shunt reactors connected to HV transmission lines is that the protection settings for these lines are often set to single-phase auto-reclosing to limit outage times. As a result, current/voltage will be induced into the faulted phase from the adjacent healthy phases. This can result in a secondary arc which develops in the arc channel of the faulted phase. A neutral earthing reactor is installed with the shunt reactor to increase the zero sequence impedance thereby limiting the effect of the secondary arc [2].

2.6.2.2 Series Reactors

Series reactors are utilised in power systems as fault current limiting devices as well as for restricting the inrush current in capacitor bank installations. These reactors inherently contain stray capacitance which results in very high frequencies during transients.

This high frequency transient could far exceed the circuit breaker TRV rating/capability. In the case of the TRV exceeding the circuit breaker rating, capacitance may be added in parallel to the fault current limiting reactors to reduce the frequency of the transient [32].

2.7 Metal Oxide Varistors (MOVs)(Zinc Oxide (ZnO) Arresters) (Surge Arresters (SAs))

The objective of a surge arrester is to protect equipment insulation from potentially harmful voltage surges. This is achieved by clamping the surge voltage to specified limits (known as the protective level) [33]. A surge arrester behaves as a variable resistor under normal system voltage conditions, the surge arrester behaves like an open circuit or infinite resistance. When an overvoltage occurs, the surge arrester conducts sufficient current such that the voltage is clamped within a specified range of peak values. The peak voltage appearing across the terminals of a surge arrester during a period of discharge current is the voltage limiting characteristic commonly referred to as the discharge voltage or residual voltage [34][35].

An arrester is typically defined by the characteristic V-I curve. In the case of metal oxide arresters, the characteristic curve is categorized into three regions [5] (refer to Figure 2-29):

- Region 1 (MCOV or pre-breakdown region): The surge arrester is not in significant conduction mode, where typically less than 1 mA of power frequency capacitive current flows through the surge arrester. This is known as the leakage current. The arrester predominantly operates within this region, where very little heat is generated. The surge arrester is highly sensitive to temperature changes within this region of the curve.
- Region 2 (TOV/Switching surge region): Current that flows through the surge arrester for this region of the V-I curve ranges from 1 mA to 2 kA and is resistive in nature. The conductivity in this region due to the overvoltage will result in a significant temperature rise of the surge arrester. After a few seconds, the surge arrester will fail due to thermal runaway. Thermal runaway of a surge arrester refers to a specific event where the continuous power loss of the surge arrester exceeds the thermal dissipation capability of the housing and connections [34].
- Region 3 (Lightning surge region): The current through the surge arrester for this region ranges between 1 kA and 100 kA. Current increases proportionally with voltage within this region. The durations of these high current surges are much shorter.

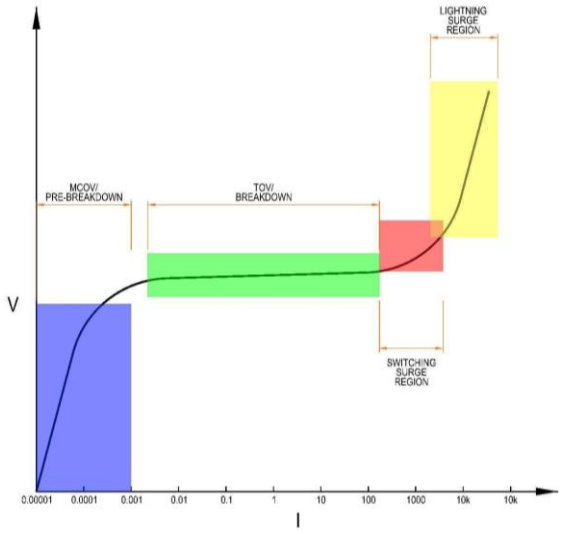

Figure 2-29: Typical V-I curve of MOV with the characteristic regions [5]

Surge Arresters are classified into two groups [34]:

- Station Class
- Distribution Class

These surge arrester classes are further categorised into their operating duties i.e. high, medium, and low duty. The operating duty of a surge arrester is its ability to absorb energy from switching events or transfer charge from lightning events and subsequently thermally recover to continuous operating

voltage conditions [34]. The thermal energy rating of an arrester is defined as the maximum specified energy that the arrester may be subjected to in three minutes specified in kJ/kV of the MCOV [34].

2.8 Probabilistic Approach to TRV Evaluation

Traditionally TRV's have successfully been analyzed using a deterministic approach. This method usually indicates that the maximum TRV occurs for a three-phase unearthed fault near the circuit breaker [3]. However, there is a higher probability of a fault occurring at a different location along the transmission line than the occurrence of a three-phase unearthed fault next to the circuit breaker.

There are currently two probabilistic approaches available for the evaluation of TRVs across circuit breaker terminals for a series compensated transmission line, using the Monte Carlo statistical approach [36] or the Kernel Density Estimation via Diffusion Process [37].

2.9 Existing Statistical Analysis Methods

2.9.1 Monte Carlo Approach

The Monte Carlo approach is a set of computational algorithms that attain a result based on repeated random sampling. The Monte Carlo involves first generating random variables having a uniform distribution and then transform them into random variables having the required distribution. Computations are performed on the sampled data to realize an output variable. Statistical analyses are then conducted on the output variable to determine the characteristics of the output data (i.e. mean, variance, reliability etc.). This random sample is a subset of a population which would likely exhibit the same properties of the population from which it is extracted.

As the variance grows, a larger number of samples are required to have the same amount of confidence.

The Monte Carlo Method was investigated in [36], which describes the maximum TRV that a circuit breaker would be exposed to during fault clearing on a series capacitor compensated transmission line. The probabilistic approach provides a more realistic evaluation of power system to understand the worst case TRV stresses that a circuit breaker may be exposed to. Typically five probabilistic criteria may be evaluated in assessing TRVs [17]:

1. Fault Type (e.g. Phase-to-Earth, Phase-to-Phase etc.)
    a. The probabilities of the fault types are developed utilizing historical data of the power system being evaluated.
2. Fault Location (along the transmission line)
3. Fault Incidence (voltage that is expressed as a function of the voltage phase angle)
4. Fault Clearing Time (determined based on the number of cycles taken to clear the fault)
5. Fault Duration (measured in seconds)

In this case the fault type, location, incidence, and fault clearing time are considered to be normally distributed while the fault duration is modelled assuming a Raleigh distribution. The conclusions of the simulations conducted indicate that there is a low probability of occurrence of higher magnitude TRVs as compared to the lower magnitude TRVs. A risk index was developed to determine the probability of an induced TRV exceeding its design value.

2.9.2 Kernel Density Estimation via Diffusion Process

Kernel Density Estimation (KDE) is a non-parametric estimation of an unknown probability density function from a given data set where conclusions can be made on the population based on the finite data sample [38]. A kernel is a weighting function which is defined and centered on a data point. Subsequently, these kernel functions are added together to result in a KDE. This result is then normalized by dividing by the number of Kernel Functions. Kernel Functions are typically:

- Non-negative functions since probabilities are non-negative.
- Symmetric on either side of the data point.
- Decrease on either side of the data point.

The bandwidth of a Kernel Function will determine how detailed the resultant KDE will result be. The larger the bandwidth, the less detailed the KDE and vice versa (see Figure 2-30).

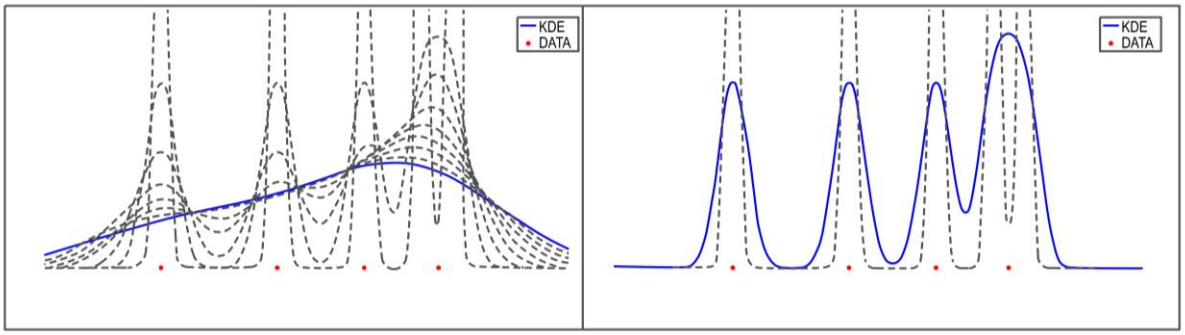

Figure 2-30: Increased bandwidth (a) vs reduced bandwidth (b) [39]

The application of the KDE was evaluated in [37]. In comparison to the Monte Carlo approach, KDE is less intensive to available computational capabilities. Moreover, the KDE approach requires fewer samples and as a result reduces the simulation time required. The approach utilized in [37] is to firstly determine the TRV and RRRV utilizing the Monte Carlo approach. A Gaussian Kernel Density Estimator is then established using the results of the Monte Carlo simulation. One of the key parameters in defining the optimal Gaussian KDE is the bandwidth. In order to achieve the optimal bandwidth, *t*, a diffusion estimator is utilized by calculating the Mean Integrated Square Error (MISE). The Probability Density Functions of the TRV and RRRV can then be plotted.

Section 2.10 presents the transient modelling theory. The factors that should be taken into consideration when developing simulation models as well as conducting the simulations are discussed.

2.10 Transient Modelling Theory

An electrical system may either be represented by a lumped parameter model or distributed parameter model. A lumped parameter model does not model surge propagation behaviour [33]. This approach is applicable where the largest dimension of the electrical system is smaller in comparison to the wavelength of the highest significant transient frequency. Distributed parameter models, in comparison to the lumped model, require a finite amount of time for a disturbance which occurs in the electrical system to be transmitted to every other point in the system. Mathematical models are utilized in representing power components which have frequency dependent parameters applicable to specific frequency ranges. As indicated previously, frequency ranges of transients are classified into four groups [7]:

- Low frequency Transients
- Slow Front Transients
- Fast Front Transients
- Very Fast Front Transients

The simulation of transient phenomena requires that the components and associated system be modelled appropriately taking into consideration the frequency range.

Since the resistance and inductance of transmission line conductors have a strong frequency dependence due to skin effect, this results in the electromagnetic waves being distorted as they propagate along the transmission line due to the different frequency components travelling at different

speeds. Therefore, appropriate distributed parameter models (which was utilized for the simulation models developed for this study) must be used when conducting TRV studies.

2.10.1 Simulation Time Step

The time step is of critical importance in determining the accuracy of the simulation. Therefore it is advised that a minimum of ten simulation time steps should fall within one period of the highest frequency that appears in the system due to the transient event (Equation 2-110) [7][8] .

$$\Delta t \leq \frac{1}{10 \times f_{max}} \tag{2-110}$$

2.10.2 Overhead Transmission Lines

The lumped and distributed-parameter models have been developed for overhead lines in the time-domain. The selection of the type of model to be used is dependent on the line length and the highest frequency of the transient phenomena being analyzed [40].

Pi-models or T-models are representative of lumped models which describe an overhead line where resistance, inductance, capacitance, and conductance are calculated at a single frequency. These models are adequate for steady state analysis. However they may also be useful at the frequencies at which the components of the model mentioned are being evaluated at [40].

Distributed parameter models are more accurate for long overhead lines. Constant-parameter and frequency-dependent parameter models are typically used for long overhead lines [40].

Table 2-6 describes factors that should be considered when modelling an overhead line.

Table 2-6: Factors to consider when modelling overhead lines [33][40]

Factors	Low Frequency Transient	Slow-Front Transient	Fast Front Transient	Very Fast-Front Transient
Overhead Line Model Representation	Multiphase model with lumped and constant parameters. Frequency Dependent model may be required for transients above 1kHz.	Multiphase distributed-parameter model for the whole length of the overhead line.	Multiphase distributed-parameter model for the whole length of the overhead line.	Single-phase distributed parameter model.
Conductor/Line Asymmetry	Important.	Important.	Important. Negligible for single-phase models.	Negligible.
Frequency Dependent Parameters	Important.	Important.	Important.	Important.
Corona Effect	May be important if the overvoltage exceeds the corona inception voltage.	Negligible.	Very Important.	Important.

Resistance, inductance, and capacitance of a transmission line are frequency dependent and are calculated at a single frequency for a constant distributed parameter transmission line model.

Resistance and inductance have a strong frequency dependence due to skin effect in the conductors and the ground plane while the capacitance and conductance have a weak frequency dependence due to their dependence to the surface area between the conductor and the ground plane. This dependence of the resistance and inductance is derived in the following equation for the internal impedance of cylindrical conductors per unit length [41]:

$$Z_{li} = \frac{1}{2\pi b\sigma\delta_c} + j\frac{1}{\omega 2\pi b\sigma\delta_c} \tag{2-111}$$

- $2\pi b$ represents the circumference of the conductor where 'b' is the outer radius of the conductor (m).
- δ_c is the skin depth or depth of penetration of the electric fields (m).
- σ represents the conductivity of the conductor (S/m).

The skin depth is defined as follows:

$$\delta_c = \frac{2}{\sqrt{\omega\mu\sigma}} \tag{2-112}$$

- μ represents the permeability of the medium (H/m).

Figure 2-31 and Figure 2-32 show the effect of frequency on the internal resistance and inductance of a conductor such as copper. Therefore, the shape of the surge gradually distorts as it propagates along the transmission line due to the different frequency components travelling at different speeds and varying attenuation factors. This emphasizes the need to accurately model transmission lines to include the frequency dependent effects in time domain transient studies [42].

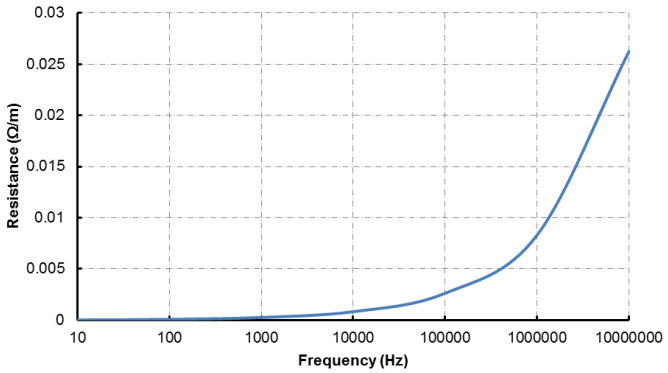

Figure 2-31: Internal AC resistance of a copper conductor

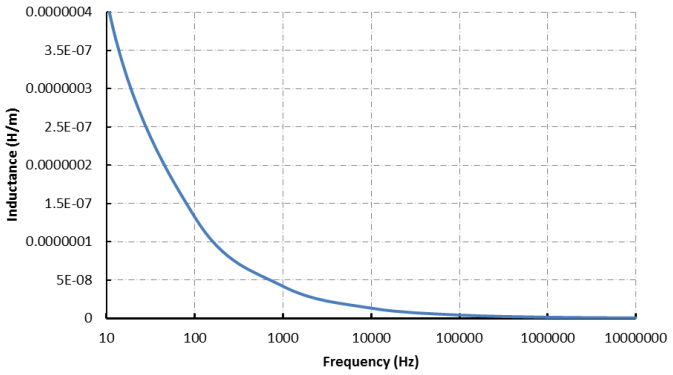

Figure 2-32: Internal inductance of copper conductor

The number of π-sections required for the correct representation of the overhead line is dependent on the highest expected transient frequency per unit length of an overhead line [7]. The maximum frequency is calculated based on the following [8]:

$$f_{max} = \frac{1}{\pi l \sqrt{LC}} \quad (2\text{-}113)$$

l: Line length
L and C are defined per unit length of overhead line conductor

The velocity of the electromagnetic wave is defined as [7][8]:

$$v = \frac{1}{\sqrt{LC}} \quad (2\text{-}114)$$

Therefore the length of a π-section should not exceed [7][8]:

$$l = \frac{v}{5 f_{max}} \quad (2\text{-}115)$$

An appraisal of existing, relevant literature by identifying, evaluating, and interpreting the research evidence is presented in section 2.11. The literature review will guide the development of the research questions and objectives by identifying the research gaps.

2.11 A literature review of TRV case studies

The following discussion is a literature review of technical papers that have relevance to the research being conducted.

The objective of the study in [43] was to determine the TRV parameters for the revised switchgear purchasing specification required for the 132 kV Jordanian Power System (JPS). The motivation for this study was the change in the network configuration that entailed the interconnection of a neighbouring power system.

The study was conducted and evaluated for two types of faults namely three-phase-to-ground faults and single-phase-to-ground faults. Two positions of faults were considered for this study, a line-side terminal fault and a busbar terminal fault. EMTP was used to conduct the study to determine the TRVs. The 132 kV network was represented in detail and the remaining network was represented by a reduced network equivalence.

The results from the study showed that the RRRV of the circuit breakers evaluated for system-fed faults ranged up to 1.8 kV/µs. As a result, the RRRV of 2 kV/µs for rated fault current was selected. The peak voltage that the circuit breakers were exposed to, reached a magnitude of 1.9 p.u. The simulations yielded RRRVs for transformer faults of up to 23.36 kV/µs. This was attributed to the transformer leakage inductance and capacitance to earth.

This study is relevant because it is similar to this research where new generation sources are connected by looping in and looping out of an existing transmission line. The above study did not consider a compensated circuit and where the fault levels are low. Just like this research, two types of faults were evaluated namely three-phase-to-ground and single-phase-to-ground.

A study on the Central Electricity Generating Board (CEGB) 400 kV power system was conducted to determine the TRV parameters for switchgear to develop a revised specification for the purchase of switchgear [44]. The reason that this study was conducted was due to the IEC specification for TRVs at the time not being adequate and often exceeded. Additionally, no parameters were specified for low fault currents.

Faults applied in this study were single-phase-to-earth and three-phase-to-earth faults. The line-side terminal fault and busbar-side terminal fault positions as well as transformer-secondary faults were evaluated. The scope of the study was limited to the 400 kV system.

The results were analysed statistically by quantifying the rate of rise of recovery voltage and peak recovery voltage as a function of the fault current. The results of the study for the first-phase-to-clear for a three-phase-to-ground fault, yielded a RRRV up to 3.18 kV/µs with most values below 1.5 kV/µs. This concluded that the RRRV rating of 2 kV/µs was acceptable. The last-phase-to-clear for the same study resulted in a RRRV up to 3.46 kV/µs. The peak recovery voltages ranged from 0.06p.u. to 1.51p.u. for the first peak voltage while the last peak voltage yielded a range of 1.04p.u. to 1.7p.u.

This study concluded that the effect of system topology changes such as line outages or the integration of additional generating capacity affected the RRRV of TRVs significantly but well below the 2 kV/ µs rating level.

This study is relevant because it is similar to this research where new generation sources are connected by looping in and looping out of an existing transmission line. In addition, the impact of line outages was also considered. The above study did not consider a compensated line and where the fault levels are low.

The results of using surge arresters to control both TRVs of a series compensated 330 km 550 kV transmission line and switching surges were discussed in [45]. Series capacitors which are an important part of the proposed study are known to increase the TRV requirements of LCBs. The sequence of opening the LCBs on the remote ends of the series compensated line (in this research this could occur when the circuit breaker at the new substation where the existing line is looped in and looped out) is critical to the impact of the TRV of the LCB being investigated.

Self-triggered protective gaps were applied to the series capacitor and showed that if they operate prior to the LCB, the TRV peak is reduced and limited. In this research, self-triggered protective gaps are not used. However, bypass circuit breakers are used and therefore similar conclusions are applicable.

The analysis of the series compensated system in North East Turkey and evaluation of various methods to limit the TRV duty of the associated LCBs for the aforementioned system were detailed in [46]. The use of surge arresters, switched opening resistors on circuit breakers, surge arresters applied across the contacts of the LCBs as well as fast bypassing of the series capacitor were investigated. The increase of TRVs is prominent due to the phenomenon of trapped charge for relatively small fault currents where the spark gap protective level is not reached and triggered.

The use of line surge arresters, as described in the previous reference, suggests that the rate of failure of these equipment is low if applied correctly. The surge arresters connected in transformer, reactor or adjacent line bays should be utilized for limiting TRVs of LCBs.

Closing resistors are commonly installed on 400 kV SF_6 circuit breakers however they are not relevant to the proposed study because the phenomenon of TRVs occurs during the opening of the circuit breakers.

A further solution was investigated which was the installation of surge arresters across the terminals of circuit breakers and grading capacitors. The surge arresters are exposed to the power frequency voltage when the circuit breaker is opened and energized at either/both terminals as well as during a switching operation of the circuit breaker. The analysis considered the voltage stress that the surge arrester installed across the circuit breaker would be exposed to, the duration for which this voltage would be applied, and the energy dissipation requirement based on the most onerous TRVs. This configuration was applied successfully in the Turkish grid.

Fast bypassing of series capacitors by using a bypass circuit breaker prior to current interruption of the circuit is also a method in limiting the TRVs that LCBs are exposed to. However, this is dependent on a high level of reliability of bypassing the series capacitor prior to fault clearing of the line. This may not be easily achieved based on various factors such as magnitude of the fault current, fault type, location,

and energy dissipation capability of the surge arrester across the series capacitor. A forced triggering of gaps may not occur as indicated previously.

Simulations were conducted at various significant points along the series compensated network. The faults applied in the network were three-phase and three-phase-to-ground faults. The LCBs were opened 80-100 ms after the fault was applied.

The TRV mitigation techniques discussed above are important considerations in the evaluation of TRVs. These mitigation techniques were not further investigated as part of this study.

This dissertation presents a study conducted on a series compensated circuit will be evaluated for future considerations. This will be achieved by integrating a voltage source by looping in and looping out (inserting a voltage source along the line) at various points along a series compensated transmission line. A three-phase-to-ground fault will be applied at various points along this circuit. The impact of varying the fault contribution of the new source on the LCB rating will be analyzed. The results of these simulations will then be compared to the conventional method based on the current configuration. The peak recovery voltage and the rate of rise of recovery voltage will be the key criteria in comparing the two approaches.

The objective of this research is not to compare the results with similar studies conducted by other utilities but rather to compare the simulated TRVs to the circuit breaker TRV ratings. This research is intended to formulate a procedure for evaluating the TRVs of LCBs connected to series and shunt compensated transmission lines.

Chapter 3 will present the high-level procedure developed for the purpose of TRV studies in an evolving series and shunt compensated transmission line. A case study will then be presented that applies the procedure developed to analyse the TRV performance of LCBs connected to an evolving series and shunt compensated transmission line. Verification of the model, that was developed on a simulation package, will be conducted against fault waveform data and the results presented. Once the model was verified, simulations were performed for the various scenarios and the analysis and results will be presented.

3 CASE STUDY: TRV EVALUATION OF LCBs CONNECTED TO AN EVOLVING SERIES AND SHUNT COMPENSATED TRANSMISSION LINE

3.1 Procedure to conduct TRV studies for LCBs connected to evolving series and shunt compensated transmission lines

Figure 3-1 presents a high-level procedure to follow to conduct a TRV study for LCBs connected to evolving series and shunt compensated transmission lines.

Firstly, the existing network data must be established. This will include the fault level of the network, the fault type to apply to the simulation model (i.e. three-phase, three-phase-to-ground etc.) and the phase angles of voltage sources. Next, the simulation model is to be developed by applying the appropriate component models. Input data such as transmission line tower geometry, conductors, conductor geometry, surge arrester V-I curves, series capacitor size damping circuit sizing, shunt reactor size etc. will be required to develop an accurate model of the network being studied. Future network plans associated to the line being studied must be identified as this will provide input to the various scenarios to be modelled and simulated. The model should then be validated against existing fault waveform recording data. Once the model is validated, the simulations for the various scenarios may be conducted. The results of the simulations will determine fault current limits that would result in the peak recovery voltage and RRRV limits being exceeded. These fault current levels will then form a trigger when these magnitudes are being reached to reassess the TRV ratings of LCBs in the circuit. This may either result in the LCB being uprated or mitigation strategies applied.

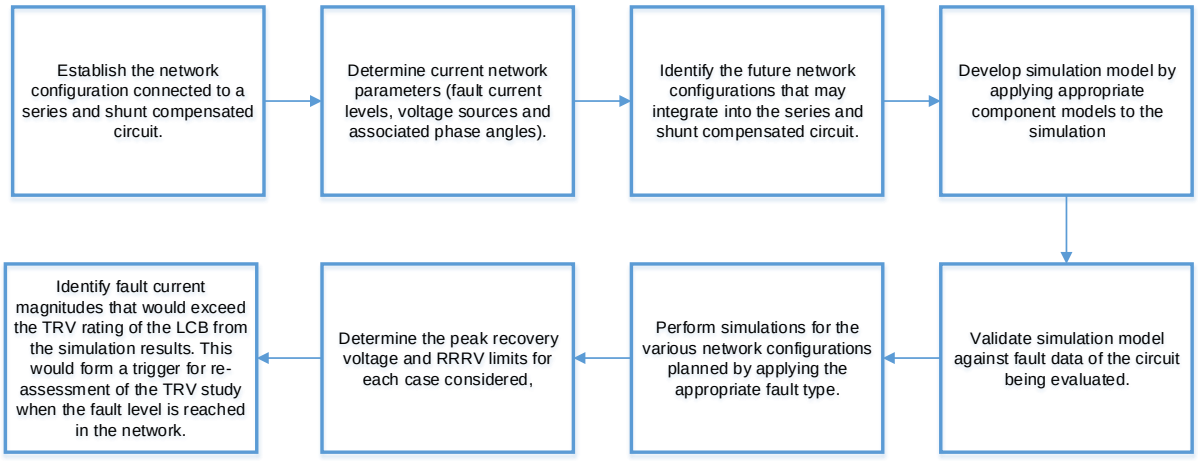

Figure 3-1: High level procedure in evaluating the TRV for LCBs connected to evolving, series and shunt compensated transmission lines

The network configuration that will be utilised in the evaluation of the TRVs for LCBs connected to a series and shunt compensated transmission line will be presented in Section 3.2.

3.2 Network Configuration

The network architecture selected is from one of the power utilities in Southern Africa (Figure 3-2). This network was selected based on the location of the network relative to the load centres being over 200 km away. Additionally, the fault level in this network is low at approximately 5 kA for three-phase faults. The series and shunt compensated transmission line investigated was Line A-B 1 which is approximately 252 km long.

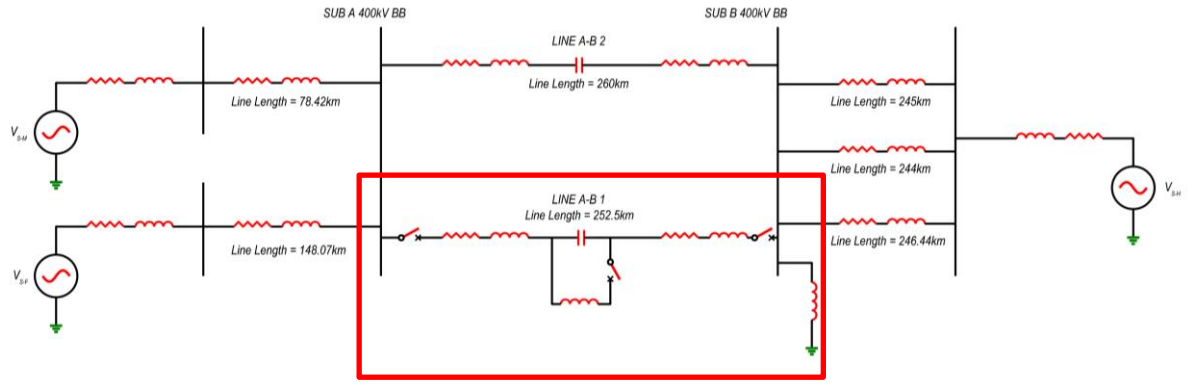

Figure 3-2: Case 1 - Base case network configuration to be analysed for the case study

A voltage source was integrated along Line A-B 1 and the resultant series compensated circuit was analysed. Though TRVs for circuit breakers are is a well-known and widely researched phenomena, this research intends to present the impact of integrating a voltage source along an existing series and shunt compensated transmission line on the TRVs. This voltage source may be representative of a renewable generation source connected through a collector distribution station which in turn connects onto the transmission network (in this case a series and shunt compensated circuit) to transmit bulk power through a power corridor to the load centres. This scenario was simulated and analysed to determine the TRV ratings of the LCBs at Sub A and B.

Two scenarios were simulated and analysed with the integration of voltage source Sub C. The second scenario (Case 2) considered a voltage source Sub C integrated between Sub A and Sub B such that the series capacity bank was between Sub A and Sub C (Figure 3-3). The position of Sub C was varied along Line A-B 1 (by varying the line length of Line A-C 1) and the fault current contribution from Sub C was also varied to evaluate the impact on the TRVs for the LCBs at Sub A and Sub C. Two line lengths for Line A-C 1 were evaluated being 200 km and 240 km respectively. The choice of the two positions specified were based on practical compensation factors that can be applied to the existing network configuration without altering the series capacitor rating. The fault current contribution from Sub C was varied between 5 kA and 10 kA. The fault current specified for Sub C (5 kA) was selected based on the fault current magnitudes observed at Sub A and Sub B in case 1. The fault current magnitude of 10 kA for Sub C was selected to observe the impact that a change in fault current contribution has on the TRV that the LCBs were exposed to.

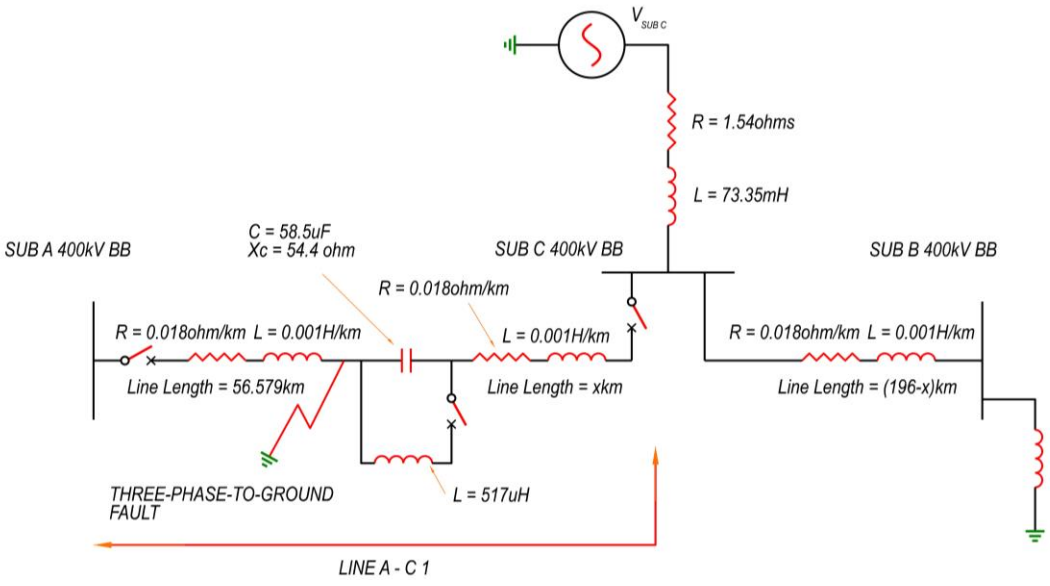

Figure 3-3: Case 2 - network configuration to be analysed for the case study

The third scenario (Case 3) considered a voltage source, Sub C, integrated between Sub A and Sub B such that the series capacity bank was between Sub B and Sub C (Figure 3-4). The position of Sub C was varied along Line A-B 1 (by varying the line length of Line B-C 1) and the fault current contribution from Sub C was also varied to evaluate the impact on the TRVs for the LCBs at Sub B and Sub C. Two line lengths for Line B-C 1 were evaluated being 212.5 km and 232.5 km respectively. The choice of the two positions specified are based on practical compensation factors that can be applied to the existing network configuration without altering the series capacitor rating. The fault current contribution from Sub C was varied between 5 kA and 10 kA. The fault current specified for Sub C (5 kA) was selected based on the fault current magnitudes observed at Sub A and Sub B in case 1. The fault current magnitude of 10 kA for Sub C was selected to observe the impact that a change in fault current contribution has on the TRV that the LCBs were exposed to.

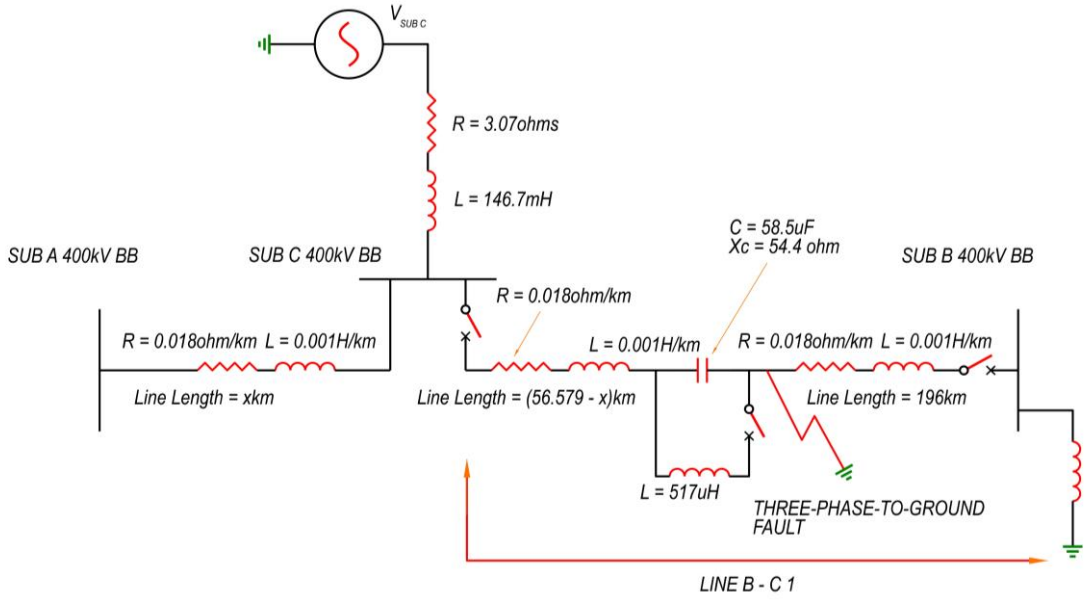

Figure 3-4: Case 3 - network configuration to be analysed for the case study

The consequence of integrating into a compensated circuit may result in stressing the existing HV equipment in the circuit due to shortening the transmission line and introducing fault current to the circuit without necessarily modifying this equipment. Therefore, the TRV capability of the existing LCBs of the compensated circuit needed to be assessed relative to the TRV stresses imposed on them. The result of this assessment from a deterministic approach may suggest that the LCBs be upgraded. The deterministic approach from an IEC perspective considers three-phase-to-ground faults as the measure for TRV evaluations.

The modelling of an electrical system requires that the components and associated systems be modelled appropriately to evaluate the transient phenomena taking into consideration the frequency range. The various components making up the network architecture (i.e. voltage sources, transmission lines, surge arresters, series capacitors and peripheral circuits) were then modelled in ATPDraw. Section 3.3 will present the modelling of the various components based on the input parameters provided.

3.3 Component Modelling

3.3.1 Overhead Transmission Line Modelling

The following diagram shows the two transmission line tower configurations utilized in the simulation (Figure 3-5).

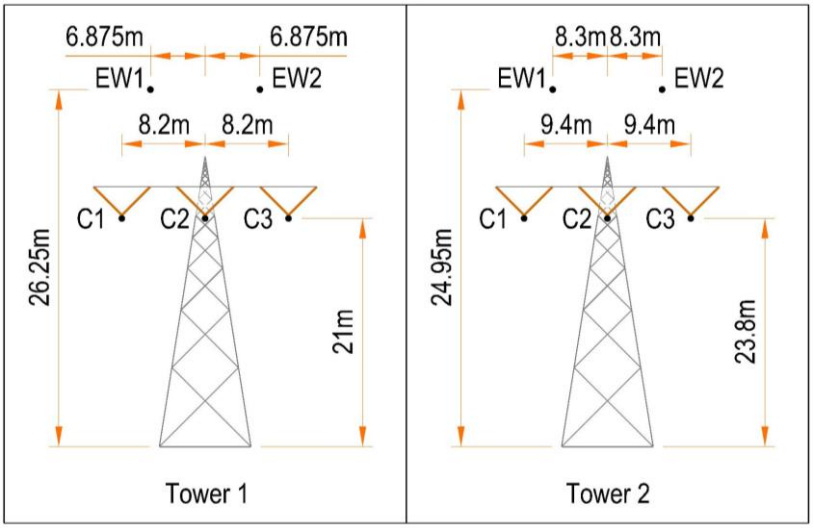

Figure 3-5: Transmission line tower configuration models

Each conductor bundle (C1, C2 and C3) consists of two sub-conductors spaced 38cm apart. The earthwire conductors were not considered for the simulation. The following transmission line steady state parameters/constants were calculated for the positive sequence metallic mode:

Table 3-1: Transmission line model parameters

Parameter	Value	Unit
Resistance		
Area	744	mm^2
Electrical Resistance	0.0437	Ω/km
Resistivity	$32.5x10^{-9}$	Ωm
Phase Spacing	9400	mm
Number of sub-conductors	2	
Sub-conductor spacing	380	mm
Conductor diameter	35	mm
Conductor radius	17	mm
D_m	11839	mm
μ	$1.26x10^{-6}$	H/m
f	50	Hz
ω	314.16	rad/s
M_r	1.96	
K_s	0.8	for M_r = 1.96
R	$13.14x10^{-6}$	Ω/m
Inductance		
L_i/L_o	0.96	for M_r = 1.97
R'	14	mm

Parameter	Value	Unit
D_{3A}	72.84	mm
L'_A	1.02×10^{-6}	H/m
Capacitance		
D_{eq}	82.13	mm
ϵ	8.85×10^{-12}	
C_A'	11.19×10^{-12}	F/m
Z_0 (Surge Impedance)	301.70	Ω

3.3.2 Source Modelling

In order to represent the network behind the circuit being studied, its Thévenin equivalent circuit was calculated to give the correct fault current (I_s) contribution at the point of connection (Figure 3-6).

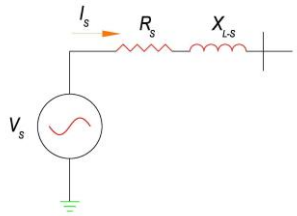

Figure 3-6: Thévenin equivalent modelling

The sources of the network modelled for the circuit being analysed were determined one busbar away. Three sources were modelled utilising the peak fault current and the associated X/R ratio at those respective busbars to determine the source impedances (Table 3-2). The input data are as follows:

Table 3-2: Input data for source impedances for the

Parameter	Source "A'	Source 'B'	Source 'C'
Peak Fault Current (kA)	4.2	3.45	3
X/R Ratio (peak)	16.77	17.59	13.69

The magnitude and polar angle of the impedance are calculated in the following manner:

$$Z = \frac{V_{L-L}}{\sqrt{3} \times \frac{I_{peak}}{\sqrt{2}}} \Omega \quad (3\text{-}1)$$

$V_{L\text{-}L}$: RMS Voltage Line-to-Line

$$\theta = \arctan\left(\frac{X}{R} ratio\right) \quad (3\text{-}2)$$

The source impedances are therefore represented as follows (Figure 3-7):

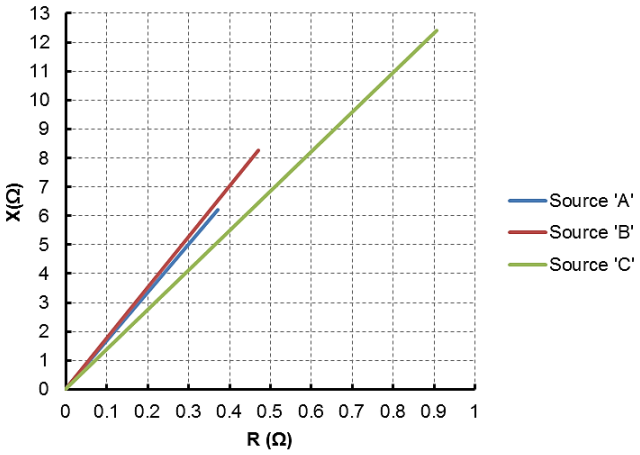

Figure 3-7: X-R diagrams of source impedances

The resistance is calculated as follows:

$$R = Z \times \cos(\theta)\Omega \tag{3-3}$$

Similarly, the inductive impedance is calculated as follows:

$$X_L = Z \times \sin(\theta)\Omega \tag{3-4}$$

The inductive impedance can then be calculated using the formula:

$$L = \frac{X_L \times 1000}{2 \times \pi \times 50} mH \tag{3-5}$$

The results of the calculations of the source impedances are showed in Table 3-3.

Table 3-3: Calculated source impedance parameters

Parameter	Source 'A'	Source 'B'	Source 'C'
Voltage (kV)	400	400	400
Z (Ω)	6.23	8.28	12.44
Angle (θ)	1.51	1.51	1.50
R (Ω)	0.37	0.47	0.91
X_L (Ω)	6.22	8.26	12.41
X (mH)	19.79	26.30	39.50

3.3.3 Surge Arrester Modelling

The surge arrester installed across the series capacitor bank was modelled with the following parameters (Table 3-4):

Table 3-4: Surge Arrester Parameters

Parameter	Value
Rated Voltage (U_r)	92.6 kV
Maximum Continuous Operating Voltage (U_{MCOV})	262 kV

The corresponding V-I curve is plotted for the surge arrester modelled (Figure 3-8).

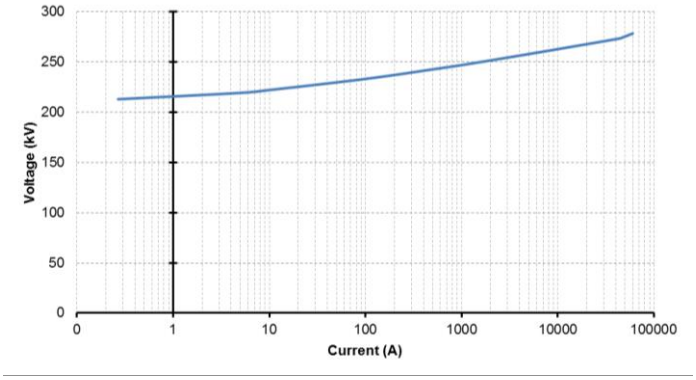

Figure 3-8: V-I curve of the surge arrester

The V-I curve data for the surge arrester can be found in Appendix 7.1.

3.3.4 Line Arrester Modelling

The arresters modelled at the remote ends of the compensated transmission line were modelled with the following parameters (Table 3-5, Figure 3-9):

Table 3-5: Line Arrester Parameters

Parameter	Value			
Rated Voltage (U_r)	312 kV			
Maximum Continuous Operating Voltage (U_{MCOV})	250 kV			
Nominal Discharge Current	20 kA			
Line Discharge Class	4			
Maximum Residual Voltage (MRV) for 8/20µs current impulse	1 kA	10 kA	20 kA	40 kA
	603.5 kV	710 kV	773.9 kV	852 kV

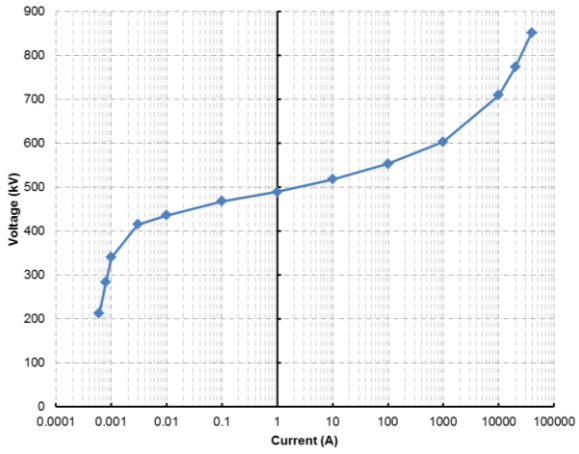

Figure 3-9: V-I curve of rated line arrester

The characteristic V-I curve data are detailed in Table 3-6:

Table 3-6: V-I data of the line arrester

Percentage (%)	Current (A)	Voltage (kV)
30	0.0006	213
40	0.0008	284
48	0.001	340.8
58.5	0.003	415.35
61.5	0.01	436.65
66	0.1	468.6
69	1	489.9
73	10	518.3
78	100	553.8
85	1000	603.5
100	10000	710
109	20000	773.9
120	40000	852

3.3.5 Series Capacitor Bank

The series capacitor bank modelled for the simulation has the following parameters (Table 3-7: Series capacitor bank parameters):

Table 3-7: Series capacitor bank parameters

Parameter	Value
Voltage (V)	400 kV
Capacitor Reactance (X_C)	54.4 Ω
Capacitance	58.5 µF
Nominal Current Rating (I)	1703 A
Capacitor Bank MVAr Rating ($\sqrt{3} \times V \times I$)	1180 MVA
Compensation Factor	68%

3.3.6 Compensation Factor

The compensation factor of the transmission line was calculated based on the ratio of the capacitor bank capacitive reactance to the transmission line inductive reactance. The details of the compensation factor are indicated below (Table 3-8: Compensation factor of existing series compensated transmission line):

Table 3-8: Compensation factor of existing series compensated transmission line

Line length	Voltage	Inductance (H/km)	Line inductive reactance	Capacitor Bank capacitive reactance	Compensation Factor
km	kV	H/km	$X_L = 2\pi fL\ (\Omega)$	$X_C = \frac{1}{2\pi fC}\ (\Omega)$	%
252.579	400	0.001018	80.79	54.4	67

3.3.7 Current Limiting Damping Circuit

The purpose of the series capacitor bank current limiting damping circuit is to allow for the discharge of the capacitor bank after the series capacitor bypass circuit breaker closes. The discharge current should be limited to the current limits of the capacitor fuses and bypass circuit breaker. The current limiting damping circuit impedance consists of the loop impedance and the reactor impedance (Figure 3-10).

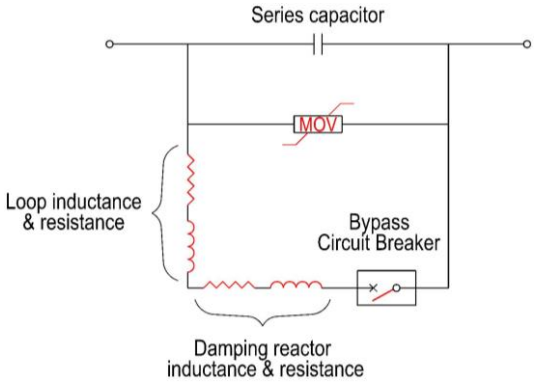

Figure 3-10: Current Limiting Damping Circuit

The parameters of the current limiting circuit modelled were as follows (Table 3-9):

Table 3-9: Current Limiting Damping circuit parameters

Parameter	Value
Loop resistance	1 mΩ
Loop inductance	20 µH
Reactor resistance	58.3 mΩ
Reactor Inductance	517 µH

The discharge frequency was calculated to be 898 Hz using Equation (2-104) where the inductance is the combination of the loop inductance and the reactor inductance.

3.3.8 Line Circuit Breaker TRV specifications

The line circuit breakers installed in the circuit being investigated have a rating of 420 kV. The line circuit breakers have the corresponding TRV ratings (Table 3-10) as discussed in section 2.3.7.

Table 3-10: TRV ratings of a 420 kV circuit breaker [4]

Test Duty	First-Pole-to-Clear	Amplitude Factor	First Reference Voltage	Time	TRV Peak Voltage	Time	RRRV
	k_{pp}	k_{af}	u_1 (kV)	t_1 (µs)	u_c (kV)	t_2 or t_3 (µs)	kV/µs
T100	1,3	1,40	334	167	624	668	2
T60	1,3	1,50	334	111	669	666	3
T30	1,3	1,54	-	-	687	137	5
T10	1,3	1,76	-	-	787	112	7
OP	2	1,25	514	334	857	1336	1,54

The data from Table 3-10 may be translated into the two and four-parameter envelope accordingly (Figure 3-11):

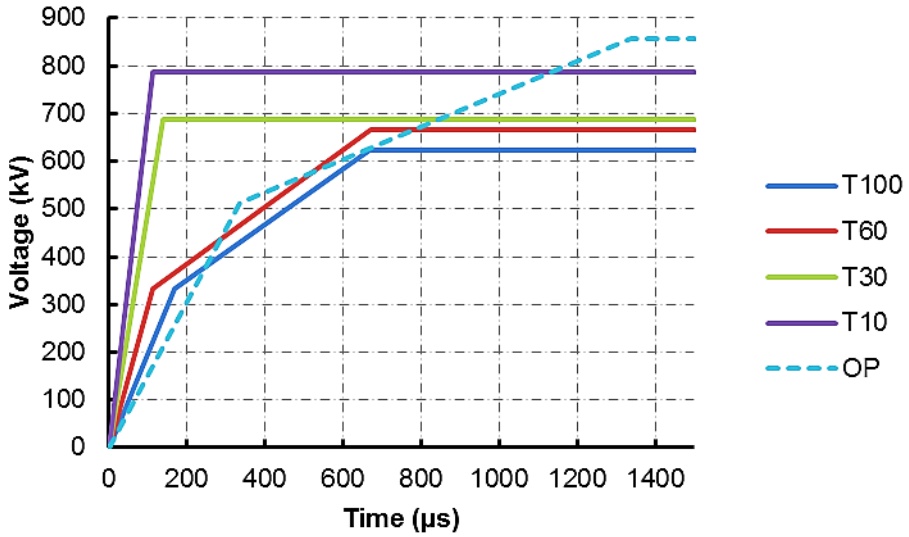

Figure 3-11: TRV ratings for various test duties of a 420 kV circuit breaker

3.3.9 Equivalent Capacitance of HV equipment

In order to accurately model a circuit for TRV evaluation, it is imperative to represent all inductances and capacitances near circuit breakers that would generate oscillations due to transient events. When three-phase faults in ungrounded systems are being examined, it is only necessary to include the positive-sequence components. Zero sequence components must be included when evaluating three-phase-to-ground faults in effectively grounded systems. When single-phase to ground faults are analysed, zero-sequence components must also be included [3].

Typically, little or no information is provided by manufacturers on the positive or zero sequence capacitance of equipment. For solidly grounded apparatus the zero-sequence capacitance is equal to the positive sequence capacitance, $C_0 = C_1$. Reference [3] provides typical ranges of capacitance for various HV equipment. Table 3-11 indicates equipment that is modelled as derived from the circuit being investigated:

Table 3-11: Equivalent capacitance of HV equipment

Equipment	Capacitance
Capacitor Voltage Transformer (362 kV)	2 150 pF - 9 500 pF
Surge Arrester	80 pF -120 pF
Current Transformer (72,5 kV – 800 kV)	150 pF – 450 pF
Bus Capacitance	8,2 pF/m – 18 pF/m
Reactor	150 pF – 250 pF
Circuit Breaker (Opening capacitance)	Not specified

3.3.10 Fault Arc Resistance

The dynamic behavior of a fault arc in a power system simulation needs to be modelled accurately in order to simulate power system transients realistically. The arc model utilized in the simulation model for this research is based on the work developed in [47]. The dynamic arc model is based on the theory of switching arcs. The dynamic arc characteristic described in [47] is based on the arc equation of *Hochrainer*:

$$\frac{dg}{dt} = \frac{1}{\tau}(G - g) \tag{3-6}$$

τ: Time constant
G: static arc conductance
g: time-varying arc conductance

The static arc conductance was shown to be defined as follows [48]:

$$G = \frac{|i|}{V_{arc} l_{arc}} \tag{3-7}$$

i: Arc current
V_{arc}: Static arc voltage gradient
l_{arc}: Static arc length

The static arc voltage gradient was concluded to be on average 15 V/cm for a range of fault current [48]. The arc length and the time constant are also considered to be constant. The time constant is defined as follows [48]:

$$\tau = \frac{\alpha I_{arc-peak}}{l_{arc}} \tag{3-8}$$

α: coefficient for heavy current arcs which is derived empirically ($2{,}85 \times 10^{-5}$)
$I_{arc\text{-}peak}$: Peak fault current

Equation (3-8) indicates that the longer the arc length, the narrower the range of the time constant. The dynamic arc conductance may be derived by applying the Laplace transform to equation (3-6):

$$sg = \frac{1}{\tau}(G - g) \tag{3-9}$$

Therefore:

$$g = \frac{G}{s\tau + 1} \tag{3-10}$$

The dynamic arc conductance may then be calculated by substituting equations (3-7) and (3-8) into equation (3-10).

The assumptions made in the cases simulated are discussed in section 3.4.

3.4 Simulation model assumptions

The capacitance of the series capacitor was fixed for all the scenarios considered in this study.

The line circuit breakers were modelled as SF_6 circuit breakers as installed in the series compensated circuit in the power system. Additionally, the Cassie and Mayr black box arc models are applicable to SF_6 circuit breakers as indicated in section 2.5 and were therefore modelled accordingly for the simulations conducted.

Typically, on long, series compensated transmission lines shunt reactors are installed at the remote ends of these lines to limit the Ferranti Effect. The system operator may still want to maintain these reactors in service for voltage control on the substation busbars when the transmission line is shortened due to the introduction of injection points. This may be a complex exercise as the shunt reactors are no longer required on the transmission line but on the busbar. In some instances, this may not be achievable as the substation may not have been initially designed to accommodate a busbar reactor. Therefore, the reactor would have to remain in service as a line reactor to control the busbar voltage. The combination of the series capacitor and the shunt reactor may have a severe impact on the TRV of the LCBs due to the line length change. For the purposes of this study, the shunt reactors remained in operation for all scenarios.

The fault sequence that the simulation model was based on is the protection philosophy of the series compensated circuit studied. Once a fault was initiated, the LCB was tripped after 65 ms. The series capacitor bypass circuit breaker was assumed to close 35 ms after the fault was initiated. A LCB reclose event was not considered as part of this study and would form part of a future investigation.

Once the network was modelled according to the parameters specified in section 3.3, the simulation model was then verified against fault waveform data from a fault recording. The verification of the model is presented in section 3.5.1. The methodology for conducting the simulations for the various cases is then presented in section 3.5.2.

3.5 Simulation methodology and accuracy

3.5.1 Simulation model accuracy

The model accuracy was verified against a fault recording for a series and shunt compensated line (Figure 3-12). The fault occurred on the 19/04/2020. The fault that occurred was a single-phase-to-ground fault (white-phase-to-ground). The fault occurred at a distance of 6.39 km from Sub A. The LCB at Sub A were tripped with a three-phase auto-reclose (ARC). The peak fault current measured on the white phase was approximately 6.2 kA. The fault current recording was measured through the Current Transformer and Capacitor Voltage Transformer installed in the line bay at Sub A. Therefore, this model was verified against the magnitudes of the load current and fault current.

In order to model the fault accurately, the duration from the last zero crossing of the current waveform prior to the fault was determined and utilized to apply the fault in the simulation. The phase angles of the voltage sources were adjusted to align the magnitude of the simulated load current to the measured load current. The measured peak load current was 193.9 A.

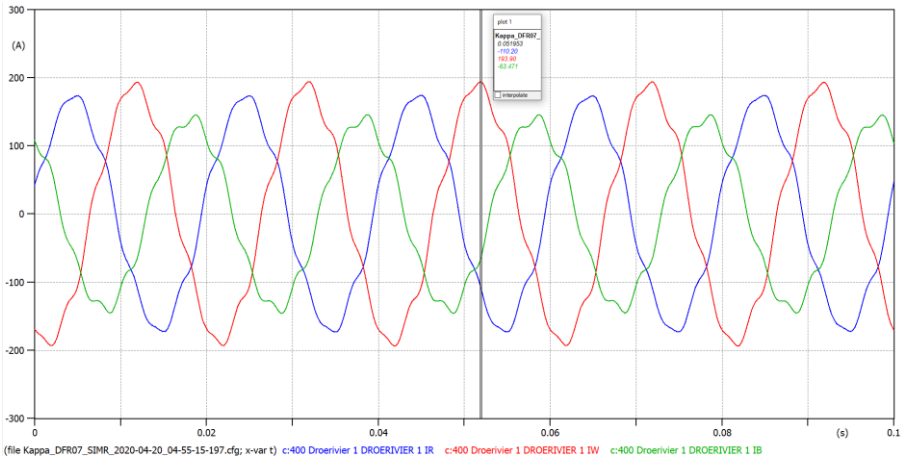

Figure 3-12: Fault recording measured peak load current [A]

The phase angles of the voltage sources were adjusted to align the magnitude of the simulated load current to the measured load current. The simulated peak load current was adjusted to 257 A which yields a 40% deviation (Figure 3-13). This significant deviation may be attributed to the actual system configuration at the time of the fault. The number of generation sources in service and network configuration will have a direct impact on the fault contribution to this circuit as well as the phase angle of the voltage sources.

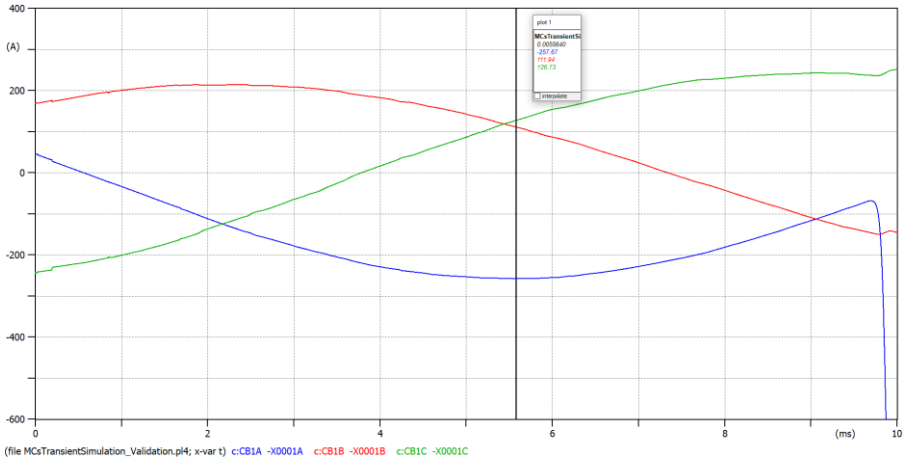

Figure 3-13: Simulated peak load current [A]

Similarly, the source impedances were adjusted to align the magnitude of the simulated fault current to the measured fault current. The measured and simulated peak fault currents were 5985 A (Figure 3-14) and 5987 A (Figure 3-15) respectively.

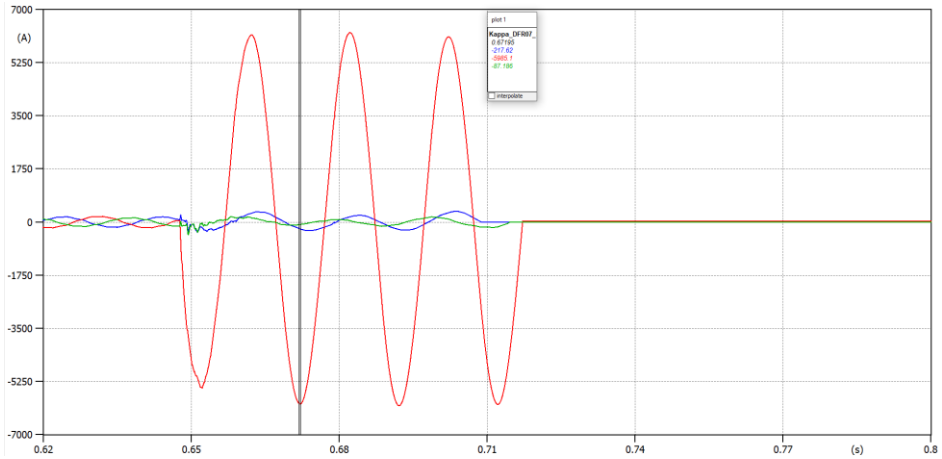

Figure 3-14: Fault recording measurement: peak fault current [A]

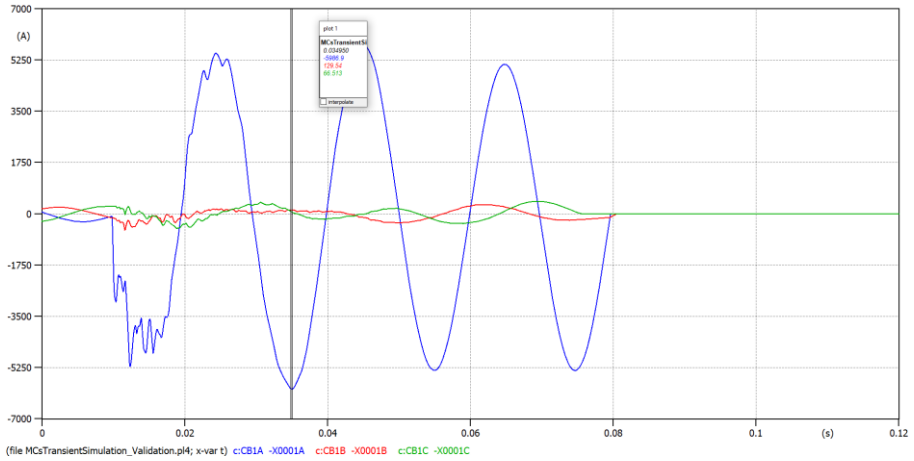

Figure 3-15: Simulated peak fault current [A]

In order to model the circuit investigated accurately, the system status needs to be known at the time of the fault (i.e. the number of generators in service and transmission lines that are out of service). Additionally, the fault recording measured data needs to be of a high bandwidth (10 MHz) to verify the simulation model for transient studies. This would be indicative of all stray capacitance requirements in the circuit being investigated.

Since 50 Hz fault current was one of the main factors in determining the TRV capability of the circuit breaker, the simulation model was deemed acceptable. This was due to the profile and magnitude of the simulated fault current being less than a 1% deviation from the magnitude of the measured fault current.

3.5.2 Sequence of the simulation procedure on ATPDraw

Once the model was verified against the fault data, the simulations were conducted based on the following sequence. In order to conduct simulations, the simulation model needed to be at steady state prior to initiating a fault. Once the fault was initiated at 15 ms, the series capacitor bank bypass circuit breaker was closed 20 ms later. The LCBs on the remote ends of the compensated circuit are subsequently opened 30 ms and 35 ms respectively after the series capacitor bank bypass circuit breaker was closed for case 1. The LCB for Sub C was opened 5 ms after the remote end LCB across the series capacitor bank for case 2.

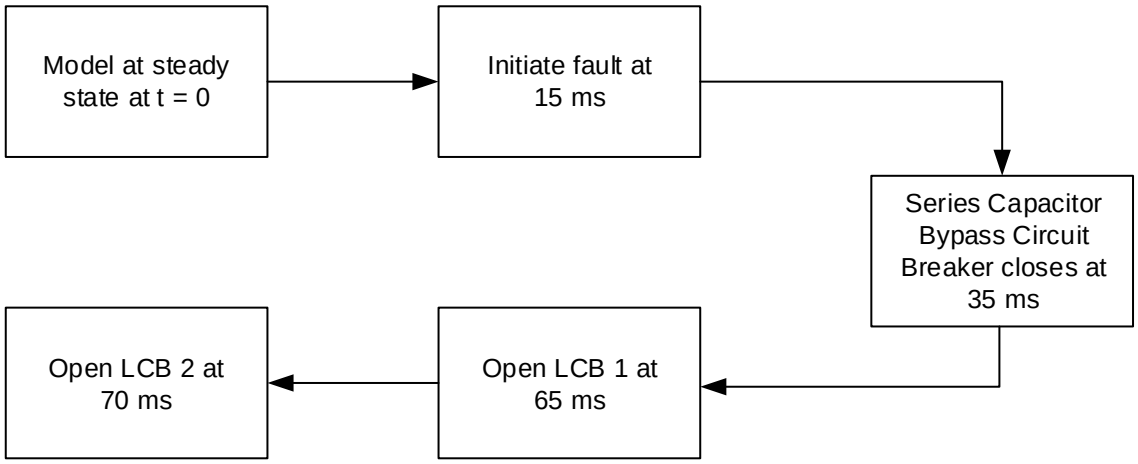

Figure 3-16: Flow diagram of the simulation algorithm

The following typical three phase voltage and current profiles are generated from the simulations conducted on ATPDraw (Figure 3-17 and Figure 3-18):

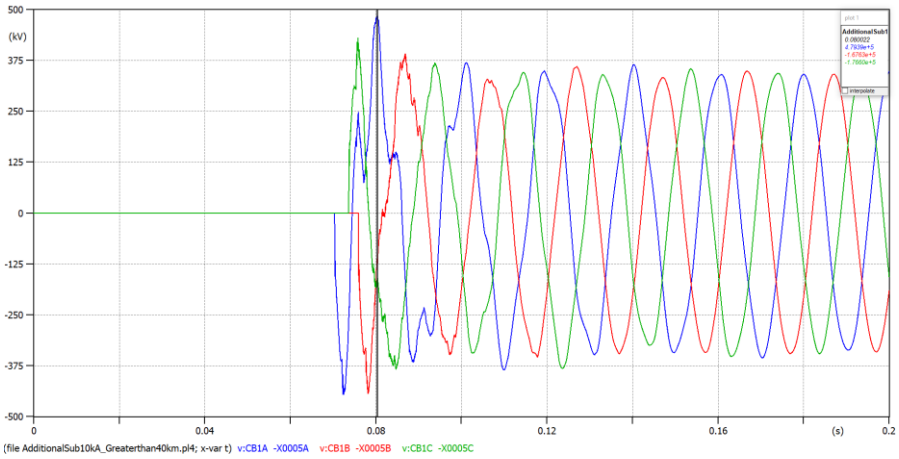

Figure 3-17: Three-phase voltage waveform across line circuit breaker contacts

The results for the above voltage waveforms are applicable for Sub C which was 240 km from Sub A (refer to Figure 3-25). Sub C contributes a fault current of 10 kA. A three-phase-to-ground fault was applied 1 km from Sub C in the direction of Sub A.

Figure 3-17 displays the voltage waveform across the circuit breaker contacts for a LCB connected in the compensated circuit. Initially all LCBs in the system being simulated are closed. Once the fault was initiated at 15 ms. A high RRRV occurs when the circuit breaker opens at a current zero crossing due to the reactance in the circuit which drives the voltage to a peak at a current zero.

The peak fault current was determined from the current measured through the LCBs shown in Figure 3-18.

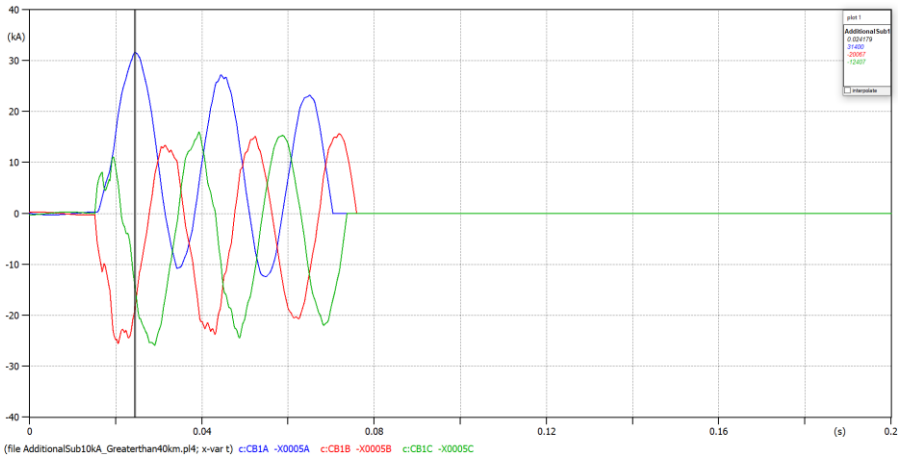

Figure 3-18: Three phase current waveform through the LCB

The peak fault current was utilised in determining the test duty of the circuit breaker. The fault current rating of the 400 kV circuit breaker installed in the compensated circuit in this instance was 50 kA. The test duty of the circuit breaker was then calculated as approximately 44% of the maximum fault current rating of the circuit breaker. Thereafter this was compared to the reference test duty as indicated in Table 3-10. The higher test duty from Table 3-10 in comparison to the calculated value was then selected. The selected test duty in this case was 60% which was associated with a four-parameter envelope. This parameter envelope was then used to evaluate the TRV capability of the line circuit breaker for a specific power system scenario.

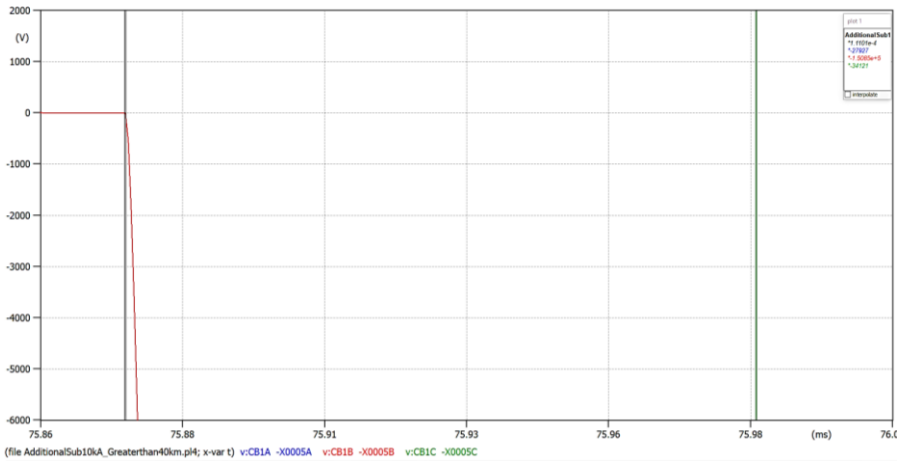

Figure 3-19: RRRV across LCB contacts

Figure 3-19 illustrates the RRRV measured across the LCB contacts of a compensated circuit. In this case the RRRV was calculated to be:

$$\frac{V}{t} = \frac{150.85kV}{111.01\mu s} = 1.36kV/\mu s \qquad (3\text{-}11)$$

This RRRV value was then compared to the reference value RRRV in accordance with the selected test duty above. In this case the reference RRRV was 3 kV/µs, therefore the RRRV rating of the CB was not exceeded.

The peak recovery voltage was then measured from the voltage waveform (Figure 3-17) which was approximately 483 kV and compared to the corresponding reference peak recovery voltage indicated in Table 3-10 for a 60% test duty (669 kV). Therefore, the peak recovery voltage was not exceeded for the line circuit breaker.

In order to accurately evaluate the TRV stress on a circuit breaker, the appropriate parameter envelope should be superimposed onto the voltage waveform obtained from the simulation. This would provide a more apparent representation of any voltage exceedances of the circuit breaker TRV capability.

The series capacitor bank discharges into the damping reactor, once the series capacitor bypass circuit breaker closes, at a measured discharge frequency of approximately 0.0011 s (Figure 3-20) which resulted in a 1% error in comparison to the calculated value in section 3.3.6.

$$f = \frac{1}{t} = \frac{1}{0.0011} = 909\ Hz \tag{3-12}$$

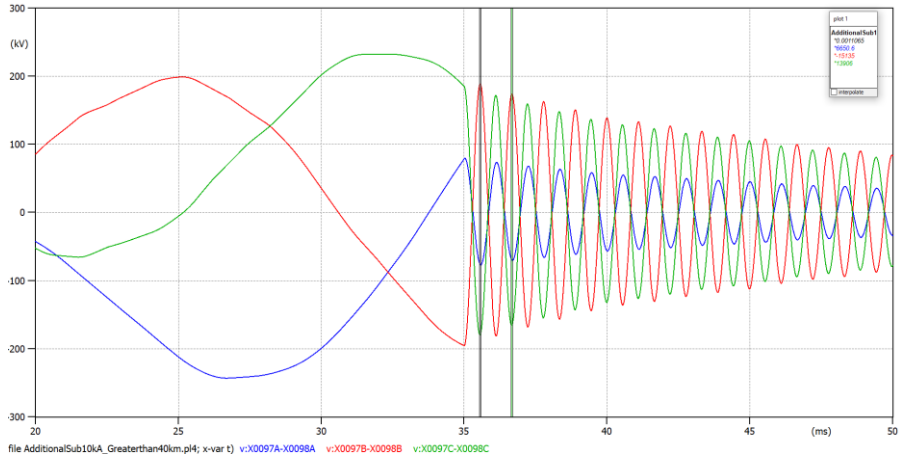

Figure 3-20: Series capacitor bank discharging into series capacitor damping reactor

The LCB arc models were based on the Cassie and Mayr black box arc model described in section 2.5. The Cassie black box arc model is representative of an arc characteristic for high currents (of the order of hundreds of amps) while the Mayr black box arc model describes the arc characteristic around current zero [20]. Figure 3-21 illustrates the arc resistance response of the LCB black box arc model during the circuit breaker contacts parting.

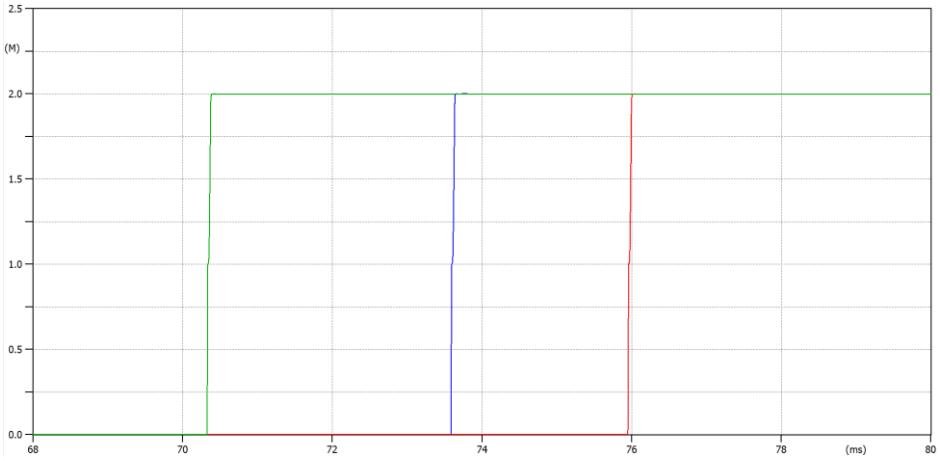

Figure 3-21: Arc resistance for LCBs at Sub C

Figure 3-22 zooms into phase A to illustrate the response of the combination of the Cassie and Mayr arc model. When the circuit breaker contacts initially part, the arc characteristic response is dominated by the Cassie arc model. The arc resistance will increase asymptotically towards 1 MΩ at which point the Mayr arc model starts to dominate the arc response. The arc resistance will then tend towards 2 MΩ. The choice of these resistance values was selected to prevent a division by zero.

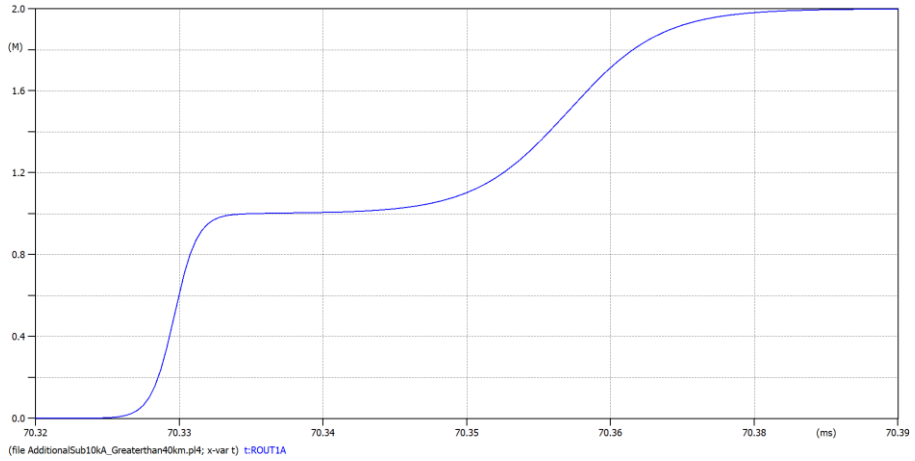

Figure 3-22: Closer view of the arc resistance response for Phase A

The fault arc resistance was modelled based on the description in section 3.3.10. The arc length used in the simulation to an earthed structure was assumed to be 3,2 m and the arc length between phases was taken to be the phase spacing which was 9,4 m. This would form the basis of the three-phase-to-ground fault applied in the simulation (Figure 3-23).

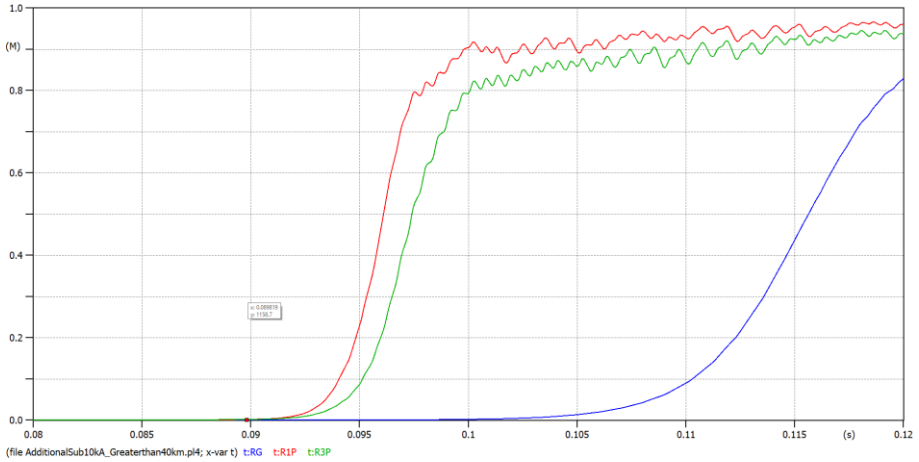

Figure 3-23: Characteristic response of fault arc resistance of three-phase-to-ground fault

Once the model was developed and verified and the sequence of conducting the simulations established, the analysis of the circuit configurations under consideration was performed. Understanding the circuit behaviour for the three cases presented is critical in ensuring that results from the simulations conducted may be verified. This is achieved by performing the circuit analysis for the three cases considered (section 3.2) for the case study. Section 3.6 will present the circuit analysis for this study.

3.6 Circuit analysis of the three circuit configurations

Circuit analysis was then performed for the three cases being considered for this study. The analysis was broken down based on the protection response of the system for a fault on the compensated circuit. The simulation was performed on ATPDraw for the corresponding case to compare with the results derived from the circuit analysis performed.

1. Case 1: Sub C not added (Figure 3-24).

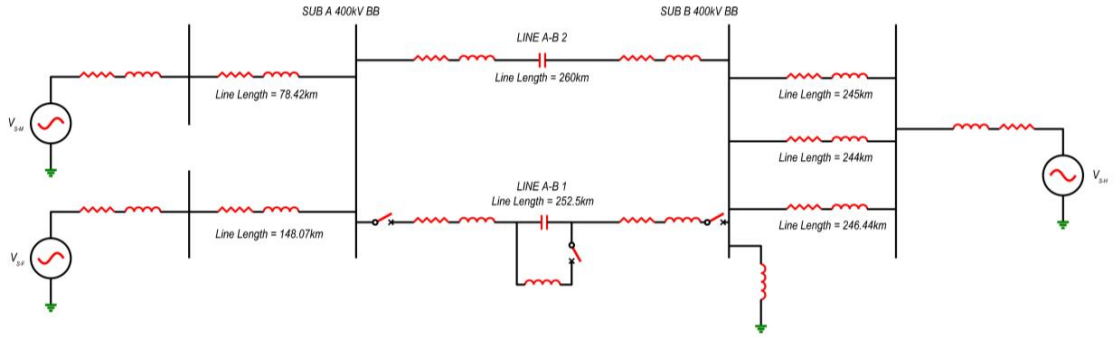

Figure 3-24: Network configuration of Case 1

2. Case 2a: Line A-C 1 which is 200 km long and Sub C is 143 km away from the series capacitor bank. The fault current contribution from Sub C was be varied between 5 kA and 10 kA. Line C-B 1 was 52.5 km long. Sub A was 56.5 km away from the series capacitor bank (Figure 3-25).
3. Case 2b: Line A-C 1 which was 240 km long and Sub C was 183 km away from the series capacitor bank. The fault current contribution of from Sub C was varied between 5 kA and 10 kA. Line C-B 1 was 12.5 km long. Sub A was 56.5 km away from the series capacitor bank (Figure 3-25).

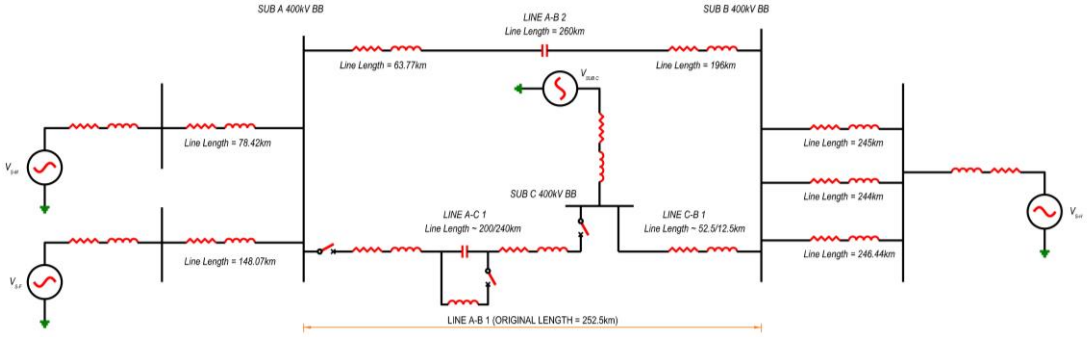

Figure 3-25: Network configuration of Case 2a and 2b

4. Case 3a: Line C-B 1 which was 232.5 km long and Sub C was 36.5 km away from the series capacitor bank. The fault current contribution of from Sub C was varied between 5 kA and 10 kA. Line A-C 1 was 20 km long. Sub A was 56.5 km away from the series capacitor bank (Figure 3-26).

5. Case 3b: Line C-B 1 - Line C-B 1 which was 212.5 km long and Sub C was 16.5 km away from the series capacitor bank. The fault current contribution of from Sub C was varied between 5 kA and 10 kA. Line A-C 1 was 40 km long. Sub A is 56.5 km away from the series capacitor bank.

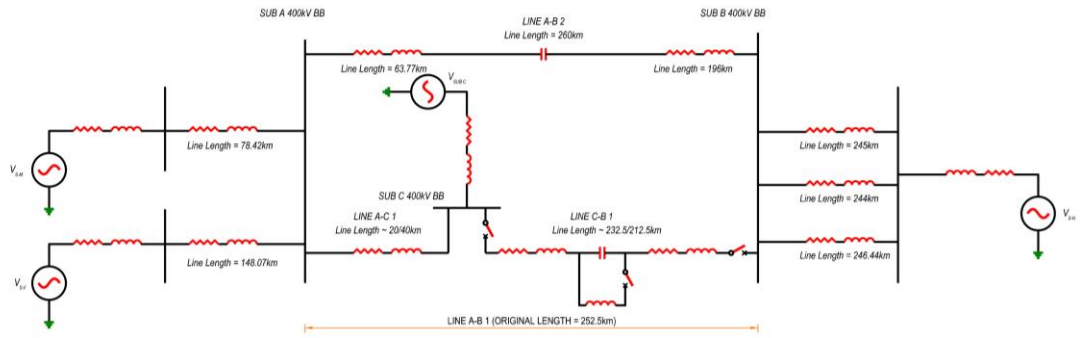

Figure 3-26: Network configuration of Case 3a and 3b

The verified model was utilised to simulate the cases presented below and the results from the simulation were compared with the results derived from the circuit analysis.

3.6.1 Case 1: No Sub C

The first case analyzed was case 1 which was the network without the integration of Sub C (Figure 3-27). This case represented the existing network configuration and informed of the current TRV capability of the LCBs at Sub A and Sub B. The series compensated transmission line was 252.5 km long with the series capacitor bank located 57 km away from Sub A. A three-phase-to-ground fault was applied along the series compensated transmission line and the TRV stresses on the LCBs at Sub A and Sub B were evaluated (Figure 3-27).

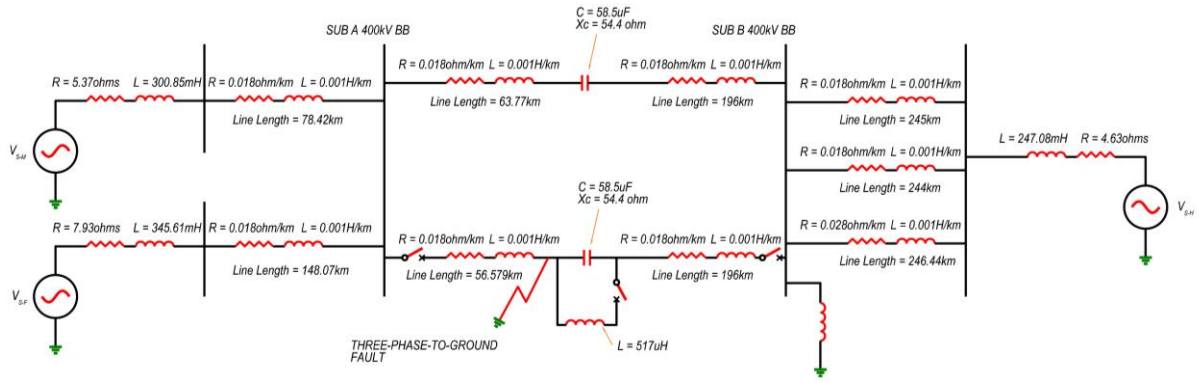

Figure 3-27: Single phase representation of the Network Configuration for Case 1 (No Sub C)

The analysis was considered in five states:

1. The network configuration was initially in steady state/pre-fault condition.
2. A three-phase-to-ground fault was applied along the series compensated transmission line with the series capacitor bank in service.
3. The three-phase-to-ground fault was still applied, and the series capacitor bank was bypassed by closing the bypass circuit breaker and putting the series capacitor bypass damping reactor into service.
4. Sub B LCB was then opened.
5. Sub A LCB was then opened and the series compensated transmission line was isolated from the network.

3.6.1.1 Steady State/Pre-fault condition (No Sub C)

The load flow study was conducted using a simulation model developed in ATPDraw. Since there were three voltage sources in this configuration, the phase angles must be known for each voltage source to accurately analyse the network (Figure 3-28). Additionally, the voltage magnitudes were considered to

be the same at 1 p.u. The LCBs at Sub A and Sub B remained closed and the series capacitor bypass circuit breaker remained opened. The line length for line A-C 1 was 252.5 km

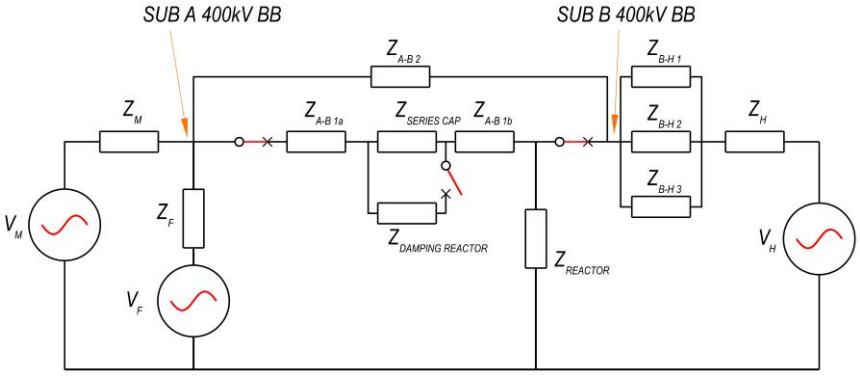

Figure 3-28: Circuit diagram of steady state pre-fault network configuration

3.6.1.2 Three-phase-to-ground fault application (No Sub C)

A three-phase-to-ground fault was applied along the series compensated transmission line at a position 1 km away from Sub A through an arc impedance (Figure 3-29).

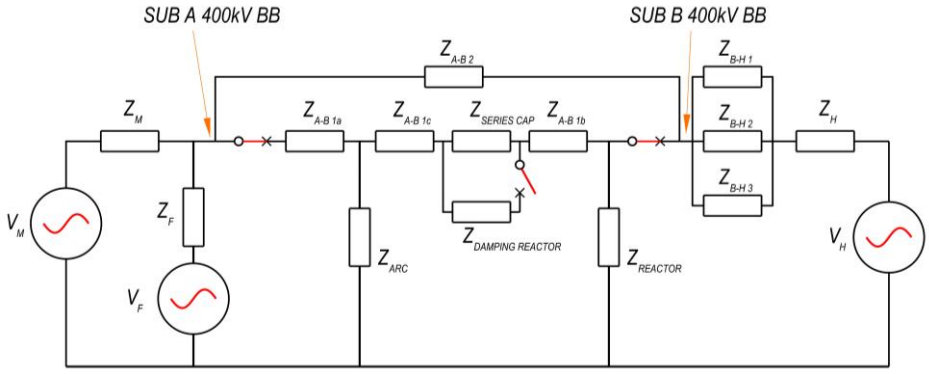

Figure 3-29: Three-phase-to-ground fault applied to the series compensated circuit (No Sub C)

A three-phase fault is a symmetrical fault which implies that the fault current magnitudes and phase angle displacement are equal. As a result, the circuit analysis may be conducted on a per phase basis.

The fault current magnitude was calculated by determining the Thévenin equivalent impedance and Thévenin equivalent open circuit voltage at the point of the fault being applied in the circuit and the arc impedance (Figure 3-30).

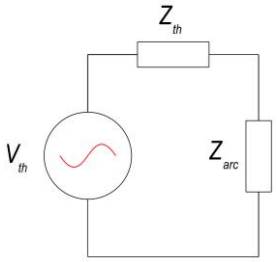

Figure 3-30: Thévenin equivalent circuit to determine fault current

The Thévenin equivalent impedance was obtained by applying a short circuit across all voltage sources and determining the impedance viewed upstream from the point of the fault (Figure 3-31).

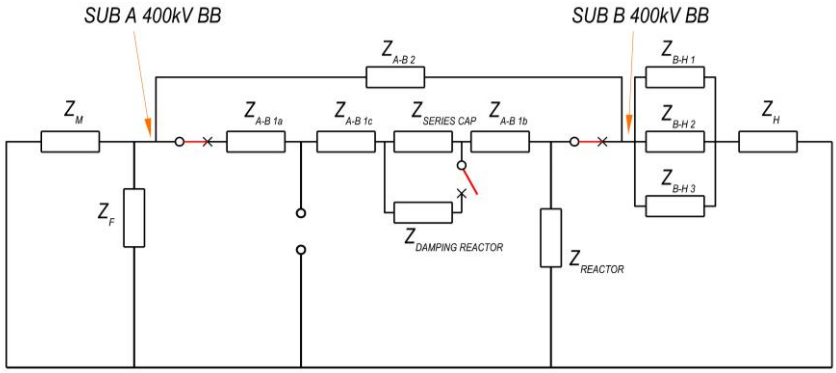

Figure 3-31: Thévenin equivalent impedance Z_{th} at the point of the fault applied (Line A-C 1)

In order to simplify the circuit, a delta -star impedance transformation was required for the impedances in the loop containing $Z_{B\text{-}H\ 1}$, $Z_{A\text{-}B\ 1a}$, $Z_{Z\text{-}B\ 1c}$, $Z_{series\ cap}$ and $Z_{A\text{-}B1b}$ (Figure 3-32).

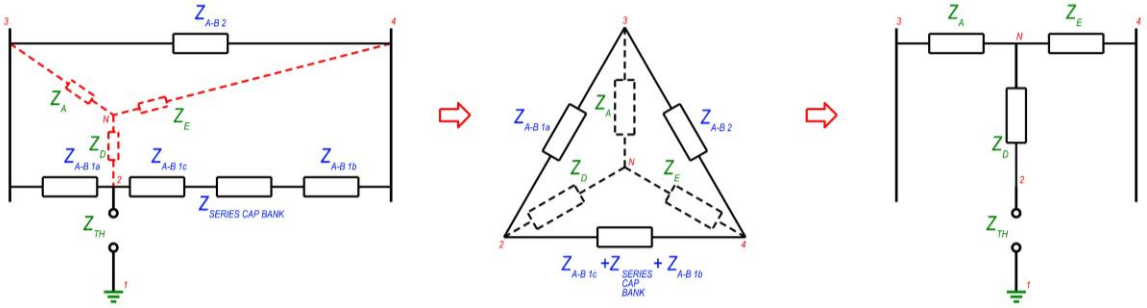

Figure 3-32: Delta- Star impedance transformation

The transformed impedances Z_A, Z_D and Z_E were determined using the following equations:

$$Z_A = \frac{(Z_{A-B\ 1a})(Z_{A-B\ 2})}{Z_{A-B\ 1a} + Z_{A-B\ 1b} + Z_{A-B\ 2}} \tag{3-13}$$

$$Z_D = \frac{(Z_{A-B\ 1a})(Z_{A-B\ 1b})}{Z_{A-B\ 1a} + Z_{A-B\ 1b} + Z_{A-B\ 2}} \tag{3-14}$$

$$Z_E = \frac{(Z_{A-B\ 1b})(Z_{A-B\ 2})}{Z_{A-B\ 1a} + Z_{A-B\ 1b} + Z_{A-B\ 2}} \tag{3-15}$$

The Thévenin impedance was reduced to the following circuit (Figure 3-33):

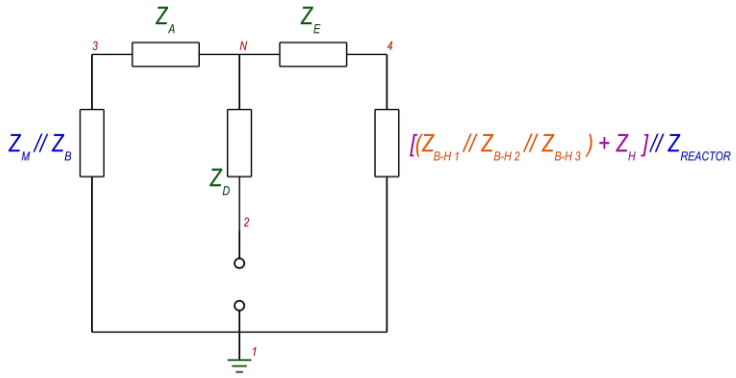

Figure 3-33: Thévenin equivalent impedance reduced circuit

The Thévenin equivalent impedance was given as:

$$Z_{th} = Z_D + \left((Z_M // Z_B + Z_A) // \left(Z_E + \left(\left((Z_{B-H\,1} // Z_{B-H\,2} // Z_{B-H\,3}) + Z_H\right) // Z_{Reactor}\right)\right)\right) \quad (3\text{-}16)$$

The Thévenin impedance Z_{th} was calculated to be 2.76 Ω + i42 Ω.

The Thévenin open circuit voltage, V_{th}, may be determined from the pre-fault steady state condition by measuring the open circuit voltage at the point of the fault. The Thévenin equivalent voltage was measured to be 283.8 kV_{rms} per phase.

The voltage gradient of an arc was taken as 1500 V/m as suggested in [48]. Taking the arc length to be the phase-to-earth clearance of 3.2 m at 400 kV [49], the arc voltage, V_{arc}, was calculated as 2.77 kV_{rms} per phase. This arc voltage was used in all calculations as this magnitude was considered constant. The simulated arc voltage was measured off the simulated waveform to be 2.27 kV_{rms} per phase.

The arc impedance, Z_{arc}, was then determined by solving the voltage divider equation since fault current flows through it (Figure 3-30):

$$V_{arc} = V_{th}\left(\frac{Z_{arc}}{Z_{arc} + Z_{th}}\right) \quad (3\text{-}17)$$

The arc impedance was then determined as follows:

$$Z_{arc} = \frac{V_{arc} Z_{th}}{V_{th} - V_{arc}} \quad (3\text{-}18)$$

The arc impedance in this case was calculated to be 0.017 Ω + i0.26 Ω.

Once the Thévenin equivalent impedance, the Thévenin equivalent open circuit voltage and the arc impedance were determined, the fault current was calculated by Ohm's law using the following equation:

$$I_{fault} = \frac{V_{th}}{Z_{th} + Z_{arc}} \quad (3\text{-}19)$$

The fault current was calculated to be 6.65 kA_{rms} per phase. The fault current measured off the simulated waveform was 5.44 kA_{rms} per phase. The difference in magnitude between the calculated fault current and the measured fault current was due to the simulation model being based on the distributed parameter model whereas the calculation was conducted based on the lumped model.

3.6.1.3 Series Capacitor Bank bypassed (No Sub C)

The series capacitor bank was then bypassed by closing the series capacitor bank bypass circuit breaker. The series capacitor bypass damping reactor was then connected to the transmission line, altering the impedance of the line (Figure 3-34).

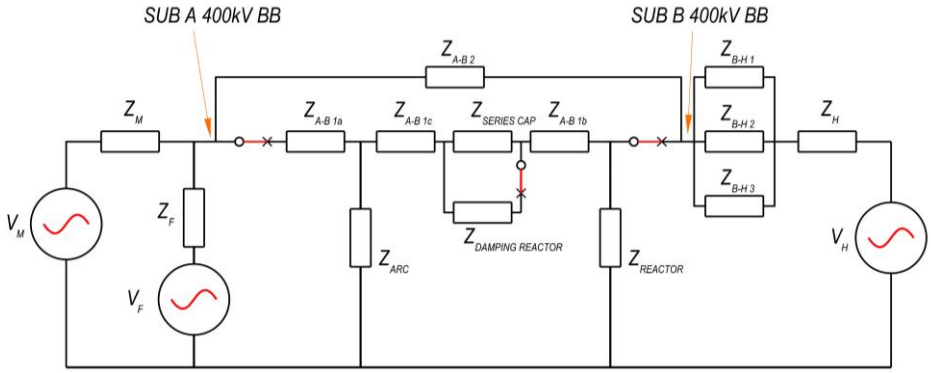

Figure 3-34: Fault applied through the arc impedance when the series capacitor bank was bypassed

A similar analysis was conducted by substituting the impedance of the series capacitor bank with the impedance of the series capacitor bank bypass reactor.

The calculation of the Thévenin equivalent impedance followed the same equation (3-16). The Thévenin equivalent impedance was calculated to be 2.91 Ω + i45.29 Ω which indicated an increase in impedance as expected when compared to when the series capacitor bank was in service.

There was a marginal change in the Thévenin equivalent open circuit voltage and the measured value was 282.7 kV_{rms} per phase.

As indicated previously the arc voltage was expected to remain constant due to the voltage gradient across the arc length remaining constant. The arc voltage measured off the simulated waveform of 2.29 kV_{rms} per phase was compared to the calculated arc voltage of 2.77 kV_{rms} per phase.

The arc impedance was then recalculated as per equation (3-18) to be 0.027+i0.43. This was an increase in magnitude in comparison to the series capacitor bank in service.

The fault current magnitude was calculated to be 6.48 kA_{rms} per phase while the fault current magnitude measured off the simulated waveform was 5.36 kA_{rms} per phase.

3.6.1.4 Sub B LCB Opens (No Sub C)

The LCB at Sub B was then opened after the series capacitor bank was bypassed (Figure 3-35). This was to prevent the LCB from being exposed to severe TRVs as a result.

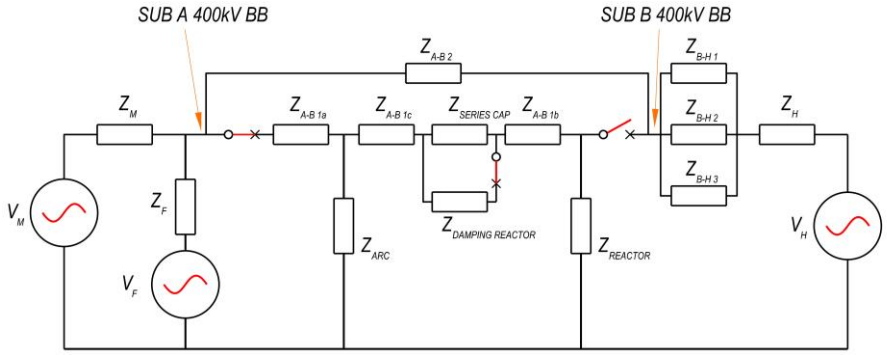

Figure 3-35: LCB at Sub B was opened after the series capacitor bank was bypassed

The Thévenin equivalent impedance was determined with the LCB at Sub B opened (Figure 3-36).

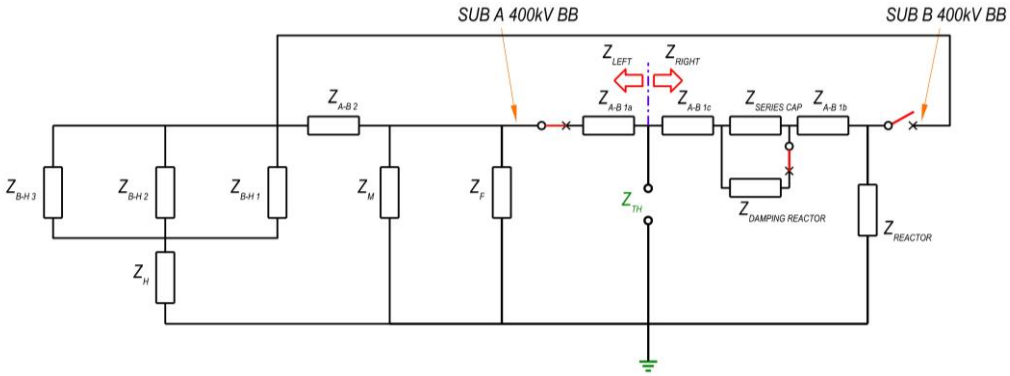

Figure 3-36: Thévenin equivalent impedance when the LCB at Sub B was opened

The impedance as seen from the point of the fault was determined as the impedance as seen from the left of the fault:

$$Z_{LEFT} = Z_{A-B\ 1a} + Z_F // Z_M // (Z_{A-B\ 2} + (Z_{B-H\ 1} // Z_{B-H\ 2} // Z_{B-H\ 3}) + Z_H) \quad (3\text{-}20)$$

And the impedance as seen from the right of the fault:

$$Z_{RIGHT} = Z_{A-B\ 1c} + Z_{DAMPING\ REACTOR} + Z_{A-B\ 1b} + Z_{REACTOR} \quad (3\text{-}21)$$

The Thévenin equivalent impedance was then determined as:

$$Z_{TH} = Z_{LEFT} // Z_{RIGHT} \quad (3\text{-}22)$$

Substituting all impedances into equations (3-20) and (3-21) and solving for the Thévenin equivalent impedance yielded a result of 2.95 Ω+i43.63 Ω.

The Thévenin equivalent open circuit voltage was measured off the simulated waveform at 283.13 kV_{rms} per phase. This indicated a marginal increase from the previous state of 282.7 kV_{rms} per phase.

The arc voltage measured off the simulated waveform was 2.26 kV_{rms} per phase which was marginally lower than the previous state.

The arc impedance was calculated to be 0.029 Ω+i0.43 Ω.

The fault current magnitude was calculated to be 6.41 kA_{rms} per phase and the fault current magnitude flowing through the arc impedance was measured off the simulated waveform to be 5.29 kA_{rms} per phase.

3.6.1.5 Sub A LCB Opens (No Sub C)

Once the LCB at Sub A opened this result in Line A-B 1 being isolated. The charge from the line capacitance of A-B 1 discharged into the fault and there was an exchange of energy between the capacitance and the inductance. The capacitance discharged at a rate determined by the magnitude of the resistance in the isolated circuit by the time constant RC. The natural frequency was determined by the magnitude of the capacitance and inductance in the isolated circuit. The combination of the R, L and C determined the transient response of the circuit (underdamped, critically damped, or overdamped).

Based on the results presented thus far, the calculated and measured values off the simulated waveforms indicated good correlation. The conclusion from the analysis indicated that the Thévenin equivalent impedance increased with each state while the magnitude of fault current decreased.

3.6.2 Sub C – Fault current contribution of 5 kA (Line A-C 1)

The second case analysed was the integration of Sub C into the series compensated transmission circuit presented in section 3.6.1. Sub C represents the integration of generation source which changes the line length of the compensated circuit while also contributing fault current. The existing line A-B 1 was split into line A-C 1 and C-B 1 with the integration of Sub C. The LCBs at Sub A and Sub C were connected across the series capacitor bank (Figure 3-37) with the line length of A-C 1 being 240 km. The fault current contribution from Sub C was 5 kA. A three-phase-to-ground fault was applied along the circuit between Sub A and Sub C.

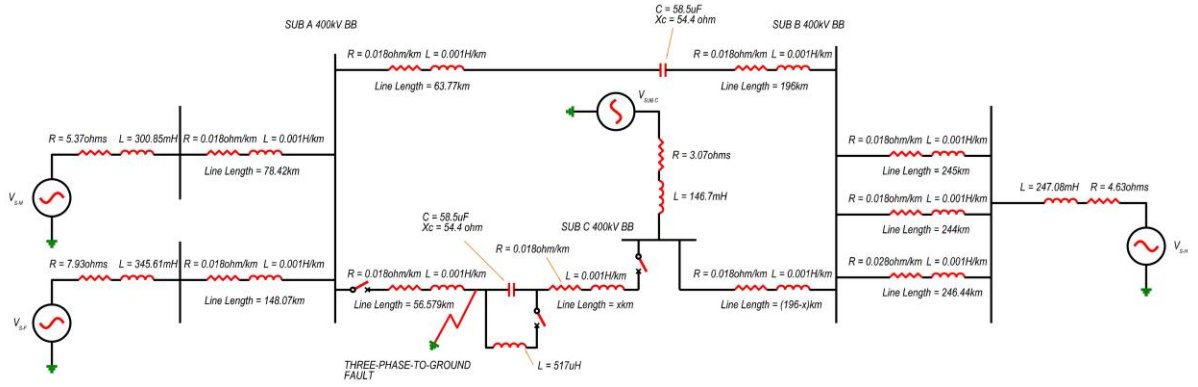

Figure 3-37: Single phase representation of the Network Configuration for Case 2: Line A-C 1 (Sub C – 5 kA contribution)

A similar analysis is presented below with the five states of the network:

1. The network configuration was initially in a steady state/pre-fault condition.
2. A three-phase-to-ground fault was applied along the series compensated transmission line with the series capacitor bank in service.
3. The three-phase-to-ground fault was still applied, and the series capacitor bank was bypassed by closing the series capacitor bypass circuit breaker and putting the series capacitor bypass damping reactor into service.
4. Sub A LCB was then opened.
5. Sub C LCB was then opened and the series compensated transmission line was isolated from the network.

3.6.2.1 Steady State/Pre-fault condition (Line A-C 1)

The load flow study was conducted with the integration of Sub C. Since there were four voltage sources in this configuration, the phase angles must be known for each voltage source (Figure 3-38). The phase angle for Sub C was selected based on the phase angles of the voltage sources adjacent to it. Additionally, the voltage magnitudes were assumed to be the same at 1 p.u. The LCBs at Sub A and Sub C remain closed and the series capacitor bypass circuit breaker remained opened. The scenario analysed was the line length of line A-C 1 being 240 km which was made up of a line length between Sub A – series capacitor bank being 56.5 km and line length between series capacitor bank to Sub C being 183.5 km. The line length for line C-B 1 was 12.6 km.

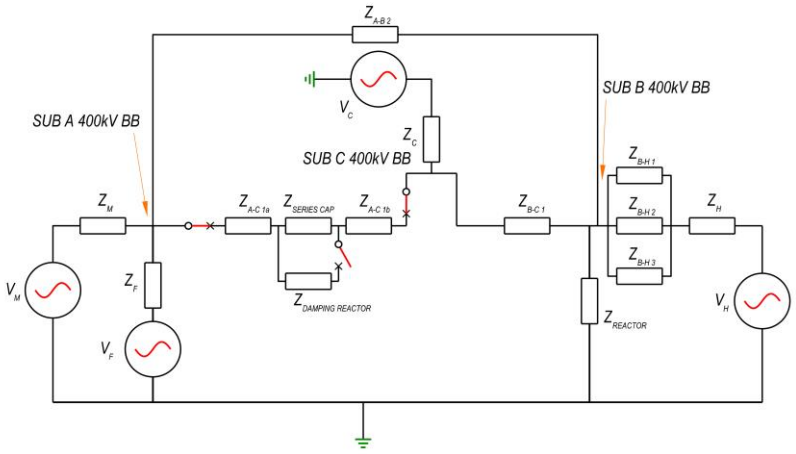

Figure 3-38: Circuit diagram of steady state pre-fault network configuration for the series compensated line A-C 1

3.6.2.2 Three-phase-to-ground fault application (Line A-C 1)

A three-phase-to-ground fault was applied 1 km away from Sub A along line A-C 1 through the arc impedance Z_{arc} (Figure 3-39).

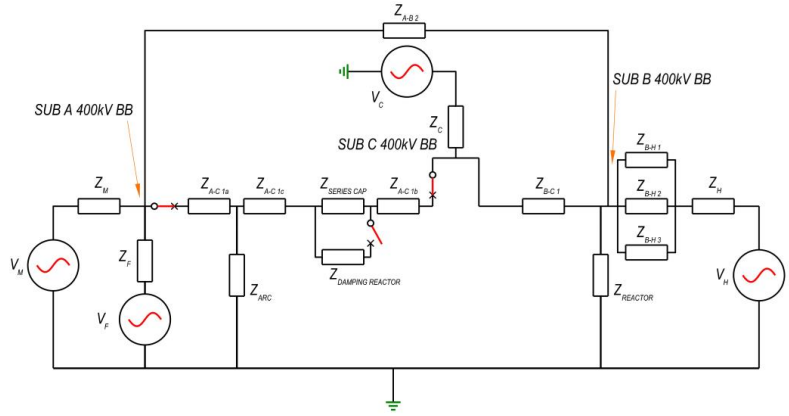

Figure 3-39: Three-phase-to-ground fault applied to the series compensated circuit Line A-C 1

The Thévenin equivalent impedance and the arc impedance were required to be calculated to determine the magnitude of fault current flowing through the arc impedance as described in section 3.6.1.2. The Thévenin equivalent impedance was determined from the circuit below (Figure 3-40):

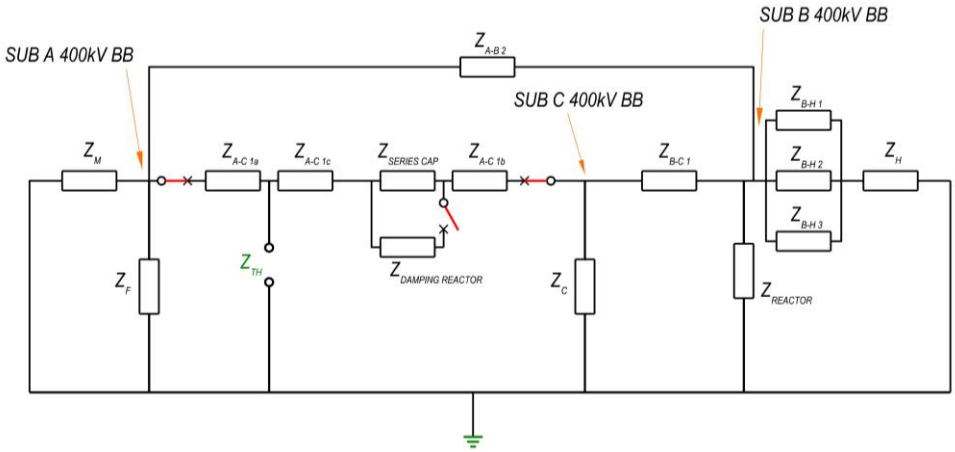

Figure 3-40: Thévenin equivalent impedance Z_{th} at the point of the fault applied (Line A-C 1)

The network impedance was simplified using the Delta-Star impedance transformation (Figure 3-41).

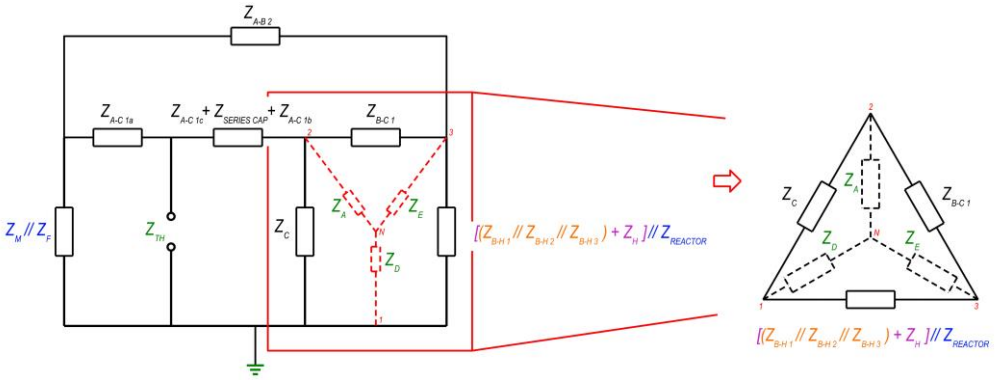

Figure 3-41: First Delta-Star impedance transformation applied to determine the Thévenin equivalent impedance (Line A-C 1)

Letting

$$Z_R = [(Z_{B-H\,1} // Z_{B-H\,2} // Z_{B-H\,3}) + Z_H] // Z_{REACTOR} \tag{3-23}$$

Then

$$Z_A = \frac{(Z_C)(Z_{B-C\,1})}{Z_C + Z_{B-C\,1} + Z_R} \tag{3-24}$$

$$Z_D = \frac{(Z_C)(Z_R)}{Z_C + Z_{B-C\,1} + Z_R} \tag{3-25}$$

$$Z_E = \frac{(Z_{B-C\,1})(Z_R)}{Z_C + Z_{B-C\,1} + Z_R} \tag{3-26}$$

The resultant equivalent impedance configuration is shown in Figure 3-42:

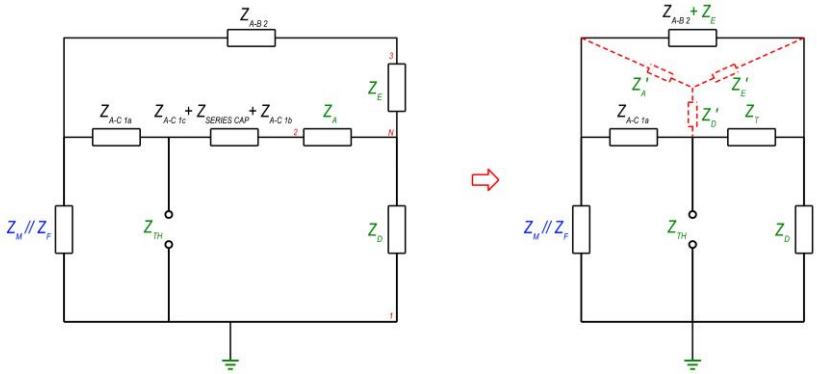

Figure 3-42: Second Delta-Star impedance transformation applied to determine the Thévenin equivalent impedance (Line A-C 1)

Where:

$$Z_T = Z_{A-C\,1c} + Z_{SERIES\,CAP} + Z_{A-C\,1b} + Z_A \tag{3-27}$$

Applying the Delta-Star impedance transformation shown in Figure 3-42 resulted in the following equations:

$$Z_A{}' = \frac{(Z_{A-C\,1a})(Z_{A-B\,2} + Z_E)}{Z_{A-C\,1a} + Z_{A-B\,2} + Z_E + Z_T} \tag{3-28}$$

$$Z_D{}' = \frac{(Z_{A-C\ 1a})(Z_T)}{Z_{A-C\ 1a} + Z_{A-B\ 2} + Z_E + Z_T} \quad (3\text{-}29)$$

$$Z_E{}' = \frac{(Z_T)(Z_{A-B\ 2} + Z_E)}{Z_{A-C\ 1a} + Z_{A-B\ 2} + Z_E + Z_T} \quad (3\text{-}30)$$

The Thévenin equivalent impedance was finally determined from Figure 3-43.

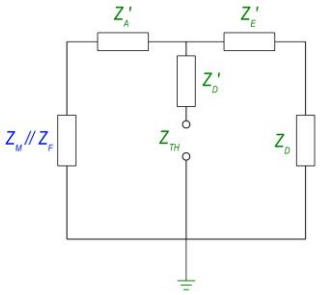

Figure 3-43: Final Thévenin equivalent impedance for a fault applied with the integration of Sub C (Line A-C 1)

The equation for Z_{th} was given as:

$$Z_{TH} = \left((Z_M//Z_F + Z_A{}')//(Z_E' + Z_D)\right) + Z_D \quad (3\text{-}31)$$

The calculated Thévenin equivalent impedance for a fault 1 km away from Sub A was 2.23 Ω+i26.46Ω.

The Thévenin equivalent open circuit voltage, V_{th}, was determined from the pre-fault steady-state condition by measuring the open circuit voltage at the point of the fault. The Thévenin equivalent voltage was measured to be 259 kV_{rms} per phase.

The arc voltage, V_{arc}, was calculated as 2.77 kV_{rms} per phase from section 3.6.2.2. This arc voltage was utilised in all calculations as this magnitude was considered constant. The arc voltage was measured off the simulated waveform to be 2.48 kV_{rms} per phase.

The arc impedance, Z_{arc}, was determined by solving equation (3-18) which resulted in 0.024 Ω+i0.29 Ω.

The fault current was calculated using equation (3-19) to be 9.65 kA_{rms} per phase. The fault current measured off the simulated waveform was 8.68 kA_{rms} per phase.

3.6.2.3 Series Capacitor Bank bypassed (Line A-C 1)

The series capacitor bank was then bypassed by closing the series capacitor bank bypass circuit breaker. The series capacitor bypass damping reactor was then connected to the transmission line, altering the impedance of the line (Figure 3-44).

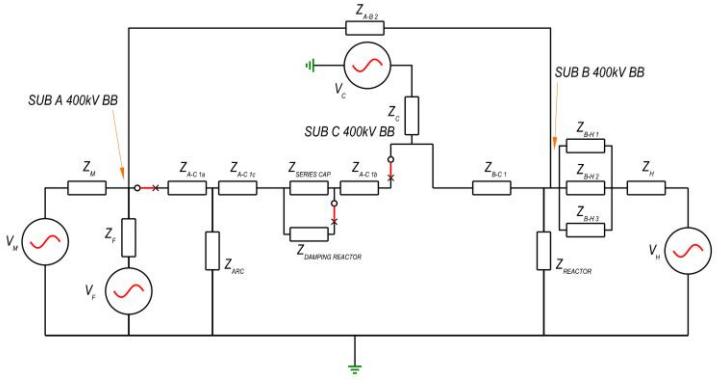

Figure 3-44: Series bypass capacitor bank circuit breaker closed Line A-C 1 (Sub C – 5 kA)

Applying the same equations as derived in section 3.6.2.2 with the series capacitor impedance replaced with the series capacitor damping reactor impedance yielded the following results:

Thévenin equivalent impedance (Z_{th}): 2.31 Ω+i29.37 Ω
Thévenin equivalent open circuit voltage: 259 kV

The arc voltage and fault current were then compared between the calculated (from equations (3-18) and (3-19)) and the measured (Table 3-12).

Table 3-12: Comparison of calculated and measured parameters for series capacitor bypass circuit

Parameter	Calculated	Measured off the simulated waveform
Arc Voltage (kV)	2.77 kV	2.55 kV
Fault Current (kA)	8.63 kA	7.92 kA

3.6.2.4 Sub A LCB Opens (Line A-C 1)

The LCB at Sub A was then opened after the series capacitor bank was bypassed (Figure 3-45).

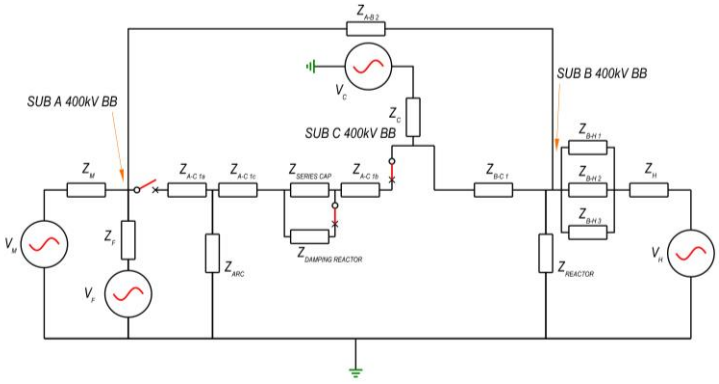

Figure 3-45: LCB at Sub A was opened after the series capacitor bank was bypassed

The Thévenin equivalent impedance was recalculated based on the change in network configuration (Figure 3-46).

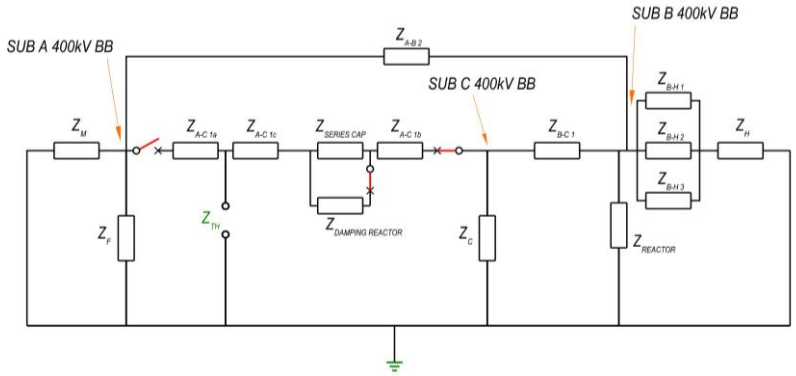

Figure 3-46: Thévenin equivalent impedance after LCB at Sub A was opened

Z_{th} was calculated as:

$$Z_{TH} = \left((Z_{B-C\,1} + Z_R)//Z_C\right) + Z_{A-C\,1b} + Z_{DAMPING\ REACTOR} + Z_{A-C\,1c} \quad (3\text{-}32)$$

Where

$$Z_R = Z_{\mathrm{REACTOR}}//\left((Z_{B-H\,1}//Z_{B-H\,2}//Z_{B-H\,3}) + Z_H\right)//\left(Z_{A-B\,2} + (Z_M//Z_F)\right) \quad (3\text{-}33)$$

The resultant Thévenin equivalent impedance was calculated to be 6.08 Ω+i99.67 Ω.

The Thévenin equivalent open circuit voltage measured from the simulation was 265.9 kV. The arc voltage and fault current were then compared between the calculated (from equations (3-18) and (3-19)) and the measured (Table 3-13).

Table 3-13: Comparison of calculated and measured parameters when the LCB at Sub A was opened

Parameter	Calculated	Measured off the simulated waveform
Arc Voltage (kV)	2.77 kV	2.64 kV
Fault Current (kA)	2.62 kA	2.5 kA

3.6.2.5 Sub C LCB Opens (Line A-C 1)

Once the LCB at Sub C opened this resulted in Line A-C 1 being isolated from the network configuration. The charge from the line capacitance of A-C 1 discharged into the fault and there was an exchange of energy between the capacitance and the inductance. The capacitance discharged at a rate determined by the magnitude of the resistance in the isolated circuit by the time constant RC. The natural frequency was determined by the magnitude of the capacitance and inductance in the isolated circuit. The combination of the R, L and C determined the transient response of the circuit (underdamped, critically damped, or overdamped).

Based on the results presented thus far, the calculated and simulated/measured values indicate good correlation. The conclusion from the analysis indicated that the Thévenin equivalent impedance increased with each state while the magnitude of fault current decreased.

3.6.3 Sub C – Fault current contribution of 5 kA (Line C-B 1)

The third case analysed was the integration of Sub C into the series compensated transmission circuit presented in section 3.6.1. The second case considered the series capacitor bank between Sub A and C. The series capacitor bank in this case was connected between Sub B and Sub C (Figure 3-47). Sub C represents the integration of generation source which changes the line length of the compensated

circuit while also contributing fault current. The fault current contribution from Sub C was 5 kA. A three-phase-to-ground fault was applied along the circuit between Sub B and Sub C.

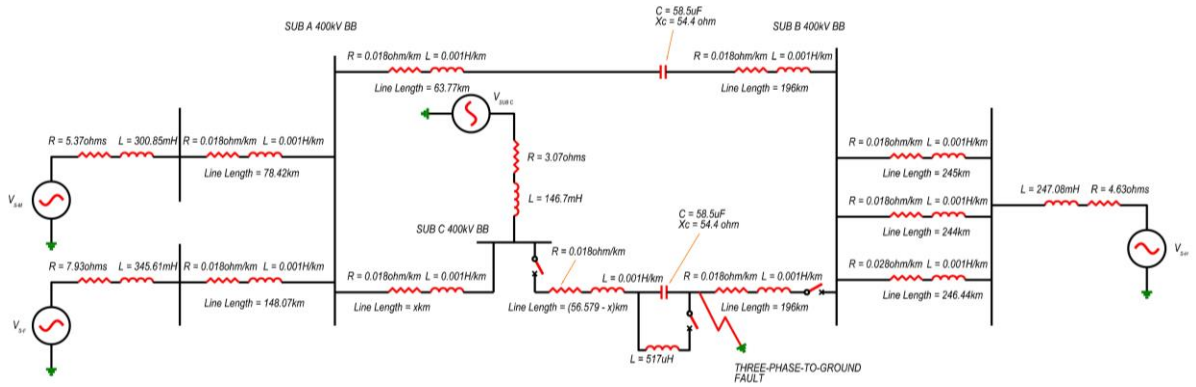

Figure 3-47: Single phase representation of the Network Configuration for Case 2: Line C-B 1 (Sub C – 5 kA contribution)

The same analysis will be presented as with the other two cases discussed.

3.6.3.1 Steady State/Pre-fault condition (Line C-B 1)

The load flow study was conducted with the integration of Sub C. Since there were four voltage sources in this configuration, the phase angles must be known for each voltage source to accurately analyse the network. The phase angle for Sub C were selected based on the phase angles of the voltage sources adjacent to it. Additionally, the voltage magnitudes were assumed to be the same at 1 p.u. The LCBs at Sub B and Sub C remained closed and the series capacitor bypass circuit breaker remained opened (Figure 3-48). The scenario analysed was the line length of line C-B 1 being 232.5 km which was made up of a line length between Sub B – series capacitor bank being 196 km and line length between series capacitor bank to Sub C being 36.5 km. The line length for line A-C 1 was 20 km.

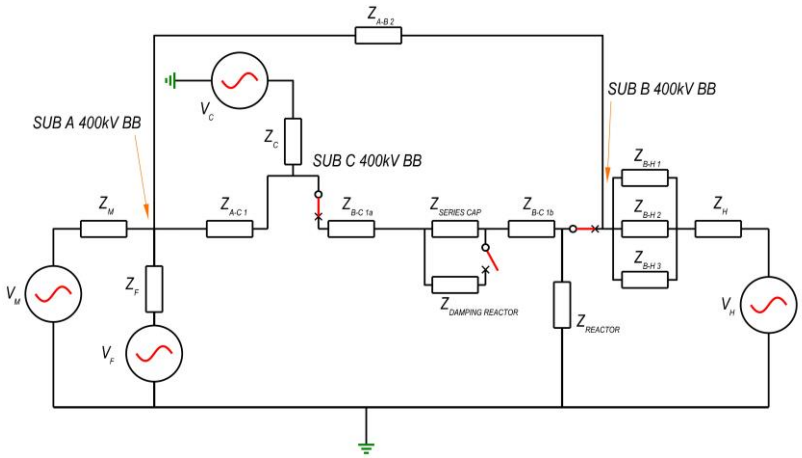

Figure 3-48: Circuit diagram of the steady state pre-fault network configuration for the series compensated line C-B 1

3.6.3.2 Three-phase-to-ground fault application (Line C-B 1)

A three-phase-to-ground fault was applied 1 km away from Sub C along line C-B 1 through the arc impedance Z_{arc} (Figure 3-49).

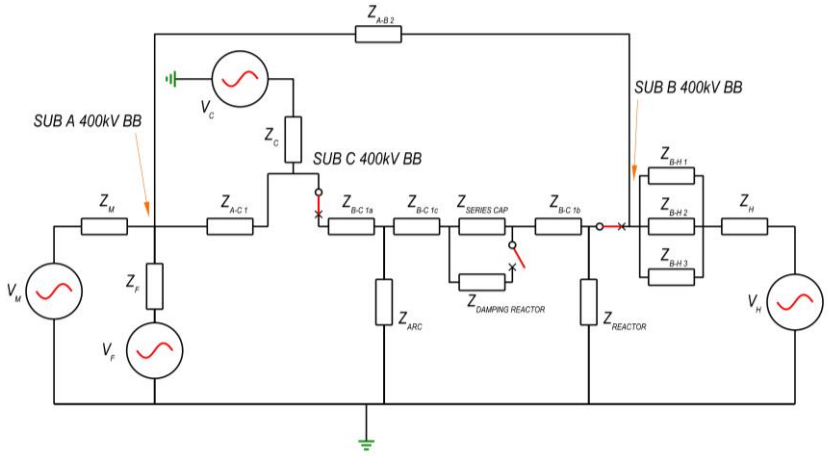

Figure 3-49: Three-phase-to-ground fault applied to the series compensated circuit Line A-C 1

The Thévenin equivalent impedance was determined from the circuit below (Figure 3-50):

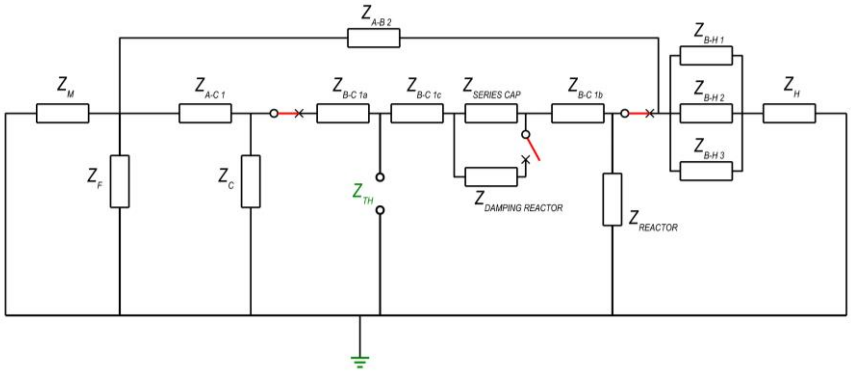

Figure 3-50: Thévenin equivalent impedance Z_{th} at the location of the fault (Line C-B 1)

The network impedance was reduced utilising the Delta-Star impedance transformation in order determine the Thévenin equivalent impedance (Figure 3-51).

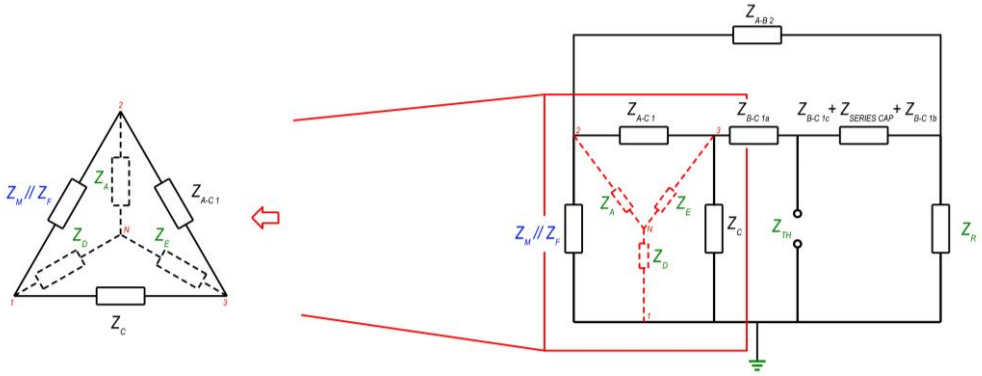

Figure 3-51: Delta-Star impedance transformation applied to determine the Thévenin equivalent impedance (Line C-B 1)

The transformed impedances were determined as follows:

$$Z_A = \frac{(Z_M // Z_F)(Z_{A-C\,1})}{(Z_M // Z_F) + Z_{A-C\,1} + Z_C} \tag{3-34}$$

$$Z_D = \frac{(Z_M//Z_F)(Z_{C1})}{(Z_M//Z_F) + Z_{A-C\,1} + Z_C} \tag{3-35}$$

$$Z_E = \frac{(Z_C)(Z_{A-C\,1})}{(Z_M//Z_F) + Z_{A-C\,1} + Z_C} \tag{3-36}$$

Where:

$$\mathrm{Z}_R = [(Z_{B-H\,1}//\mathrm{Z}_{\mathrm{B-H\,2}}//\mathrm{Z}_{\mathrm{B-H\,3}}) + \mathrm{Z}_{\mathrm{H}}]//\mathrm{Z}_{\mathrm{REACTOR}} \tag{3-37}$$

A second Delta-Star impedance transformation was required to determine the Thévenin equivalent impedance (Figure 3-52).

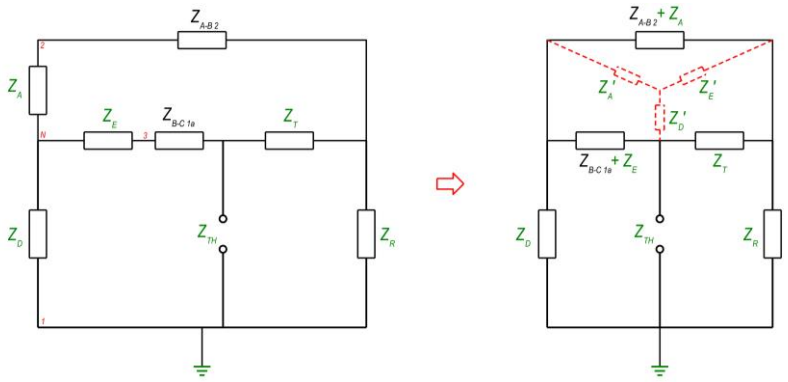

Figure 3-52: Second Delta-Star impedance transformation applied to determine the Thévenin equivalent impedance (Line C-B 1)

Letting Z_T=$Z_{C\text{-}B\ 1c}$+$Z_{SERIES\ CAP}$+$Z_{C\text{-}B\ 1b}$, the transformed impedances were determined as follows:

$$Z_A{}' = \frac{(Z_{B-C\,1a} + Z_E)(Z_{A-B\,2} + Z_A)}{Z_{B-C\,1a} + Z_E + Z_{A-B\,2} + Z_A + Z_T} \tag{3-38}$$

$$Z_D{}' = \frac{(Z_{B-C\,1a} + Z_E)(Z_T)}{Z_{B-C\,1a} + Z_E + Z_{A-B\,2} + Z_A + Z_T} \tag{3-39}$$

$$Z_E{}' = \frac{(Z_{A-B\,2} + Z_A)(Z_T)}{Z_{B-C\,1a} + Z_E + Z_{A-B\,2} + Z_A + Z_T} \tag{3-40}$$

The Thévenin equivalent impedance was determined as follows:

$$Z_{th} = \big((Z_A' + Z_D)//(Z_E{}' + Z_R)\big) + Z_D{}' \tag{3-41}$$

The calculated Thévenin equivalent impedance for a fault 1 km away from Sub A was 1.54 Ω+i22.93 Ω.

The measured Thévenin equivalent open circuit voltage was 256.3 kV_{rms} per phase.

The arc voltage, V_{arc}, was calculated as 2.77 kV_{rms} per phase from section 3.6.2.2. This arc voltage was utilised in all calculations as this magnitude was considered constant. The arc voltage measured off the simulated waveform was measured to be 2.5 kV_{rms} per phase.

The arc impedance, Z_{arc}, was determined by solving equation (3-18) which resulted in 0.017 Ω+i0.25 Ω.

The fault current was calculated using equation (3-19) to be 11.03 kA_{rms} per phase. The fault current measured off the simulated waveform was 10 kA_{rms} per phase.

3.6.3.3 Series Capacitor Bank bypassed (Line C-B 1)

The series capacitor bank was then bypassed by closing the series capacitor bank bypass circuit breaker. The series capacitor bypass damping reactor was then connected to the transmission line, altering the impedance of the line (Figure 3-53).

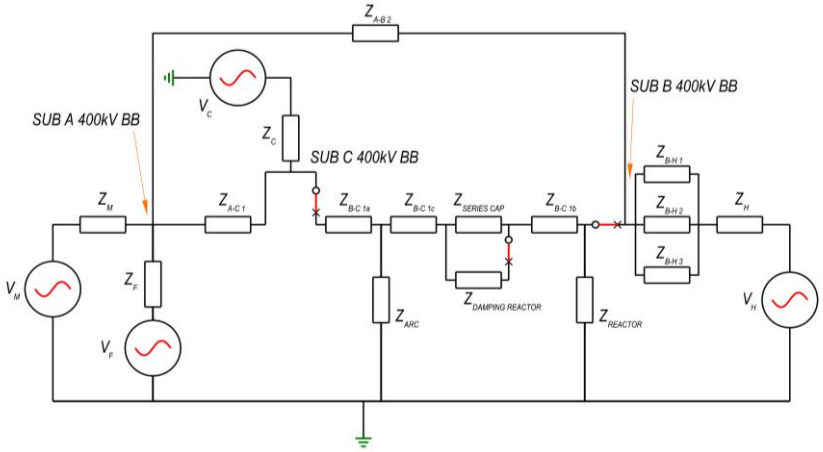

Figure 3-53: Series bypass capacitor bank circuit breaker closed Line C-B 1 (Sub C – 5 kA)

Applying the same equations as derived in section 3.6.3.2 with the series capacitor impedance replaced with the series capacitor damping reactor impedance yielded the following results:

Thévenin equivalent impedance (Z_{th}): 0.017 Ω+i0.26 Ω
Thévenin equivalent open circuit voltage: 255 kV

The Thévenin equivalent open circuit voltage measured from the simulation was 265.9 kV. The arc voltage and fault current were then compared between the calculated (from equations (3-18) and (3-19)) and the measured (Table 3-14).

Table 3-14: Comparison of calculated and measured parameters for series capacitor bypass circuit

Parameter	Calculated	Measured off the simulated waveform
Arc Voltage (kV)	2.77 kV	2.55 kV
Fault Current (kA)	10.64 kA	9.77 kA

3.6.3.4 Sub B LCB Opens (Line C-B 1)

The LCB at Sub B was then opened after the series capacitor bank was bypassed (Figure 3-54).

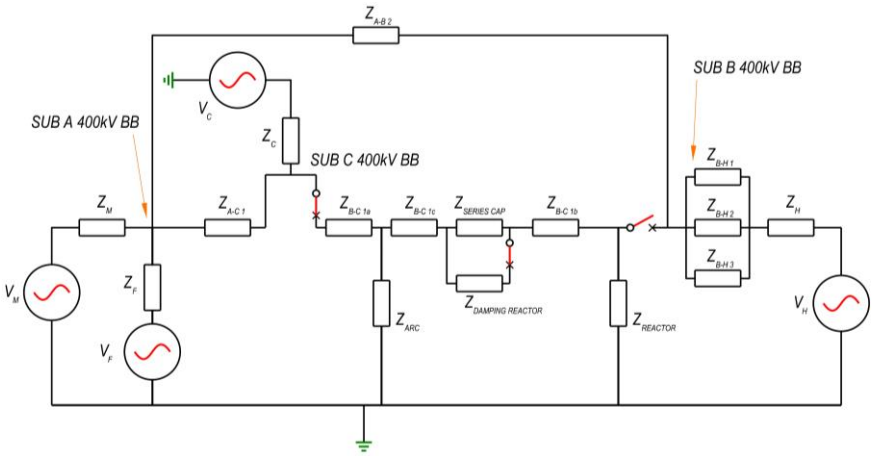

Figure 3-54: LCB at Sub B was opened after the series capacitor bank was bypassed

The Thévenin equivalent impedance was recalculated based on the change in network configuration (Figure 3-55).

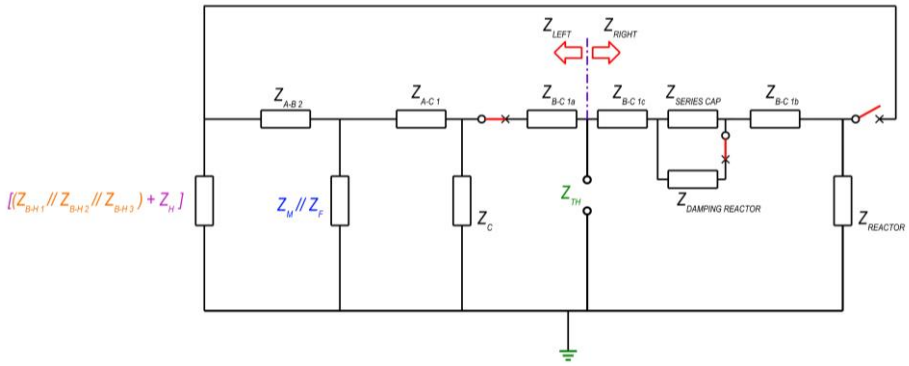

Figure 3-55: Thévenin equivalent impedance after LCB at Sub B was opened

Z_{th} was calculated as seen from the fault:

$$Z_{th} = Z_{LEFT} // Z_{RIGHT} \tag{3-42}$$

Where

$$Z_{LEFT} = \left(\left(\left((Z_T + Z_{A-B\,2}) // (Z_M // Z_F)\right) + Z_{A-C\,1}\right) // Z_C\right) + Z_{B-C\,1a} \tag{3-43}$$

$Z_T = (Z_{B\text{-}H\,1} // Z_{B\text{-}H\,2} // Z_{B\text{-}H\,3}) + Z_H$

$$Z_{RIGHT} = z_{B-C\,1c} + Z_{DAMPING\ REACTOR} + Z_{B-C\,1b} + Z_{REACTOR} \tag{3-44}$$

The resultant Thévenin equivalent impedance was calculated to be 1.6 Ω+i24.11Ω.

The Thévenin equivalent open circuit voltage measured from the simulation was 254.03 kV. The arc voltage and fault current were then compared between the calculated (from equations (3-18) and (3-19)) and the measured (Table 3-15).

Table 3-15: Comparison of calculated and measured parameters when the LCB at Sub B was opened

Parameter	Calculated	Measured off the simulated waveform
Arc Voltage (kV)	2.77 kV	2.55 kV
Fault Current (kA)	10.4 kA	9.57 kA

3.6.3.5 Sub C LCB Opens (Line C-B 1)

Once the LCB at Sub C opened this resulted in Line C-B 1 being isolated from the network configuration. The charge from the line capacitance of C-B 1 discharged into the fault and there was an exchange of energy between the capacitance and the inductance. The capacitance discharged at a rate determined by the magnitude of the resistance in the isolated circuit by the time constant RC. The natural frequency was determined by the magnitude of the capacitance and inductance in the isolated circuit. The combination of the R, L and C determined the transient response of the circuit (underdamped, critically damped, or overdamped).

Based on the results presented thus far, the calculated and simulated/measured values indicated good correlation. The conclusion from the analysis indicated that the Thévenin equivalent impedance increased with each state while the magnitude of fault current decreased.

Once the simulations were conducted by varying the various parameters in accordance with the three cases described, the results were consolidated and are presented below in section 3.7. The analysis of each individual case is presented in detail.

3.7 Simulation Results

Simulations were conducted for three scenarios:

Case 1: Sub C not added (Figure 3-56).

The circuit of interest was the series compensated transmission line A - B 1 of length 252.5 km. A three-phase-to-ground fault was applied between Sub A and Sub B along line A-B 1. The magnitude of the series capacitor bank was considered fixed for all cases considered.

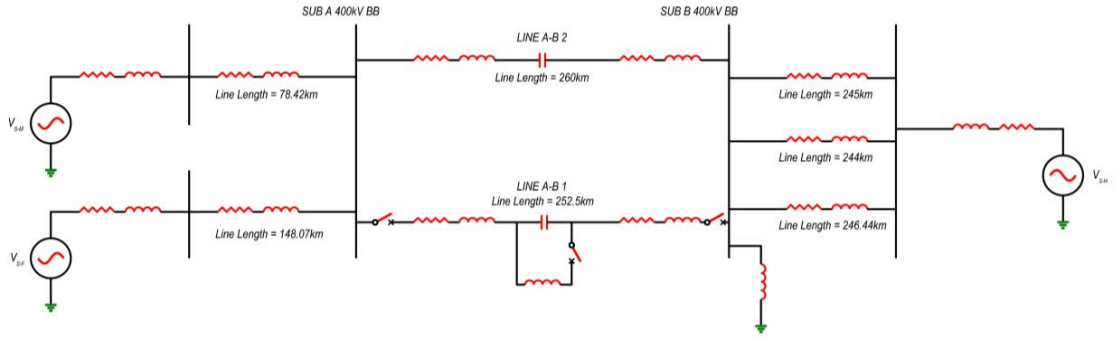

Figure 3-56: Network configuration of Case 1

Case 2a: Line A-C 1 - Sub C integrated with a fault contribution of 5 kA

Line A-B 1 was split into two lines by looping in and out of Sub C resulting in two lines, line A-C 1 and line C-B 1. The series capacitor bank was located along line A-C 1 (Figure 3-57). The first scenario considered was for the new voltage source (Sub C) to have a fault contribution of 5 kA. The line length between Sub A and Sub B was fixed at 252.5 km and the distance between Sub A and the series capacitor bank was fixed at 56.5 km. The magnitude of the series capacitor bank was considered fixed

for all cases evaluated. The position of Sub C was selected such that the compensation factor did not exceed 90%. As a result, the line lengths selected for A-C 1 were 200 km and 240 km, resulting in line C-B 1 being 52.5 km to 12.5 km in length respectively.

Case 2b: Line A-C 1 - Sub C integrated with a fault contribution of 10 kA

The configuration of Case 2b was the same as Case 2a however the fault current contribution was increased from 5 kA 10 kA (Figure 3-57).

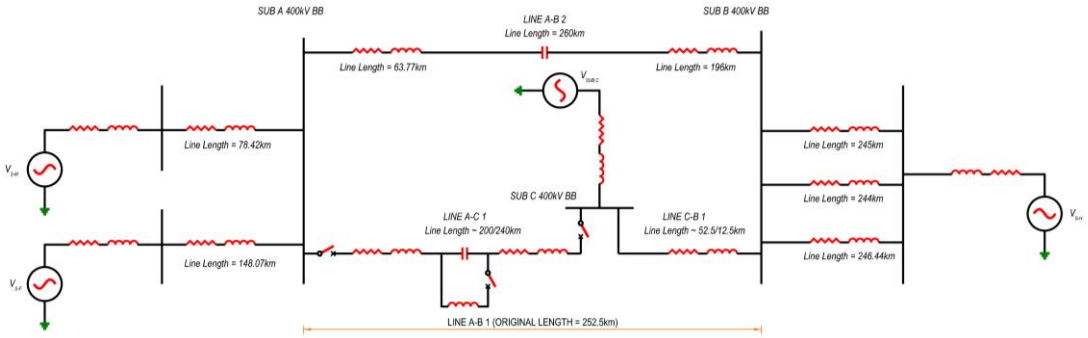

Figure 3-57: Network configuration of Case 2a and 2b

Case 3a: Line C-B 1 - Sub C integrated with a fault contribution of 5 kA

Case 3a entailed line A-B 1 being split into two lines by looping in and out of Sub C resulting in two lines, line A-C 1 and line C-B 1. The series capacitor bank was located along line C-B 1 (Figure 3-58). This scenario considered the new voltage source (Sub C) to have a fault contribution of 5 kA. The line length between Sub A and Sub B was fixed at 252.5 km and the distance between Sub A and the series capacitor bank was fixed at 56.5 km. The magnitude of the series capacitor bank was considered fixed for all cases considered. The position of Sub C was selected such that the compensation factor did not exceed 90%. As a result, the line lengths selected for C-B 1 were 212.5 km and 232.5 km, resulting in line A-C 1 being 40 km to 20 km in length respectively.

Case 3b: Line C-B 1 - Sub C integrated with a fault contribution of 10 kA

The configuration of Case 3b was the same as Case 2a however the fault current contribution was increased from 5 kA 10 kA (Figure 3-58).

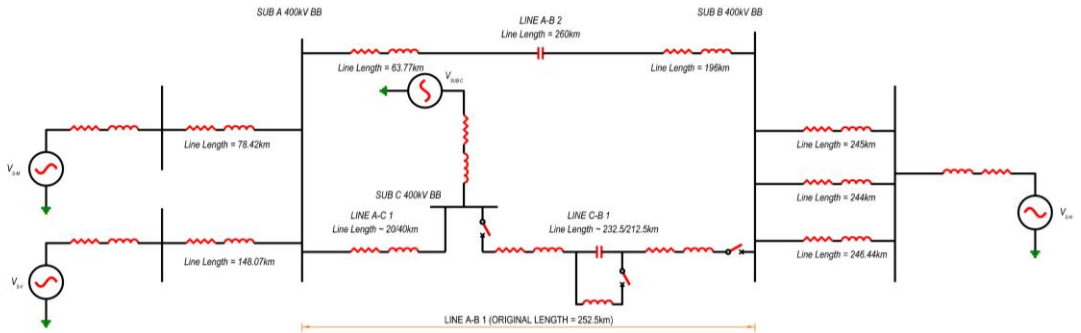

Figure 3-58: Network configuration of Case 3a and 3b

The key criteria (peak recovery voltage and RRRV which is defined by the parameter envelope) were then evaluated based on the simulation methodology described in section 3.5.1. The following sections presents the results of the simulations conducted as indicated above.

3.7.1 Simulation Results: Case 1

The first case was simulated which entailed not integrating Sub C (Figure 3-59). The circuit investigated was the series compensated transmission line between Sub A and Sub B, line A-B 1. The length of the transmission line was 252.5 km and the series capacitor bank was located 56.5 km away from Sub A. A damping reactor of magnitude 517 µH was installed across the series capacitor.

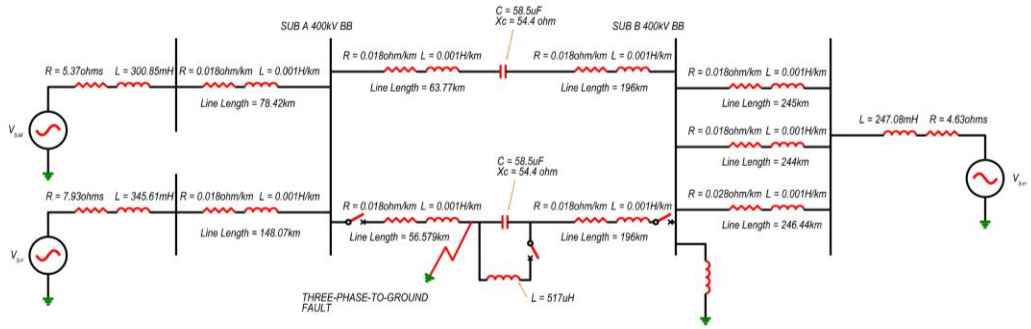

Figure 3-59: Single Line Diagram of Case 1

The compensation factor for the base case was determined in section 3.3.6. A three-phase-to-ground fault was applied at various points along the transmission line. Sub A was used as a reference point for all fault positions applied in the scenarios considered.

The peak fault current through the LCBs at Sub A and Sub B were determined first (Figure 3-61 and Figure 3-62). The maximum magnitude of the peak fault current was determined over the duration of the fault. The reason for this was to establish the test duty of the circuit breaker for the various simulations which determined the circuit breaker TRV capability.

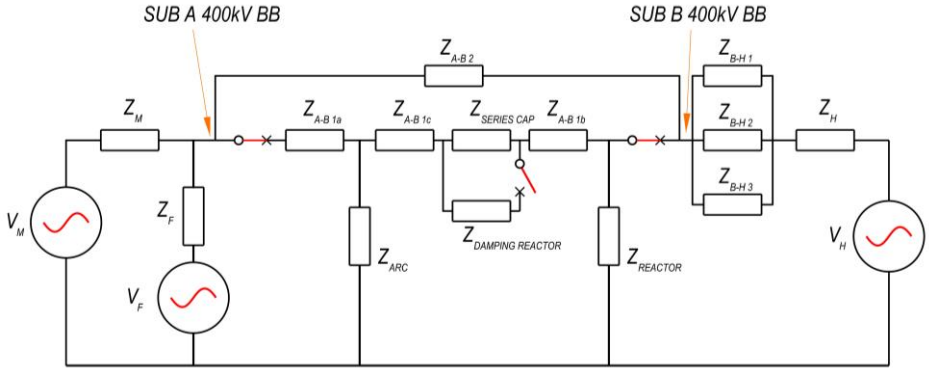

Figure 3-60: Circuit configuration of case 1

Sub A supplied the full fault current to the fault and to Sub B for faults up until the surge impedance was matched for line impedance A-B 1a at 170 km (Figure 3-60). The fault current reduced as the distance between the position of the fault applied to the LCB at Sub A increased (Figure 3-61). This was due to the increase in impedance of the transmission line between the LCB and the fault position. A step change increase in magnitude for faults just after the series capacitor bank was observed. This was due to the effective impedance of the transmission line from Sub A to the fault being reduced. Subsequently the magnitude of the peak fault current decreased with an increase in distance from the series capacitor bank to the fault position in the direction of Sub B. The peak fault current then had an increase in magnitude of peak fault current at approximately 170 km from Sub A. This was attributed to surge impedance matching of transmission line A-B 1a. This correlated with the current profile for Sub B (Figure 3-62) for faults observed at 170 km from Sub B. The maximum peak short circuit current was approximately 8 kA and 6.6 kA for the LCBs at Sub A and Sub B respectively.

The fault current at Sub B was supplied by Sub A up until the surge impedance of line A-B 1a was reached at 170 km. Fault current was then supplied from Sub B to the fault for fault positions between 170 km to 252.5 km away from Sub A. There was a dip in fault current for faults occurring approximately 20 to 30 km away from Sub B. This may be attributed to the current split between the fault and the line reactor of Sub B feeder bay.

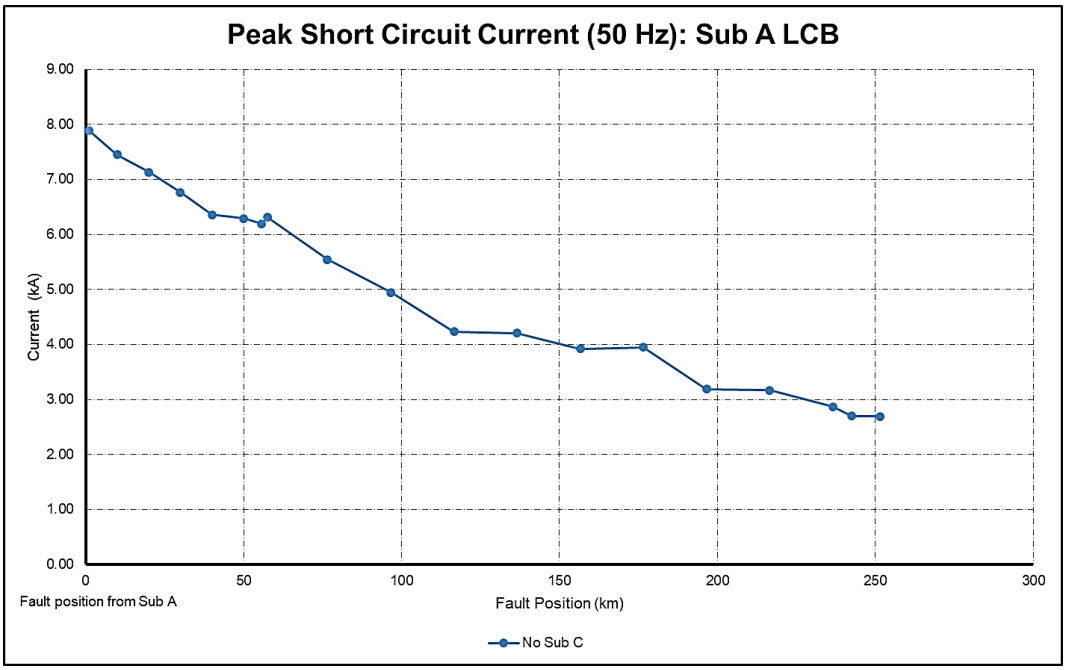

Figure 3-61: Peak fault current (50 Hz) for LCBs at Sub A – Case 1

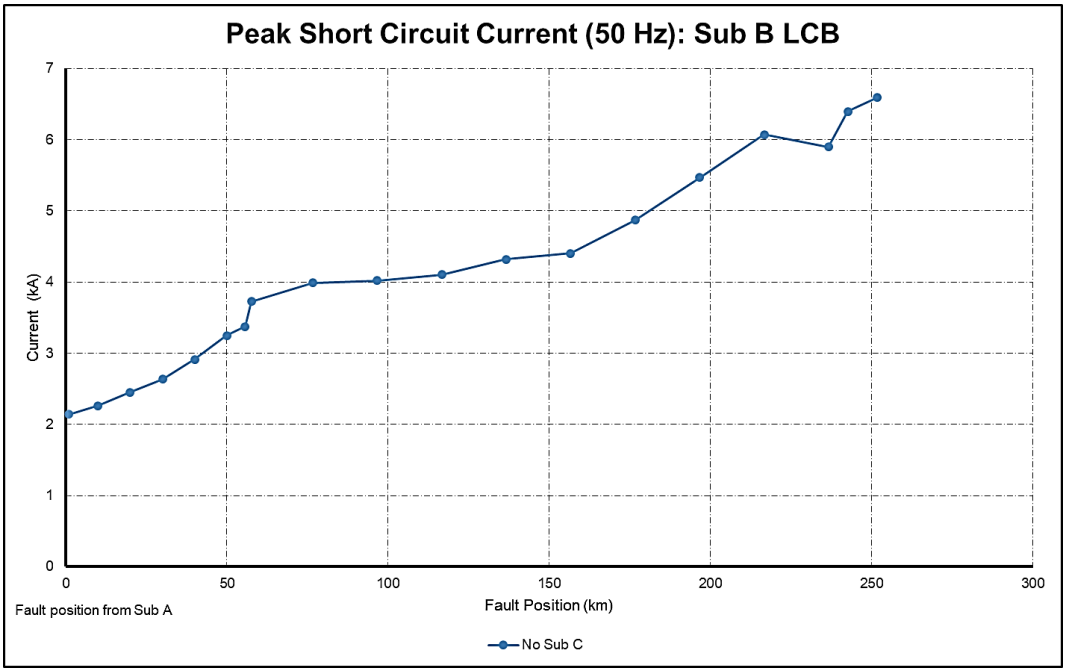

Figure 3-62: Peak fault current (50 Hz) for LCBs at Sub B – Case 1

The test duty of a circuit breaker is the ratio of the magnitude of fault current flowing through the circuit breaker to the maximum fault current rating of the circuit breaker. The test duties for each simulation were then derived as described in section 3.5.2 and plotted for both LCBs at Sub A and Sub B (Figure 3-63 and Figure 3-64). These test duties were then utilised to determine the parameter envelopes to be

selected for evaluation of the LCBs TRV capability at the various fault positions. The test duty is proportional to fault current. The maximum test duty for both LCBs was 30%. This indicated that the LCBs were to be assessed against the two-parameter envelope.

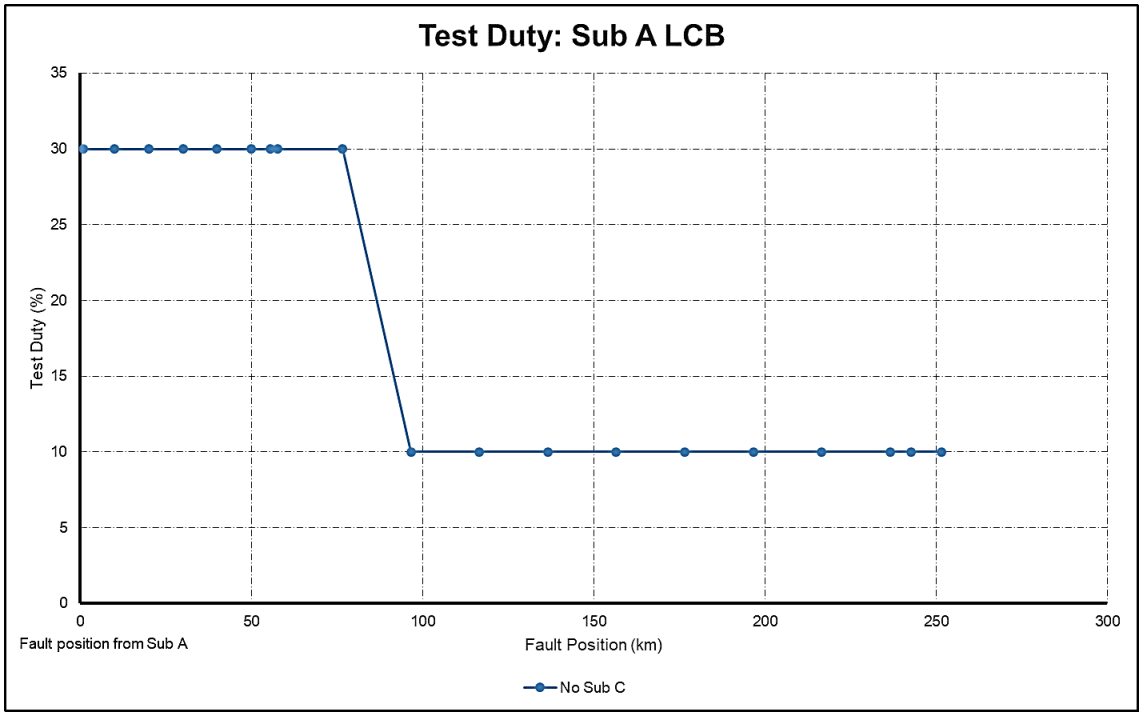

Figure 3-63: Test duties for LCBs at Sub A – Case 1

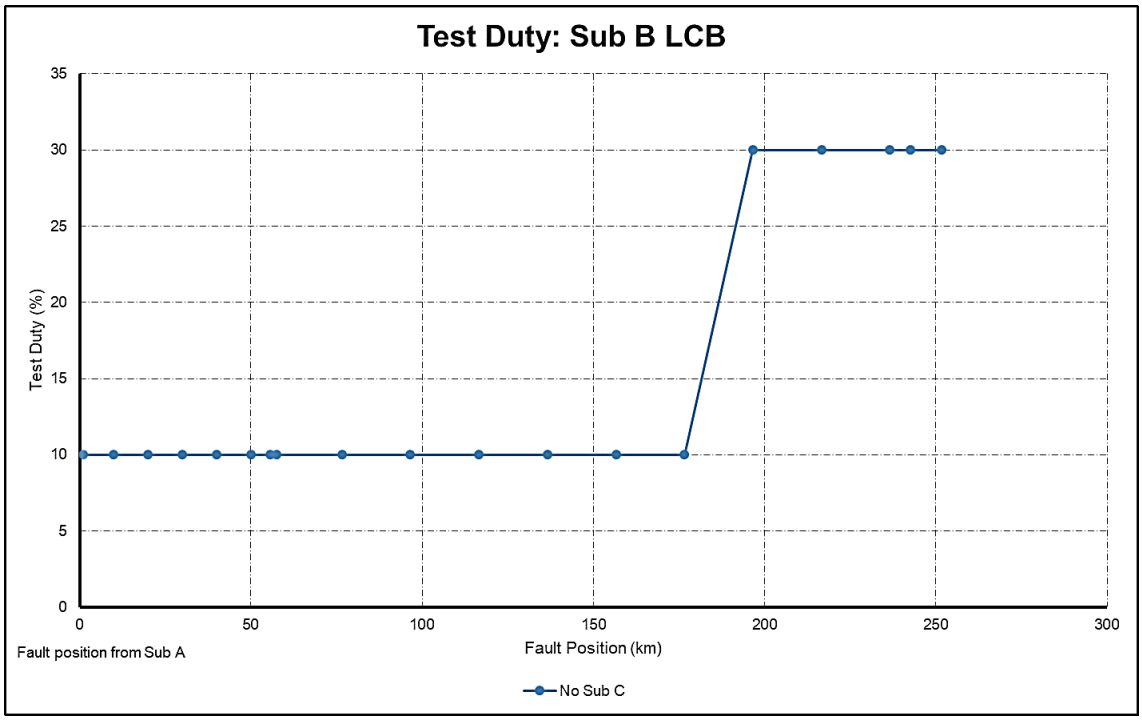

Figure 3-64: Test duties for LCBs at Sub B – Case 1

Figure 3-65 shows the peak recovery voltage profile for the LCB at Sub A for faults applied at varied positions along the transmission line. The voltage at Sub A was inversely proportional to the fault position for faults up until the series capacitor bank. There was a peak observed between 50 km and

80 km away from Sub A. The reason for this was due to the Thévenin equivalent impedance reaching surge impedance and the network delivers maximum current to the fault.

The peak recovery voltages marginally exceeded the circuit breaker peak recovery voltage limit at this point (Figure 3-66). However, there is a margin of safety catered for when selecting the TRV parameter envelope based on the test duty of the circuit breaker.

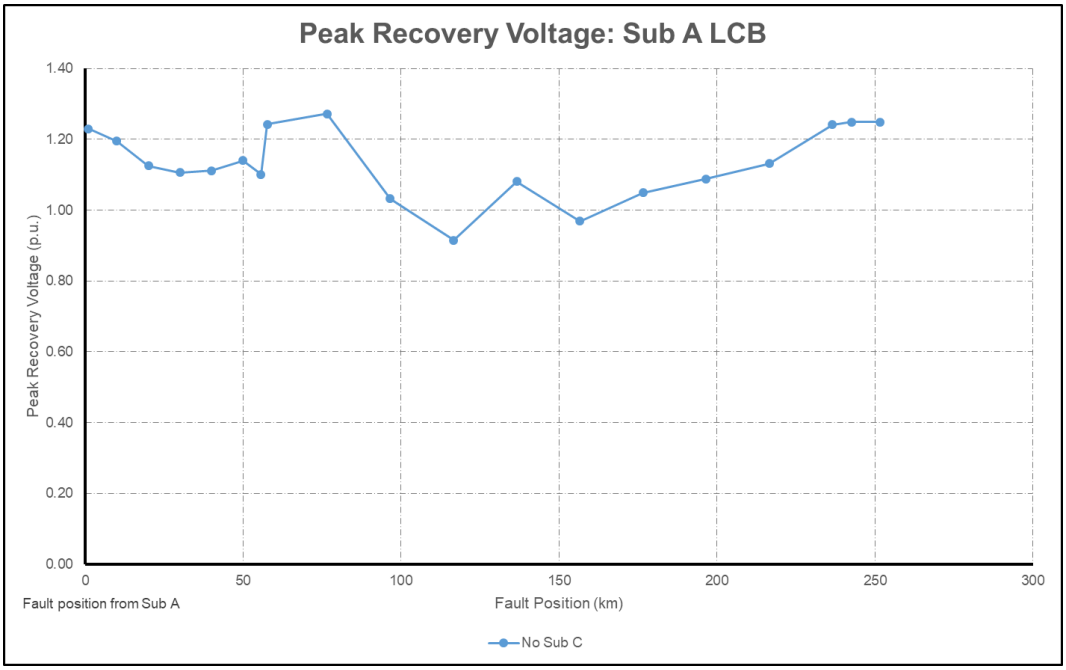

Figure 3-65: Peak recovery voltage profile for LCBs at Sub A – Case 1

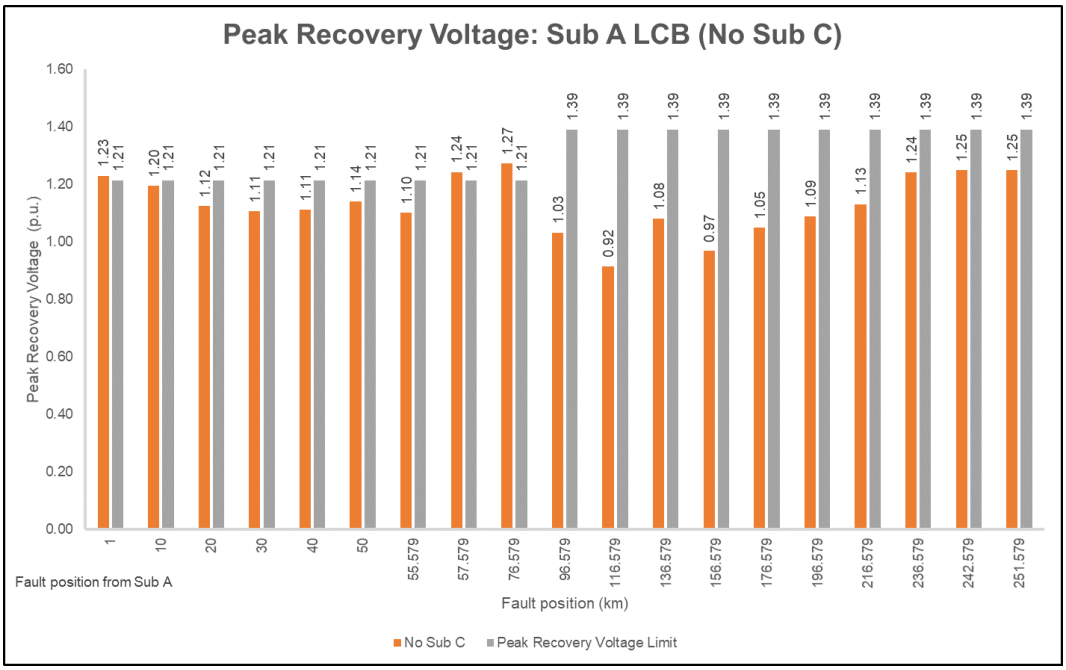

Figure 3-66: Peak recovery voltages and limits for LCBs at Sub A – Case 1

There was a notable peak of the recovery voltage observed at approximately 140 km away from Sub A (Figure 3-65) and may be attributed to the combination of the transient response on the line side (indicated in the red voltage profile of Figure 3-67) of the LCB at Sub A as well the voltage reflections

of the fault impedance. The profile of the line side voltage suggests a highly underdamped response of the circuit after the LCB was opened. The voltage profile indicated in green is the source side transient response and the blue voltage profile is the TRV of the LCB at Sub A.

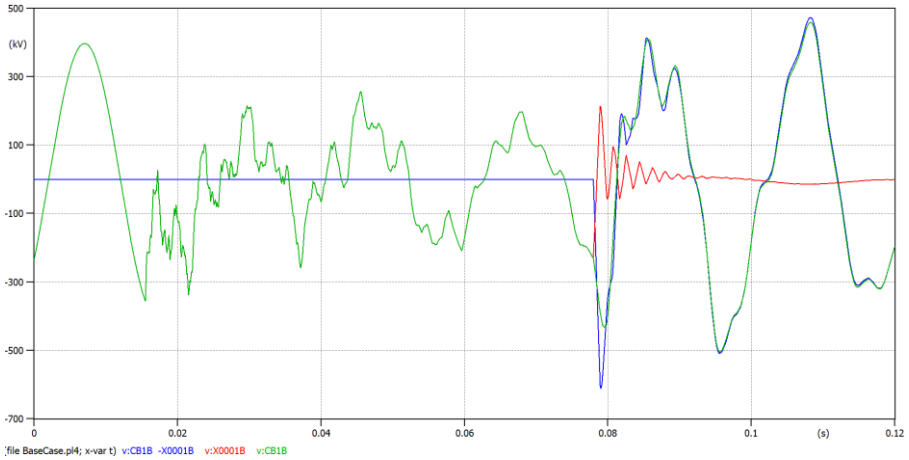

Figure 3-67: Underdamped response of Sub A LCB for a fault at 140 km away from Sub A

For faults from approximately 160 km away from Sub A, the inductive reactance of the transmission line starts dominating. As a result, the voltage starts to lead the current. Since the LCB opens at a current zero, the magnitude of voltage for which the LCB opened, increased with an increase in distance of the fault position from Sub A.

The peak recovery voltage profile for the LCB at Sub B followed the same voltage profile as Sub A (Figure 3-68) however the effect of the series capacitor bank was not significant due to the magnitude of the inductive reactance of the transmission line being significantly larger than the magnitude of the capacitive reactance of the capacitor bank. The peak recovery voltages that the LCB at Sub B was exposed to did not exceed its peak recovery voltage limits (Figure 3-69).

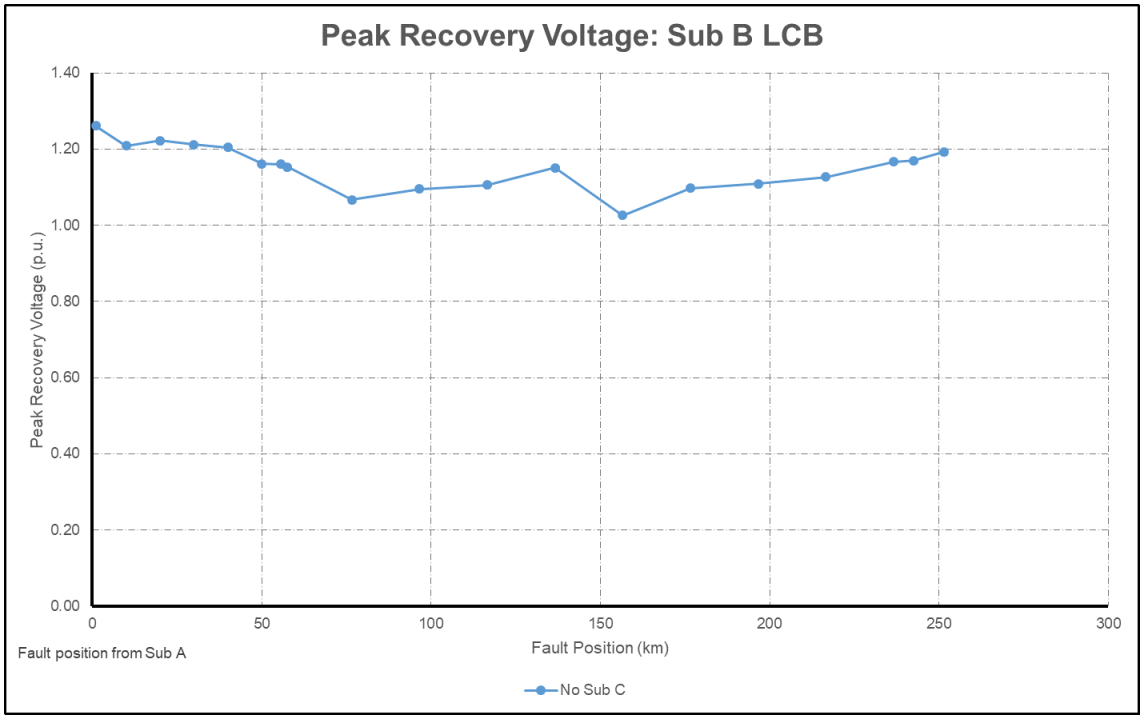

Figure 3-68: Peak recovery voltage profile for LCBs at Sub B – Case 1

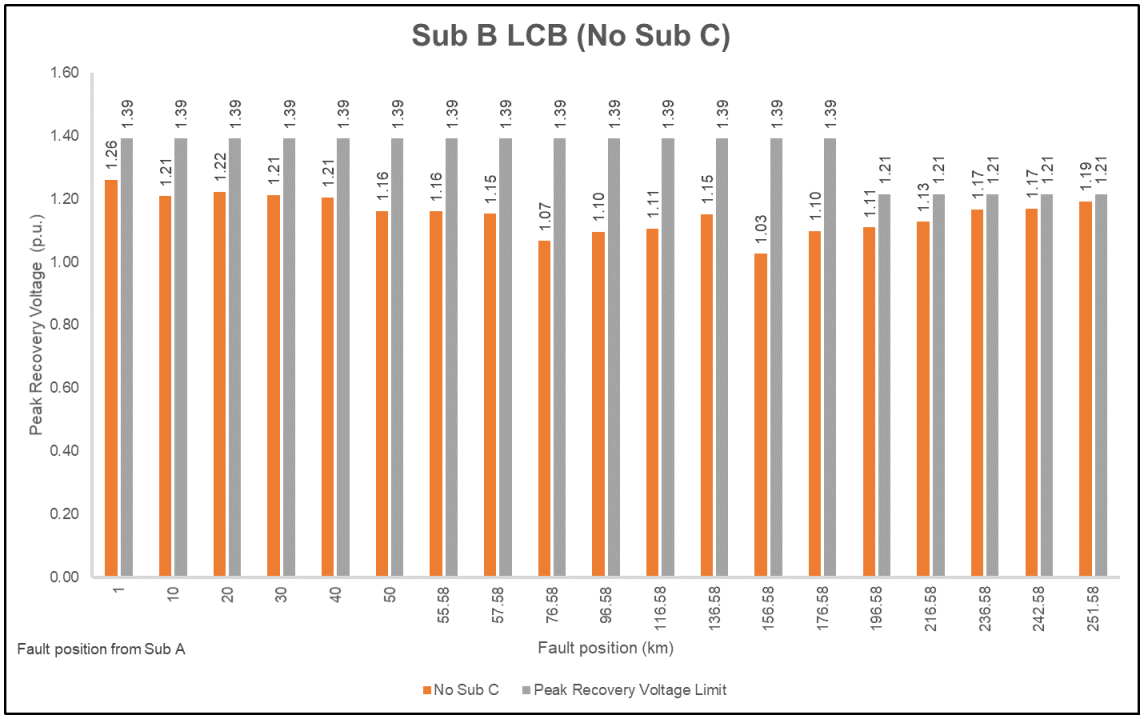

Figure 3-69: Peak recovery voltages and limits for LCBs at Sub B – Case 1

The RRRV of the LCBs for all three scenarios were evaluated in a similar manner (Figure 3-70).

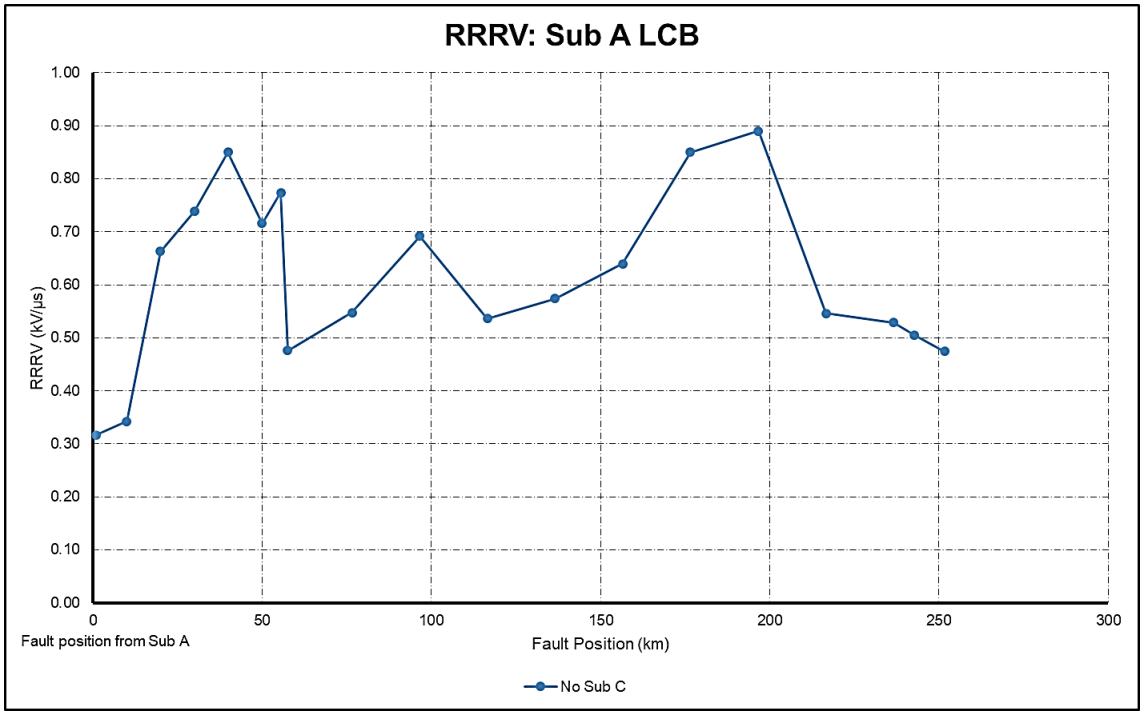

Figure 3-70: RRRV profile for LCBs at Sub A – Case 1

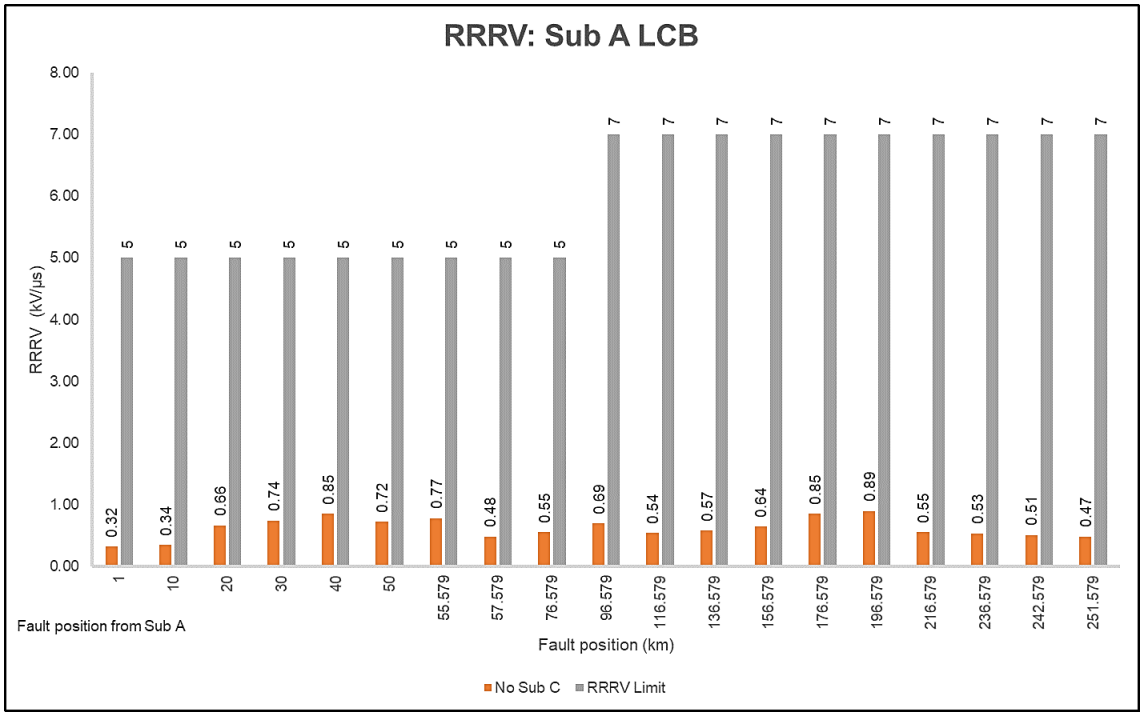

Figure 3-71: RRRV and limits for LCBs at Sub A – Case 1

The measurements were taken at the inception of the LCB opening and the voltage recorded after a duration of 112 µs once the LCB opens for a test duty of 10% and 137 µs for a test duty of 30%. The RRRV is calculated based on the equation below [3]:

$$RRRV = \sqrt{2}\omega M I_{SC} Z_0 \tag{3-45}$$

ω: angular velocity [rad/s]
M: Test Duty
I_{SC}: Fault Current rating of the circuit breaker [A]
Z_0: Surge Impedance [Ω]

The RRRV was expected to be at its highest for faults in close proximity to the LCB (within the first 10 km). However, the saw-tooth response of the peak recovery voltage for faults up to 20 km from the LCB reduced the RRRV. Therefore, the RRRV was calculated from the point at which the LCB opened until the first peak to get a more accurate result. A peak RRRV was observed at approximately 80 km from Sub A. This was attributed to the Thévenin equivalent impedance reaching the surge impedance at this point. A peak was also observed between 170 km and 200 km from Sub A due to the surge impedance of line A-C 1a being matched.

The RRRV for the LCB at Sub A was evaluated against the RRRV limit corresponding to specific test duties. The RRRV was not exceeded in the base case for the LCB at Sub A as indicated in Figure 3-71.

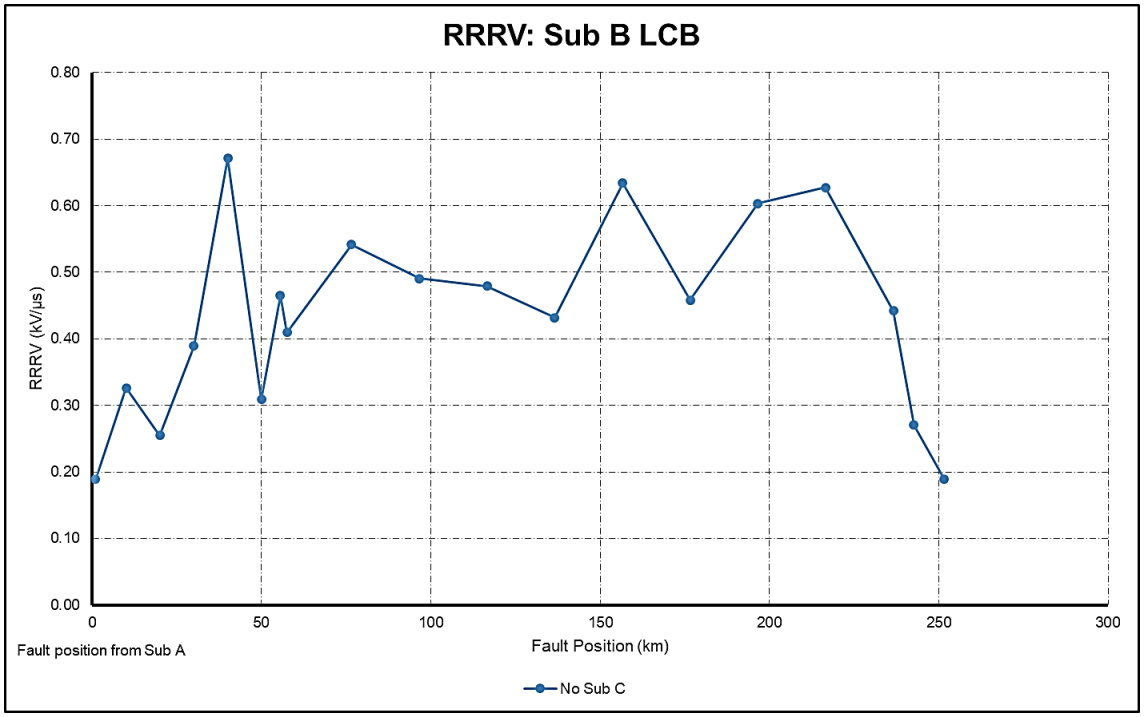

Figure 3-72: RRRV profile for LCBs at Sub B – Case 1

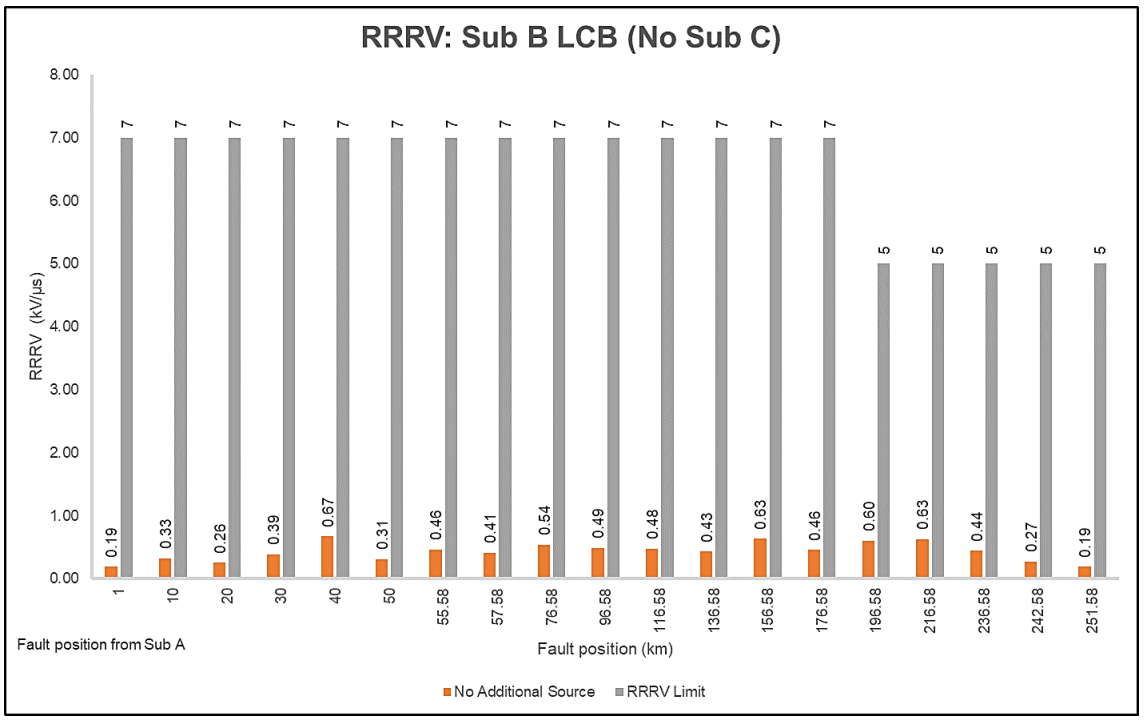

Figure 3-73: RRRV and limits for LCBs at Sub B – Case 1

Similarly, the RRRV for the LCB at Sub B was evaluated (Figure 3-72). The RRRV profile for the LCB at Sub B was similar to that of Sub A. However the magnitude of the RRRV for a fault at approximately 170 km from Sub A reached a low point due to the surge impedance being matched in line A-C 1a The RRRV did not exceed the RRRV limit as indicated in Figure 3-73.

3.7.2 Simulation Results: Case 2a (Sub C – 5 kA)

Simulations were then conducted for the Case 2 which entailed integrating a voltage source, Sub C, along the series compensated transmission line, A-B 1, as discussed in section 3.7.1. Line A-B 1 was split into two lines by looping in and out of Sub C resulting in line A-C 1 and line C-B 1. The series capacitor bank was located along line A-C 1.

The first scenario considered was for the new voltage source (Sub C) to have a fault contribution of 5 kA (Figure 3-74). The line length between Sub A and Sub B was fixed at 252.5 km and the distance between Sub A and the series capacitor bank was fixed at 56.5 km. In order to integrate Sub C at 200 km and 240 km from Sub A, line A-C 1b would have to be increased from 143 km to 183 km respectively. Line C-B 1 would decrease from 52.5 km to 12.5 km (Figure 3-57).

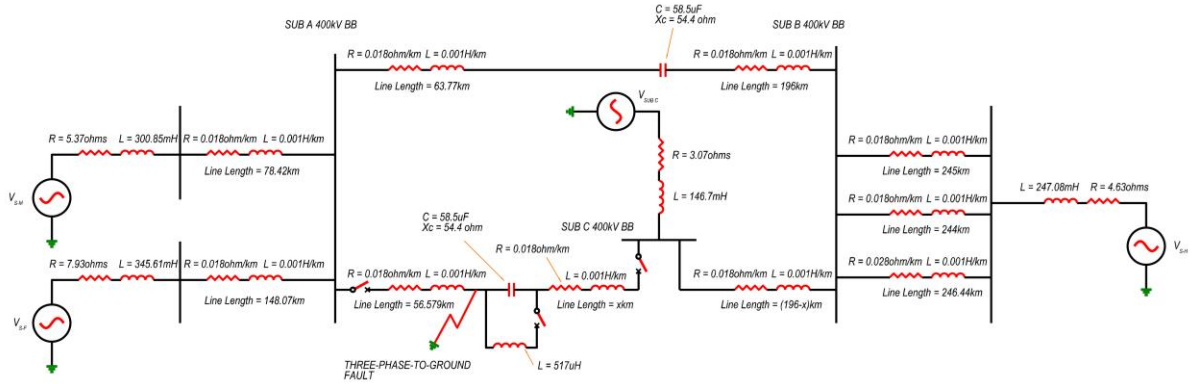

Figure 3-74: Single Line Diagram of Case 2a

The details of the source impedance of Sub C is as follows (Table 3-16):

Table 3-16: Sub C source impedance parameters

Parameter	Sub C
Peak Fault Current (kA)	5
X/R Ratio (peak)	15

The parameters of the series capacitor bank remained fixed for all the simulations conducted. Therefore, the compensation factor varied for simulations conducted for each position of Sub C and the corresponding transmission line lengths. The compensation factor was varied between 71% and 85% as indicated below (Table 3-17):

Table 3-17: Compensation factor for studies conducted for Line A- C 1

Line length (km)	Line Configuration	Inductance	Line inductive reactance (Ω)	Capacitor Bank Capacitive Reactance (Ω)	Compensation Factor
km		H/km	$X_L = 2\pi f L\ (\Omega)$	$X_C = \frac{1}{2\pi f C}\ (\Omega)$	%
200	A – C 1	0.001018	63.97	54.4	85%
240	A – C 1		76.77		71%

Compensation factors exceeding 90% were not considered as this was deemed impractical from an application perspective.

The first two cases that were evaluated were:

- Line A-C 1 which was 200 km long and Sub C was 143 km away from the series capacitor bank. The fault current contribution of from Sub C was 5 kA. Line C-B 1 was 52.5 km long. Sub A was 56.5 km away from the series capacitor bank.
- Line A-C 1 which was 240 km long and Sub C was 183 km away from the series capacitor bank. The fault current contribution of from Sub C was 5 kA. Line C-B 1 was 12.5 km long. Sub A was 56.5 km away from the series capacitor bank.

The peak fault currents were evaluated for the above scenarios (Figure 3-75 and Figure 3-76).

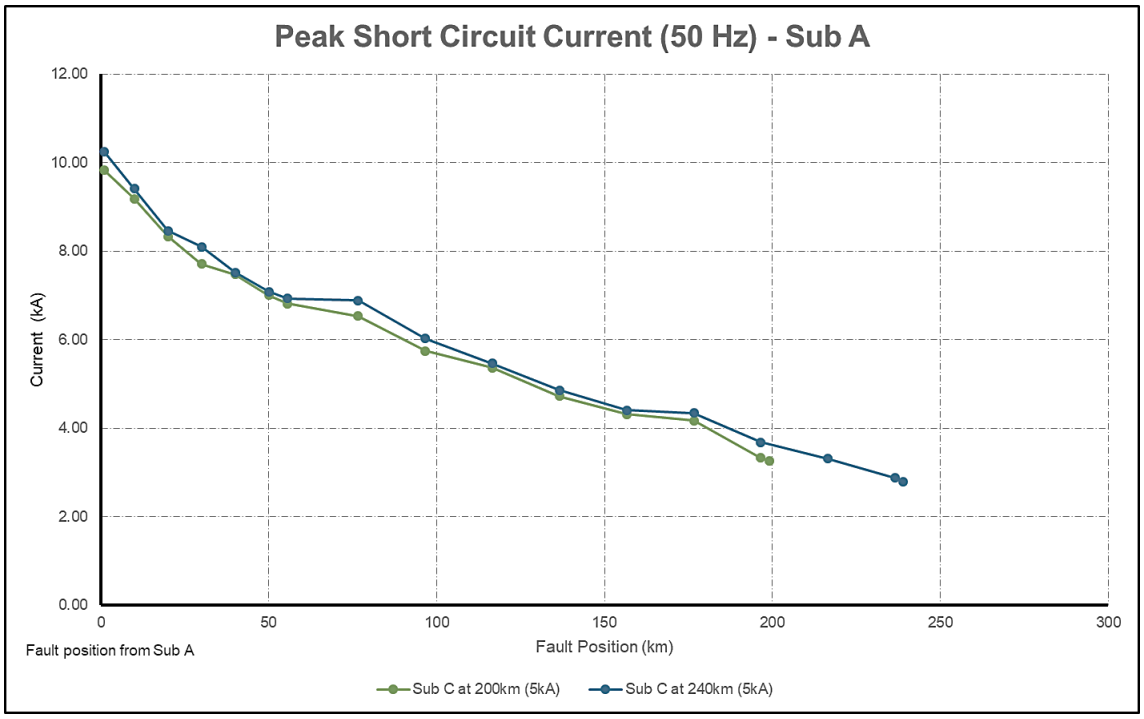

Figure 3-75: Peak fault current (50 Hz) for LCBs at Sub A – Case 2a

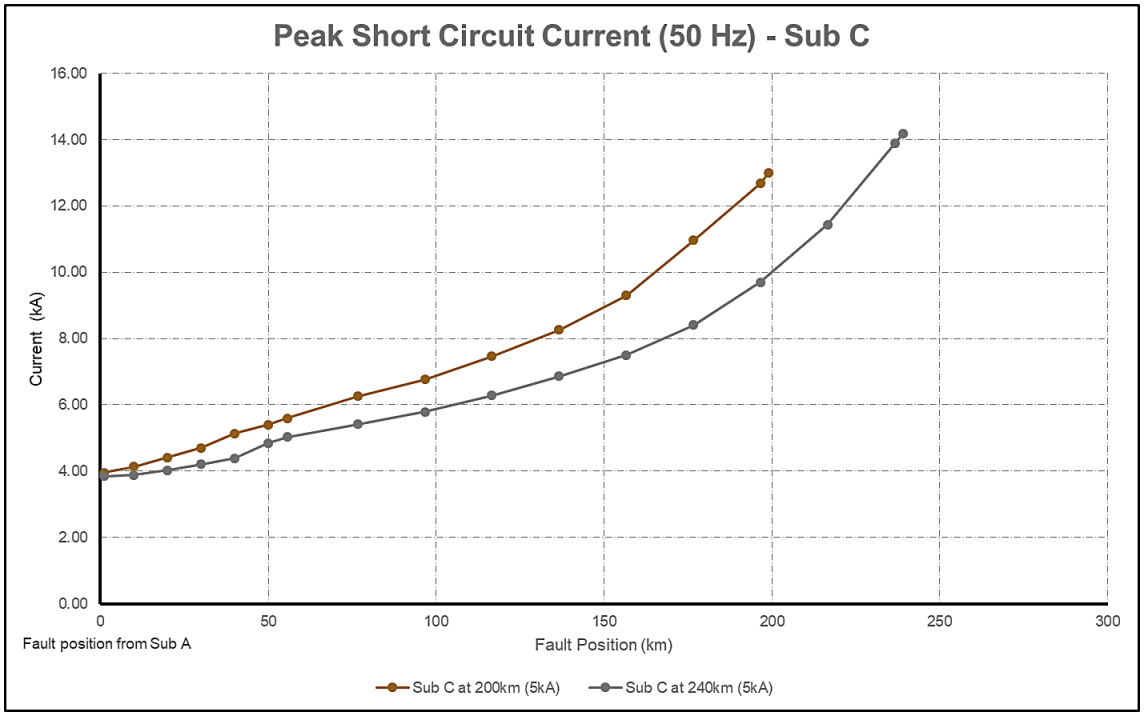

Figure 3-76: Peak fault current (50 Hz) for LCBs at Sub C– Case 2a

The current profile for Sub A in Figure 3-75 indicated that the magnitude of fault current contribution through Sub A for the same fault position with respect to Sub A increased as the line length of A-C 1 increased from 200 km to 240 km. The reason for this was due to reducing the line length and impedance of line C-B 1. The step increase in current for faults just after the series capacitor bank was not as prominent as in the case without Sub C. The fault current peak observed at 170 km away from Sub A was due to the surge impedance matching of line A-C 1a.

The current profile for the current through the LCB at Sub C is presented in Figure 3-76. The fault current supplied by Sub C was dependent on the voltage divider that was applied between $Z_{A\text{-}C\ 1b}$ and $Z_{B\text{-}C\ 1}$. As $Z_{A\text{-}C\ 1b}$ increased, the voltage at Sub C busbar increased resulting in a decrease in fault current contribution from Sub C (Figure 3-77).

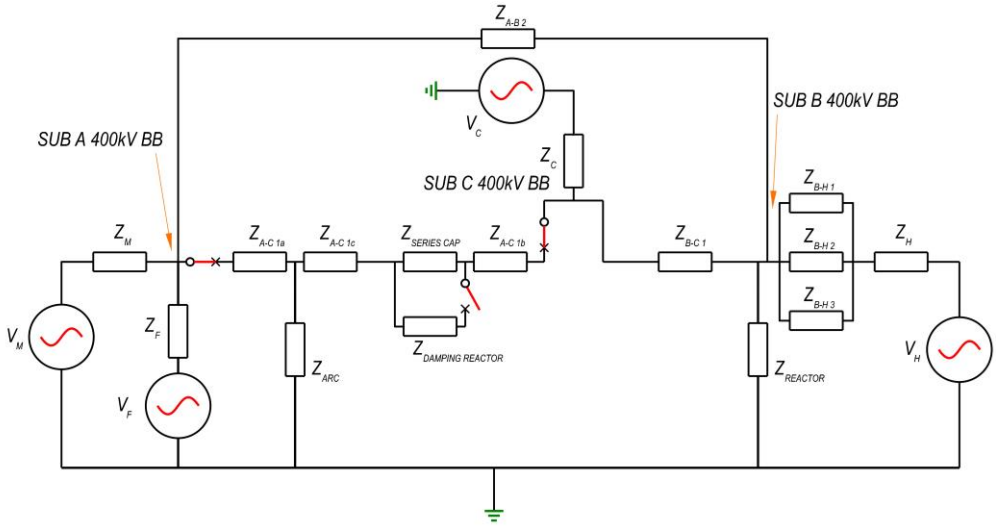

Figure 3-77: Circuit configuration of case 2a

The highest peak short circuit current magnitudes measured through the LCBs at Sub A with the integration of Sub C at 200 km and 240 km were approximately 10 kA and 11 kA respectively for faults located 1 km away from Sub A (Figure 3-75). The fault current through Sub A increased from 8 kA (without the integration of Sub C) to 10 kA (with the integration of Sub C). This increase was attributed to the additional fault current contribution from Sub C in comparison to case 1.

The test duties for both LCBs at Sub A (Figure 3-78) and Sub C (Figure 3-79) were between 10% and 30% for both line lengths 200 km and 240 km respectively. Therefore, the TRV of the LCBs were evaluated against the two parameter envelopes for the respective test duties. The LCB at Sub A operated at a 30% test duty for fault positions up to 116 km from Sub A in comparison to Sub A in case 1 (30% test duty for faults up to 96 km from Sub A).

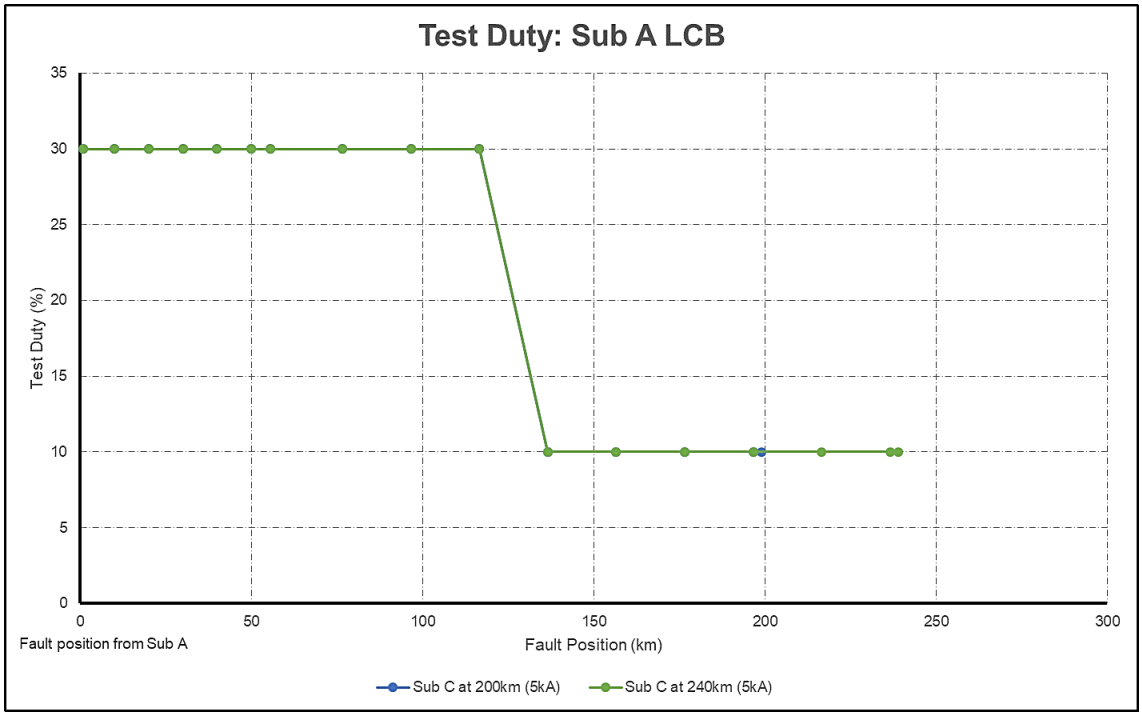

Figure 3-78: Test duties for LCBs at Sub A – Case 2a

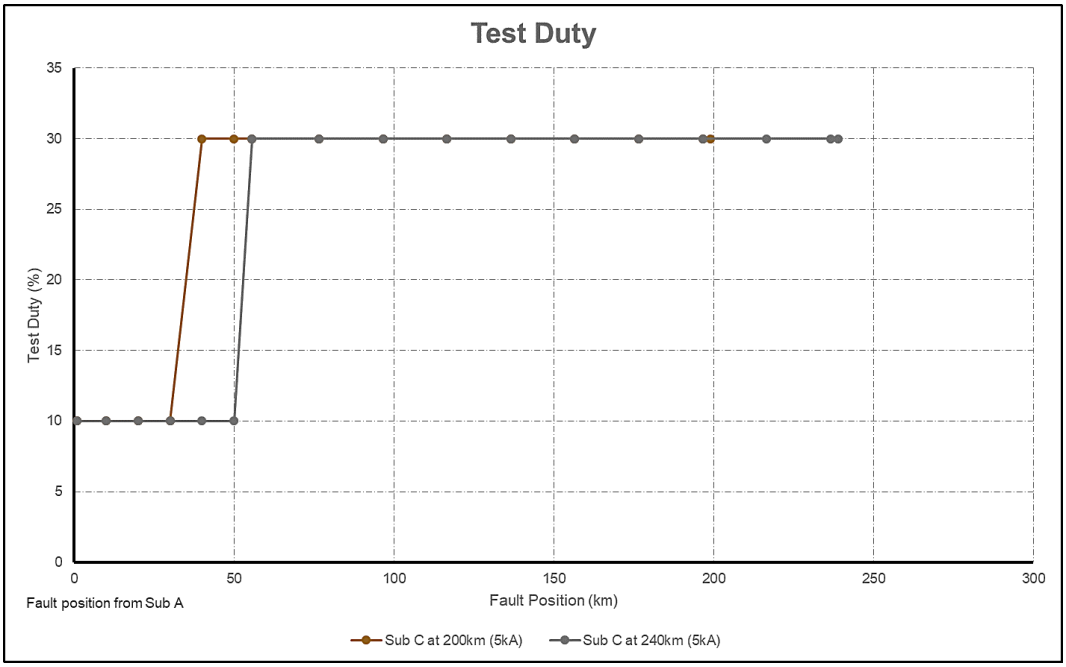

Figure 3-79: Test duties for LCBs at Sub C – Case 2a

The voltage profiles below (Figure 3-80) indicates that the peak recovery voltages that the LCB at Sub A was exposed to. There was a spike in peak recovery voltage at approximately 70 km due the surge impedance matching of the Thévenin equivalent impedance. The voltage profiles then track each other closely. There was another spike observed on the peak recovery voltage, this time due to the surge impedance matching of the line A-C 1.

The voltage profiles for the peak recovery voltages for Sub C are shown below (Figure 3-81). There are two peaks on the profile (for line A-C 1 being 240 km) that are observed. The peak near 40 km may be attributed to the impedance of line A-C 1b getting close to its surge impedance value.

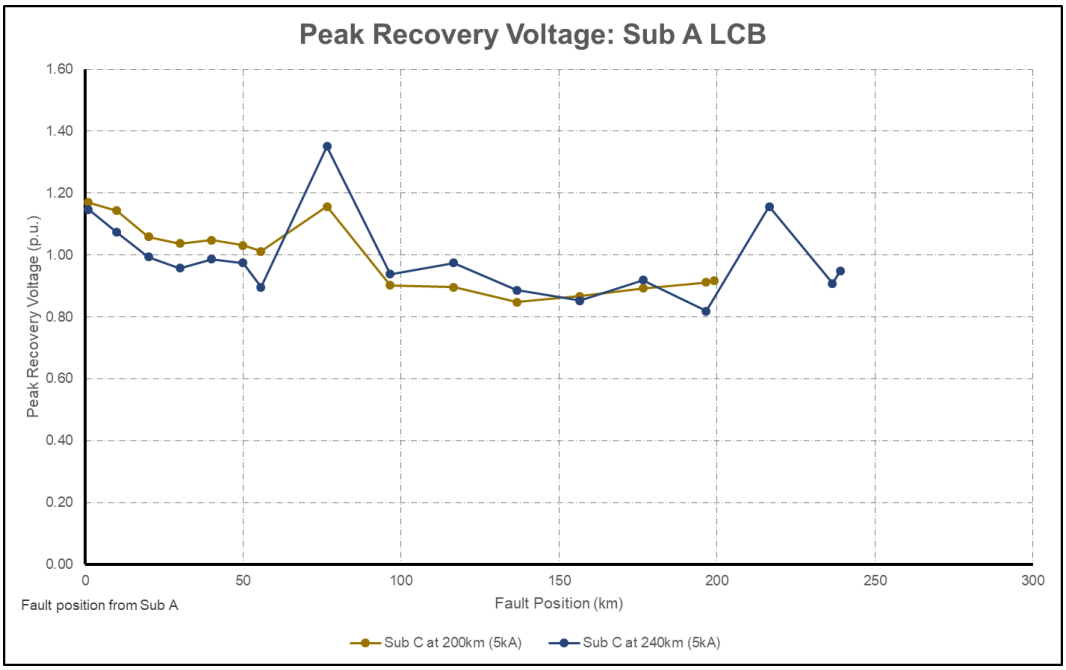

Figure 3-80: Peak Recovery Voltage profiles for LCBs at Sub A for line lengths of 200 km and 240 km for Line A-C 1: Case 2a

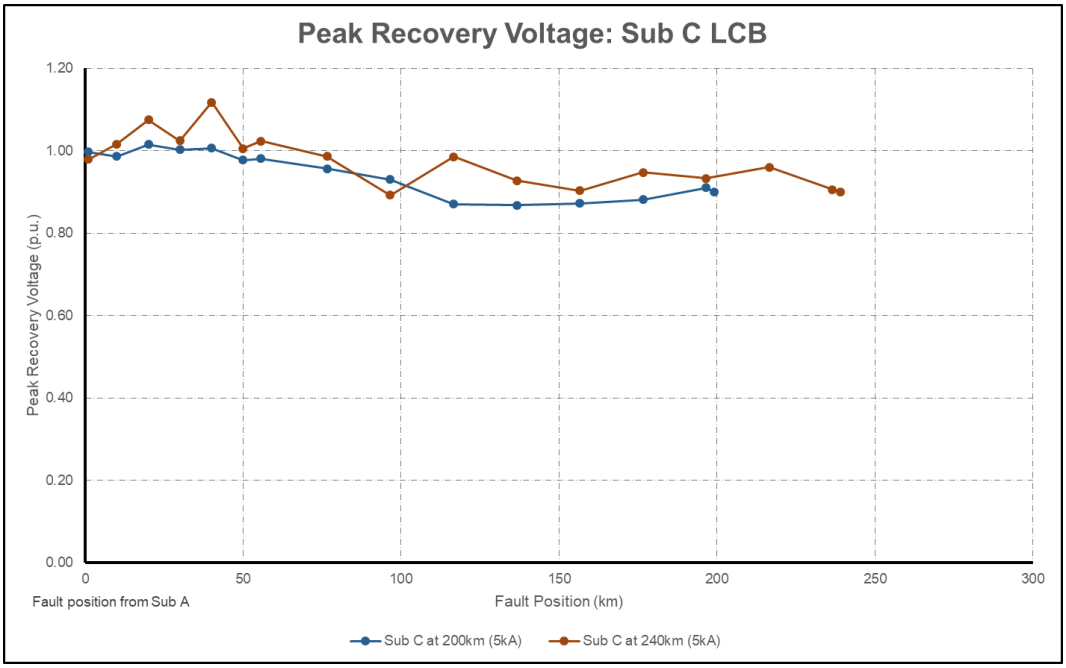

Figure 3-81: Peak Recovery Voltage profiles for LCBs at Sub C for line lengths of 200 km and 240 km for Line A-C 1: Case 2a

The second peak at approximately 130 km from Sub A may be attributed to the underdamped response and voltage reflections that the line side terminal of the LCB was exposed to (Figure 3-82).

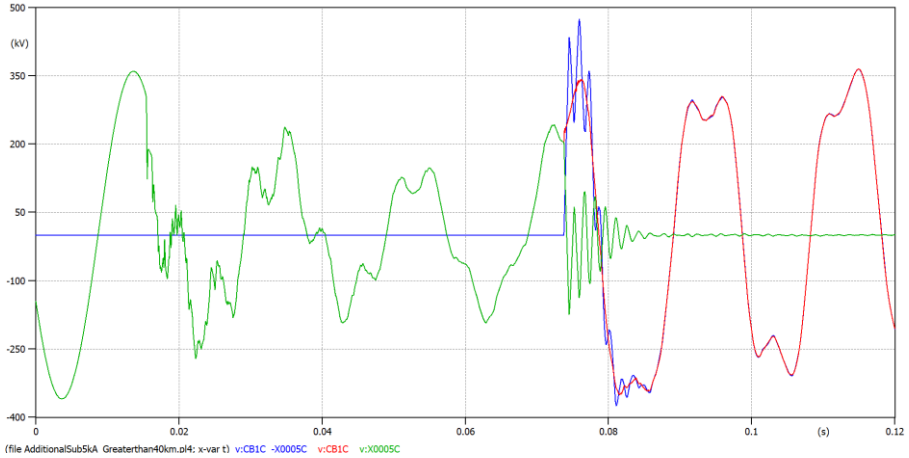

Figure 3-82: Underdamped Response at the line side terminal of the LCB at Sub C for a fault approximately 140 km from Sub A – Case 2a

The increase in voltage from Sub C to Sub A that was observed was due to the influence of the inductive reactance which causes the voltage to lead the current resulting in the LCB opening at higher magnitudes of voltage.

The peak recovery voltages for the LCB at Sub A were compared against its peak recovery voltage limits (Figure 3-83 and Figure 3-84). The LCB does not exceed the limits for line length of A-C 1 being 200 km (Figure 3-83). The peak recovery voltage was however exceeded for a fault at 76.5 km away from Sub A for line length of A-C 1 being 240 km (Figure 3-84). This was due to the Thévenin equivalent impedance reaching its surge impedance.

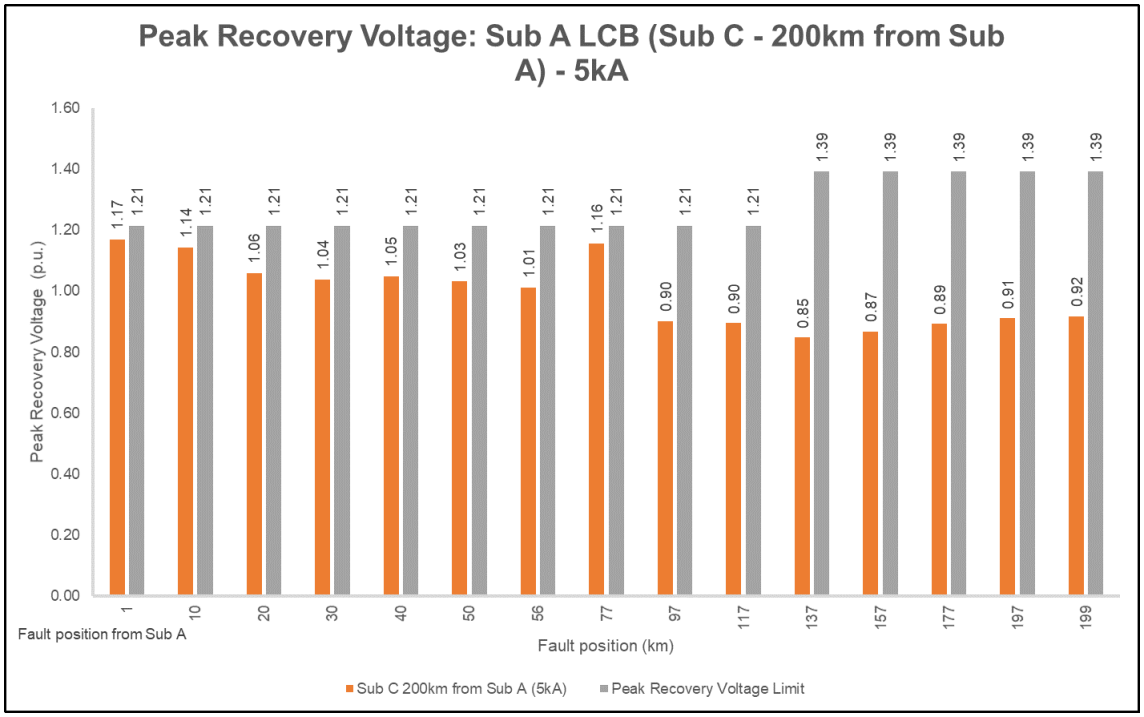

Figure 3-83: Peak Recovery Voltage profiles for the LCB at Sub A for Sub C at 200 km – Case 2a

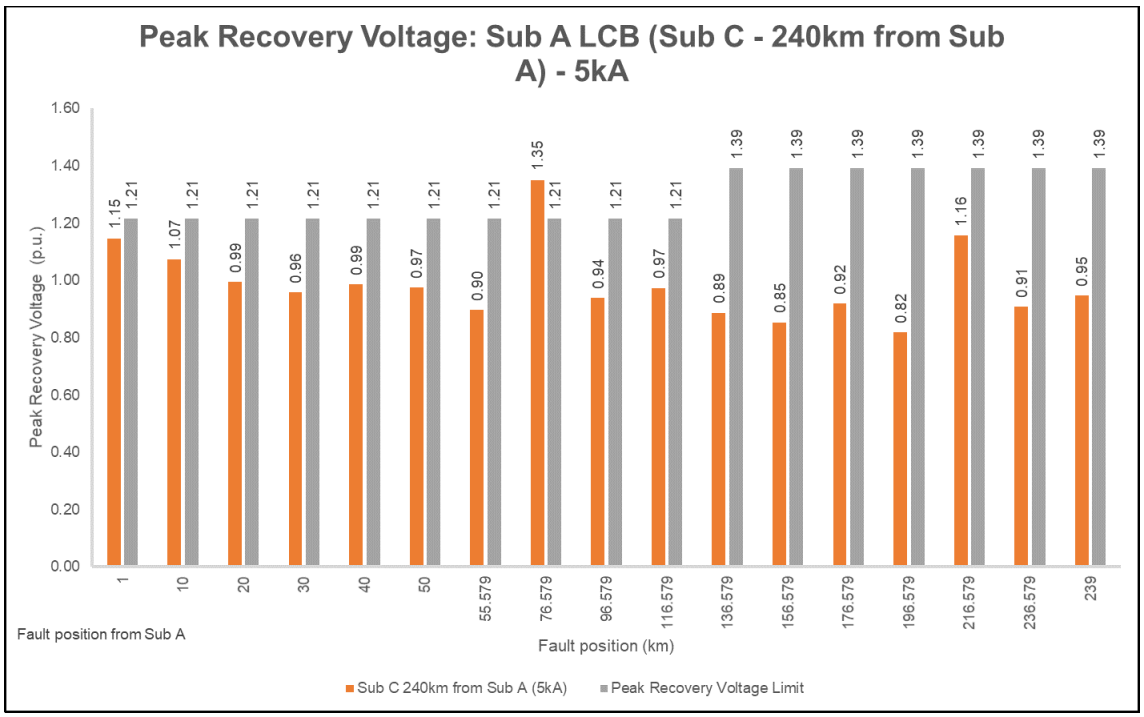

Figure 3-84: Peak Recovery Voltage profiles for the LCB at Sub A for Sub C at 240 km – Case 2a

The peak recovery voltages for the LCB at Sub C were compared against its peak recovery voltage limits (Figure 3-85 and Figure 3-86). The LCB did not exceed the limits in both instances.

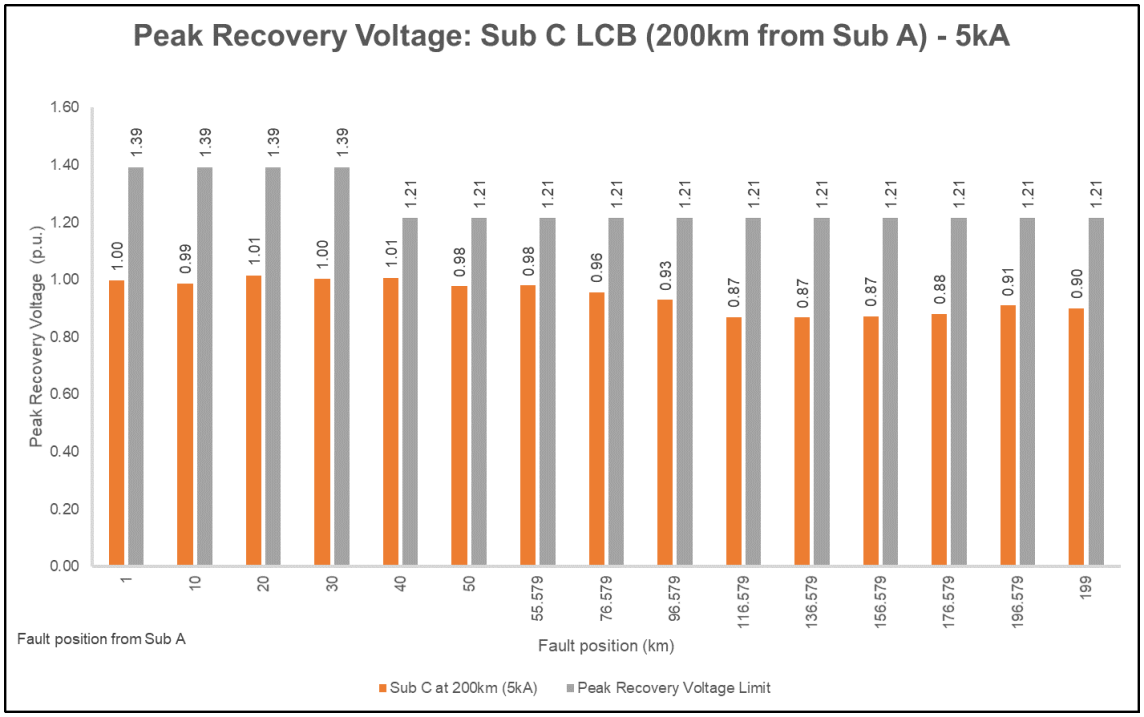

Figure 3-85: Peak Recovery Voltage profiles for the LCB at Sub C for Sub C at 200 km– Case 2a

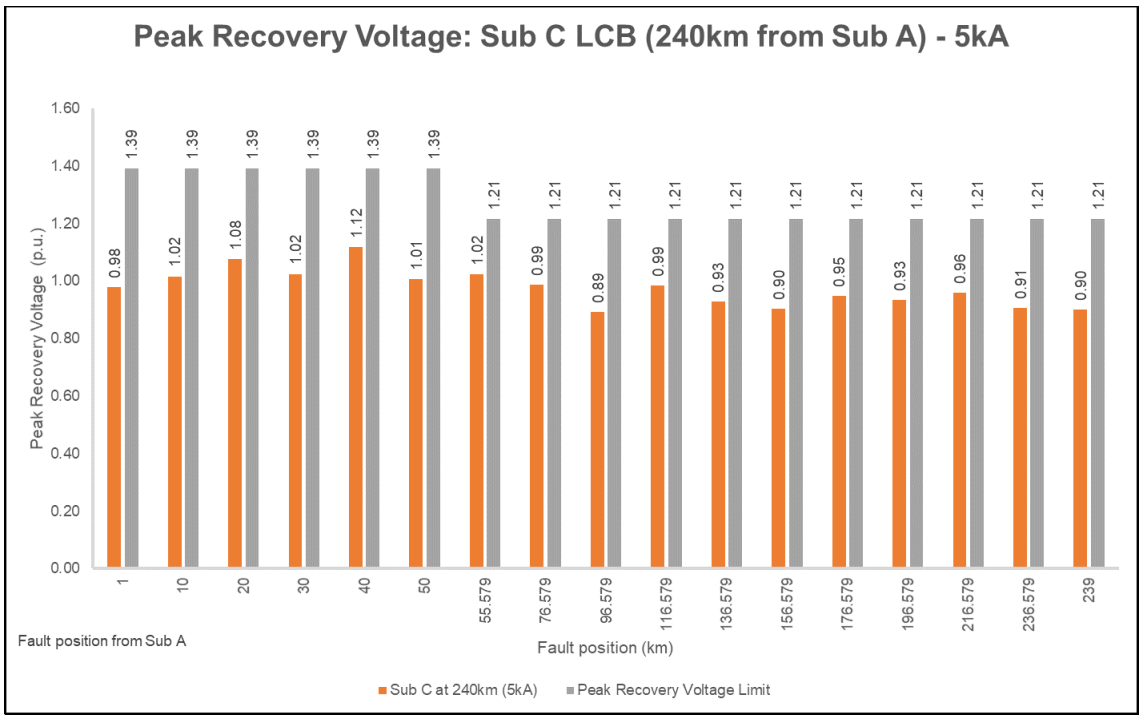

Figure 3-86: Peak Recovery Voltage profiles for the LCB at Sub C for Sub C at 240 km – Case 2a

The RRRV were evaluated for the LCBs at Sub A for the two scenarios presented (Figure 3-87 and Figure 3-88). The measurements were taken at the inception of the LCB opening and the voltage recorded after a duration of 112 µs once the LCB opened for a test duty of 10% and 137 µs for a test duty of 30%. The LCBs were recorded to be within the acceptable limits as indicated.

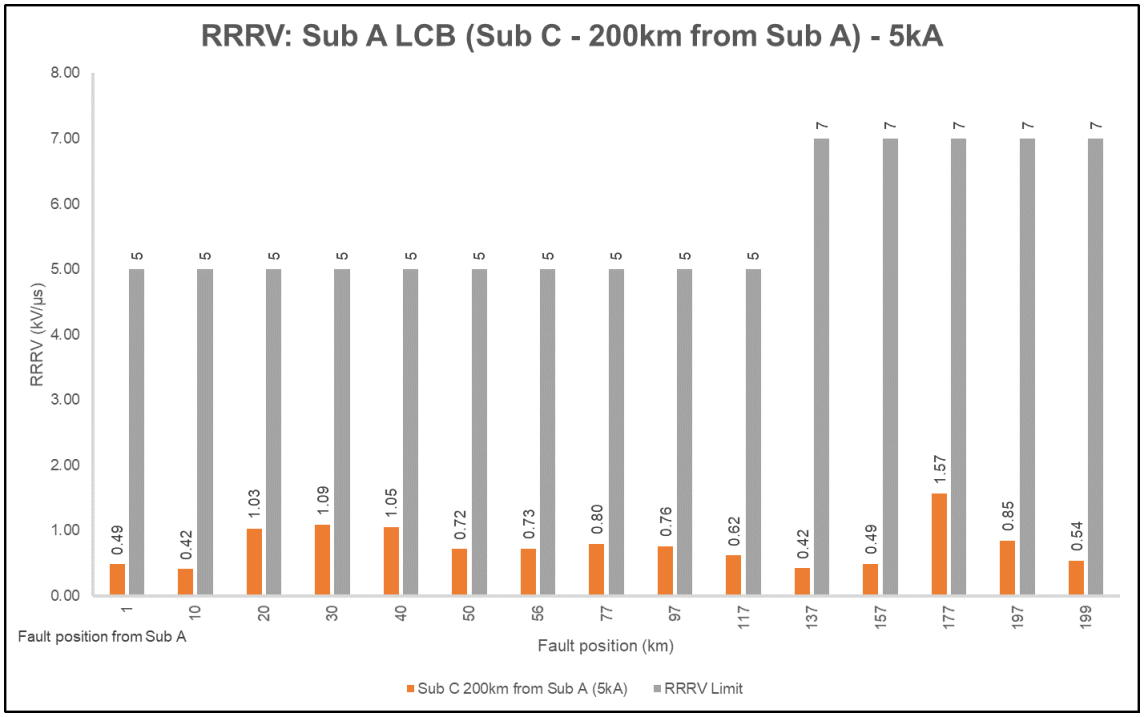

Figure 3-87: RRRV for the LCB at Sub A for Sub C at 200 km – Case 2a

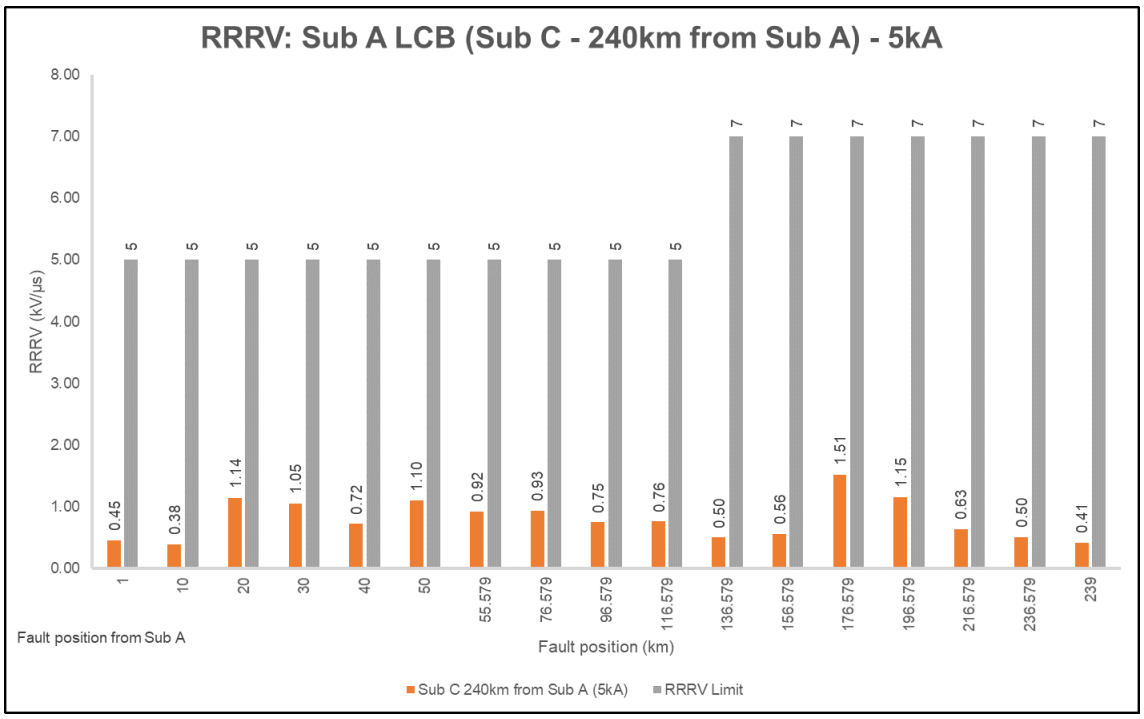

Figure 3-88: RRRV for the LCB at Sub A for Sub C at 240 km – Case 2a

The same exercise was conducted to assess the RRRV of the LCB at Sub C and was found to be within acceptable limits (Figure 3-89 and Figure 3-90). The measurements were taken at the inception of the LCB opening and the voltage recorded after a duration of 112 µs once the LCB opened for a test duty of 10% and 137 µs for a test duty of 30%.

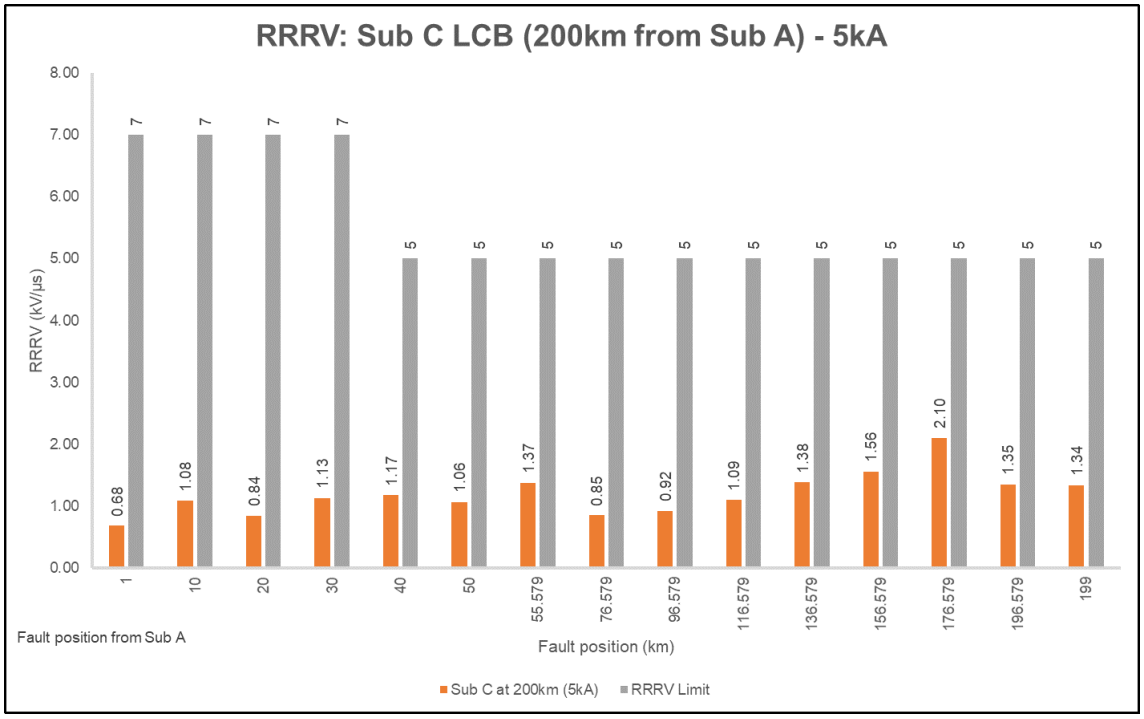

Figure 3-89: RRRV for the LCB at Sub C for Sub C at 200 km – Case 2a

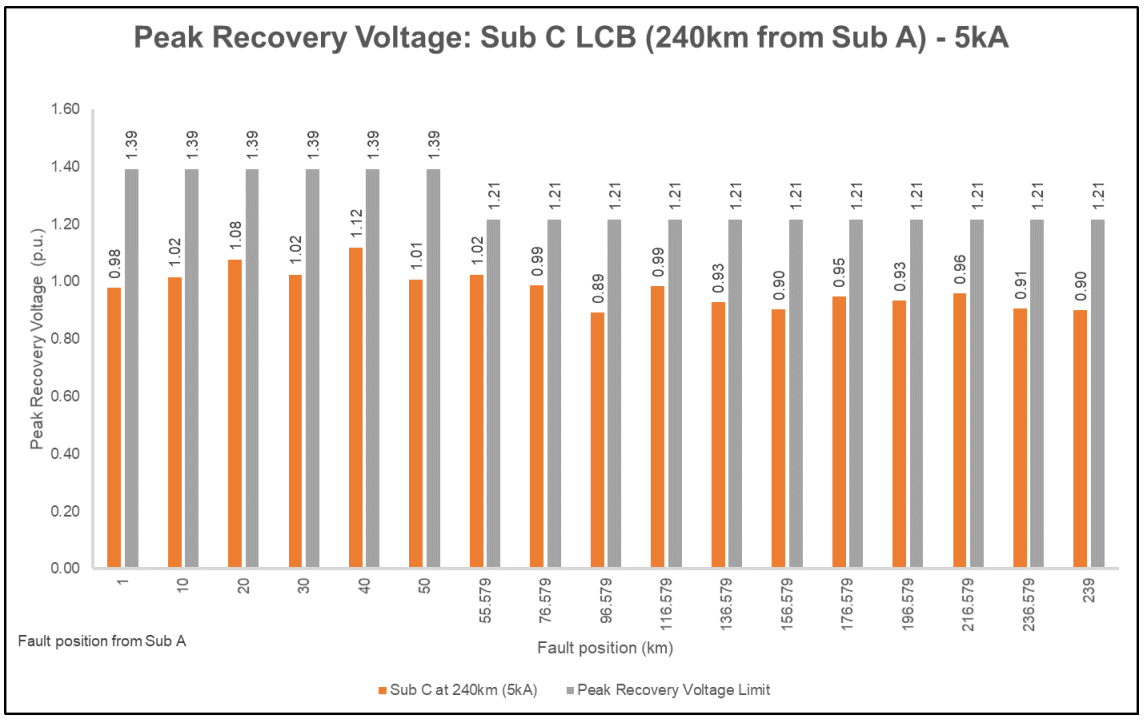

Figure 3-90: RRRV for the LCB at Sub C for Sub C at 240 km – Case 2a

3.7.3 Simulation Results: Case 2b (Sub C – 10 kA)

The simulations were repeated for the same scenarios discussed in section 3.7.2 however the fault current contribution for Sub C was increased to 10 kA. Voltage Source Sub C was integrated along the series compensated transmission line, A-B 1, as discussed in section 3.7.2. Line A-B 1 was split into two lines by looping in and out of Sub C resulting in lines A-C 1 and C-B 1 (Figure 3-57). The series capacitor bank was located along line A-C 1. The first scenario considered was for the new voltage source (Sub C) to have a fault contribution of 10 kA (Figure 3-91).

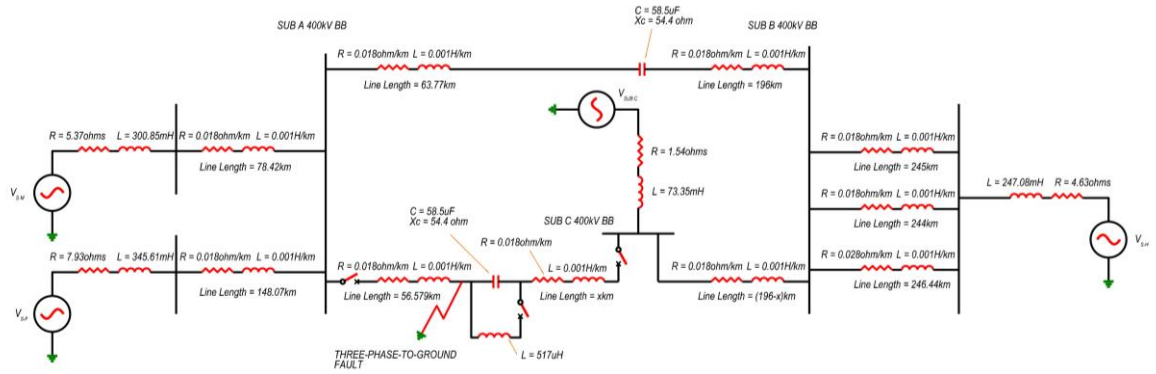

Figure 3-91: Single Line Diagram of Case 2b (Sub C at 10 kA)

The details of the source impedance of Sub C are shown below (Table 3-18):

Table 3-18: Sub C source impedance parameters (10 kA) – Case 2b

Parameter	Sub C
Peak Fault Current (kA)	10
X/R Ratio (peak)	15

The second set of cases that were evaluated were:

- Line A-C 1 which was 200 km long and Sub C was 143 km away from the series capacitor bank. The fault current contribution of from Sub C was 10 kA. Line C-B 1 was 52.5 km long. Sub A was 56.5 km away from the series capacitor bank.
- Line A-C 1 which was 240 km long and Sub C was 183 km away from the series capacitor bank. The fault current contribution of from Sub C was 10 kA. Line C-B 1 was 12.5 km long. Sub A was 56.5 km away from the series capacitor bank.

The same analysis was conducted as per section 3.7.2 however the source impedance for Sub C was changed to produce a fault current of 10 kA. The fault current was evaluated first to determine the test duty of the LCBs.

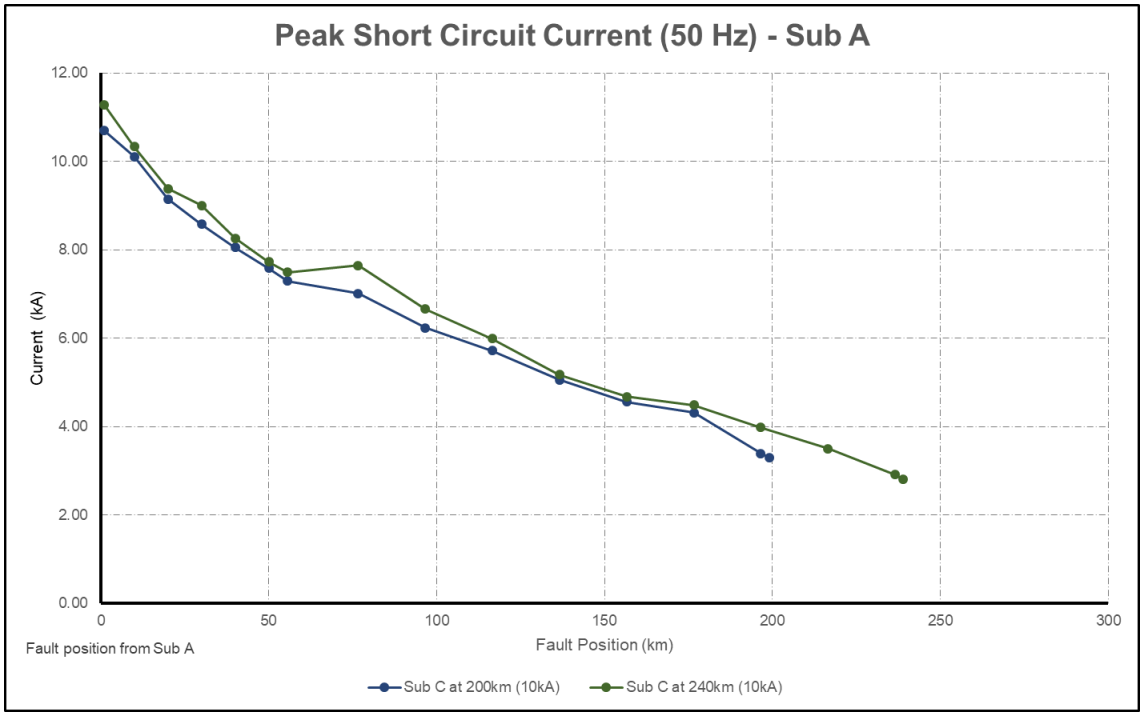

Figure 3-92: Peak fault current (50 Hz) for LCBs at Sub A – Case 2b

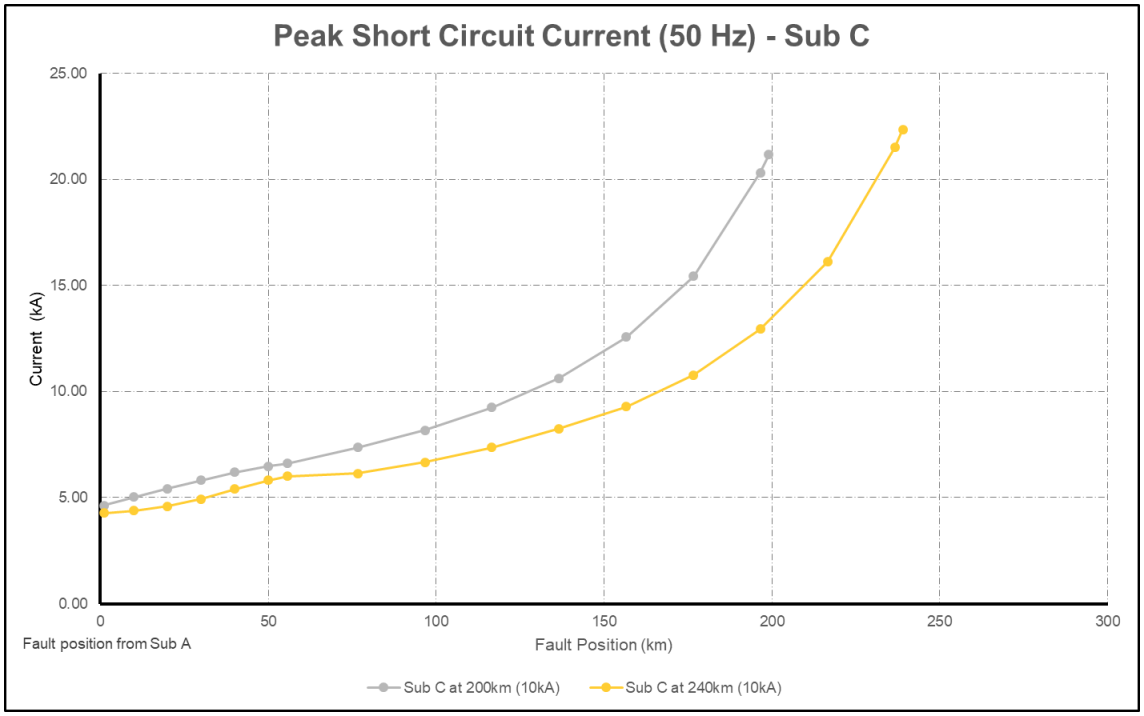

Figure 3-93: Peak fault current (50 Hz) for LCBs at Sub C– Case 2b

The fault current profiles indicated above (Figure 3-92 and Figure 3-93) follow a similar trend as that of the fault current profiles presented in Figure 3-75 and Figure 3-76 respectively. The magnitudes of the fault current have increased as follows (Table 3-19):

Table 3-19: Comparison of fault currents for LCBs at Sub A and Sub C

LCB	Fault Current Magnitudes (kA)			
	Line A-C 1 length = 200 km		Line A-C 1 length = 240 km	
	Sub C LCB 5 kA	Sub C LCB 10 kA	Sub C LCB 5 kA	Sub C LCB 10 kA
Sub A	10 kA	11.7 kA	10.7 kA	11.5 kA
Sub C	13 kA	22 kA	14.3 kA	23 kA

The fault current through the LCBs at Sub C indicate a significant increase (69% increase for line A-C 1 at 200 km and 60.8% increase for line A-C 1 at 240 km) with the change in source impedance at Sub C.

The test duties for both LCBs at Sub A (Figure 3-94) and Sub C (Figure 3-95) were between 10% and 30% for both line lengths 200 km and 240 km respectively for the fault contribution of 10 kA from Sub C. Therefore, the TRV of the LCBs were evaluated against the two-parameter envelopes for the respective test duties. The LCB at Sub A operated at a 30% test duty for fault positions up to 116 km from Sub A in comparison to Sub A in case 1 (30% test duty for faults up to 96 km from Sub A).

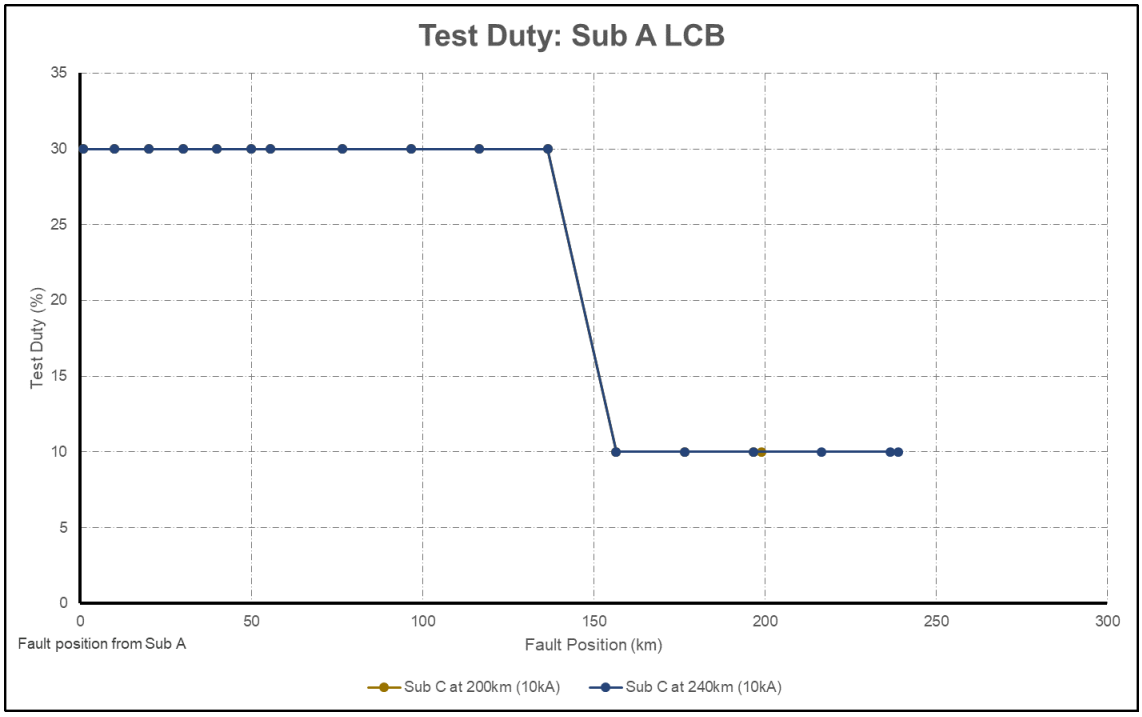

Figure 3-94: Test duties for LCBs at Sub A – Case 2b

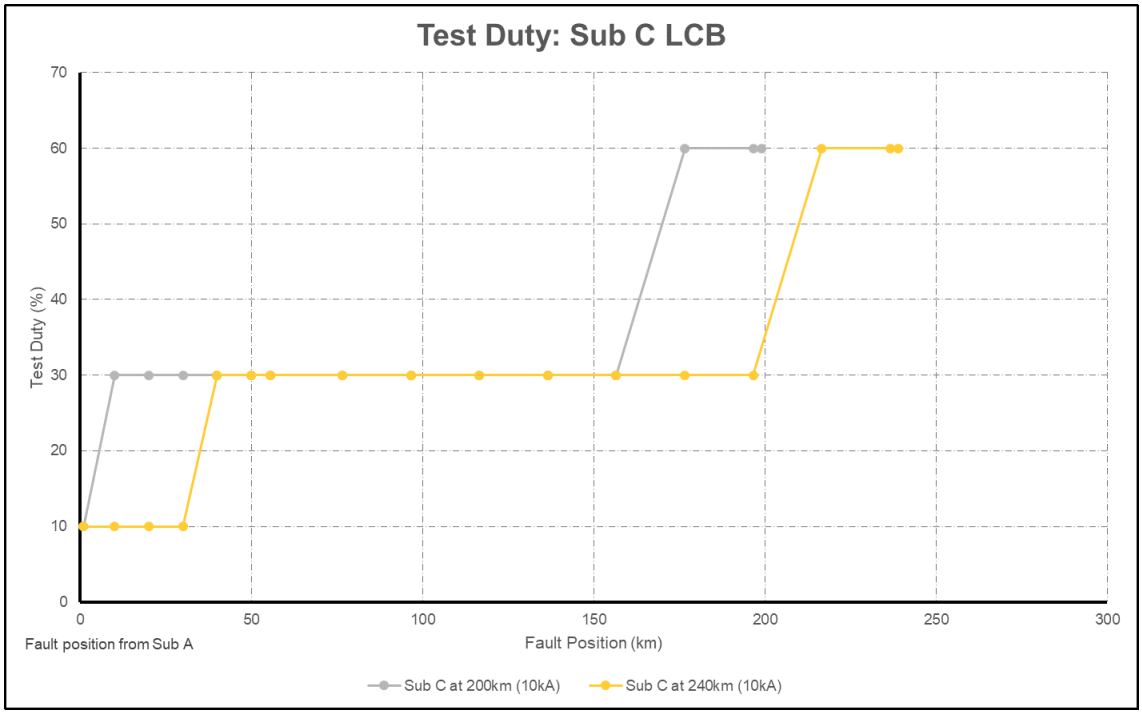

Figure 3-95: Test duties for LCBs at Sub C – Case 2b

The test duty for the LCB at Sub A remained within the range of 10% and 30% (Figure 3-94). However the breaker operated at a maximum test duty of 30% for faults up to 136 km in comparison to the previous case (Figure 3-78) which operated up to 116 km at a maximum test duty 30%.

The test duty of the LCB at Sub C increased from a maximum test duty of 30% (Figure 3-79) to a maximum test duty of 60% for a fault contribution of 10 kA through the LCB at Sub C (Figure 3-95).

The LCB operated at a test duty of 60% for faults up to 20 km away from Sub C for the line length of A - C 1 being 200 km. The LCB then operated at a test duty of 30% for faults from 20 km to 170 km away from Sub C at which point the test duty of the LCB dropped to 10%.

The LCB operated at a test duty of 60% for faults up to 35 km away from Sub C for the line length of A - C 1 being 240 km. The LCB then operated at a test duty of 30% for faults from 35 km to 200 km away from Sub C at which point the test duty of the LCB dropped to 10%.

The peak recovery voltages of the LCBs at Sub A and C for line length of A-C 1 being 200 km and 240 km respectively were analysed. The peak recovery voltage profile for Sub A (Figure 3-96) followed the same profile as the previous case (refer to Figure 3-80). There was however an increase in voltage of the profile.

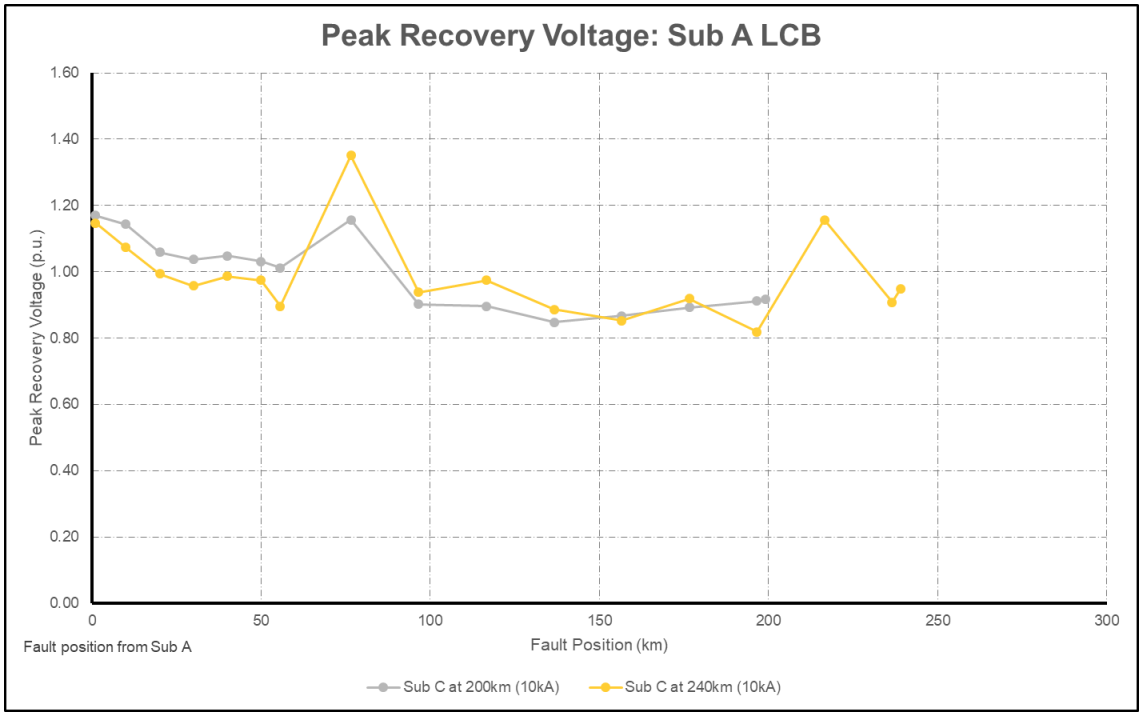

Figure 3-96: Peak Recovery Voltage profiles for LCBs at Sub A for line lengths of 200 km and 240 km for Line A-C 1 - Case 2b

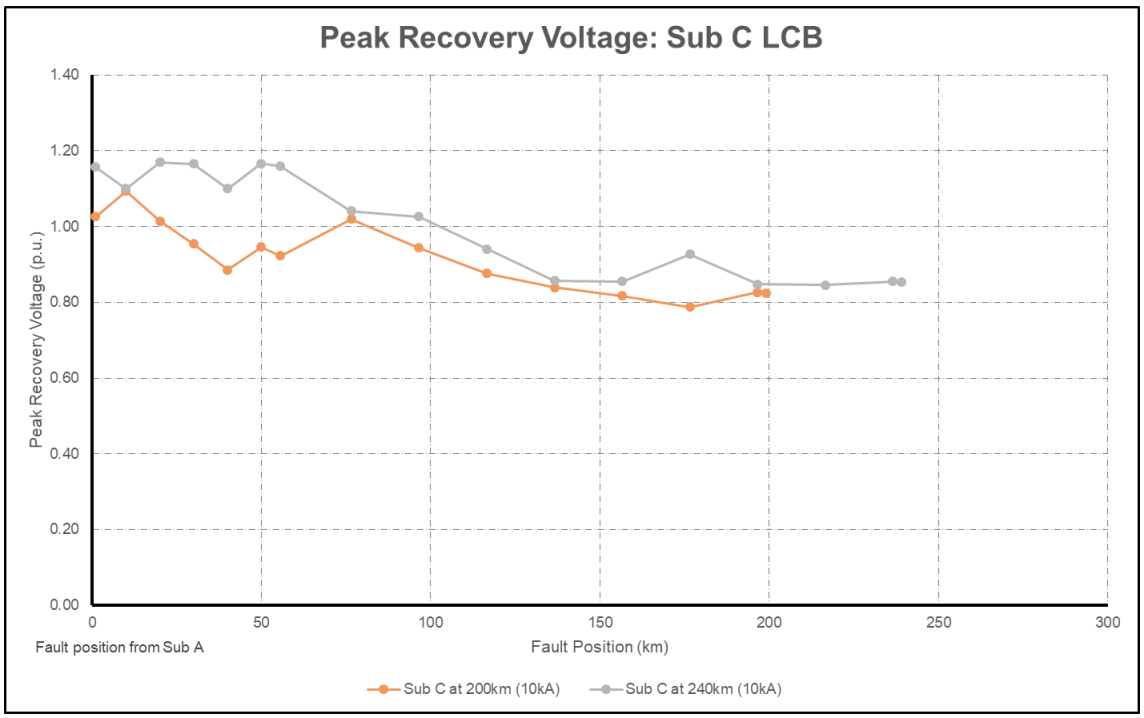

Figure 3-97: Peak Recovery Voltage profiles for LCBs at Sub C for line lengths of 200 km and 240 km for Line A-C 1 - Case 2b

The increase in fault current contribution of Sub C elevated the peak recovery voltage profile for both line lengths of A-C 1 being 200 km and 240 km. The peak recovery voltage profile of Sub C increased with respect to fault position away from Sub C (Figure 3-97). This was due to the influence of the inductive reactance along the transmission line which results in the voltage leading the current.

Looking at the peak recovery voltage profile for the LCB at Sub C for the line length of A-C 1 being 200 km away from Sub A, there were two peaks that occurred at 20 km away from Sub A and 80 km away from Sub A. They were attributed to the surge impedances being reached for line A-C 1b and the Thévenin equivalent impedance respectively.

The peak recovery voltage profile of for the LCB at Sub C for the line length of A-C 1 being 240 km away from Sub A, indicated two peaks that occur at 90 km away from Sub A and 170 km away from Sub A. They were attributed to the surge impedances being reached for the Thévenin equivalent impedance and the line A-C 1a respectively.

The peak recovery voltage that the LCB at Sub A was exposed to under the line length scenarios of A – C 1 being 200 km and 240km exceeded its peak recovery voltage limits in both instances (Figure 3-98 and Figure 3-99). The peak recovery voltage was close to if not exceeding the limit for at least 40% of the line (Figure 3-99). This indicated that a significant portion of the circuit was at risk. Therefore, a recommendation would be to consider mitigation approaches such as arresters connected across the terminals of the LCB to limit the TRV across the LCB. As a worst-case approach, the breaker may be uprated to the next breaker current or voltage rating.

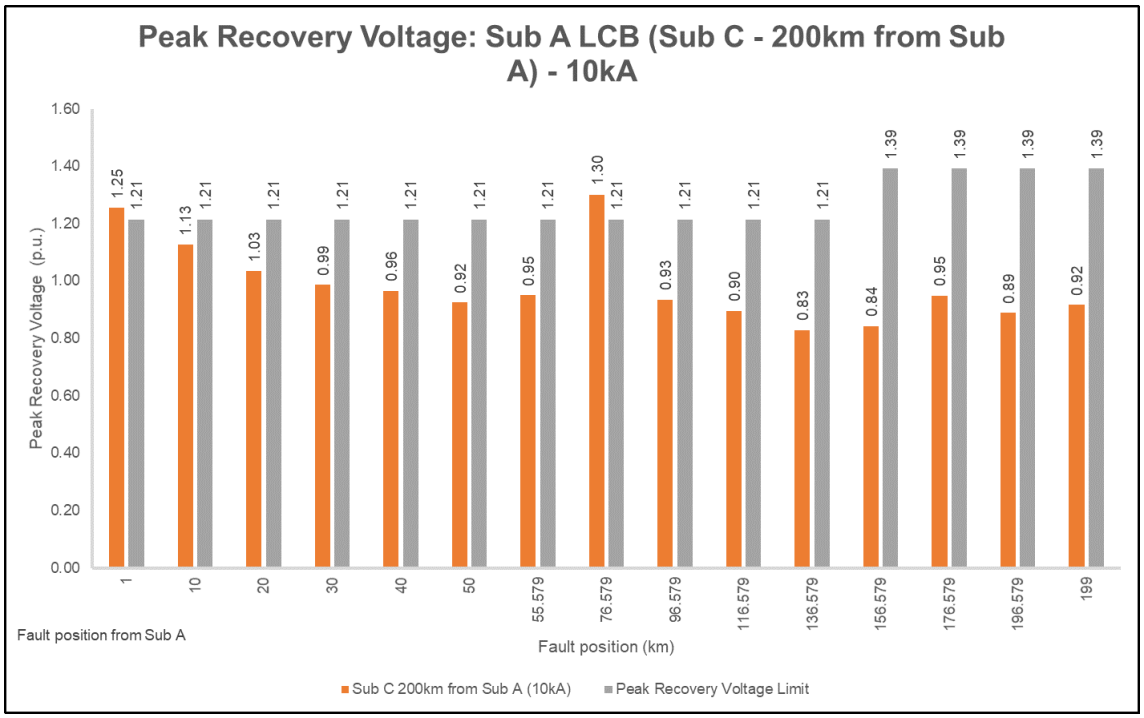

Figure 3-98: Peak Recovery Voltage profiles for the LCB at Sub A for Sub C at 200 km – Case 2b

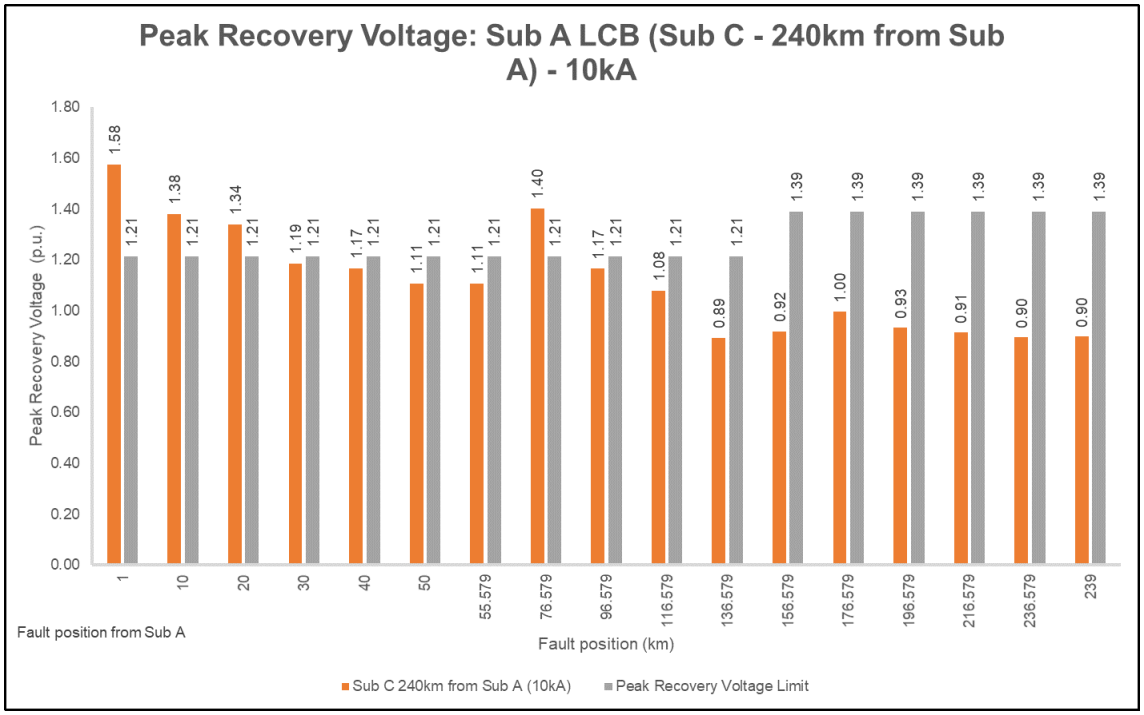

Figure 3-99: Peak Recovery Voltage profiles for the LCB at Sub A for Sub C at 240 km – Case 2b

The peak recovery voltage that the LCB at Sub C was exposed to under the line length scenarios of A – C 1 being 200 km and 240km did not exceed its peak recovery voltage limits in both instances (Figure 3-100 and Figure 3-101). However, the actual peak recovery voltage got close to its peak recovery voltage limit. A further increase in the fault current contribution of Sub C could have resulted in exceeding the limit.

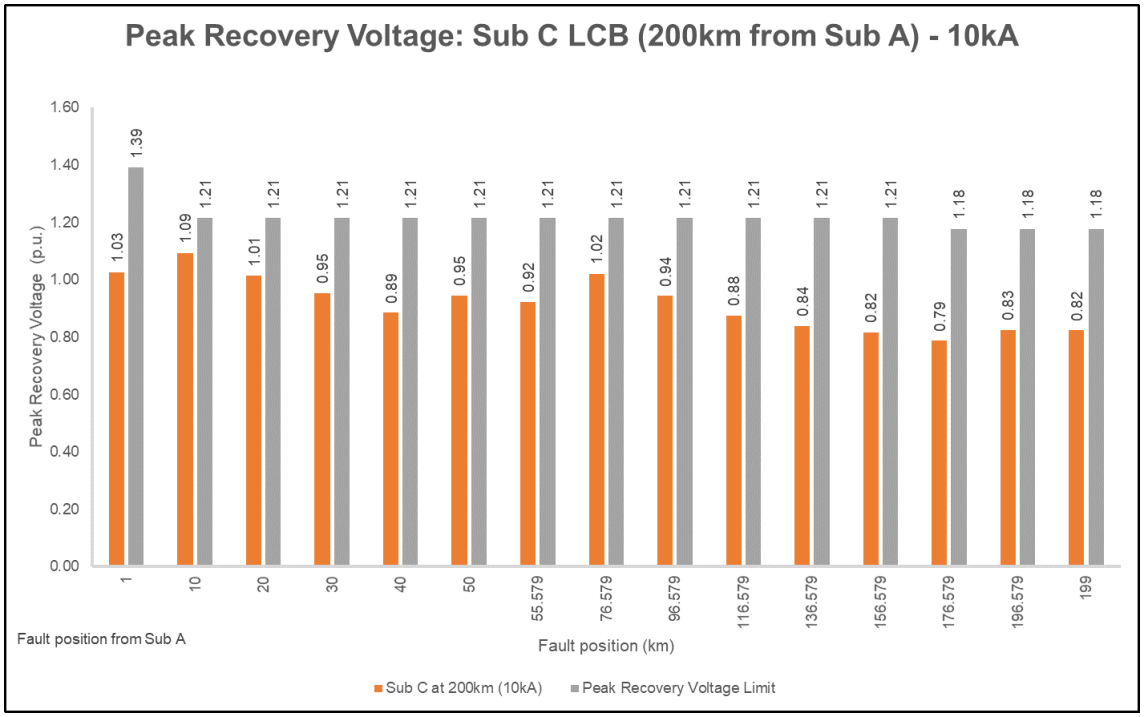

Figure 3-100: Peak Recovery Voltage profiles for the LCB at Sub C for Sub C at 200 km – Case 2b

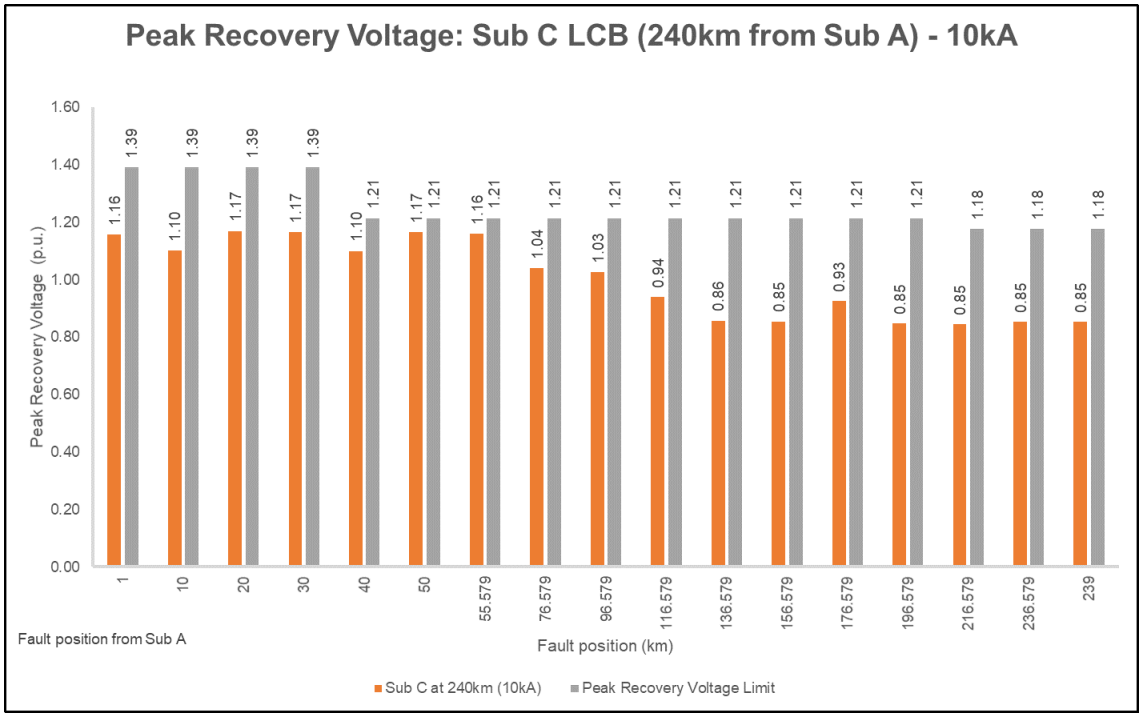

Figure 3-101: Peak Recovery Voltage profiles for the LCB at Sub C for Sub C at 240 km – Case 2b

The RRRV were evaluated for the LCBs at Sub A for the two scenarios presented (Figure 3-102 and Figure 3-103). The measurements were taken at the inception of the LCB opening and the voltage recorded after a duration of 112 µs once the LCB opened for a test duty of 10% and 137 µs for a test duty of 30%. The LCBs were recorded to be within the acceptable limits as indicated.

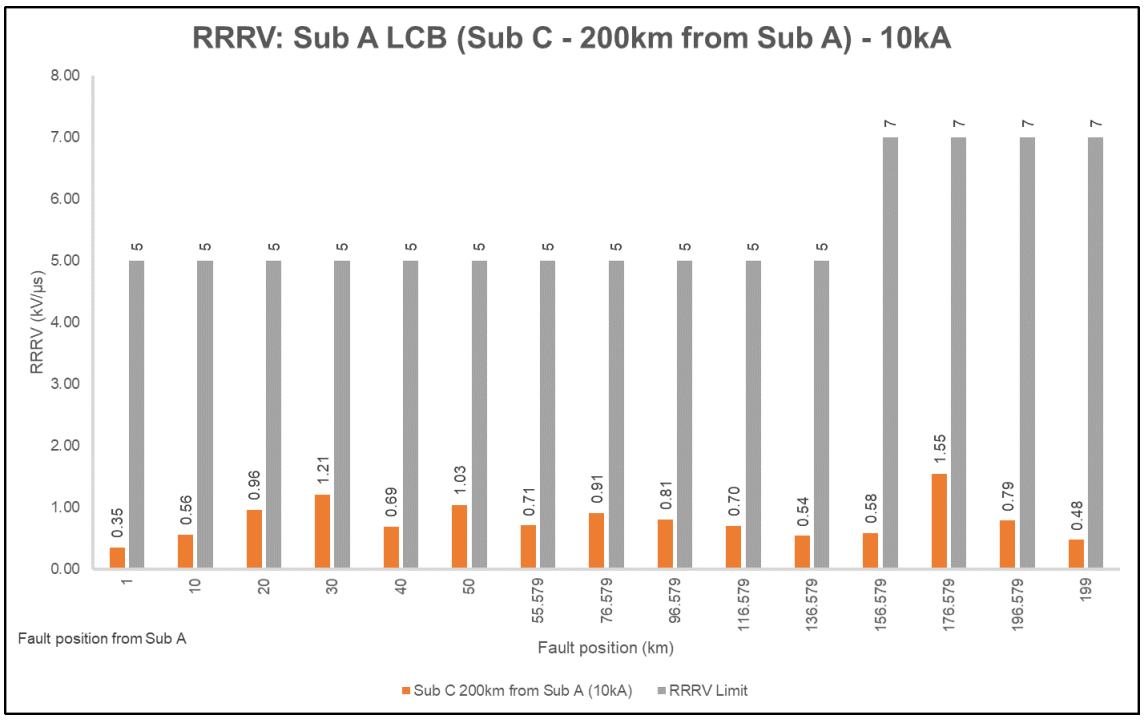

Figure 3-102: RRRV for the LCB at Sub A for Sub C at 200 km – Case 2b

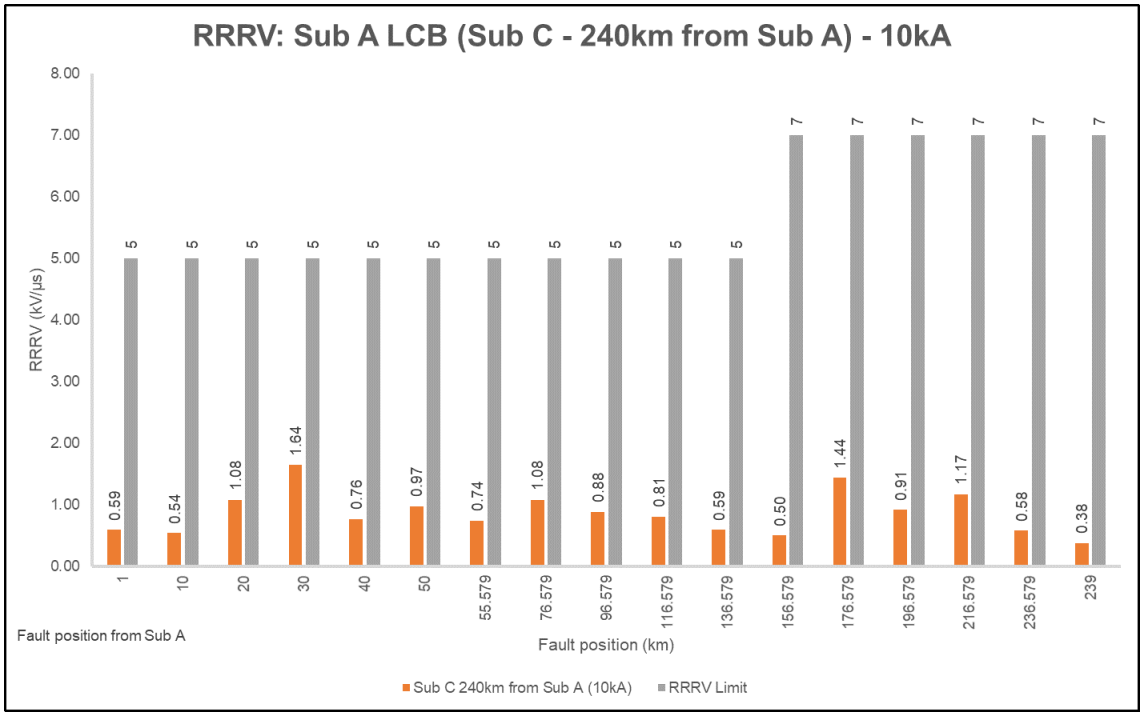

Figure 3-103: RRRV for the LCB at Sub A for Sub C at 240 km – Case 2b

The RRRV were evaluated for the LCBs at Sub A for the two scenarios presented (Figure 3-104 and Figure 3-105). The measurements were taken at the inception of the LCB opening and the voltage recorded after a duration of 112 µs once the LCB opened for a test duty of 10%, 137 µs for a test duty of 30% and 111 µs for a test duty of 60%. The LCBs were recorded to be within the acceptable limits as indicated. However, the RRRV reached the RRRV limit for a fault at 176 km (Figure 3-104) and 216 km (Figure 3-105).

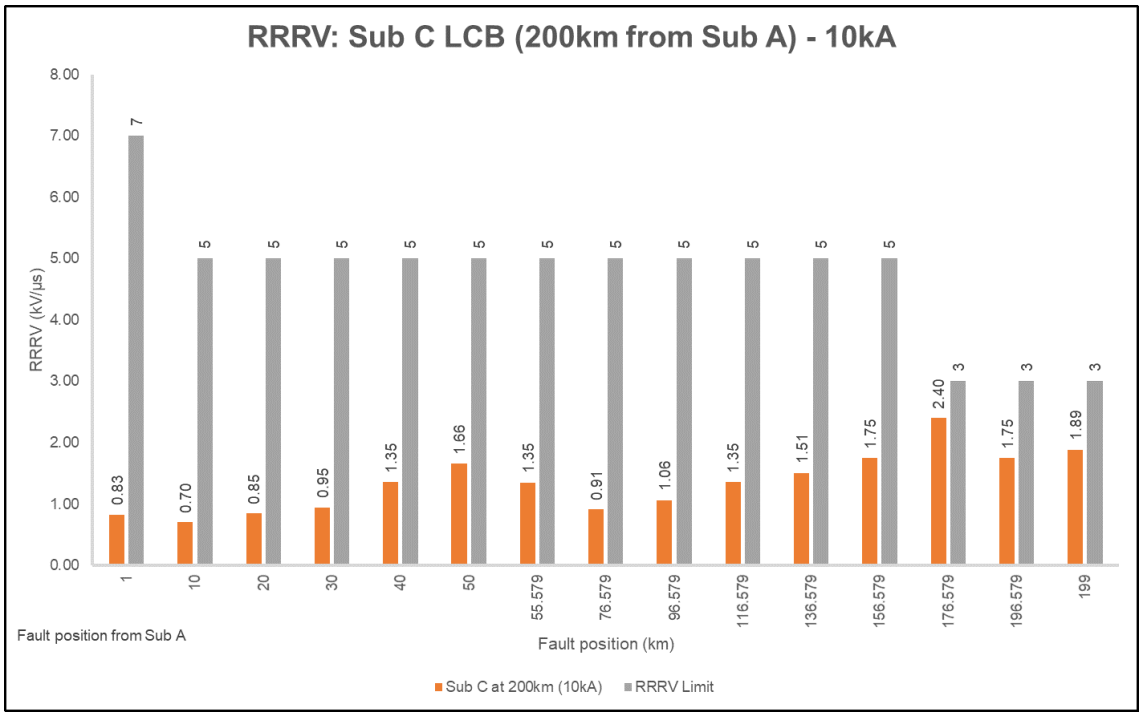

Figure 3-104: RRRV for the LCB at Sub C for Sub C at 200 km – Case 2b

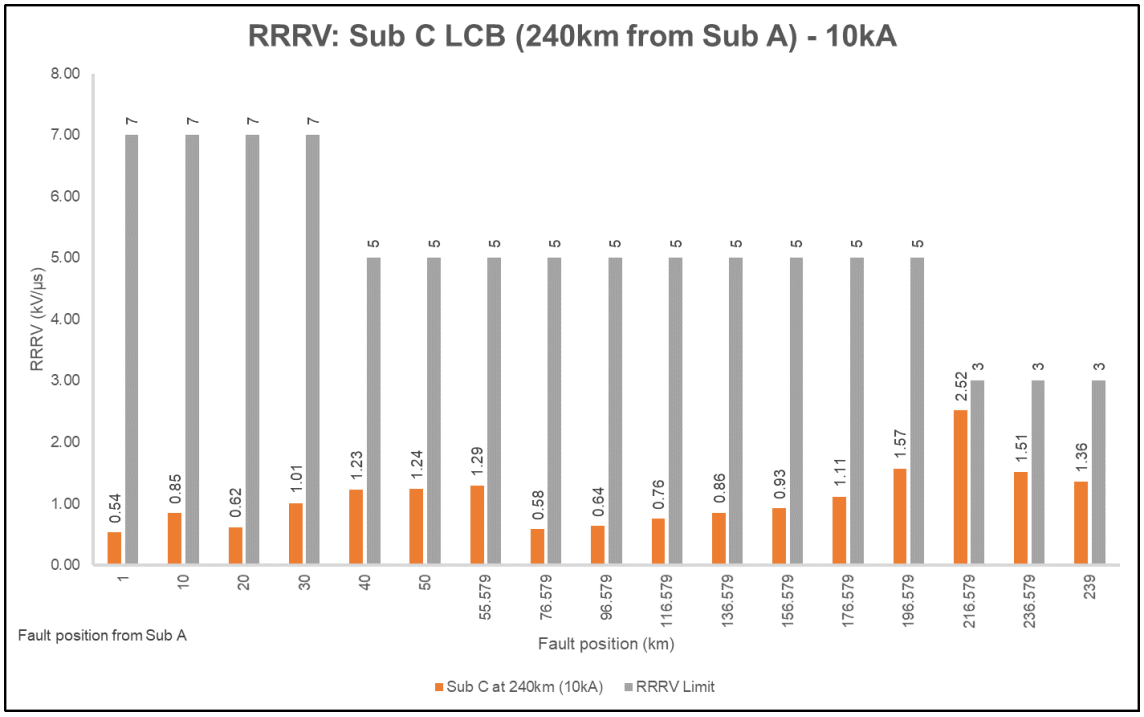

Figure 3-105: RRRV for the LCB at Sub C for Sub C at 240 km – Case 2b

3.7.4 Simulation Results: Case 3a (Sub C – 5 kA)

Simulations were then conducted for the Case 3 which entailed integrating a voltage source, Sub C, along the series compensated transmission line A-B 1, resulting in the line C-B 1, as discussed in section 3.7. Line A-B 1 was split into two lines by looping in and out of Sub C resulting in line A-C 1 and line C-B 1. The series capacitor bank was located along line C-B 1.

The first scenario considered was for the new voltage source (Sub C) to have a fault contribution of 5 kA (Figure 3-106). The line length between Sub A and Sub B was fixed at 252.5 km and the distance between Sub A and the series capacitor bank was fixed at 56.5 km. In order to integrate Sub C at 212.5 km and 232.5 km from Sub B, the resultant line A-C was 40 km to 20 km in length respectively (Figure 3-58).

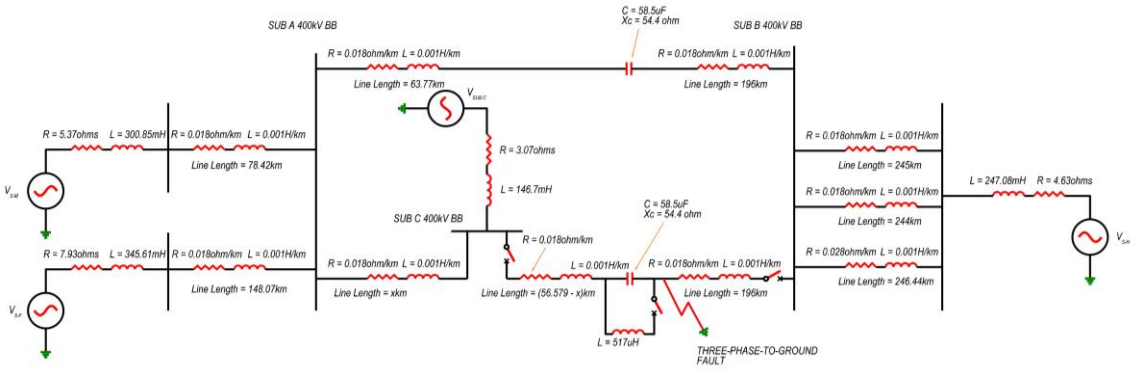

Figure 3-106: Single Line Diagram of Case 3a

The details of the source impedance of Sub C is as follows (Table 3-20):

Table 3-20: Sub C source impedance parameters (5 kA)

Parameter	Sub C
Peak Fault Current (kA)	5
X/R Ratio (peak)	15

The magnitude of the series capacitor bank remained fixed for all simulations conducted. Therefore, the compensation factor varied for simulations conducted for each position of Sub C and the corresponding transmission line lengths. The compensation factor was varied between 73% and 80% as indicated below (Table 3-21):

Table 3-21: Compensation factor for studies conducted for Line B - C 1

Line length (km)	Line Configuration	Inductance	Line inductive reactance (Ω)	Capacitor Bank Capacitive Reactance (Ω)	Compensation Factor
km		H/km	$X_L = 2\pi fL\ (\Omega)$	$X_C = \frac{1}{2\pi fC}\ (\Omega)$	%
212.5	B – C 1	0.001018	69.28	54.4	80%
232.5	B – C 1		75.68		73%

Compensation factors exceeding 90% were not considered as this was deemed impractical from an application perspective.

The second set of cases that were evaluated were:

- Line C-B 1 which was 212.5 km long and Sub C was 40 km away from Sub A. The fault current contribution of from Sub C was 5 kA.
- Line C-B 1 which was 232.5 km long and Sub C was 20 km away from Sub A. The fault current contribution of from Sub C was 5 kA.

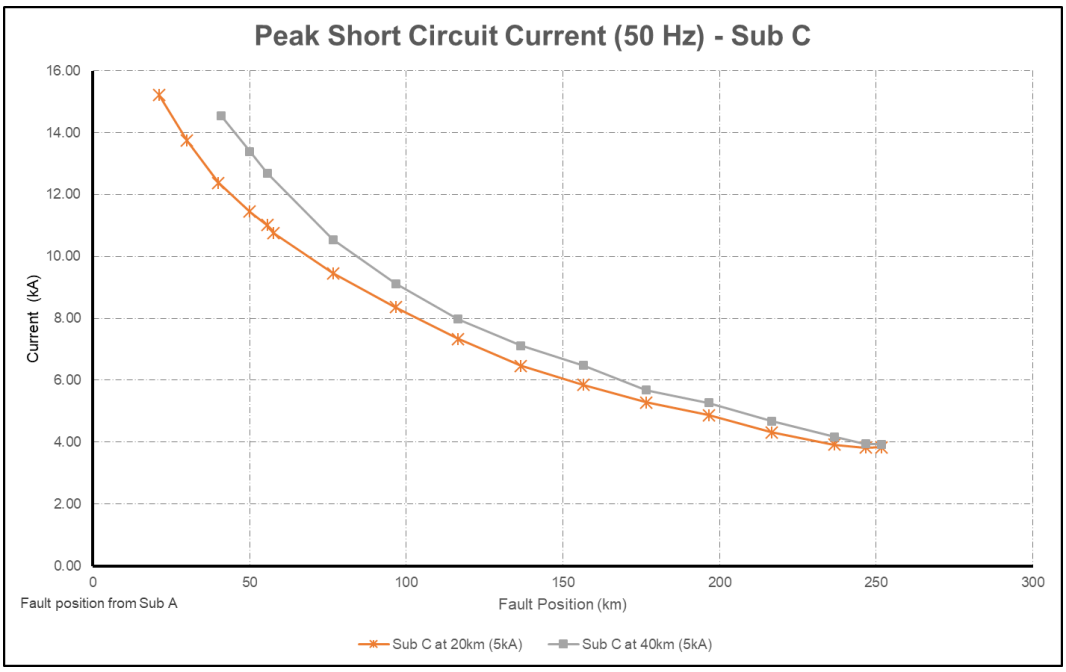

Figure 3-107: Peak fault current (50 Hz) for LCBs at Sub C – Case 3a

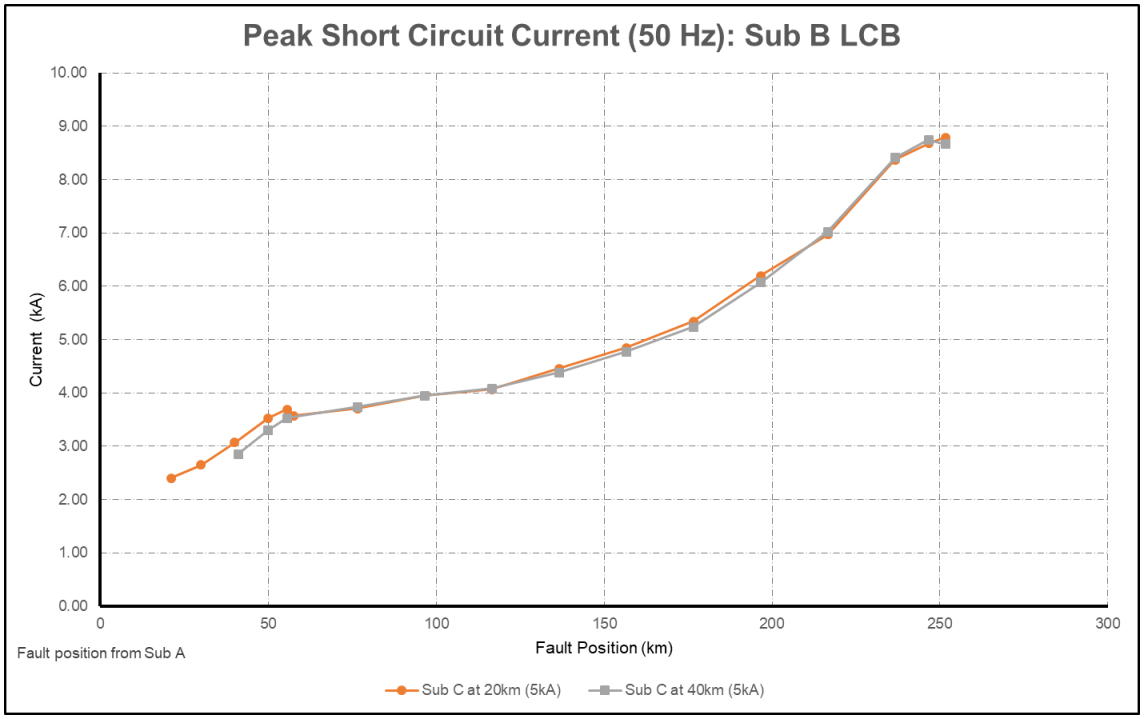

Figure 3-108: Peak fault current (50 Hz) for LCBs at Sub B– Case 3a

The current profiles for Sub C in Figure 3-107 indicates that the magnitude of fault current for the same fault position with respect to Sub A yielded a higher fault current for a shorter line length C-B 1. The fault current supplied by Sub C was dependent on the voltage divider that was applied between $Z_{A\text{-}C\ 1}$ and $Z_{B\text{-}C\ 1a}$. As $Z_{A\text{-}C\ 1a}$ increases, the voltage at Sub C busbar increases resulting in a decrease in fault current contribution from Sub C (Figure 3-109).

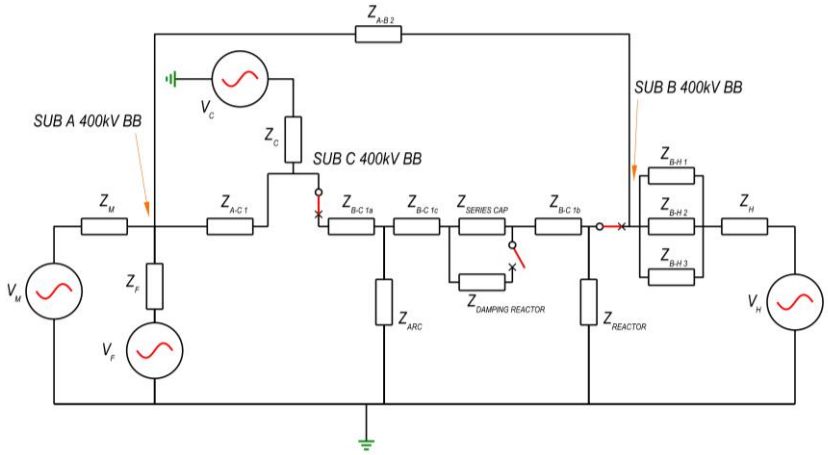

Figure 3-109: Circuit configuration of case 3a

The current profile for the LCB at Sub B in (Figure 3-108) indicates that the magnitude of fault current contribution through Sub B for the same fault position with respect to Sub A increased as the line length of A-C 1 increased from 212.5 km to 232.5 km. Applying the current divider rule (Figure 3-110) the current through the LCB at Sub C and Sub B may be derived (refer to section 3.6.3.2.) as indicated.

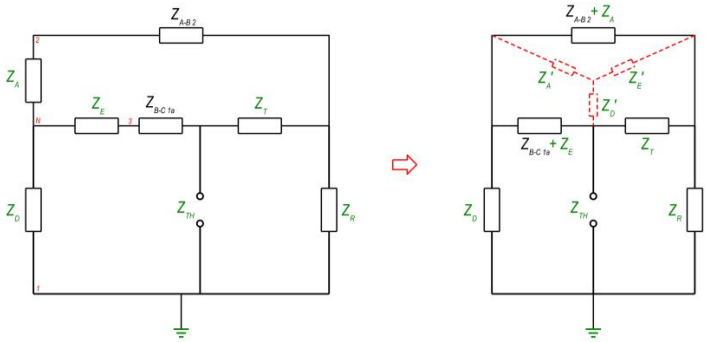

Figure 3-110: Fault current split from the fault to Sub C and Sub B

The test duties for LCB at Sub C (Figure 3-111) was between 10% and 60% while the test duty of the LCB Sub B (Figure 3-112) was between 10% and 30% for both line lengths of C-B 1 being 212.5 km and 232.5 km respectively for the fault contribution of 5 kA at Sub C. Therefore, the TRV capabilities of the LCBs was evaluated against the two parameter envelopes for test duties between 10% and 30% and the four-parameter envelope for the test duty of 60%.

The LCB at Sub C operated at a 60% test duty for fault positions from the LCB at Sub C up to 10 km of the line length when line C-B 1 was 232.5 km long (Figure 3-111). The test duty then drops to 30% for faults between 30 km and approximately 150 km from the LCB at Sub A of the total line length. The test duty dropped further to 10% for faults occurring for the remaining line length.

The test duty for the LCB at Sub C operated between 10% and 30% when the line length of C-B 1 was 212 km.

The test duty profiles for the LCB at Sub B for both line lengths of C-B 1 (212.5 km and 232.5 km) were similar (Figure 3-112) due to the fault current magnitudes through the LCB at Sub B being similar (Figure 3-108) for both line lengths of C-B 1 being evaluated in this case.

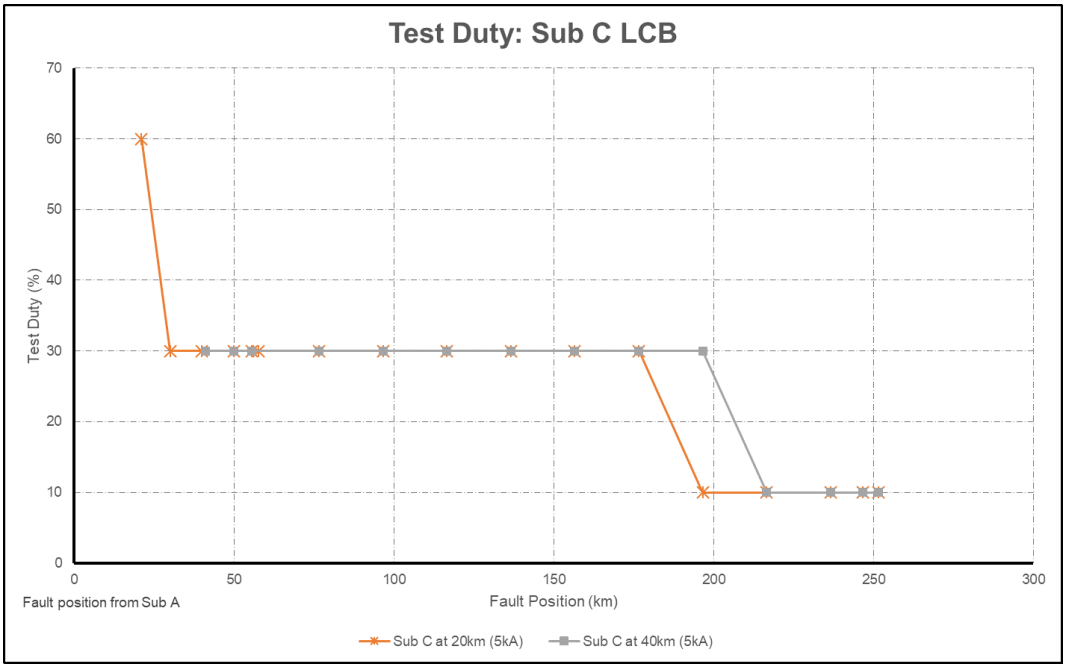

Figure 3-111: Test duties for LCBs at Sub C – Case 3a

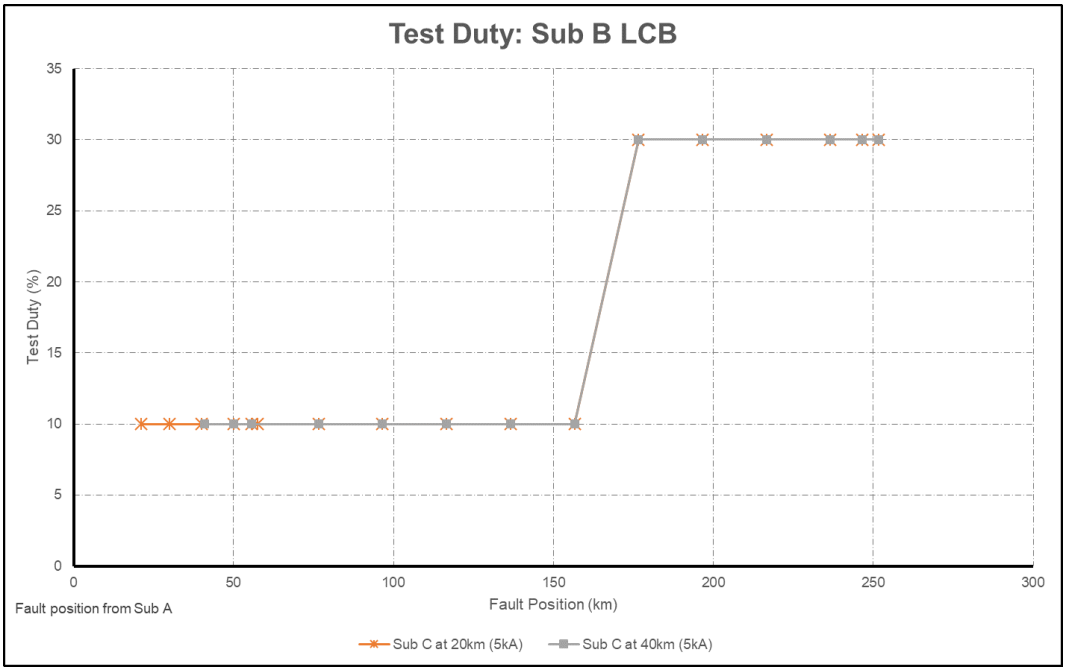

Figure 3-112: Test duties for LCBs at Sub B – Case 3a

The voltage waveform for the peak recovery voltages for Sub C are shown below (Figure 3-113). There are two peaks on the voltage profile (for line C- B 1 being 232.5 km) that were observed for the peak recovery voltage for the LCB at Sub C. This may be attributed to the capacitive reactance observed in Line B-C 1a. The current increased through this branch and boosted the peak recovery voltage for faults after the series capacitor bank. Another voltage peak was observed at approximately 160 km from Sub A (line B-C 1a line length is 232.5 km). This was due to line B-C 1a reaching its surge impedance value.

The peak voltage observed for the peak recovery voltages at the LCB at Sub C when C-B 1 was 212.5 km was due to the Thévenin impedance which reached its surge impedance for a fault 140 km away from Sub A. The second peak was due to B-C 1a reaching its surge impedance for a fault 200 km away from Sub A.

Voltage peaks for the peak recovery voltages of Sub B were observed at approximately 50 km from Sub A (line B-C 1b line length is 232.5 km) and 140 km from Sub A (Figure 3-114). This was due to B-C 1b and the Thévenin impedance reaching their surge impedance values for faults at those respective locations.

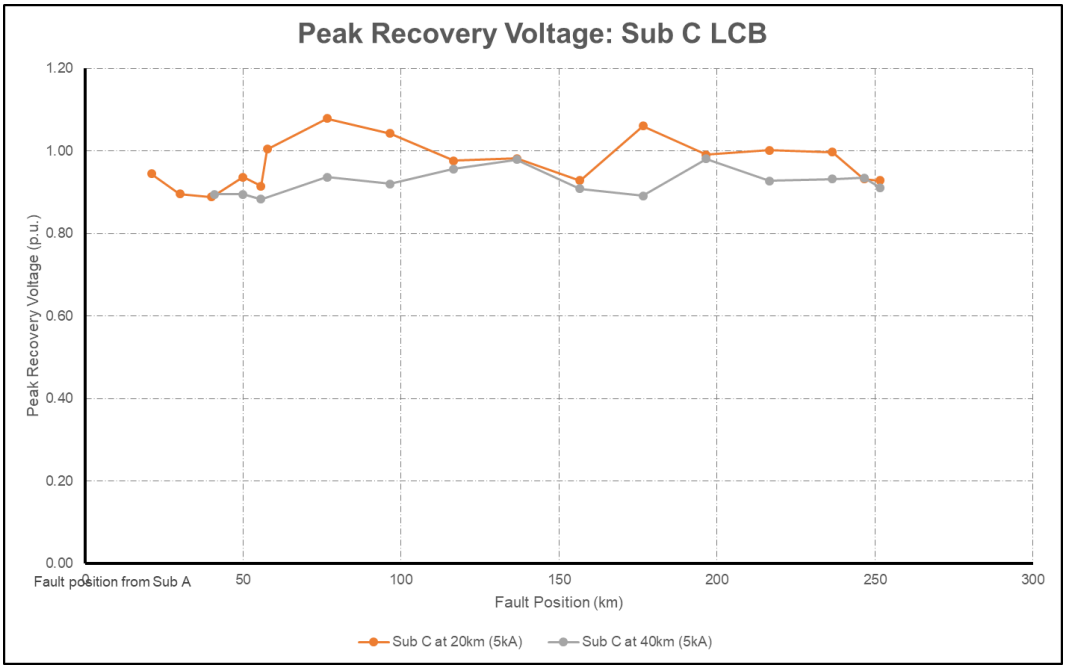

Figure 3-113: Peak Recovery Voltage profiles for LCBs at Sub C for line lengths of 20 km and 40 km for Line C-B 1 – Case 3a

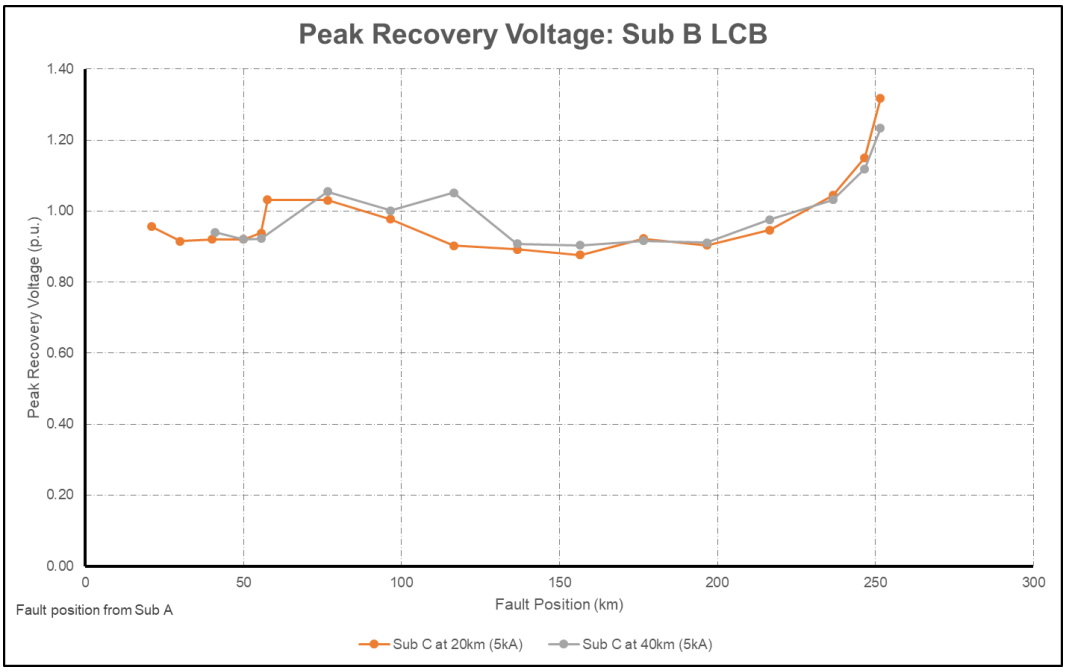

Figure 3-114: Peak Recovery Voltage profiles for LCBs at Sub B for line lengths of 20 km and 40 km for Line C-B 1 – Case 3a

The peak recovery voltages for the LCB at Sub B were compared against its peak recovery voltage limits (Figure 3-115 and Figure 3-116). The LCB at Sub B exceeded its limits for both line lengths evaluated when faults were applied 251 km away from Sub A. A recommendation would be to apply surge arresters across the circuit breaker terminals to limit the TRV that the LCB at Sub B is exposed to. Additionally, there is a high probability that the LCB may exceed its TRV capability for higher fault currents. This should be taken into consideration if uprating the breaker is to be considered.

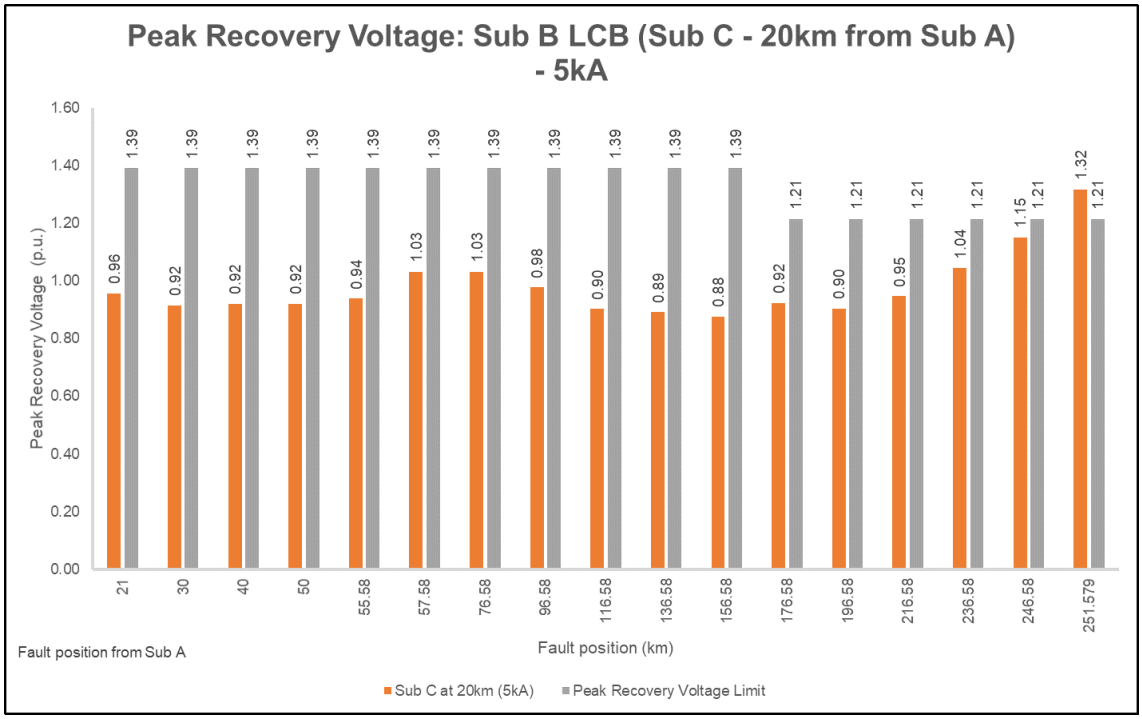

Figure 3-115: Peak Recovery Voltage profiles for the LCB at Sub B for Sub C at 20 km – Case 3a

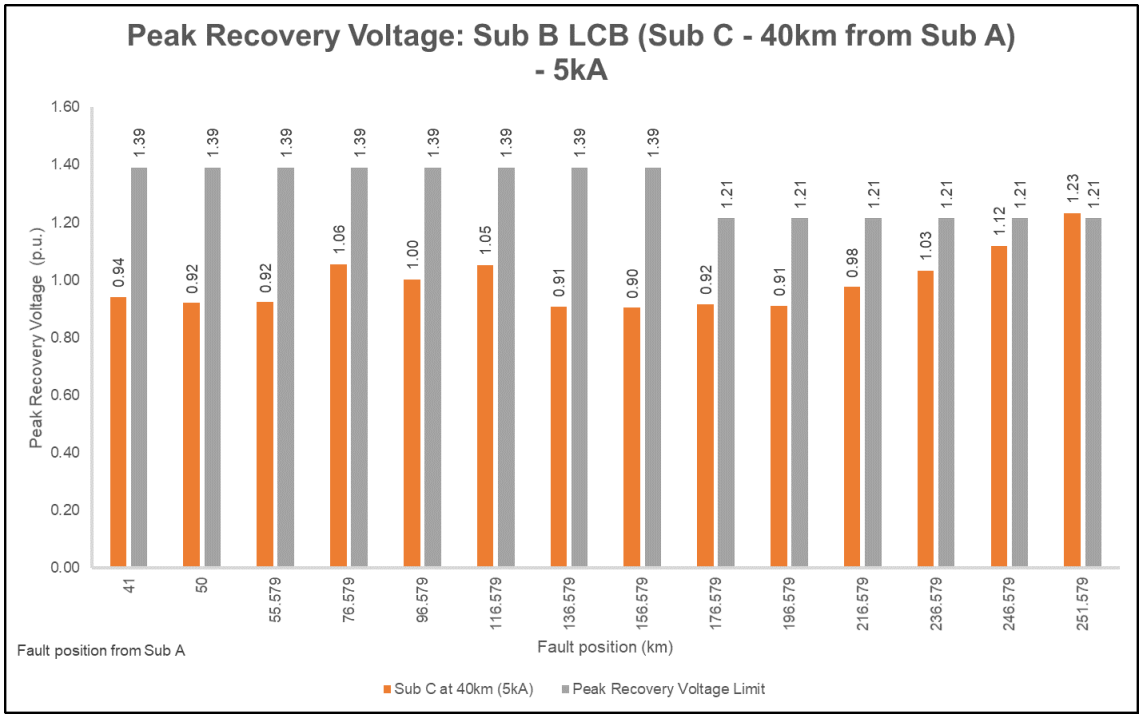

Figure 3-116: Peak Recovery Voltage profiles for the LCB at Sub B for Sub C at 40 km – Case 3a

The peak recovery voltages for the LCB at Sub C were then compared against its peak recovery voltage limits (Figure 3-117 and Figure 3-118). The LCB at Sub C did not exceed its limits for both line lengths evaluated.

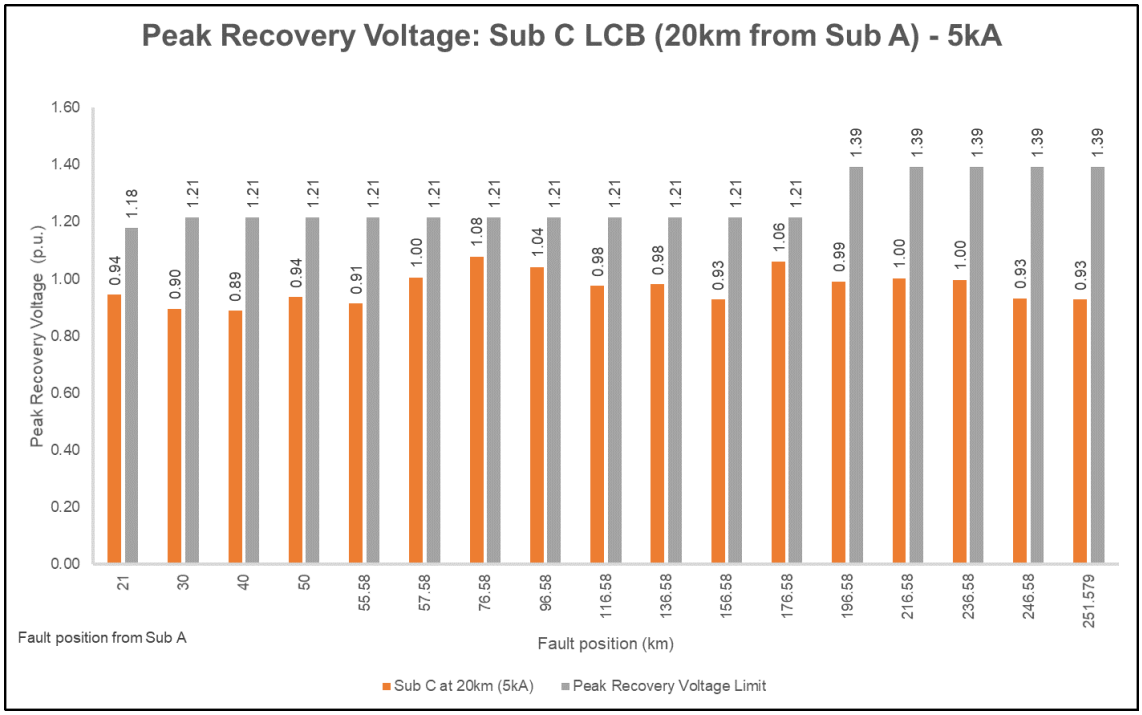

Figure 3-117: Peak Recovery Voltage profiles for the LCB at Sub C for Sub C at 20 km – Case 3a

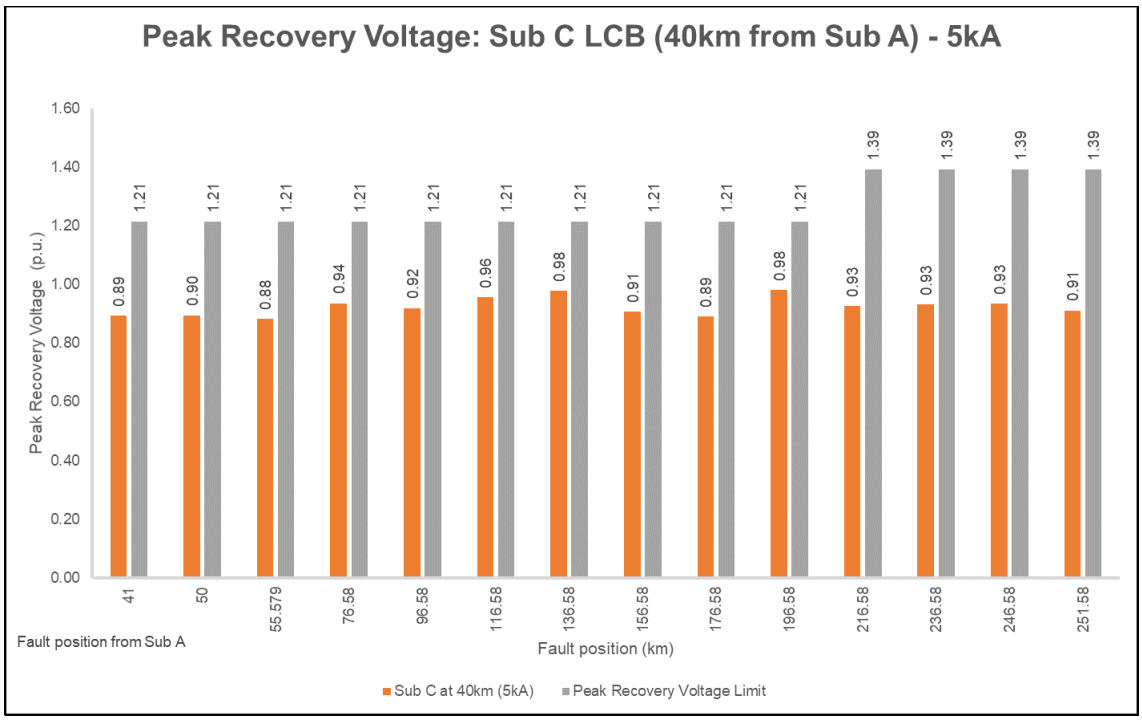

Figure 3-118: Peak Recovery Voltage profiles for the LCB at Sub C for Sub C at 40 km – Case 3a

The RRRV were evaluated for the LCBs at Sub B for the two scenarios presented below (Figure 3-119 and Figure 3-120). The measurements were taken at the inception of the LCB opening and the voltage recorded after a duration of 112 µs once the LCB opens for a test duty of 10% and 137 µs for a test duty of 30%. The LCBs were recorded to be well within the acceptable limits as indicated.

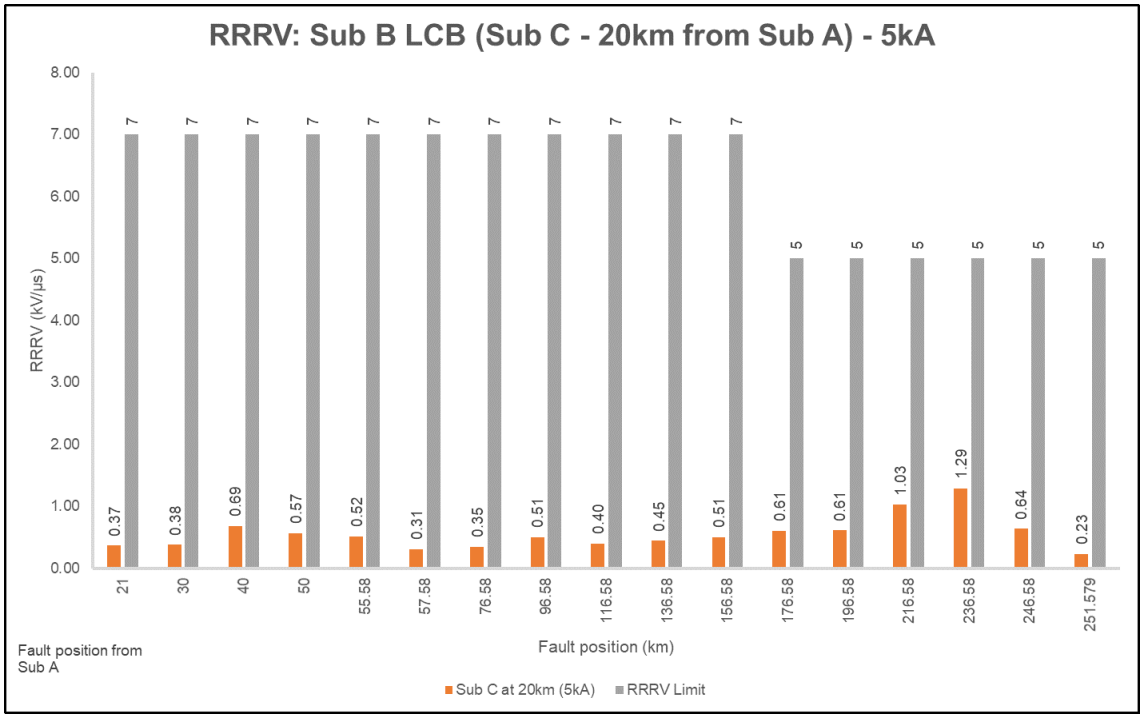

Figure 3-119: RRRV for the LCB at Sub B for Sub C at 20 km– Case 3a

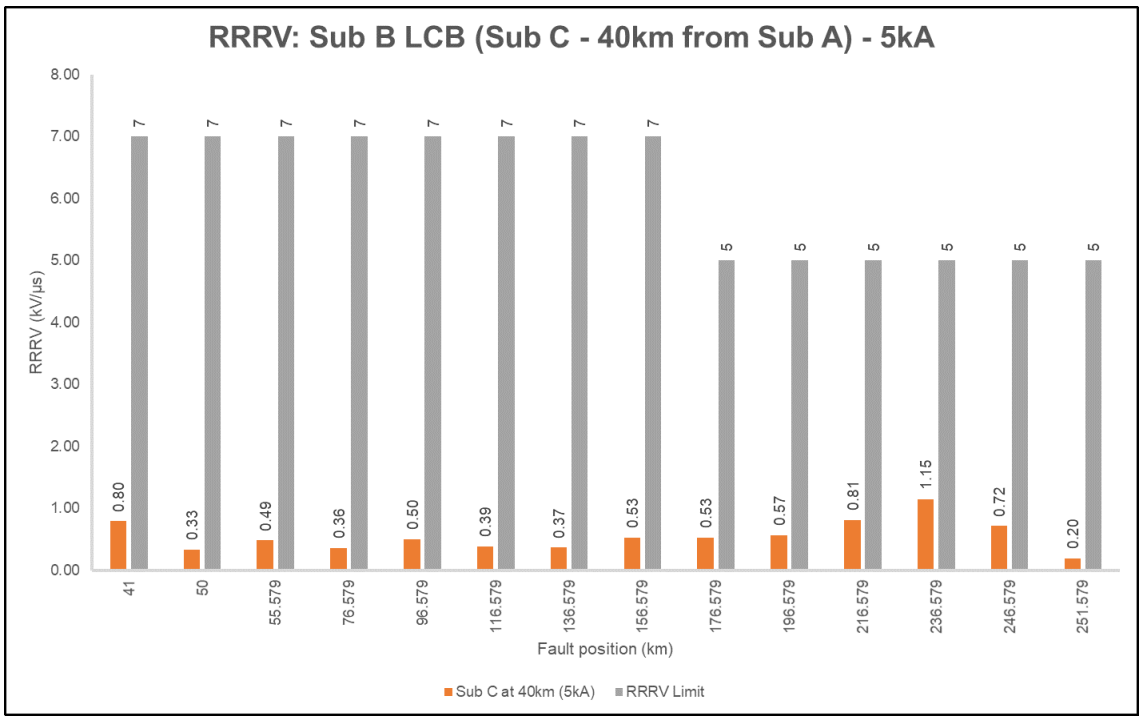

Figure 3-120: RRRV for the LCB at Sub B for Sub C at 40 km – Case 3a

The RRRV were evaluated for the LCBs at Sub C for the two scenarios presented below (Figure 3-121 and Figure 3-122). The measurements were taken at the inception of the LCB opening and the voltage recorded after a duration of 112 µs once the LCB opens for a test duty of 10%, 137 µs for a test duty of 30% and 111 µs for a test duty of 60%. The LCBs were recorded to be well within the acceptable limits as indicated.

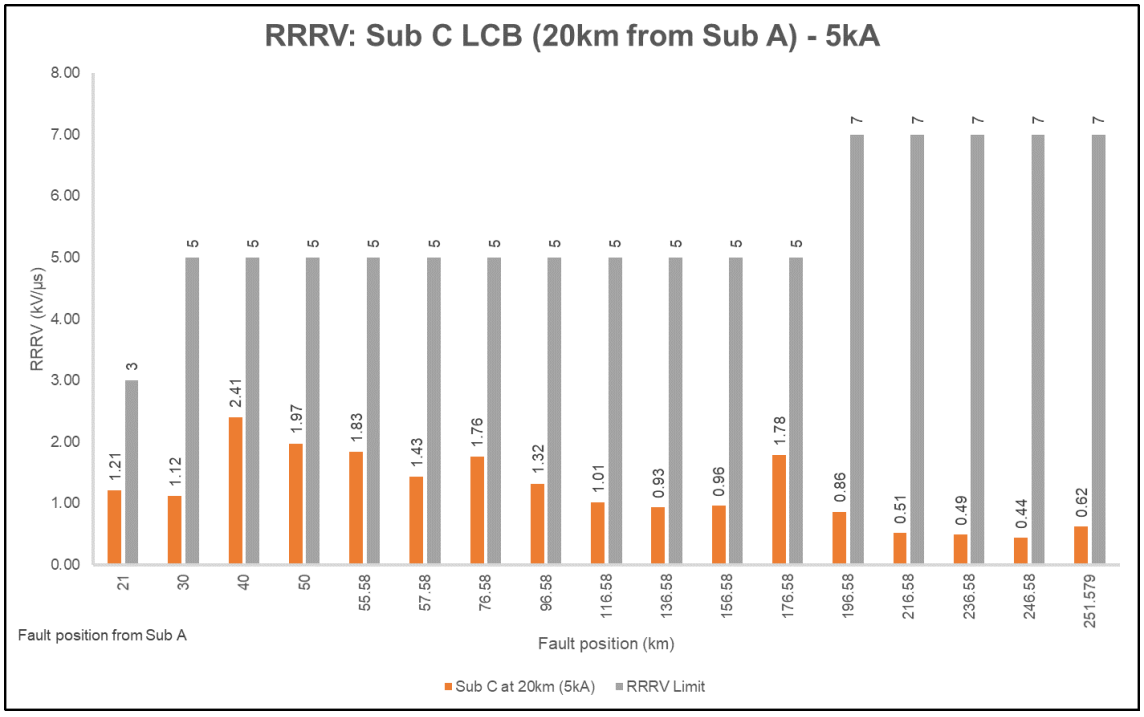

Figure 3-121: RRRV for the LCB at Sub C for Sub C at 20 km from Sub A – Case 3a

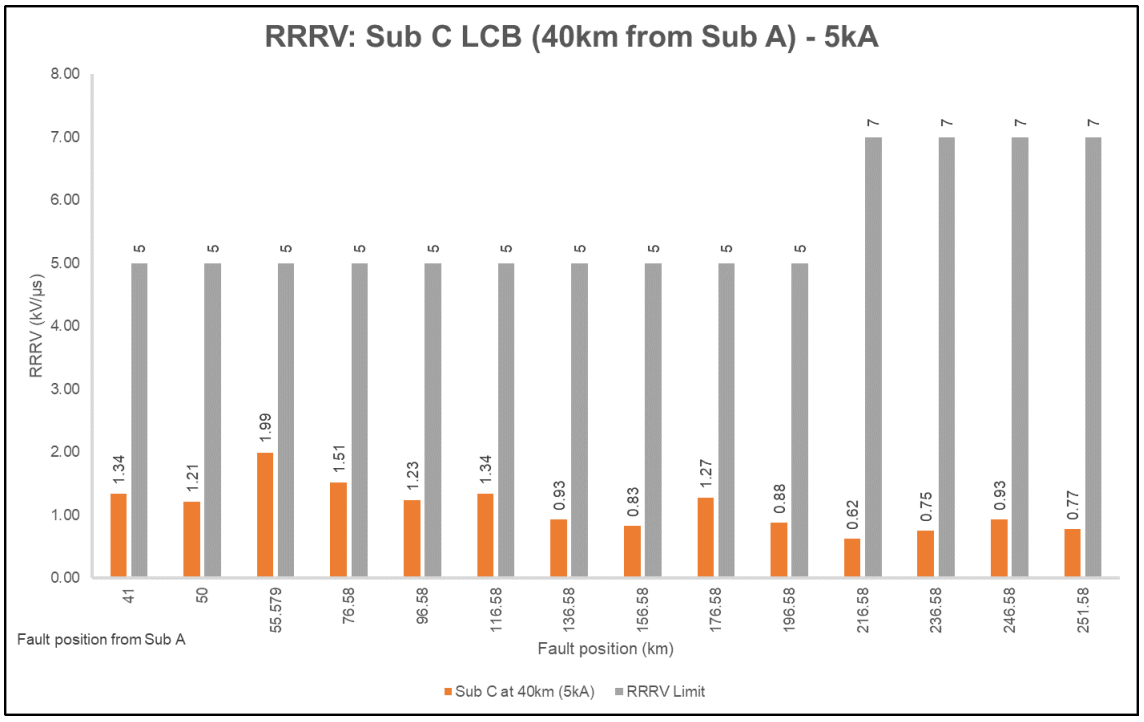

Figure 3-122: RRRV for the LCB at Sub C for Sub C at 40 km from Sub A – Case 3a

3.7.5 Simulation Results: Case 3b (Sub C – 10 kA)

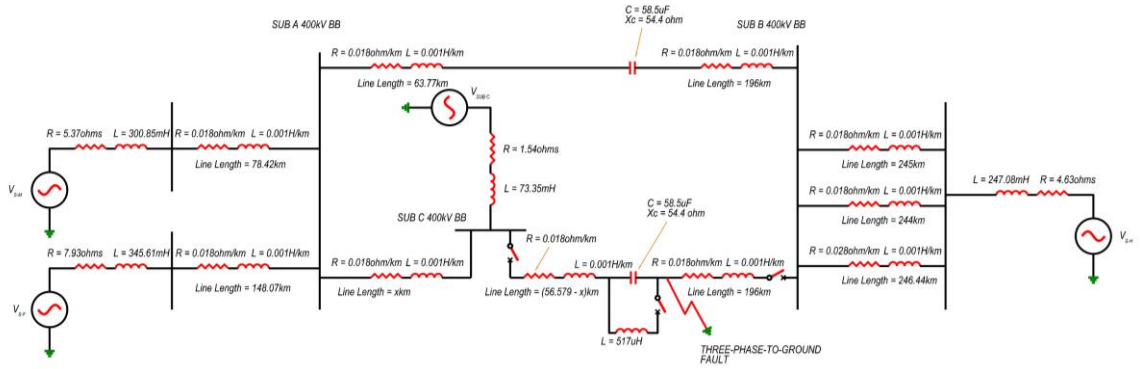

Figure 3-123: Single Line Diagram of Case 3b

The third set of cases that were evaluated were:

- Line C-B 1 which was 212.5 km long and Sub C was 40 km away from Sub A. The fault current contribution of from Sub C was 10 kA.
- Line C-B 1 which was 232.5 km long and Sub C was 20 km away from Sub A. The fault current contribution of from Sub C was 10 kA.

The same analysis was conducted as per section 3.7.4 however the source impedance for Sub C was adjusted to produce a fault current of 10 kA. The fault current was evaluated first to determine the test duty of the LCBs.

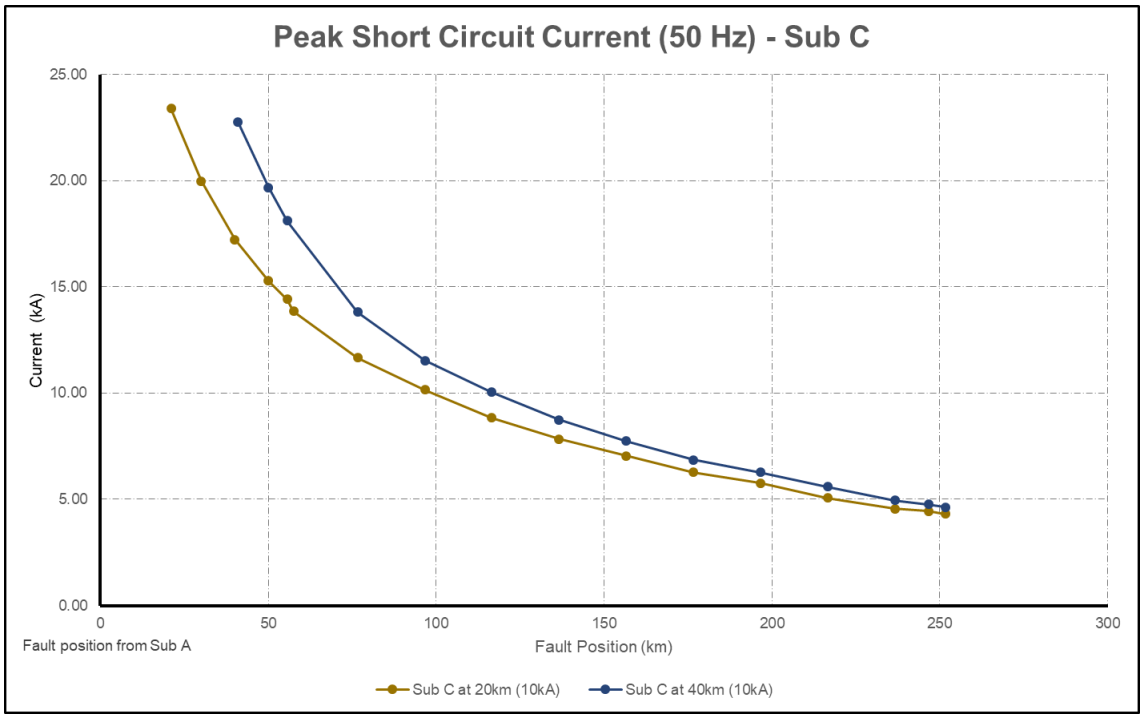

Figure 3-124: Peak fault current (50 Hz) for LCBs at Sub B – Case 3b

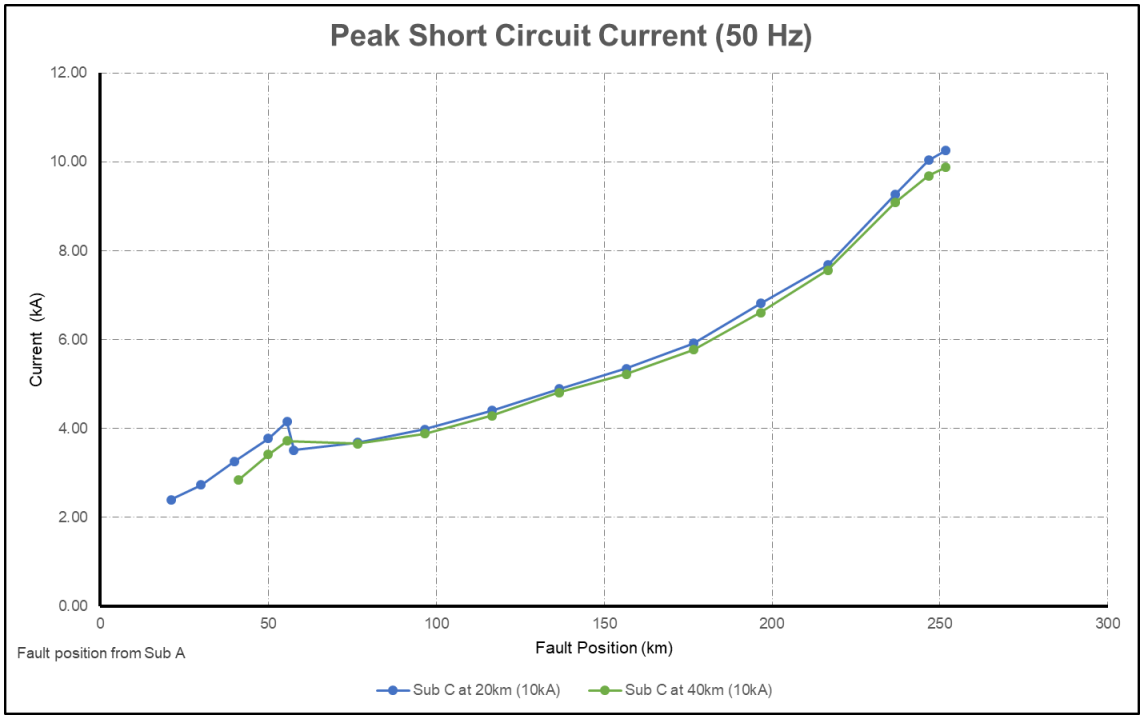

Figure 3-125: Peak fault current (50 Hz) for LCBs at Sub C– Case 3b

The fault current profiles indicated above (Figure 3-124 and Figure 3-125) follow a similar trend as that of the fault current profiles presented in Figure 3-107 and Figure 3-108 respectively. The magnitudes of the fault current increased as follows:

Table 3-22: Comparison of fault currents for LCBs at Sub A and Sub C

LCB	Fault Current Magnitudes (kA)			
	Line C-B 1 length = 212.5 km		Line C-B 1 length = 232.5 km	
	Sub C LCB 5 kA	Sub C LCB 10 kA	Sub C LCB 5 kA	Sub C LCB 10 kA
Sub B	8.7 kA	9.8 kA	8.8 kA	10.3 kA
Sub C	14.5 kA	22.8 kA	15.2 kA	23.4 kA

The fault current through the LCBs at Sub C indicated a significant increase (57% increase for line C-B 1 at 212.5 km and 54% increase for line C-B 1 at 232.5 km) with the change in source impedance at Sub C (Table 3-22).

The test duties for the LCBs at Sub B and Sub C (Figure 3-127) remained within the same range when compared to the case where the fault contribution of Sub C was 5 kA (Figure 3-112).

The LCB at Sub C operated at a test duty of 60% for faults within the first 4% and 13% of line C-B 1 of length 232.5 km (Sub C was 20 km away from Sub A) where the fault current contribution from Sub C was 5 kA (Figure 3-111) and 10 kA (Figure 3-126) respectively. The LCB at Sub C operated at a test duty of 30% for 17% more of the line length when the fault current contribution of Sub C was 10 kA in comparison to the case where the fault current contribution was 5 kA.

The test duty of the LCB at Sub C increased from 30% to 60 % for faults within the first 5% of line C - B 1 from Sub A when the line length was 212.5 km (Sub C was 40 km away from Sub A) and the fault current contribution of Sub C increased from 5 kA (Figure 3-112) to 10 kA (Figure 3-127).

The LCB at Sub B operates at a test duty of 30% for faults within the first 33% and 41% of line C-B 1 of length 232.5 km (Sub C was 20 km away from Sub A) where the fault current contribution from Sub C was 5 kA (Figure 3-112) and 10 kA (Figure 3-127) respectively. The LCB at Sub B operates at a test duty of 30% for 9% more of the line length when the fault current contribution of Sub C was 10 kA in comparison to the case where the fault current contribution was 5 kA.

The test duty of the LCB at Sub B increased from 10% to 30 % for 10% more of the line C - B 1 from Sub A when the line length was 212.5 km (Sub C was 40 km away from Sub A) and the fault current contribution of Sub C increased from 5 kA (Figure 3-112) to 10 kA (Figure 3-127).

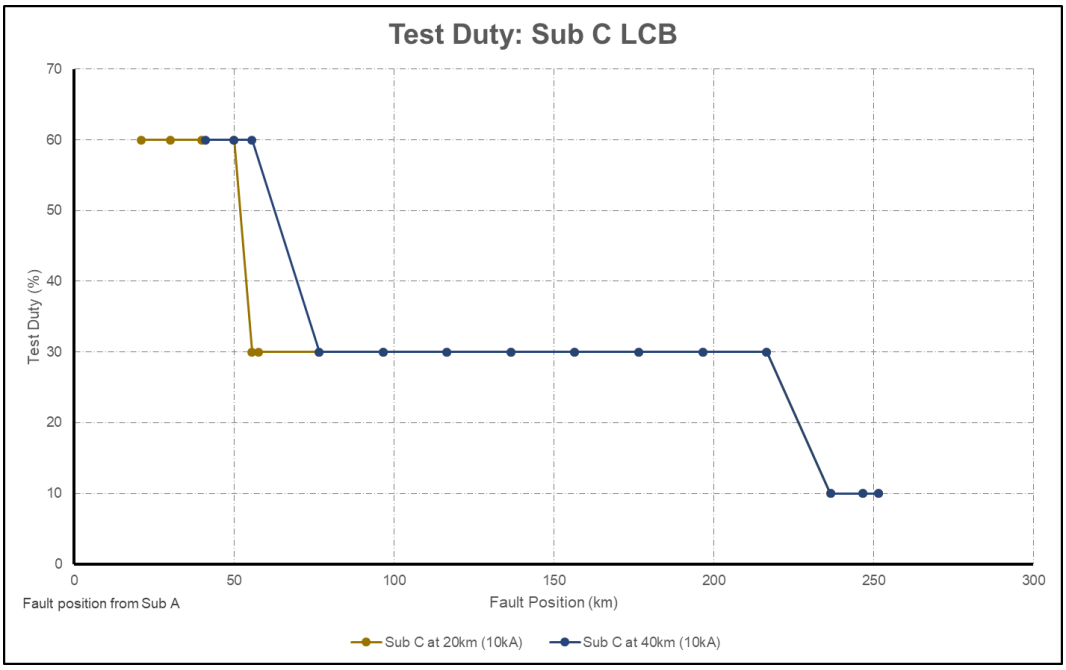

Figure 3-126: Test duties for LCBs at Sub C – Case 3b

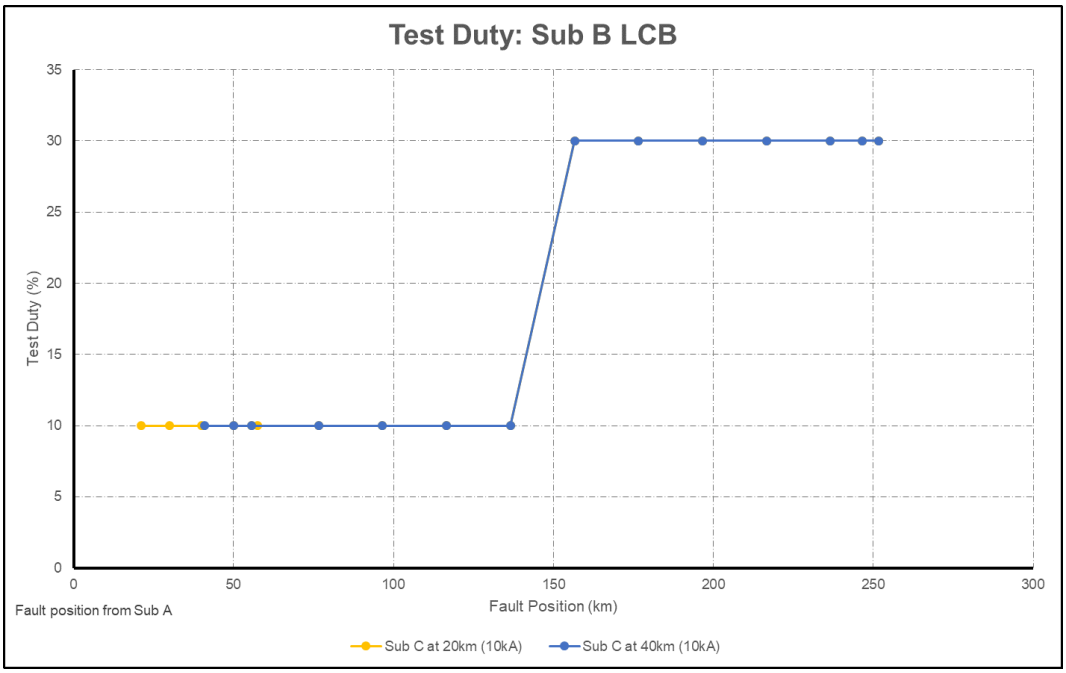

Figure 3-127: Test duties for LCBs at Sub B – Case 3b

The peak recovery voltages of the LCBs at Sub B and C for line length of B-C 1 being 212.5 km and 232.5 km respectively were analysed. The peak recovery voltage profile for Sub C (Figure 3-128) followed the same profile as the previous case (refer to Figure 3-113). There was however an increase in voltage of the profile. Additionally, the voltage peaks that were observed were due to surge impedance matching.

The peak recovery voltage profile for the LCB at Sub B followed a similar profile as that in Figure 3-114.

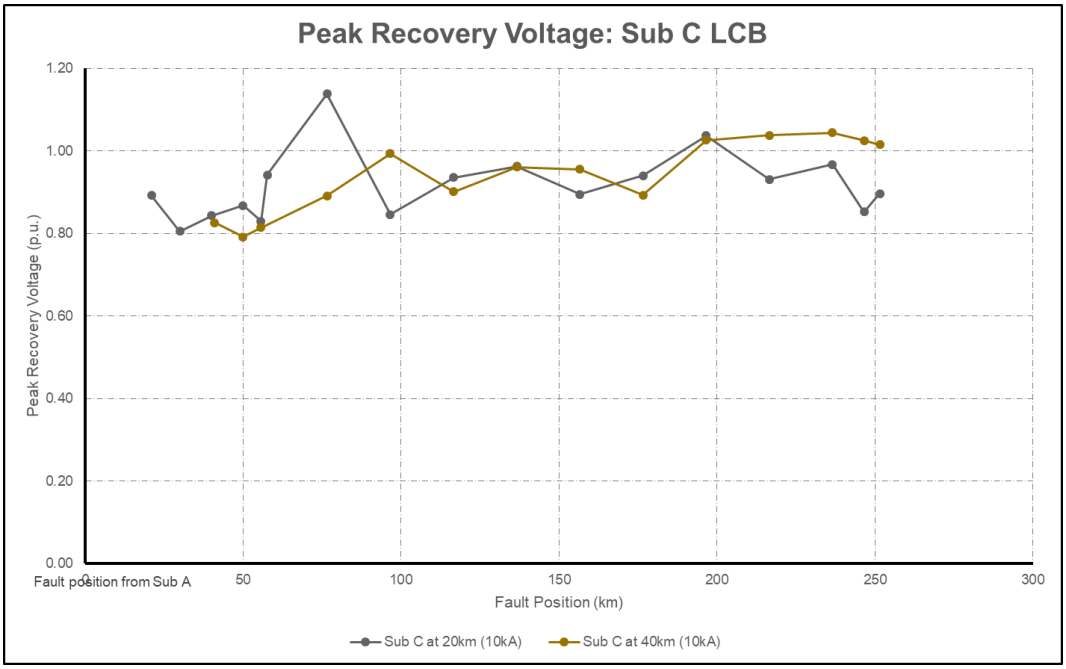

Figure 3-128: Peak Recovery Voltage profiles for LCBs at Sub C for line lengths of 212.5 km and 232.5 km for Line C-B 1 – Case 3b

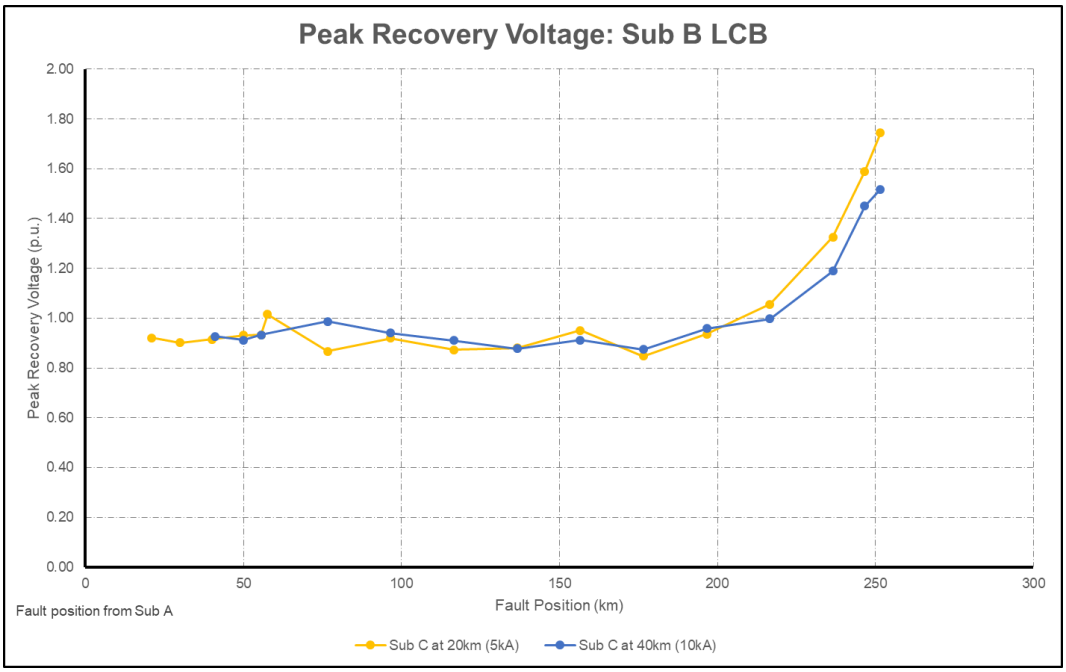

Figure 3-129: Peak Recovery Voltage profiles for LCBs at Sub B for line lengths of 212.5 km and 232.5 km for Line C-B 1 – Case 3b

The peak recovery voltage limit for the LCB at Sub B were exceeded for both line lengths of C-B 1 (Figure 3-130 and Figure 3-131). The peak recovery voltage exceeds limit for the first 20 km of line C-B 1 in both cases. Additionally, the peak recovery voltages were fairly high for approximately 40% of line C-B 1 in both cases. A recommendation would be to either investigate the benefit of installing surge arresters across the LCB terminals. The second option would be to uprate the LCB as a further increase in fault current will pose a higher risk to the LCB failing.

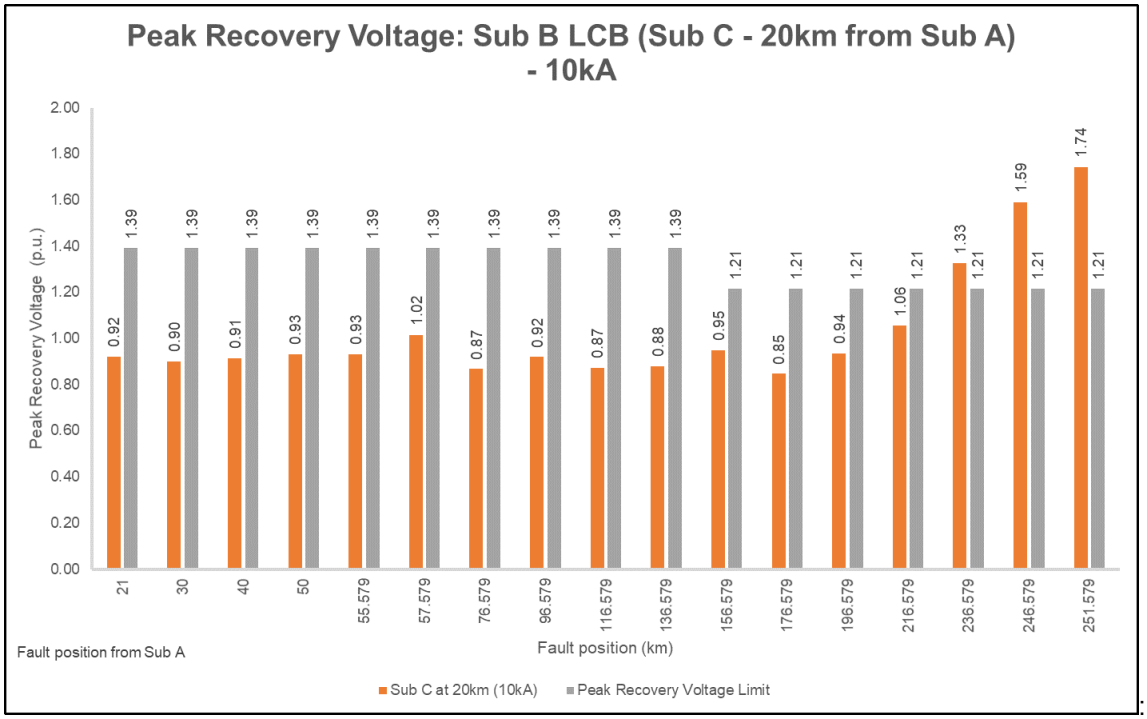

Figure 3-130: Peak Recovery Voltage profiles for the LCB at Sub B for Sub C at 20 km – Case 3b

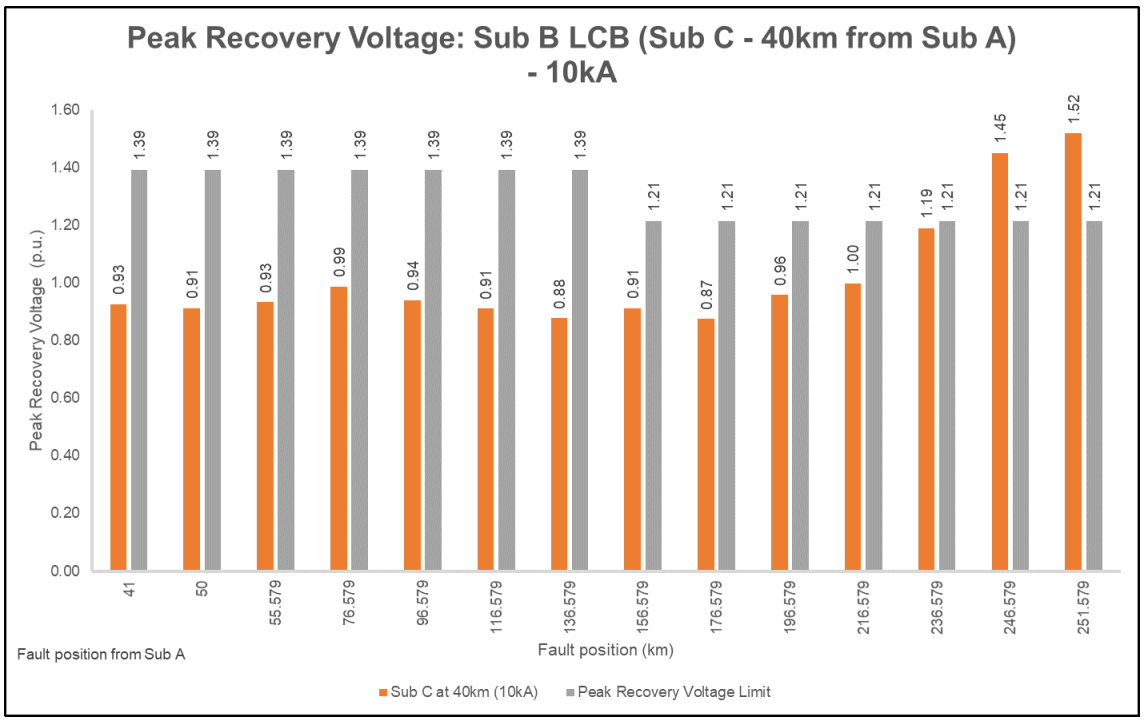

Figure 3-131: Peak Recovery Voltage profiles for the LCB at Sub B for Sub C at 40 km – Case 3b

The peak recovery voltage limit for the LCB at Sub C did not exceed the peak recovery voltage limits for both line lengths of C-B 1 (Figure 3-132 and Figure 3-133). However, the peak recovery voltages are close to their limits and the recommendation would be to either install surge arresters across the LCB terminals or uprate the LCB.

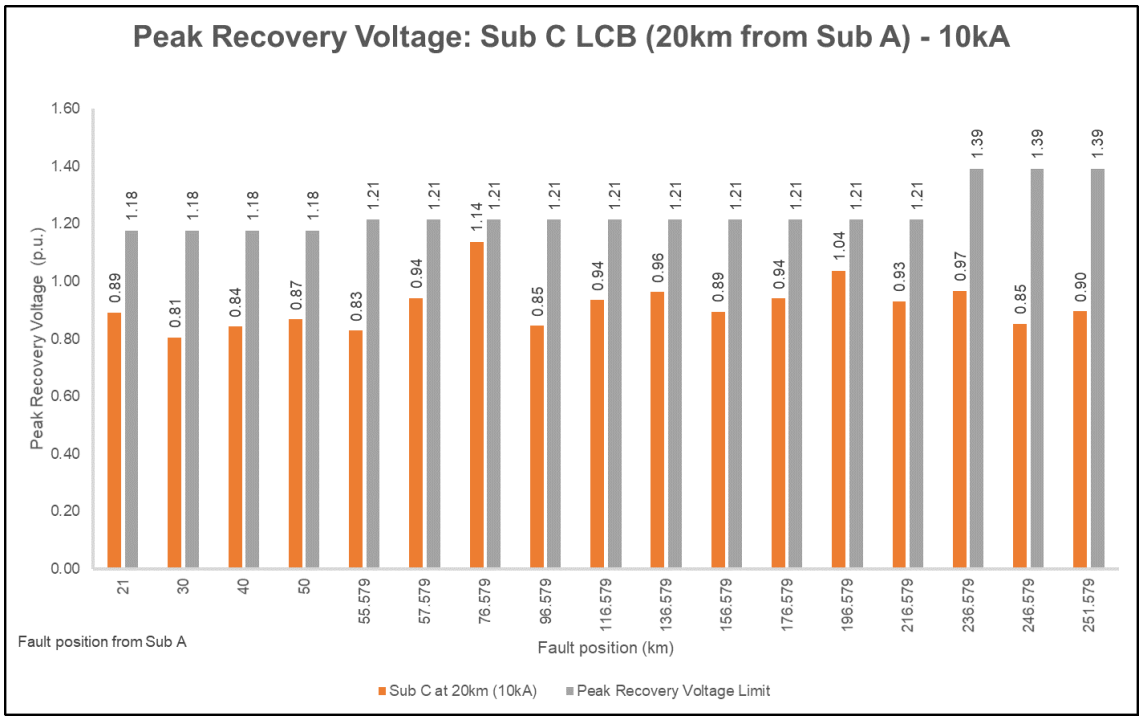

Figure 3-132: Peak Recovery Voltage profiles for the LCB at Sub C for Sub C at 20 km – Case 3b

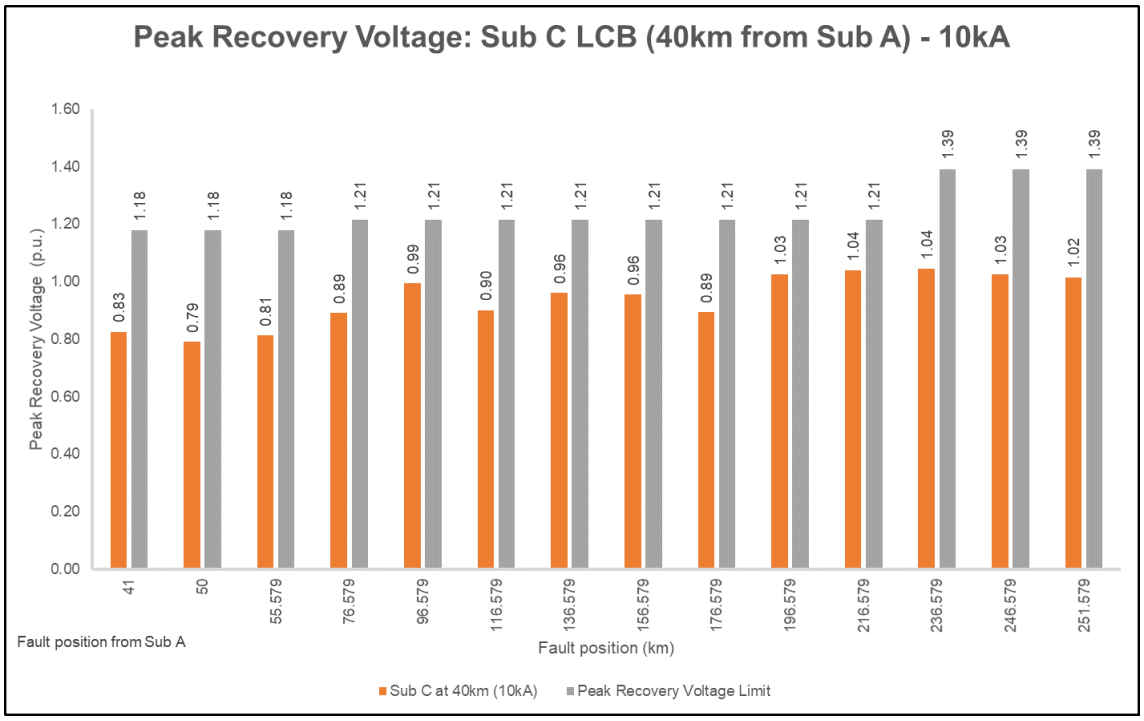

Figure 3-133: Peak Recovery Voltage profiles for the LCB at Sub C for Sub C at 40 km – Case 3b

The RRRV were evaluated for the LCBs at Sub B for the two scenarios presented below (Figure 3-134 and Figure 3-135). The measurements were taken at the inception of the LCB opening and the voltage

recorded after a duration of 112 µs once the LCB opened for a test duty of 10% and 137 µs for a test duty of 30%. The LCBs were recorded to be well within the acceptable limits as indicated.

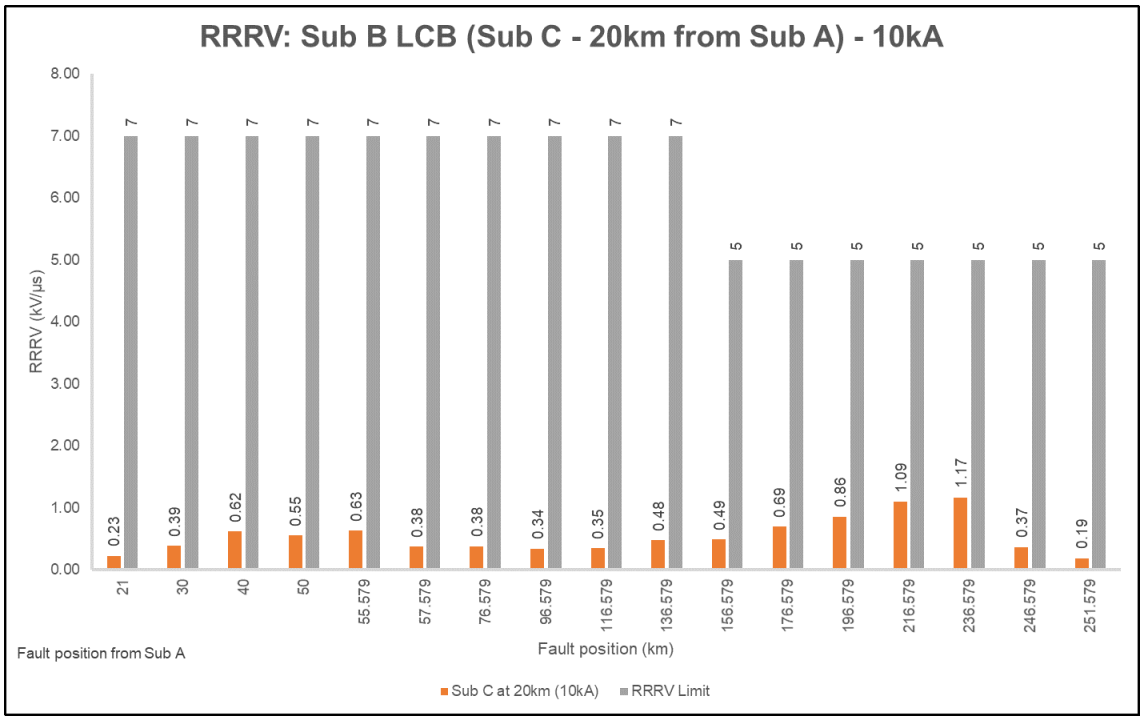

Figure 3-134: RRRV for the LCB at Sub B for Sub C at 20 km – Case 3b

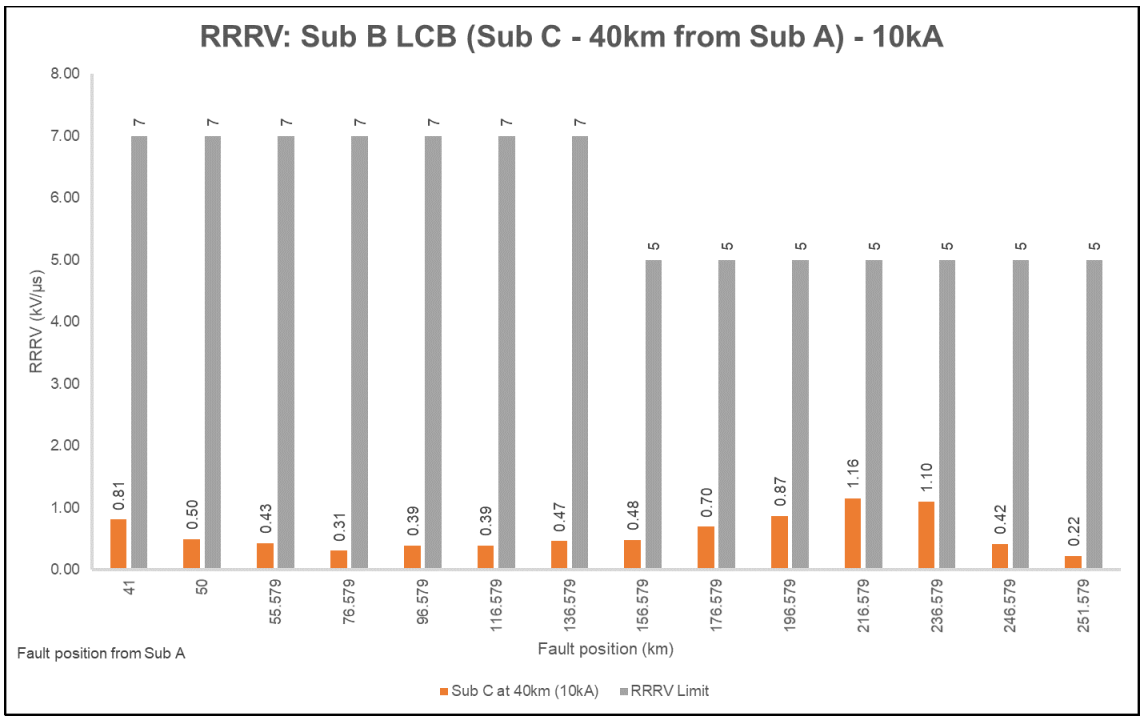

Figure 3-135: RRRV for the LCB at Sub B for Sub C at 40 km – Case 3b

The RRRV were evaluated for the LCBs at Sub C for the two scenarios presented below (Figure 3-136 and Figure 3-137). The measurements were taken at the inception of the LCB opening and the voltage recorded after a duration of 112 µs once the LCB opens for a test duty of 10%, 137 µs for a test duty of 30% and 111 µs for a test duty of 60%. The LCB at Sub C marginally exceeded its RRRV rating for a

fault 20 km away from Sub A where the line length of C-B 1 was 232.5 km (Figure 3-136). The RRRV increased substantially for an increase in fault current in comparison to the RRRV for the LCB at Sub C with a fault current contribution of 5 kA (Figure 3-121). The probability of exceeding the RRRV limit for three-phase-to-ground faults before the series capacitor bank increases with an increase in fault current in this scenario. The RRRV rating for the LCB at Sub C where the line length of C-B 1 was 212.5 km nears its RRRV limit for faults 1 km before the series capacitor bank (Figure 3-137). This scenario also indicates an increase in probability of exceeding the RRRV limits for an increase in the magnitude of three-phase-to-ground faults.

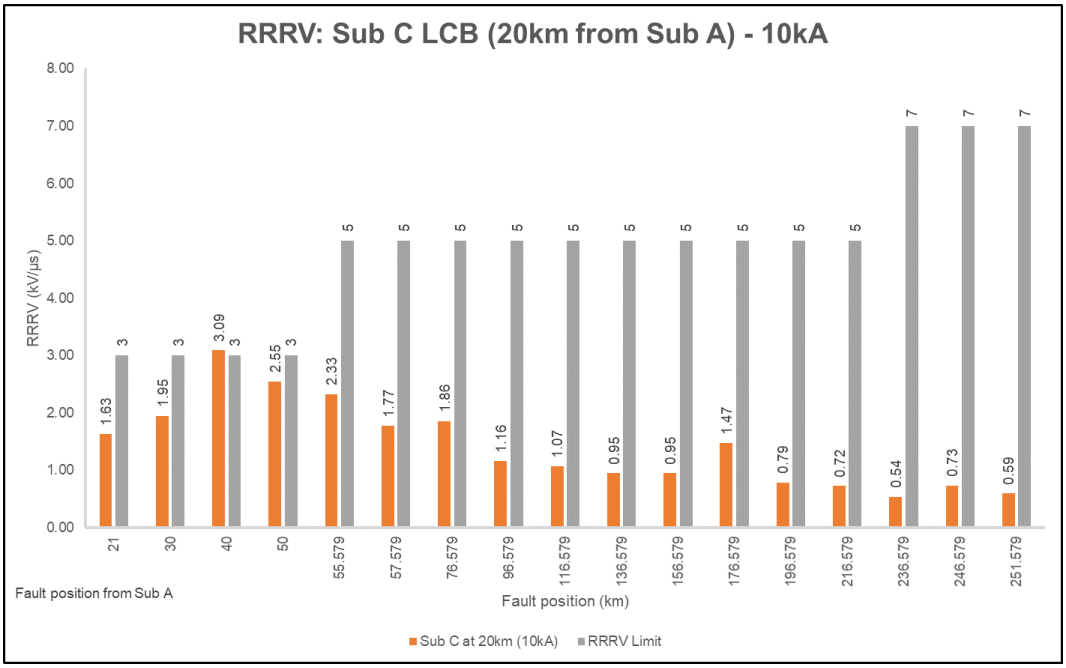

Figure 3-136: RRRV for the LCB at Sub B for Sub C at 20 km – Case 3b

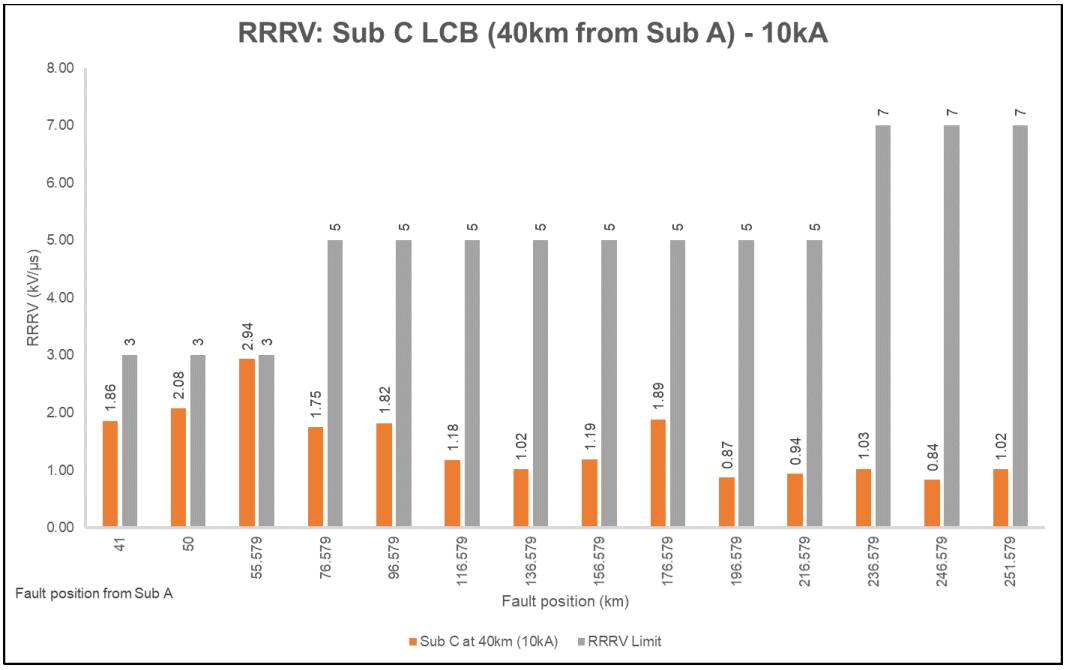

Figure 3-137: RRRV for the LCB at Sub B for Sub C at 40 km – Case 3b

3.7.6 Series Compensated Transmission Line Protection Malfunction

One of the challenges associated with series compensated transmission lines is the ability of the impedance protection systems to operate correctly. This is discussed in detail in section 2.6.1.2. The objective of this section is to present the consequence of the protection systems failing to operate. In this example, either the line protection system fails to detect the fault along the transmission line and the series capacitor bypass circuit breaker consequently fails to close or the series capacitor bypass circuit breaker fails to close due to a malfunction. The LCBs close after the protection system responds and the series capacitor bank circuit breaker remains opened. There is a trapped charge on the transmission line that is observed and an elevated TRV that the LCB is exposed to.

The following example further illustrates this aspect. Sub C was connected 240 km away from Sub A. A three-phase-to-ground fault was applied 10 km away from Sub A and was initiated after 15 ms. Thereafter the LCB at Sub A opened at 65 ms and the LCB at Sub C opened last at 70 ms. The peak recovery voltage and the RRRV were used to determine if the LCB ratings were exceeded.

The magnitude of fault current flowing through the LCB at Sub A was 9 kA_{rms} per phase (Figure 3-138). This translates to a test duty of the LCB at 30%.

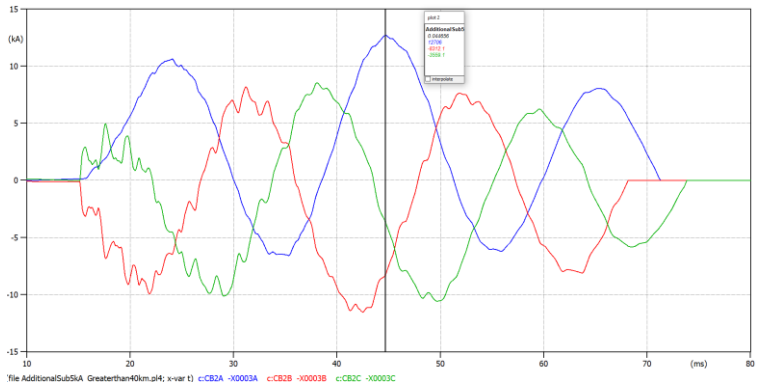

Figure 3-138: Fault current through LCB at Sub A

The peak recovery voltage that the LCB at Sub A was exposed to was 670 kV_{peak} (Figure 3-139). This was within the peak recovery voltage limit of 687 kV for a circuit breaker at 30% test duty. The corresponding RRRV for the LCB was 0.37 kV/µs for a circuit breaker at test duty of 30% which was also lower than the limit of 5 kV/ µs.

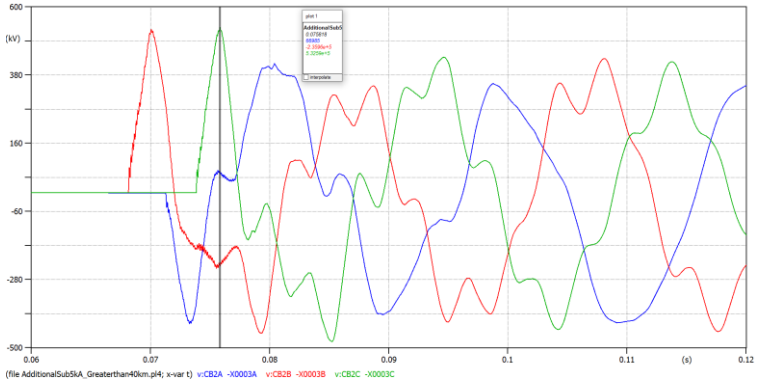

Figure 3-139: Voltage profile of TRV across the LCB terminals at Sub A

The magnitude of fault current flowing through the LCB at Sub C was 9 kA_{rms} per phase (Figure 3-140). This translates to a test duty of the LCB at 10%.

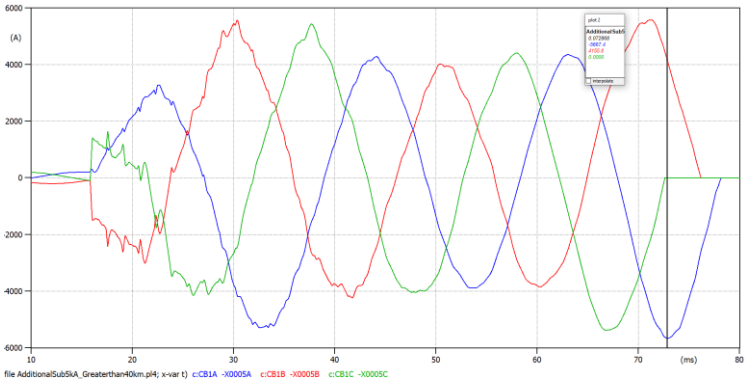

Figure 3-140: Fault current through LCB at Sub C

The peak recovery voltage that the LCB at Sub C was exposed to was 950 kV_{peak} (Figure 3-141). This exceeds the peak recovery voltage limit of 787 kV for a circuit breaker at 10% test duty. This was due to the trapped charge of the series capacitor bank. The MOV across the series capacitor bank limits the voltage due to the trapped charge. The TRV exceeds 1 MV in the absence of the MOV.

The corresponding RRRV for the LCB was 0.96 kV/µs for a circuit breaker at test duty of 10% which was lower than the limit of 7 kV/µs.

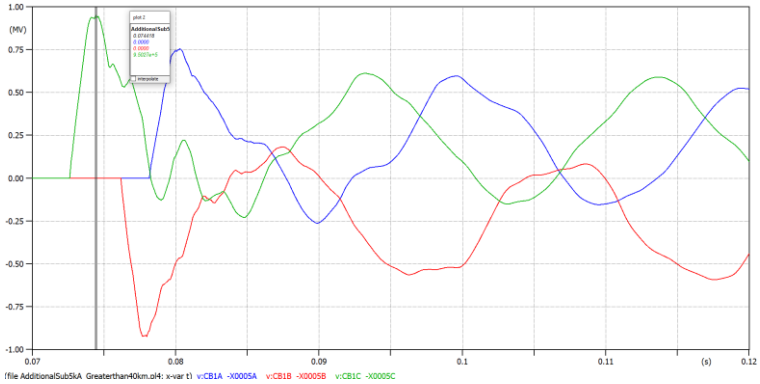

Figure 3-141: Voltage profile of TRV across the LCB terminals at Sub C

Figure 3-142 shows the trapped charge on the transmission line after the LCBs are opened.

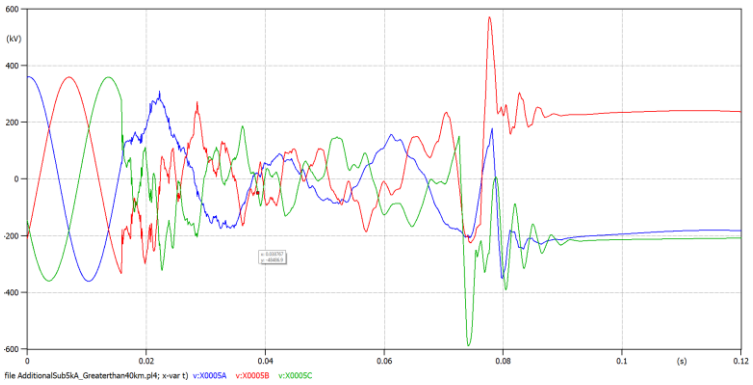

Figure 3-142: Trapped charge due to the series capacitor bank seen after 80 ms

This example highlights the importance of applying appropriate protection system settings on an impedance protection system for a series compensated transmission line. The consequence of the protection system to respond correctly to a fault detected could be detrimental to the LCBs resulting in the loss of the line and possibly busbars in the event of a bus zone trip.

Chapter 4 presents a discussion of the results highlighting the influence of integrating a voltage source along a series and shunt compensated transmission line. The effects of varying the line length as a result of integrating a voltage source, as well as varying the fault current are presented.

4 DISCUSSION OF RESULTS

The two parameters associated with the TRV rating of a circuit breaker are the peak recovery voltage and the RRRV. The following discussion of results will focus on the two parameters indicated with respect to the factors that were varied (i.e. fault current, integration of voltage source along the series compensated circuit and varying the position of this new voltage source). The following discussion will be presented for each voltage source evaluated (i.e. Sub A, Sub B and Sub C).

4.1 Peak Recovery Voltages and RRRVs for Sub A

The peak recovery voltage profile was presented for the LCB at Sub A for faults applied at varied positions along the transmission line in the following cases:

- Case 1: No Sub C
- Case 2a: Sub C contributing fault current magnitude of 5 kA. Sub C was located 200 km and 240 km from Sub A. Series capacitor bank was between Sub A and Sub C
- Case 2b: Sub C contributing fault current magnitude of 10 kA for line lengths of 200 km and 240 km away from Sub A. Series capacitor bank was between Sub A and Sub C.

Upon fault initiation, the voltage seen at the LCB at Sub A is inversely proportional to the fault position for faults up until the series capacitor bank. When the protection system triggers the LCB to open, the voltage on the source terminal of the LCB transitions from the voltage perceived during the fault to system voltage. The transient response on the source is dependent on the power system damping (i.e. overdamped or underdamped).

The line voltage on the line side terminal of the LCB at Sub A is then dependent on the line capacitance which will discharge into the fault. Again, the response of the system change on the line side is dependent on the damping offered by the transmission line between the line side terminal and the fault.

The voltage profile of the peak recovery voltage at Sub A followed the apparent impedance of a compensated circuit as shown in Figure 2-26.

Figure 4-1 indicates that the peak recovery voltage was influenced by the magnitude of the fault current. The higher the fault current, the higher peak recovery voltages that the LCB at Sub A was exposed to.

There is a peak observed between 50 km and 80 km away from Sub A. The reason for this was due to the Thévenin equivalent impedance reaching surge impedance and the network delivered maximum current to the fault.

The peak recovery voltages marginally exceeded the circuit breaker peak recovery voltage rating for Case 1. However, there is a margin of safety catered for when selecting the TRV parameter envelope based on the test duty of the circuit breaker.

The integration of Sub C (Case 2a and Case 2b) resulted in the peak recovery voltage rating being exceeded for terminal or short line faults (up to 20 km) or for faults after the series capacitor bank from Sub A as a result of either an increase in fault current or increase in line length between Sub A and Sub C.

The peak recovery voltage rating was exceeded by a maximum margin of 7% when Sub C was 200 km away from Sub A and the fault current contribution from Sub C was increased from 5 kA to 10 kA. The exceedances occurred for faults applied 1 km away from Sub A and 76 km away from Sub A.

The same assessment was conducted when Sub C was located 240 km away from Sub A and the fault current contribution of Sub C was increased from 5 kA to 10 kA. The peak recovery voltage exceeded its limits from a margin of 11% at 5 kA fault current contribution from Sub C to 15% at 10 kA fault current

contribution from Sub C for faults applied after the series capacitor bank at a distance of 76 km from Sub A. The peak recovery voltage limits were exceeded for faults applied between 1 km and 20 km from Sub A when the fault current contribution from Sub C was 10 kA. The limits were exceeded by a margin of 30% at 1 km to 10% at 20 km. There were no peak recovery voltage rating exceedances observed when the fault current contribution from Sub C was 5 kA for faults applied between 1 km and 20 km away from Sub A.

Increasing the line length between Sub A and Sub C (from 200 km to 240 km) while maintaining the fault current contribution from Sub C to 5 kA resulted in the peak recovery voltage being exceeded for faults after the series capacitor bank from Sub A (76 km from Sub A) by a margin of 12%.

Increasing the line length between Sub A and Sub C (from 200 km to 240 km) while maintaining the fault current contribution from Sub C to 10 kA resulted in the peak recovery voltage rating being exceeded for faults terminal or short line faults (up to 1 km away from Sub A) by a margin of approximately 30%.

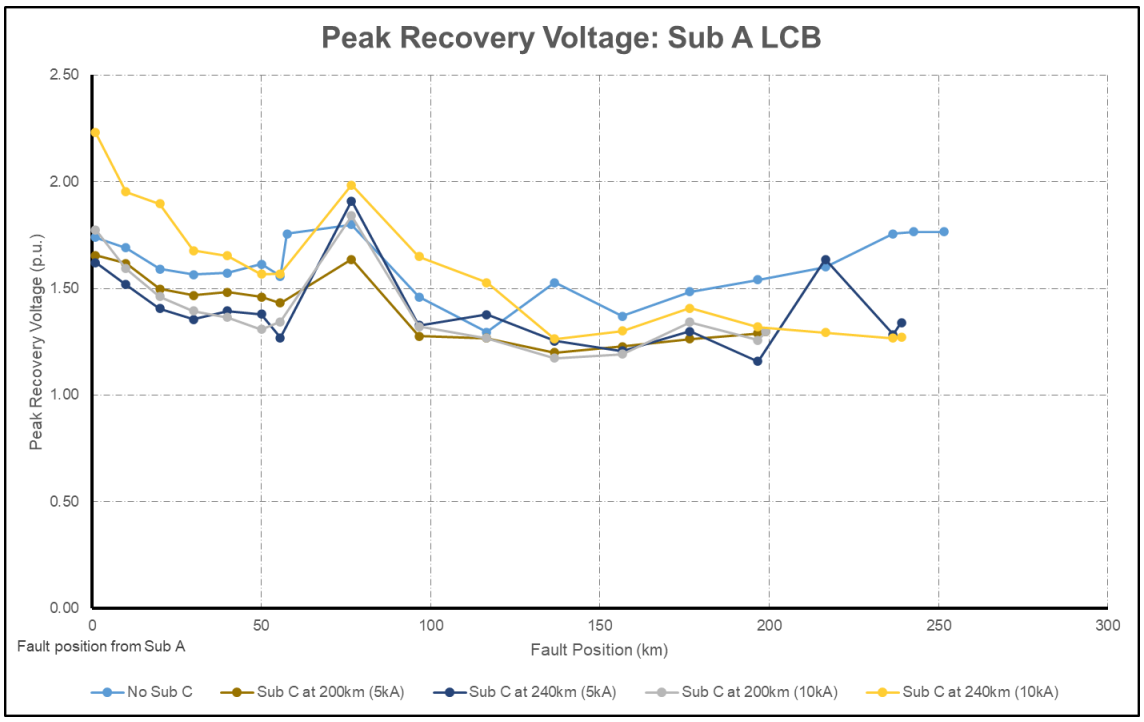

Figure 4-1: Peak recovery voltage profiles for Sub A LCB

Figure 4-2 presents the RRRVs that the LCB at Sub A were exposed to. The RRRV was expected to be at its highest for faults in close proximity to the LCB (within the first 10 km). However, the saw-tooth response of the peak recovery voltage for faults up to 20 km from the LCB reduces the RRRV. Therefore, the RRRV should be calculated from the point at which the LCB opens until the first peak to get a more accurate result.

A peak RRRV was observed at approximately 80 km from Sub A. This was attributed to the Thévenin equivalent impedance reaching the surge impedance at this point. A peak was also observed between 170 km and 200 km from Sub A due to the surge impedance of line A-C 1a being matched. The RRRV for Sub A was within the rating in all instances.

Figure 4-2 indicates that the RRRV is proportional to fault current magnitude.

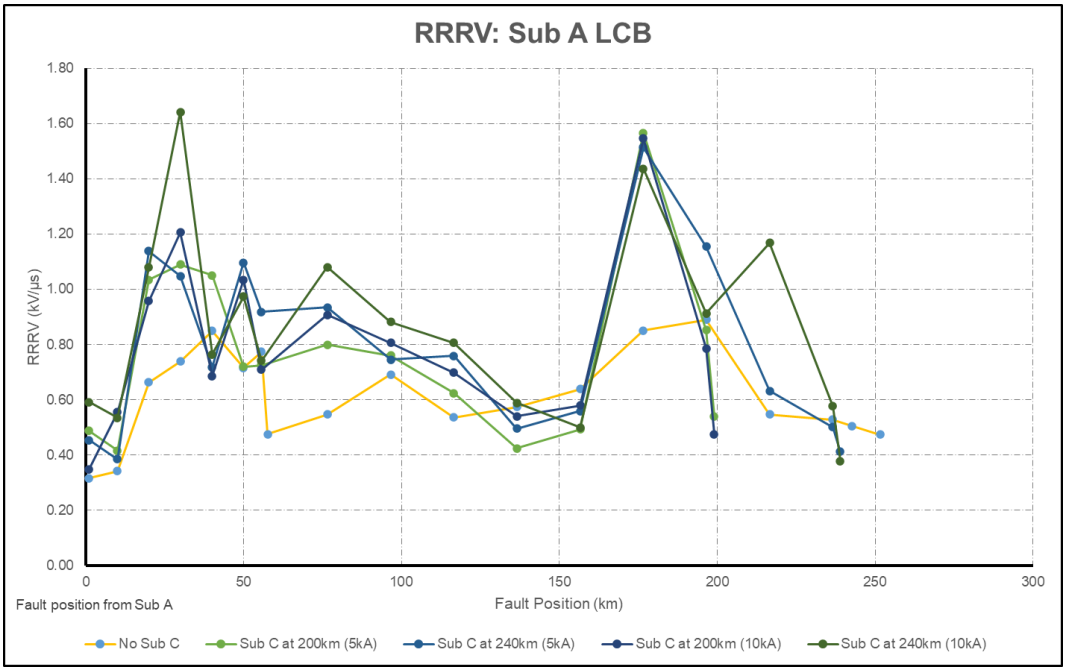

Figure 4-2: RRRV profiles for Sub A LCB

4.2 Peak Recovery Voltages and RRRVs for Sub B

The peak recovery voltage profile was presented for the LCB at Sub B for faults applied at varied positions along the transmission line in the following cases:

- Case 1: No Sub C
- Case 3a: Sub C contributing fault current magnitude of 5 kA and located at positions 20 km and 40 km away from Sub A (Line B-C 1 was 232.5 km and 212.5 km long respectively). The series capacitor bank was located between Sub B and Sub C. Faults were applied at varied positions along the transmission line between Sub B and Sub C however the fault position was with reference from Sub A.
- Case 3b: Sub C contributing fault current magnitude 10 kA and located at positions 20 km and 40 km away from Sub A (Line B-C 1 was 232.5 km and 212.5 km long respectively). The series capacitor bank was located between Sub B and Sub C. Faults were applied at varied positions along the transmission line between Sub B and Sub C however the fault position was with reference from Sub A.

The LCB at Sub B was within its peak recovery voltage rating for faults applied at all fault positions evaluated in the instance of Case 1.

The integration of Sub C (Case 3a and Case 3b) resulted in the peak recovery voltage rating being exceeded for terminal or short line faults (up to 20 km) from Sub B as a result of either an increase in fault current or increase in line length between Sub B and Sub C.

The peak recovery voltage rating was exceeded when Sub C was 20 km away from Sub A (Line B-C 1 was 232.5 km) and the fault current contribution from Sub C was increased from 5 kA to 10 kA. The limit was exceeded by a margin of 8% for a fault applied 1 km away from Sub B and the fault current contribution from Sub C was 5 kA. The margin of exceedance increased to 44% for a fault applied 1 km away from Sub B for a fault current contribution of 10 kA from Sub C. The limits were also exceeded for faults applied up to 16 km away from Sub B when the fault current contribution from Sub C was 10 kA by a margin of 9%.

The same assessment was conducted when Sub C was located 40 km away from Sub A (Line B-C 1 was 212.5 km) and the fault current contribution of Sub C was increased from 5 kA to 10 kA. The peak recovery voltage exceeded the LCB rating by a maximum margin of 25%. The limits were exceeded for faults applied at 1 km away from Sub B by a margin of 1% when the fault current contribution from Sub C was 5 kA. This indicates that a reduction in the line length reduced the peak recovery voltages that the LCB at Sub B is exposed to. The peak recovery voltage ratings were exceeded when the fault current contribution from Sub C was increased to 10 kA for faults applied at 1 km and 6 km away from Sub B by margins of 25% and 19% respectively.

Increasing the line length between Sub B and Sub C (from 212.5 km to 232.5 km) while maintaining the fault current contribution from Sub C to 5 kA resulted in the peak recovery voltage rating being exceeded for terminal or short line faults (1 km away from Sub B) from a margin of approximately 1% to 8%.

The peak recovery voltage ratings were exceeded when the fault contribution from Sub C was maintained at 10 kA and the line length between Sub B and Sub C was increased from 212.5 km to 232.5 km. The ratings were exceeded for terminal or short-line faults (1 km and 6 km away from Sub B) when Line B-C 1 was 212.5 km by a maximum margin of approximately 8% to approximately 43% when the line length of B-C 1 was increased to 232.5 km. The margin was exceeded for faults applied between 1 km and 16 km away from Sub B

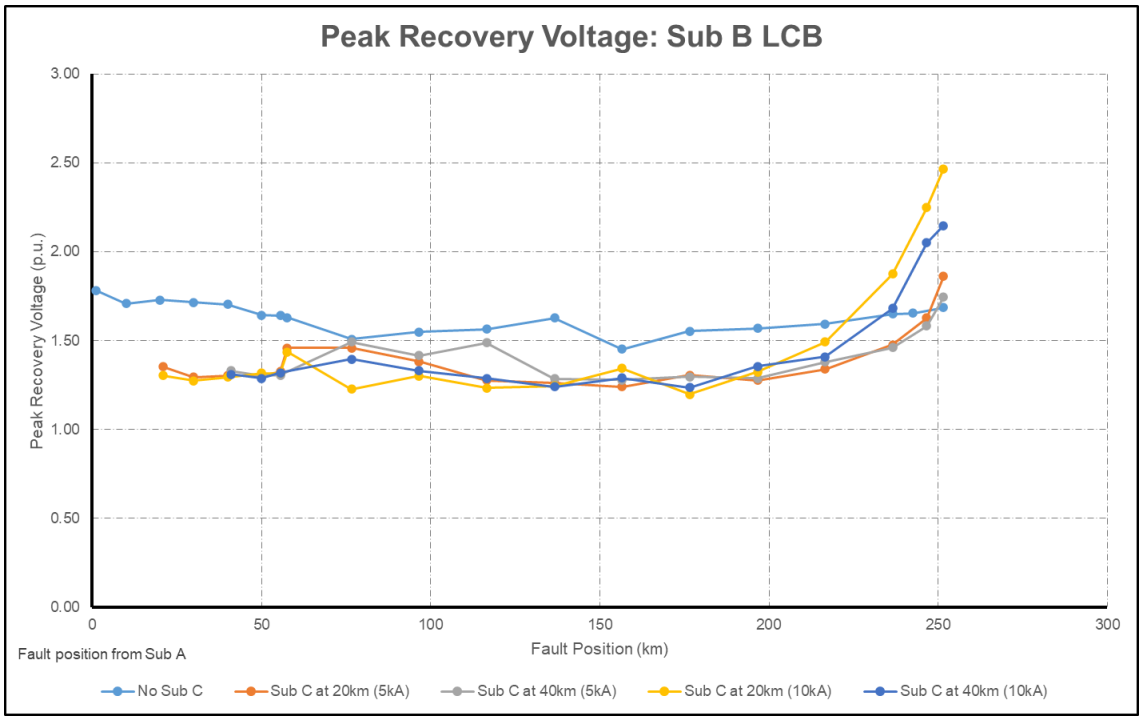

Figure 4-3: Peak recovery voltage profiles for Sub B LCB

Figure 4-4 presents the RRRVs that the LCB at Sub B were exposed to. As in the case of the LCB at Sub A (Figure 4-2) the RRRV was expected to be at its highest for faults in close proximity to the LCB (within the first 10 km). However, the saw-tooth response of the peak recovery voltage for faults up to 20 km from the LCB reduces the RRRV. The LCBs were recorded to be well within the acceptable limits as indicated.

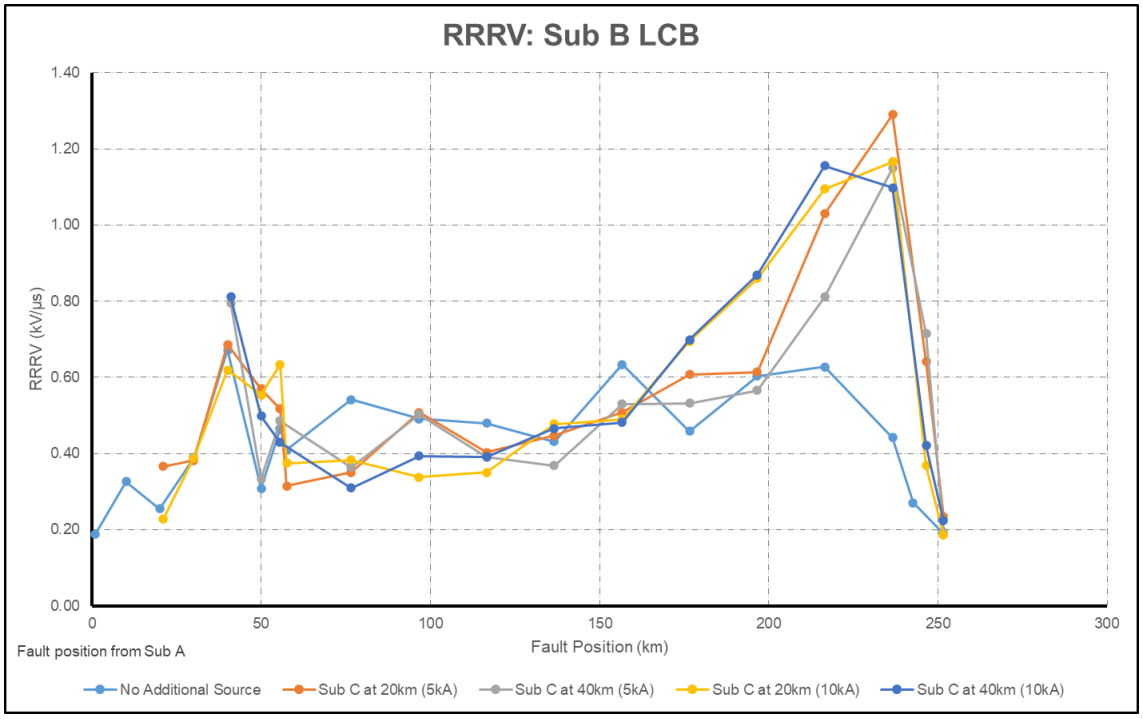

Figure 4-4: RRRV profiles for Sub B LCB

4.3 Peak Recovery Voltages and RRRVs for Sub C

The TRV analysis for the LCB at Sub C was conducted for the two cases assessed:

- Case 2: The integration of Sub C between Sub A and Sub B such that the series capacitor was between Sub A and Sub C. Sub C contributing fault current magnitude of 5 kA (Case 2a) and 10 kA (Case 2b). Sub C was located 200 km and 240 km from Sub A.
- Case 3: The integration of Sub C between Sub A and Sub B such that the series capacitor is between Sub B and Sub C. Sub C was contributing fault current magnitude of 5 kA (Case 3a) and 10 kA (Case 3b) and located at positions 20 km and 40 km away from Sub A (Line B-C 1 was 232.5 km and 212.5 km long respectively). Faults were applied at varied positions along the transmission line between Sub B and Sub C however the fault position was with reference from Sub A.

The integration of Sub C (Case 2a and Case 2b) indicated that the peak recovery voltage ratings for the LCB at Sub C were not exceeded for all cases (Figure 4-5). However, it must be noted that the test duty on the LCB suggested that the TRVs that the LCB at Sub C was exposed to were more onerous than what the LCB at Sub A was exposed to. Any further increases in magnitude of fault current through Sub C would result in the LCB exceeding its peak recovery voltage rating. The peak recovery voltage profile also indicates that the increase in line length results in higher peak recovery voltages.

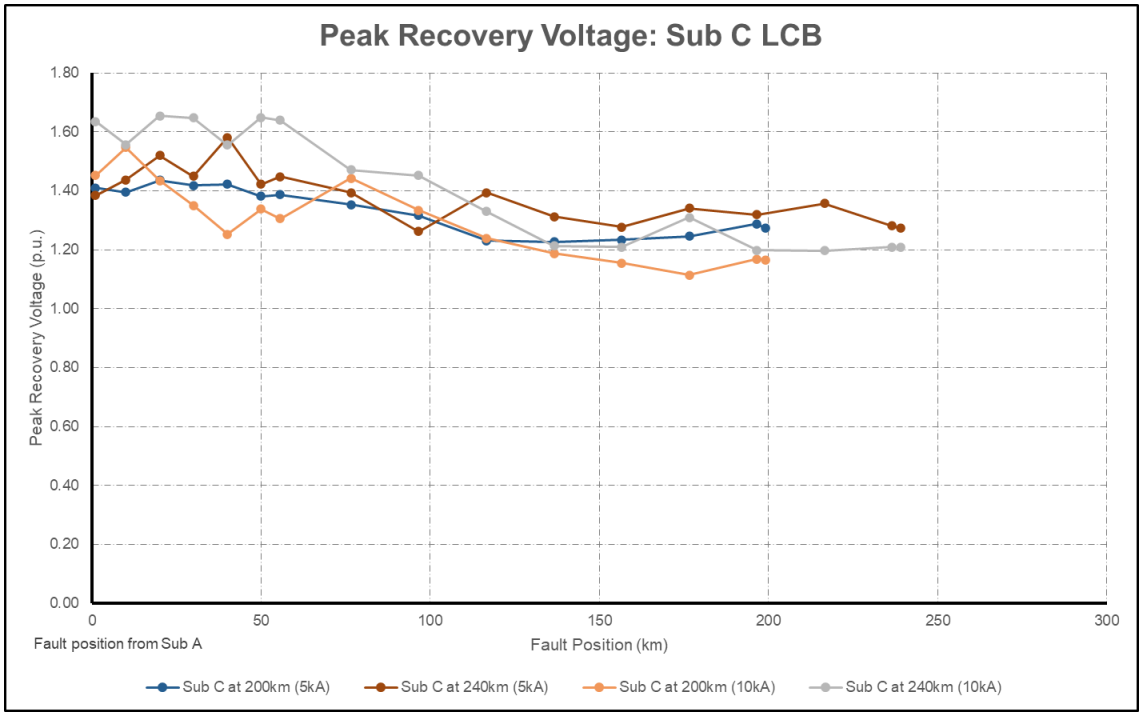

Figure 4-5: Peak recovery voltage profiles for Sub C LCB for Cases 2a and 2b

The integration of Sub C (Case 2a and Case 2b) indicated that the RRRV limits for the LCB at Sub C were not exceeded for all cases (Figure 4-6). However, the RRRV reached much higher magnitudes in comparison to the RRRV that the LCB at Sub A was exposed to (Figure 4-2). The RRRV profiles (Figure 4-6) also indicate that the RRRV is proportional to the fault current and line length.

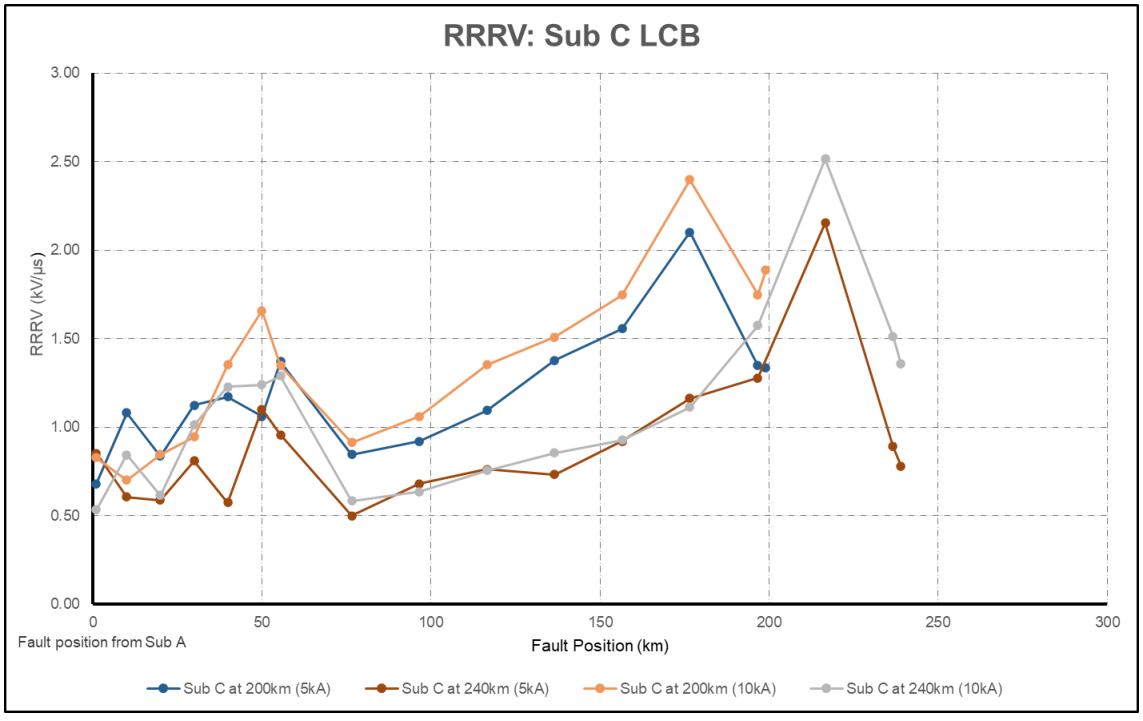

Figure 4-6: RRRV profiles for Sub C LCB for Case 2a and 2b

The integration of Sub C (Case 3a and Case 3b) indicated that the peak recovery voltage ratings for the LCB at Sub C were not exceeded for all cases (Figure 4-7). However, it must be noted that the test duty on the LCB suggested that the TRVs that the LCB at Sub C was exposed to were more onerous

than what the LCB at Sub B was exposed to. Any further increases in magnitude of fault current through Sub C would result in the LCB exceeding its peak recovery voltage rating. The peak recovery voltage profile also indicated that the increase in line length results in higher peak recovery voltages.

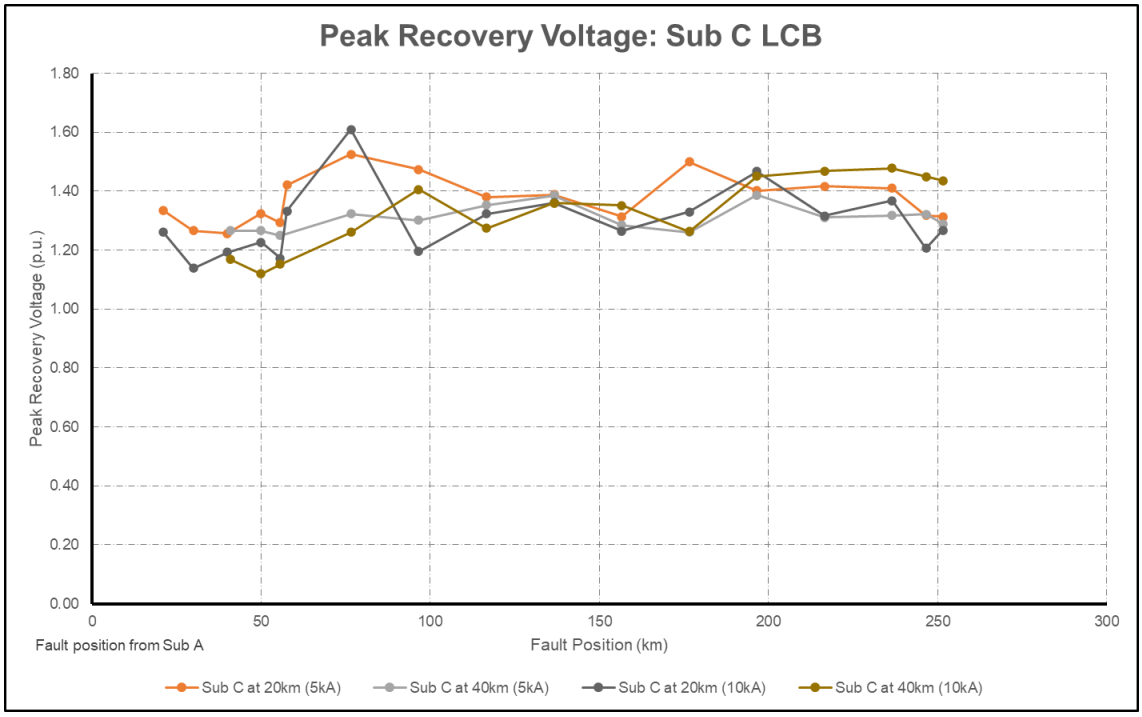

Figure 4-7: Peak recovery voltage profiles for Sub C LCB for Cases 3a and 3b

The integration of Sub C (Case 3a and Case 3b) indicated that the RRRV ratings for the LCB at Sub C were not exceeded for all cases (Figure 4-8). However, the RRRV reaches much higher magnitudes in comparison to the RRRV that the LCB at Sub A was exposed to (Figure 4-4). The RRRV profiles (Figure 4-8) also indicate that the RRRV is proportional to the fault current and line length.

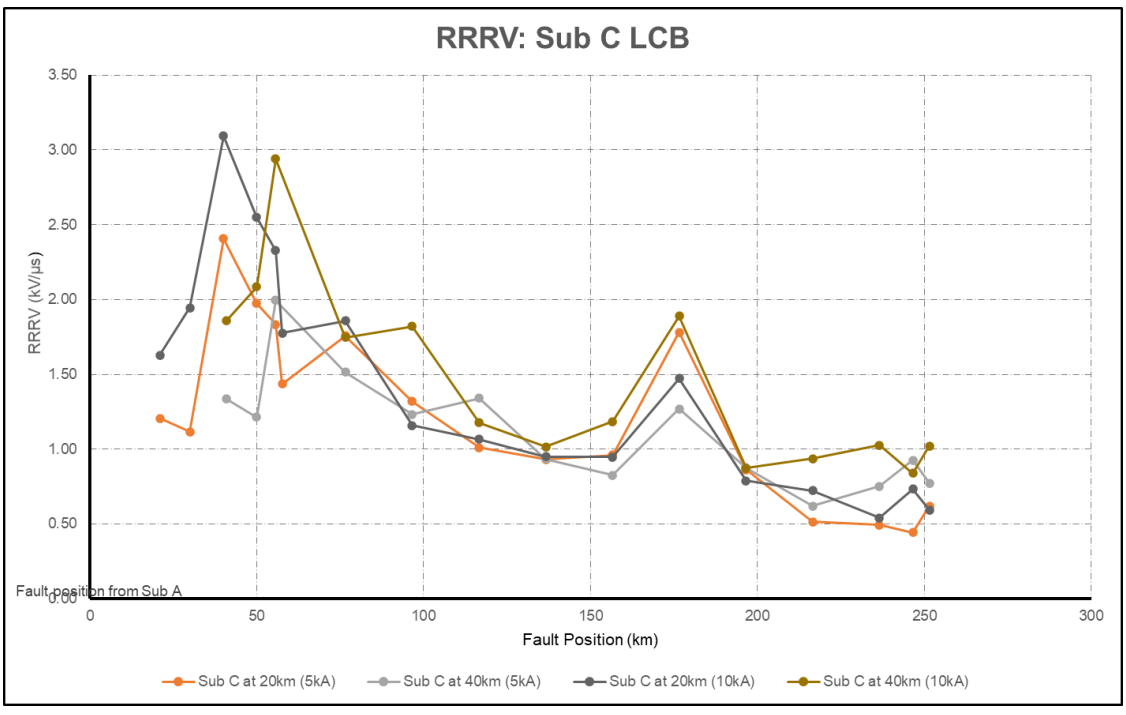

Figure 4-8: RRRV profiles for Sub C LCB for Case 3a and 3b

5 CONCLUSION

The need to investigate the TRV stresses on LCBs connected to evolving, series and shunt compensated transmission lines arises from the requirement to integrate new renewable energy sources into existing compensated transmission line corridors.

The key parameters that are used in assessing the LCB TRV performance are the peak recovery voltage as well as the rate of rise of recovery voltage.

This research highlighted that fault current is one of the fundamental factors that influence the required TRV rating of a circuit breaker. An increase in the fault level may result in either the peak recovery voltage or RRRV reaching or exceeding the LCB rating.

A change in the network configuration may also influence the required TRV rating of a circuit breaker by introducing additional stresses that may be imposed on the circuit breaker. The peak recovery voltage applied to LCBs connected to series and shunt compensated circuits have been shown to be susceptible to a change in the line lengths. An increase in line length could result in the peak recovery voltage ratings of the LCBs being exceeded.

Therefore, as part of network planning studies which indicate an increase in fault level of the network, a TRV study should be conducted for the LCBs. A change in the network configuration should also initiate an evaluation on the TRV stresses on the LCBs as a result of the change.

The boundary conditions on the performance of the LCB should be established under the initial conditions of the system configuration. This will guide the system planner in sensitising when mitigations need to be considered or the LCBs need to be upgraded with respect to TRV performance under evolving conditions.

The study also showed that the compensation factor does not have an influence on the required TRV rating of the circuit breaker if the protection systems of a series and shunt compensated circuit operates correctly under fault conditions. However, in the event of a maloperation of the protection system with the series capacitor bypass circuit breaker failing to close under fault conditions, this could result in the LCBs being exposed to severe TRVs. In this instance the compensation factor becomes a significant consideration for the evaluation of TRVs for LCBs.

Based on the above conclusions derived, this dissertation has validated the procedure developed in evaluating TRVs of LCBs connected to evolving series and shunt compensated lines.

5.1 Future work and recommendations

The following is recommended as future work when considering TRVs of LCBs in evolving, series and shunt compensated circuits:

- ITRVs associated to LCBs installed in series and shunt compensated transmission circuits.
- Sizing of surge arresters installed across series capacitor banks.
- Probabilistic approach to evaluating TRVs of LCBs connected in evolving, series and shunt compensated transmission lines.
- The impact of ARC to be evaluated on the TRV performance of LCBs connected in evolving, series and shunt compensated transmission lines.

6 REFERENCES

[1] "SAPP Annual Report 2019." [Online]. Available: http://www.sapp.co.zw/annual-reports
[2] G. Li and Z. Xiang, "Experience with Equipment for Series and Shunt Compensation," Cigre, Technical Brochure 693, Jul. 2017.
[3] *IEEE Guide for the Application of Transient Recovery Voltage for AC High Voltage Circuit Breakers*.
[4] *High-Voltage Switchgear and Control Gear - Part 100: Alternating-Current Circuit-Breakers*, vol. SANS 62271-100:2017. 2017.
[5] A. R. Hileman, *Insulation Coordination of Power Systems*. CRC Press, 1999.
[6] *IEEE Standard for Insulation Coordination - Definitions, Principles and Rules*, vol. IEEE Std C62.82.1-2010. 2011.
[7] "Guidelines for Representation of Network Elements when calculating Transients," Cigre, Technical Brochure 39, 2000.
[8] *Insulation co-ordination, Part 4: Computational guide to insulation co-ordination and modelling of electrical networks*, no. IEC TR60071-4. 2004.
[9] L. van der Sluis, *Transients in Power Systems*. John Wiley & Sons Ltd, 2001.
[10] D. Dufournet, "Transient Recovery Voltage (TRVs) for High-Voltage Circuit Breakers Part 1," San Antonio (USA), Sep. 19, 2013.
[11] D. F. Peelo, *Current Interruption Transients Calculation*. John Wiley and Sons Ltd., 2014.
[12] G. Catenacci, L. Paris, J.-P. Couvreux, and M. Pouard, "Transient Recovery Voltages in French and Italian High-Voltage Networks," *IEEE Transactions on Power Apparatus and Systems*, vol. PAS-86 No. 11, Nov. 1967.
[13] G. B. Thomas, J. Hass, and C. Heil, *Thomas' Calculus Early Transcendentals*, 14th ed. Pearson, 2018.
[14] A. Greenwood, *Electrical Transients in Power Systems*. John Wiley & Sons Inc., 1991.
[15] W. M. Leeds and D. J. Povejsil, "Out-of-Phase Switching Voltages and Their Effect on High-Voltage Circuit Breaker Performance," Jan. 1952.
[16] D. Durfournet, A. Janssen, and et al., "Switching Phenomena for EHV and UHV Equipment," Cigre, 570, Feb. 2014.
[17] K. Arp, K.-D. Basel, V. Biewendt, and K. Blum, *ABB Switchgear Manual*, 10th ed. STAR Deutschland GmbH, 1999.
[18] K. Nakanishi, *Switching Phenomena in High-Voltage Circuit Breakers*. Marcel Dekker Inc., 1991.
[19] R. Barrault, D. Dufournet, W. Hermann, and et al, "Practical application of arc physics in circuit breakers. Survey of calculation methods and application guide.," Cigre, Working Group 13.1, 1984.
[20] E. Haginomori, T. Koboyashi, J. Arai, and H. Ikeda, *Power System Transient Analysis Theory and Practice using Simulation Programs (ATP-EMTP)*. John Wiley and Sons Ltd., 2016.
[21] D. Andersson, R. Barrault, D. Dufournet, and M. Hrabovsky, "Applications of Black Box Modelling to Circuit Breakers," Cigre, Working Group 13.01, Aug. 1993.
[22] T. E. Browne Jr., "A study of A-C arc behaviour near current zero by means of mathematical models," *AIEE*, vol. 67, pp. 141–153, 1948.
[23] R. D. Garzon, *High Voltage Circuit Breakers Design and Applications*. Marcel Dekker Inc., 1997.
[24] F. Iliceto, E. Ciniera, and G. Asan, "TRVs across Circuit Breakers of Series Compensated Lines. status with present technology and analysis for the Turkish 420-kV Grid," *IEEE Transactions on Power Delivery*, vol. Volume 7, Number 2, Apr. 1992.
[25] P. Ijumba-Kamera, "Existing Series Capacitors in the Eskom Transmission Network," Eskom, GP_16/17, Mar. 2016.
[26] E. Bakie, C. Westhoff, N. Fischer, and J. Bell, "Voltage and current inversion challenges when protecting series-compensated lines - A case study.," presented at the 69th Annual Conference for Protective Relay Engineers, 2016.
[27] "A linearized model for MOV-protected series capacitors," *IEEE*, vol. PWRS-2, No. 4, Nov. 1987.
[28] M. Bamber, M. Bergstrom, A. Darby, S. Darby, G. Elliot, and et al, *Network Protection and Automation Guide*, First. Alstom Grid, 2011.
[29] Z. Emin, M. Martinez-Duro, and et al., "Resonance and Ferroresonance in Power Networks," Cigre, 569, Feb. 2014.
[30] D. D. Wilson, "Series Compensated Lines Voltages Across Circuit Breakers and Terminals caused by Switching."
[31] J. K. Bladow and T. L. Weaver, "Switching Surge Control for the 500kV California-Oregon Transmission Project," presented at the Cigre Paris, Sep. 1990.
[32] D. Dufournet, "Transient Recovery Voltage (TRVs) for High-Voltage Circuit Breakers Part 2," San Antonio (USA), Sep. 19, 2013.

[33] J. C. Das, *Transients in Electrical Systems: Analysis, Recognition and Mitigation*. McGraw Hill, 2010.
[34] *Surge Arrester Part 4: Metal-oxide surge arresters without gaps for a.c. systems*, vol. SANS 60099-4:2014. 2014.
[35] J. Woodworth, "Understanding Arrester Discharge Voltage," Dec. 04, 2008. http://www.arresterworks.com/arresterfacts/pdf_files/understanding_arrester_discharge_voltage.pdf
[36] S. O. Faried and S. Aboreshaid, "Stochastic Evaluation of Transient Recovery Voltages Across Circuit Breakers of Series Capacitor Compensated Transmission Lines," *IEEE Transactions on Power Delivery*, vol. 16, Number 1, Jan. 2001.
[37] M. H. Zakernejad, M. Mohammadi, and M. Mehrtash, "A New Approach for Probabilistic Evaluation of Transient Recovery Voltage Across Circuit Breakers in TCSC Compensated Transmission Lines," presented at the 29th Power System Conference - 2014 Tehran, Iran.
[38] A. C. Guidoum, "Kernel Estimator and Bandwidth Selection for Density and its Derivatives," University of Science and Technology Houari Boumediene., Course Notes, Oct. 2015.
[39] J. Guttag, "Monte Carlo Simulation," 2016. [Online]. Available: https://youtu.be/OgO1gpXSUzU
[40] J. A. Martinez-Velasco, *Power System Transients: Parameter Determination*. CRC Press, 2010.
[41] B. Guru and H. R. Hiziroglu, *Electromagnetic field theory fundamentals*, Second. Cambridge University Press, 2004.
[42] P. Gomez, "Validation of ATP Transmission Line Models for a Monte Carlo study of switching transients," presented at the North American Power Symposium, 2007.
[43] M. F. Abusharkh, M. H. Abdel-Rahman, and H. M. El-Zayyat, "Transient Recovery Voltage (TRV) conditions on the Jordanian 132 kV system," presented at the Cigre Session, Paris, Sep. 1992.
[44] P. K. Basak and P. G. Parrott, "Survey of TRV conditions on the CEGB 400 kV system," *IEE Proceedings*, vol. 128, no. 6, Nov. 1981.
[45] B. L. Avent, D. F. Peelo, J. H. Sawada, and B. C. Hydro, "Application of 500 kV Circuit Breakers on Transmission line with MOV protected series capacitor bank," presented at the Cigre Session, Paris, 2002.
[46] F. M. Gatta, F. Iliceto, and S. Lauria, "TRVs across the circuit breakers of series compensated lines analysis, design and operation in the 420 kV Turkish Grid," presented at the Cigre Session, Paris, 2002.
[47] M. Kizilcay and T. Pniok, "Digital Simulation of Fault Arcs in Power Systems," *European Transactions on Electrical Power*, vol. 1, no. 1, Feb. 1991.
[48] A. T. Johns, R. K. Aggarwal, and Y. H. Song, "Improved techniques for modelling fault arcs on faulted EHV transmission systems," *IEE Proceedings: Generation, Transmission Distribution*, vol. 141, no. 2, Mar. 1994.
[49] A. J. S. Groenewald, *Eskom Substation Layout Design Guideline, Insulation coordination and electrical clearances*. 2011.

7 APPENDICES

7.1 V-I data for Surge Arrester

I (kA)	Voltage (kV)
0.00027	213
0.005	219
0.010	222
0.1	233
0.5	243
1	247
1.5	250
2	252
2.5	253
3	254
3.5	256
4	256
4.5	257
5	258
6	259
7	260
7.5	261
8	261
9	262
10	263
12	264
15.8	266
17.7	267
20	268
25	269
30	271
35	272
40	273
45	274
50	275
55	277
60	278